3RD-SCEEER
June 2020
P-ISSN: 1814-5892
E-ISSN: 2078-6069
www.ijeee.edu.iq

Iraqi Journal

For Electrical And Electronic Engineering

IJEEE

Proceedings of The 3rd Scientific Conference of Electrical and Electronic Engineering Researches (SCEEER) (15-16) JUNE 2020 | BASRAH / IRAQ

Open Acess

IJEEE University of Basrah College of Engineering

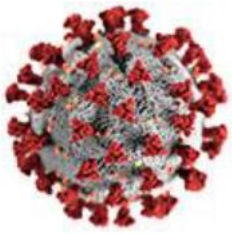

The 3rd Scientific Conference of Electrical and Electronic Engineering Researches (SCEEER)

15-16 JUNE 2020

BASRAH / IRAQ

http://www.sceeer.ijeee.edu.iq

CONFERENCE PROGRAMME BOOKLET

Electrical Engineering Department

College of Engineering

University of Basrah

COMMITTEES

Scientific Committee

- Prof. Dr. Abdulkareem S. Abdullah (Chairman)
- Prof. Dr. Ali F. Marhoon (Member)
- Prof. Dr. Fadhil R. Tahir (Member)
- Prof. Dr. Haider M. Alsabbagh (Member)
- Assist. Prof. Dr. Ramzy S. Ali (Member)
- Assist. Prof. Dr. Abbas H. Abbas (Member)

Organizing Committee

- Assist. Prof. Dr. Ammar A. Aldair (Chairman)
- Assist. Prof. Dr. Mofeed T. Rashid (Member)
- Assist. Prof. Dr. Falih M. Alnahwi (Member)
- Assist. Prof. Dr. Ali K. Abdulabbas (Member)
- Dr. Auday B. Al-Mayyahi (Member)
- Dr. Husham L. Swadi (Member)

Coordinating Committee

- Assist. Prof. Dr. Abdulmuttalib T. Rashid (Chairman)
- Assist. Prof. Dr. Basil H. Jasim (Member)
- Assist. Prof. Dr. Ali A. Abduljabar (Member)
- Dr. Khalid M. Addulhassan (Member)
- Dr. Habeeb J. Nakad (Member)
- Dr. Osama Y. Al-Atbee (Member)
- Dr. Fatemah K. Al– Assfor (Member)
- Dr. Wasan A. Wali (Member)
- Mrs. Maha K. Gentab (Member)

وقائع المؤتمر العلمي الثالث لابحاث الهندسة الكهربائية والالكترونية

15-16 حزيران 2020

البصرة – العراق

الجلسه الافتتاحيه (8:30-9:00)صباحاً (عن طريق FCC) ID: mmrali2

- عزف النشيد الوطني
- قرائة آيات من القران الكريم
- قرائة سورة الفاتحة ترحماً على ارواح شهداء العراق
- كلمة السيد عميد كلية الهندسة المحترم

جامعة البصرة

كلية الهندسة

قسم الهندسة الكهربائية

Monday 15/06/2020

9:00-12:00 AM Session 1: Chair **Dr. Ammar A. Aldair (FCC ID: mmrali2)**

No.	ID	Name the paper	Names of Authors	Time
1	1570641908	Outdoor & Indoor Quadrotor Mission	**Baqir Nassir Abdul-Samed, Ammar A. Aldair**	9:00-9:15
2	1570641914	Simulation Model of Cold Rolling Mill	**Waleed I. Breesam Khearia A. Mohamad Mofeed T. Rashid**	9:15-9:30
3	1570642077	Design of a Wide Dual-Band Coplanar Probe Feed Antenna for WLANs Applications	**Nabil Eyad Abdulhussein Abdulkareem S. Abdullah**	9:30-9:45
4	1570642252	Encrypted Vehicular Communication Using Wireless Controller Area Network	**Mohammed Al-Qaraghuli Saadaldeen Rashid Ahmed Muhammad Ilyas**	9:45-10:00
5	1570642656	The Influence of Concave Pectoral Fin Morphology in the Performance of Labriform Swimming Robot	**Farah Abbas Naser Mofeed Turky Rashid**	10:00-10:15
6	1570643609	The Design and Implementation of a Single-Actuator Soft Robot Arm for Lower Back Pain Reduction	**Alaa Al-Ibadi**	10:15-10:30
7	1570644508	Healthcare Monitoring and Analytic System Based Internet of Thing	**Bahaa. S.Mostafa Abbas Hussain miry Tariq.M.Salman**	10:30-10:45
8	1570644527	WSNs and IoT Their Challenges and applications for Healthcare and Agriculture A Survey	**Mohammed Mehdi Saleh**	10:45-11:00
9	1570644557	Robotics Path Planning Algorithms using Low-Cost IR Sensor	**Israa Sabri A. AL-Forati Abdulmuttalib T. Rashid**	11:00-11:15
10	1570644670	Two Algorithms For Static Polygon Shape Formation Control	**Bayadir A. Issa Abdulmuttalib T. Rashid**	11:15-11:30
11	1570644839	Enhancing Reading Advancement Using Eye Gaze Tracking	**Saadaldeen Ahmed Mustafa latif fadhil Salwa Khalid Abdulateef**	11:30-11:45
12	1570644889	Two Dimensional Path Planning with Static Polygon Obstacles Avoidance	**Duaa Ahmed Ramadhan Abdulmuttalib T. Rashid Osama T. Rashid**	11:45-12:00

Monday 15/06/2020

9:00-11:45 AM Session 2: Chair **Dr. Mofeed T. Rashid (FCC ID: mofid766)**

No.	ID	Name the paper	Names of Authors	Time
1	1570644947	Adaptive Energy Management System for Smart Hybrid Microgrids	**Bilal Naji Alhasnaw** **Basil H. Jasim**	9:00-9:15
2	1570645168	Robotic Glove for Rehabilitation Purpose Review	**Yahya salim ahmed** **Auns Q. Al-Neami** **Saleem lateef**	9:15-9:30
3	1570645187	Enhancement the Sensitivity of waveguide Coated ZnO thin films Role of Plasma irradiation	**Marwan Hafeedh Younus** **Mouyad Abdullah Ahmed** **Ghazwan Ghazi. Ali**	9:30-9:45
4	1570645256	Synchronization and tracking control of a novel 3 dimensional chaotic system	**Basil H. Jasim** **Mofeed T. Rashid** **Khulood Moosa Omran**	9:45-10:00
5	1570645259	Design and implementation of monitoring and warning (IOT) system for electricity poles	**Jumana Amer AL-Hammoudi** **Basil H. Jasim**	10:00-10:15
6	1570645262	Control Strategy of Reactive Power Sharing in an Islanded Microgrids	**Ali Q. Almousawi** **Ammar A. Aldair**	10:15-10:30
7	1570645297	Novel Memory Structures in QCA Nano Technology	**Ali H. Majeed** **Esam Alkaldy** **Mohd S. Zainal** **Danial MD. Nor**	10:30-10:45
8	1570645310	Automatic Storage and Retrieval System using the Optimal Path Algorithm	**Hanan M. Hameed** **Abdulmuttalib Turky Rashid** **Kharia A. Al Amry**	10:45-11:00
9	1570646082	Design a Compact Coplanar Wideband Antenna Used in Radio Frequency Identification Systems	**Sufyan Hazaa Ali** **Ahmed Hameed Reja** **Yousif Azzawi Hachim**	11:00-11:15
10	1570648530	Fair and Balance Demand Response application in Distribution Networks	**Ibrahim H. Al-Kharsan** **Ali.F. Marhoon** **Jawad Radhi Mahmood**	11:15-11:30
11	1570649530	Performance of Non-Orthogonal Multiple Access (NOMA) with Successive Interference Cancellation (SIC)	**Ali K. Marzook** **Hayder J. Mohammed** **Hisham L. Swadi Roomi**	11:30-11:45

Table of Contents:

Article Title	Page
Outdoor & Indoor Quadrotor Mission	**1**
Design of a Wide Dual-Band Coplanar Probe Feed Antenna for WLANs Applications	**13**
Encrypted Vehicular Communication Using Wireless Controller Area Network	**17**
The Design and Implementation of a Single-Actuator Soft Robot Arm for Lower Back Pain Reduction	**25**
Healthcare Monitoring and Analytic System Based Internet of Thing	**30**
WSNs and IoT Their Challenges and applications for Healthcare and Agriculture: A Survey	**37**
Robotics Path Planning Algorithms using Low-Cost IR Sensor	**44**
Two Algorithms For Static Polygon Shape Formation Control	**53**
Enhancing Reading Advancement Using Eye Gaze Tracking	**59**
Two Dimensional Path Planning with Static Polygon Obstacles Avoidance	**65**
Adaptive Energy Management System for Smart Hybrid Microgrids	**73**
Robotic Glove for Rehabilitation Purpose: Review	**86**
Enhancement the Sensitivity of waveguide Coated ZnO Thin Films: Role of Plasma Irradiation	**93**
Synchronization and Tracking Control of A Novel 3 Dimensional Chaotic System	**99**
Design and Implementation of Monitoring and Warning (IOT) System for Electricity Poles	**105**
Control Strategy of Reactive Power Sharing in an Islanded Microgrids	**112**
Novel Memory Structures in QCA Nano Technology	**119**
Automatic Storage and Retrieval System using the Optimal Path Algorithm	**125**
Fair and Balance Demand Response application in Distribution Networks	**139**
Performance of Non-Orthogonal Multiple Access (NOMA) with Successive Interference Cancellation (SIC)	**152**

Open Access
Iraqi Journal for Electrical and Electronic Engineering
Conference Article

Outdoor & Indoor Quadrotor Mission

Baqir Nassir Abdul-Samed[1], Ammar A. Aldair[2]
[1,2] Electrical Engineering Department, University of Basrah, Basrah, Iraq

Correspondence
*Baqir Nassir Abdul-Samed
Electrical Engineering Department,
University of Basrah, Basrah, Iraq
Email: bakir_68@hotmail.com

Abstract
The last few years Quadrotor became an important topic, many researches have implemented and tested concerning that topic. Quadrotor also called an unmanned Aerial Vehicle (UAV), it's highly used in many applications like security, civil applications, aid, rescue and a lot of other applications. It's not a conventional helicopter because of small size, low cost and the ability of vertical and takeoff landing (VTOL). The models kept an eye on quadrotors were presented, the advancement of this new kind of air vehicle is hindered for a very long while because of different reasons, for example, mechanical multifaceted nature, enormous size and weight, and challenges in charge particularly. Just as of late a lot of interests and endeavors have been pulled in on it; a quadrotor has even become a progressively discretionary vehicle for useful application. Quadrotor can be used in variable, different , outdoor and indoor missions; these missions should be implemented with high value of accuracy and quality. In this work two scenarios suggested for different two missions. First mission the quadrotor will be used to reach different goals in the simulated city for different places during one flight using path following algorithm. The second mission will be an indoor arrival mission, during that mission quadrotor will avoid obstacles by using only Pure pursuit algorithm (PPA). To show the benefit of using the new strategy it will compare with a victor field histogram algorithm (VFH) which is used widely in robotics for avoiding obstacles, the comparison will be in terms of reaching time and distance of reaching the goal. The Gazebo Simulator (GS) is used to visualize the movement of the quadrotor. The gazebo has another preferred position it helps to show the motion development of the quadrotor without managing the mathematical model of the quadrotor. The Robotic Operating System (ROS) is used to transfer the data between the MATLAB Simulink program and the Gazebo Simulator. The diversion results show that, the proposed mission techniques win to drive the quarter on the perfect route similarly at the limit with regards to the quadrotor to go without hitting any obstacle in the perfect way.

KEYWORDS: Quadrotor, PPA, path following, obstacle avoidance, VFH, Gazebo, ROS.

I. INTRODUCTION

In recent years, the unmanned aerial vehicle (UAV) becomes more popular than the winged helicopter because the UAV has the ability of vertical takeoff and landing, which needs a small place for takeoff and landing. Moreover, the cost of the UAV is cheap and its structure is simple. For these reasons, the UAV has superiority over the winged helicopter in applying in many application fields such as rescue, search, surveillance, interdiction, and transportation. The dynamic model of quadrotor UAV consists of inherent nonlinearity which makes it not easy to analyze [1-3]. UAV is a very complex, so it will need an accurate algorithm for navigation safely during attempts to complete the different missions. Different algorithms have been suggested and tested for path flowing for mobile robots like Bug1, Bug2, Tangent Bug…etc.

Pure pursuit algorithm (PPA) one of the common path flowing algorithms, so it will be used to navigate the quad--rotor during different tasks [2,3,4].

PPA will force the quadrotor to follow a desired path in either outdoor or indoor. The desired path should be clear of Obstacle so that the quadrature dose not hits and destroyed, for that reason it should need an extra algorithm for obstacle avoidance, also it needs for a quadrotor itself a more of component like sensors to detect these obstacles, this of course will lead to more cost, more complicated, extra weight and longtime processing.

In this paper path following algorithm has been used alone (especially in a well-known environment) to map the path of the quadrotor. It will be possible to make the quadrotor keep away from obstacle to achieve the goal.

Two scenarios suggested and tested to achieve that idea. First one was about moving quadrotor inside a simulated city to reach different goals by flying high to avoid obstacles. Second one about indoor mission with well-known environment, the quadrotor used to move to the target while

avoiding obstacles in the way *without* using any *obstacle avoidance algorithm*. Finally, the suggested strategy of using only path following algorithm (PPA) for avoiding obstacles compared with the (VFH) algorithm to show the advantages of using that kind of strategy.

The MATLAB used to implement the simulation for the proposed scenarios with the aid of gazebo & ROS. G**azebo** is an open-source 3D robotics simulator. Gazebo was a component in the Player Project from 2004 through 2011. Gazebo integrated the ODE physics engine, Open Graphic library rendering, and support code for sensor simulation and actuator control. In 2011, Gazebo became an independent project supported by Willow Garage. In 2012, Open Source Robotics Foundation (OSRF) became the steward of the Gazebo project. OSRF changed its name to Open Robotics in 2018.

Gazebo can use multiple high-performance physics engines, such as ODE, Bullet, etc. (the default is ODE). It provides realistic rendering of environments including high-quality lighting, shadows, and textures. It can model sensors that "see" the simulated environment, such as laser range finders, cameras (including wide-angle), Kinect style sensors, etc.[4]

Gazebo simulator used to show the 3D environment of moving quadrotor. Robotic operating system (ROS) will be used as a coordinator between MATLAB and gazebo.
The results show that effectiveness of the proposed scenarios of flying the quadrotor in different environments.

II. QUADROTOR BASIC CONCEPTS

Quadrotor convenient in many applications due to it's a low cost, structure, simplicity and ability of vertical takeoff landing (VTOL). Different models and structure suggested to be suitable of different missions. [3,5].

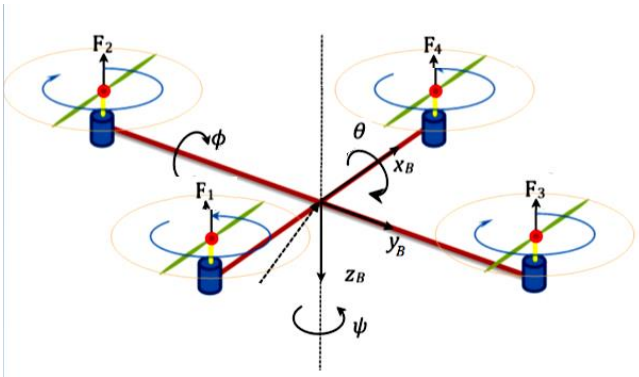

Figure (1) Motor forces of quadrotor

The quarter has four propellers to generate the suitable forces (F_1,F_2,F_3 and F_4) for takeoff, following the trajectory and landing as shown in Figure 1.

The four propellers can be considered as two pairs:
The propeller1 and propeller4 as the first pair while propeller2 and propeller3 as the second pair. In order to balance the torques and make the UAV stabile during the maneuver, the first pair should rotate clockwise while the second pair should rotate counterclockwise or vice versa[5,6,7] .As shown in Figure (2).

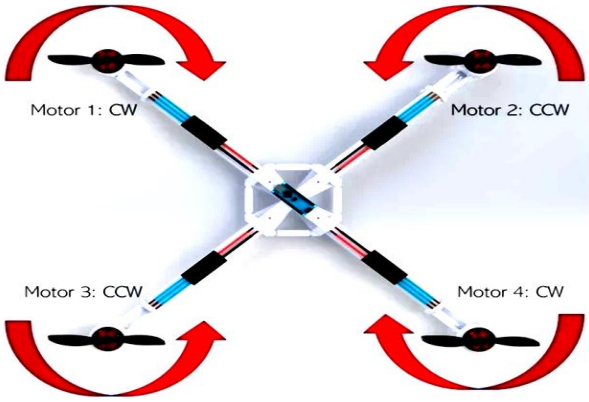

Figure (2) rotation of four motors

A quadrotor has six-degree of freedom (6 DOF): three-degree of freedom represents the *rotational movements*, while the other three-degree of freedom represents the *translation movements*. Quadrotor movements dynamics are simple it depends on the changing speed of the four motors. The changing speed creates the following movements: forward, backward, up, down, right rotation and left rotational [6,8]. Fig. 3 shows the six-degree of freedom of quadrotor

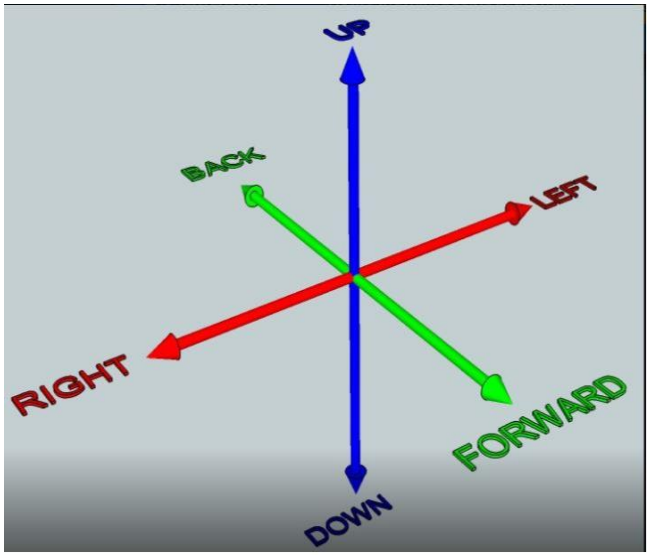

Figure (3) quadrotor six degrees of freedom

To control movements of the quadrotor for different directions like right, left, up and down, these movements can be done by changing the relative speeds of the motors in a way like: -

- Verticals

  It's sometimes called throttle, the movements along the z-axes, this can be achieved by increasing (up) or decreasing (down) the speed of the four motors. Shown in figure 1.

- Yaw movement (ψ)
  The quadrotor moves right or left depends on the speeds of the clockwise or counter clockwise rotation pair of motors. As shown in figure 1

- Roll movements (Ø)
  This movement can be achieved by changing the speed of the left or right pairs of motors. As shown in figure 1

- Pitch movement (Θ)
  This movement causes the quadrotor moving front or back by changing the speed of the front or back pair of motors. As shown in figure 1.

III. PURE PURSUIT ALGORITHM (PPA)

PPA used here to drive and guide the quadrotor to follow a desired path to complete its mission during giving waypoints for single and multi-goals.
PPA widely applied to achieve path following problem for the mobile robots. It is a geometrical method depends on the calculating the curvature that followed by the vehicle to the desired path point. The curvature that connects the current position of the vehicle and the next point on the desired trajectory is constructed (lookahead point).
Figure 4 shows the geometry of the pure pursuit algorithm. [9,10,11]

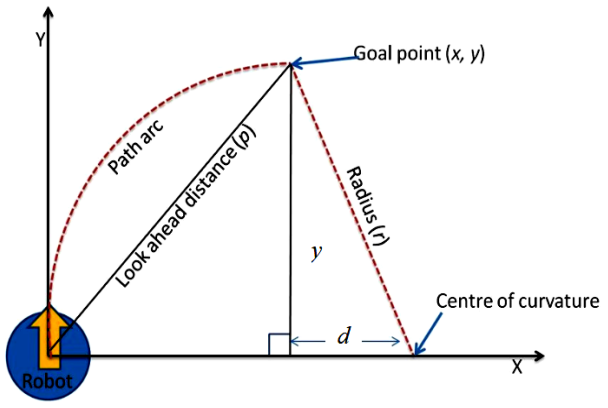

Figure (4) geometry of PPA

According to the pure pursuit algorithm, the quadrotor should move from the current point (0,0) to the goal point through a number of the next points (lookahead point) to reach the goal point (*x, y*) . It can increase or decrease the next point location to reach the goal fast or slow but that will affect on the smoothness and accuracy of the desired path. [9]

Equation of the larger triangle can be written: -

$$l^2 = x^2 + y^2 \quad (1)$$

The line segment on the x (d) given by: -

$$d = r - x \quad (2)$$

For the smallest triangle the relation is: -

$$r^2 = d^2 + y^2 \quad (3)$$

By solving (1) to (3) the curvature (ρ) can be calculated as: -

$$\rho = \frac{1}{r} = \frac{2x}{l^2} \text{ OR } r = \frac{l^2}{2x} \quad (4)$$

The curvature of the path arc obtained in (4) determines the steering wheel angle of the quadrotor [9]

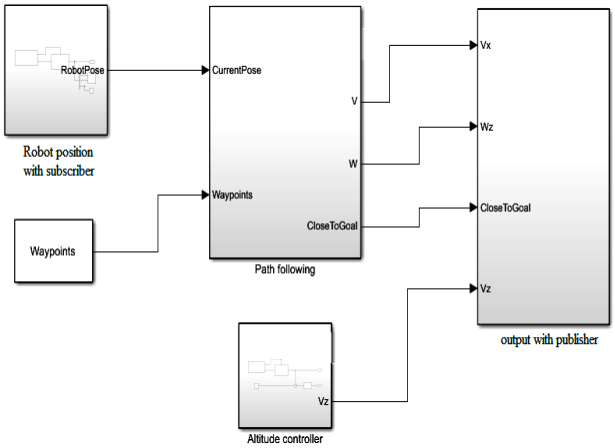

Figure (5) PPA MATLAB simulation

Figure 5 shows the PPA simulation in MATLAB which will connected to Gazebo simulator through ROS to show the quadrotor movement for different environments that will used in the suggested scenarios

IV ROS AND GAZEBO

The simulation of the quadrotor movements implemented by using a 3D Gazebo simulator (GS) to show the simulated world when quadrotor completes different missions. Using gazebo helps to build different environments, even it can be import objects or models from the online library of gazebo or from other 3d graphics programs like solidworks , CAD and SketchUp. The gazebo is not connected directly to MATLAB Simulink , ROS will be the in the middle between MATLAB and gazebo .ROS receive commands from MATLAB and forward it to Gazebo (mainly control signals) to adjust the quadrotor path to the goal , as well as some information should fed to the MATLAB about the current position of the quadrotor all this achieved by the *publisher*. After quadrotor moves again ROS will be responsible to send the new location of the quadrotor to the MATLAB to adjust the angular velocity to enable the quadrotor to choose the best path towards goal using the path following algorithm this will be achieved by *subscriber*. As shown in figure 6 [12,13,14]

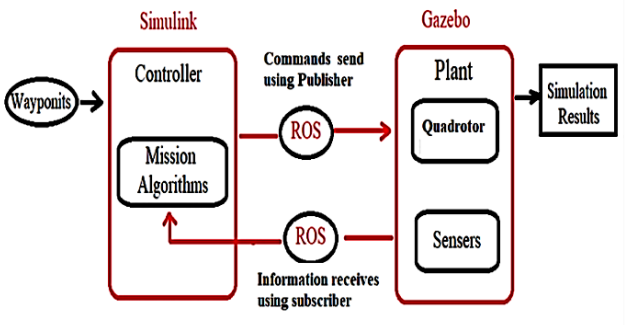

Figure (6) Simulink connected to Gazebo via ROS

V SIMULATION AND RESULTS

Many researches introduced different navigation algorithms for mobile robots likes bug1, bug 2, tangent bug A*….. etc. Each one these algorithms has different applications with some drawbacks, for instant bug algorithms influenced by sensor readings which make the robot slow, A* from other hand is time consuming and not suitable for path with many loops.

In this work we will concentrate on using the pure pursuit algorithm (PPA) to solve the navigation problem of the quadrotor .As mentioned earlier, PPA a geometric algorithm used widely to solve path following problem.PPA will force the quadrotor to move from the current point to the next point until reaching the goal with adjustment linear and angular velocity delivered to the quadrotor to take the best path towards goal .

After reaching goal, PPA stops the quadrotor by sending Goal position to the MATLAB and this is making the linear and angular velocity equals to zero (hold) . All the operation achieved by using the quadrotor sensors to send the position to updates to the MATALB which leads to adjust the quadrotor desired path towards the goal.

Two scenarios suggested and tested to show the ability of the PPA to control the quadrotor path to reach goals. 3D Gazebo used to design two worlds. First one is a simulated city; the second one is a maze with well-known environment the Simulation provides an excellent environment to show the quadrotor flying in the simulated worlds.

First Scenario (outdoor mission)

The first scenario is an outdoor mission it was about using the quadrature to complete several missions and reaching different goals inside a simulated city. The simulated city assumed to have all necessary requirements, designed using 3D gazebo. Quadrotor will fly from start point to the first goal and approach ground in the goal using PPA , then it will fly again to the 2nd goal and so on until reaches the last goal and will landing finally there .

Simulated city consiste of all necessary requirments including :

- Fire station & Trucks
- Diffeernt models of houses
- Gas Station
- Trees
- Grocery stors
- Bus station
- Police Office
- Cras
- Caffe

Second Scenario (path following like obstacle avoidance algorithm) (PFLOA)

The second scenario has different gazebo environments and it will be using new strategy for enable the quadrotor fly from the start point to the goal point though some obstacles. Accomplishing this purpose, led to use an obstacle avoidance algorithm. Many obstacle algorithms used and implemented, these algorithms need extra software, hardware or both. Of course, this will make the robot more expensive, slow because of extra weight and large time for processing, mostly this will used in both known and unknown environments.

In this work, it's assumed that the mobile robot or in our case the quadrotor will fly in well-known environment. It can be determined the position of obstacles, free spaces and shortest path to the goal in each time quadrotor passes an obstacle. This is achieved by making the quadrotor follow a waypoint all the way from start point to the goal. It can minimize or maximize the number of waypoints and this is of course will influence on the path accuracy. Taking a sharp turn from point to point to overcome the obstacle will leads to minimize the time to reach final destination.

The new strategy was very successful and very efficient making the quadrotor avoid different types of obstacles without hitting any of them and in a short time. To show the effectiveness of the suggested strategy for avoiding obstacles, it will compare the results with vector field histogram (VFH) method of avoiding obstacles which is used widely in robotics in terms of time, speed, distance and safety.

After simulation for both algorithms, it is found that the Path following like obstacle avoidance algorithm was fast and take less time than Vector field histogram with also short distance compare to VFH.

PFLOA = 2:09:43 (minute: second: fraction of sec.)

VFH = 2:29:39

First Scenario

Figure 7 shows the enviroment of the simulated city used for nevigation of the quadrotor from the start point .

Figure (7) simulated city

Figure 8 shows the first target house No.1

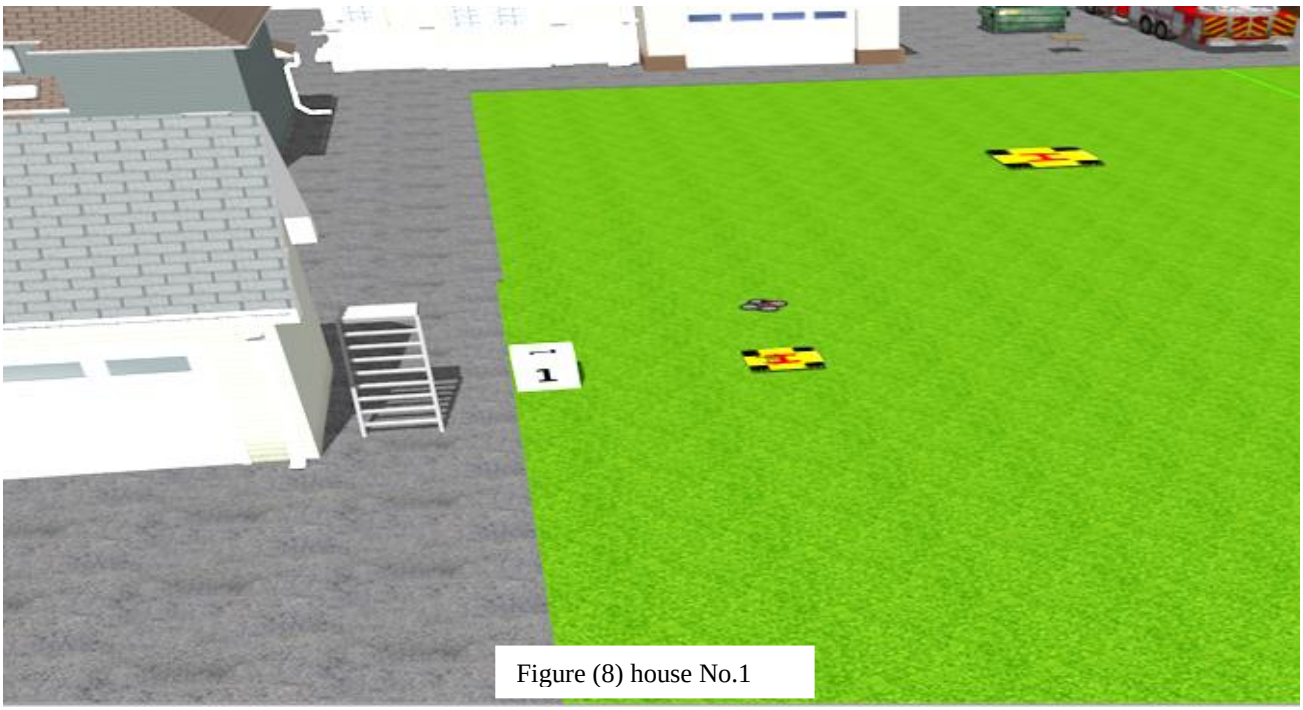

Figure (8) house No.1

Figure 9 shows the second target house no.2

Figure (9) house No.2

Figure 10 shows the third target Fire station.

Figure (10) Fire station

Figure 11 shows the 4th target Grocery store

Figure (11) Grocery store

Figure 12 shows the targets no.5 and the last one the Caffe

Figure (12) Caffe

Second Scenario

Figure 13 show the obstacle environment using 3D gazebo.

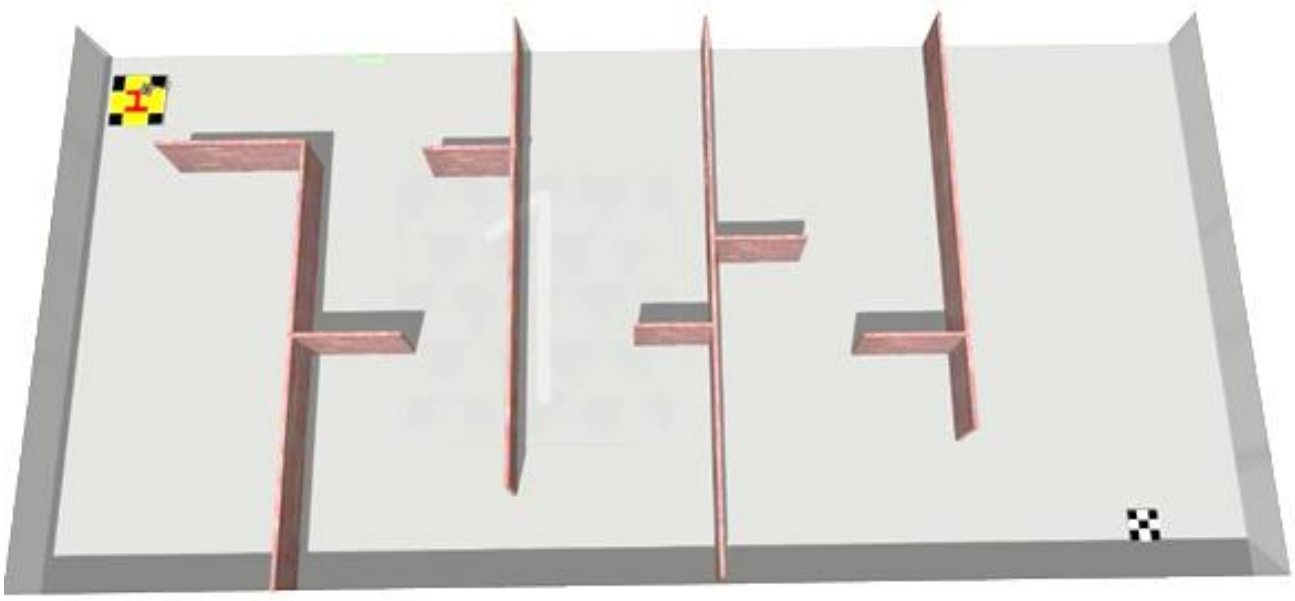

Figure (13) obstacle environment

Figure 14 show the first obstacle

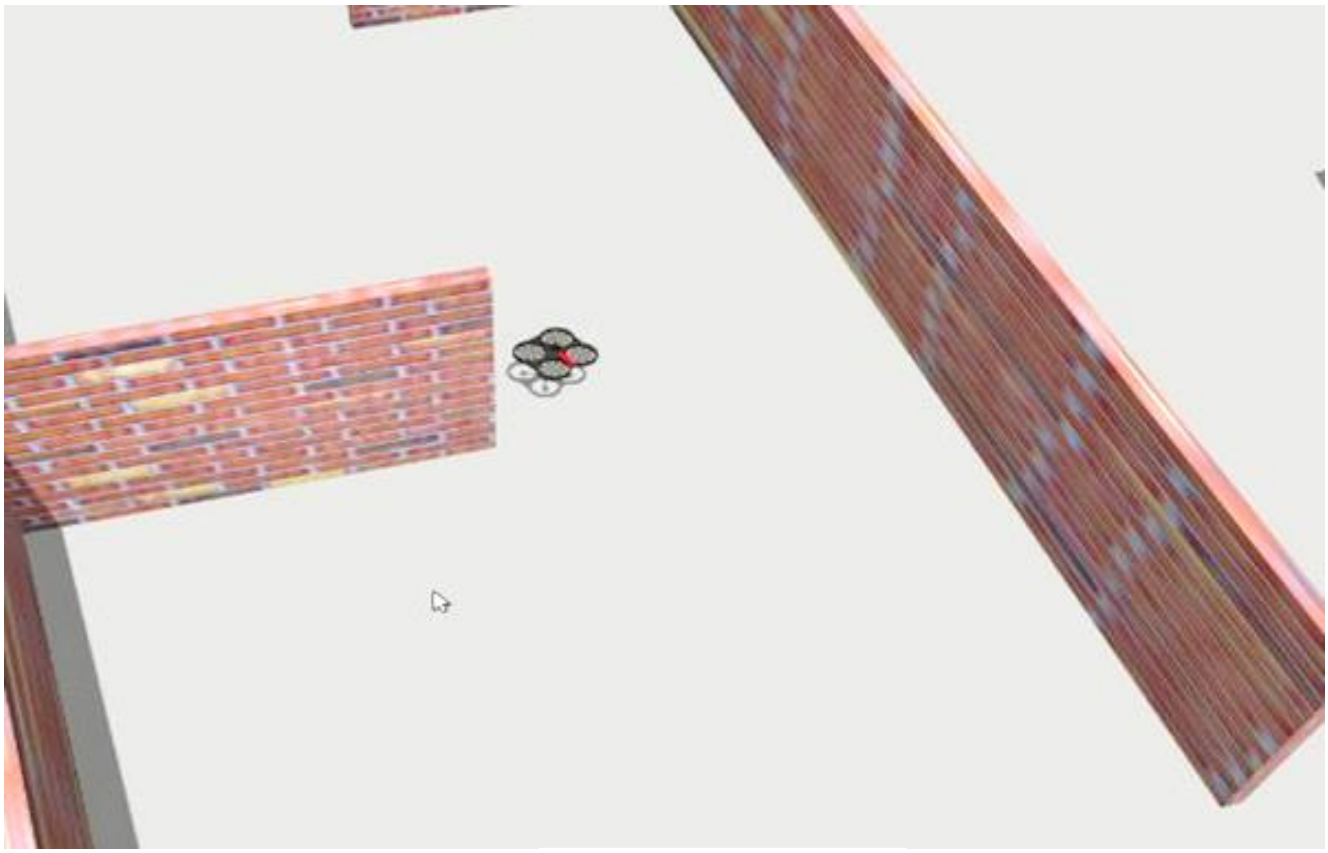

Figure (14) First obstacle

Figure 15 shows the 2nd obstacle

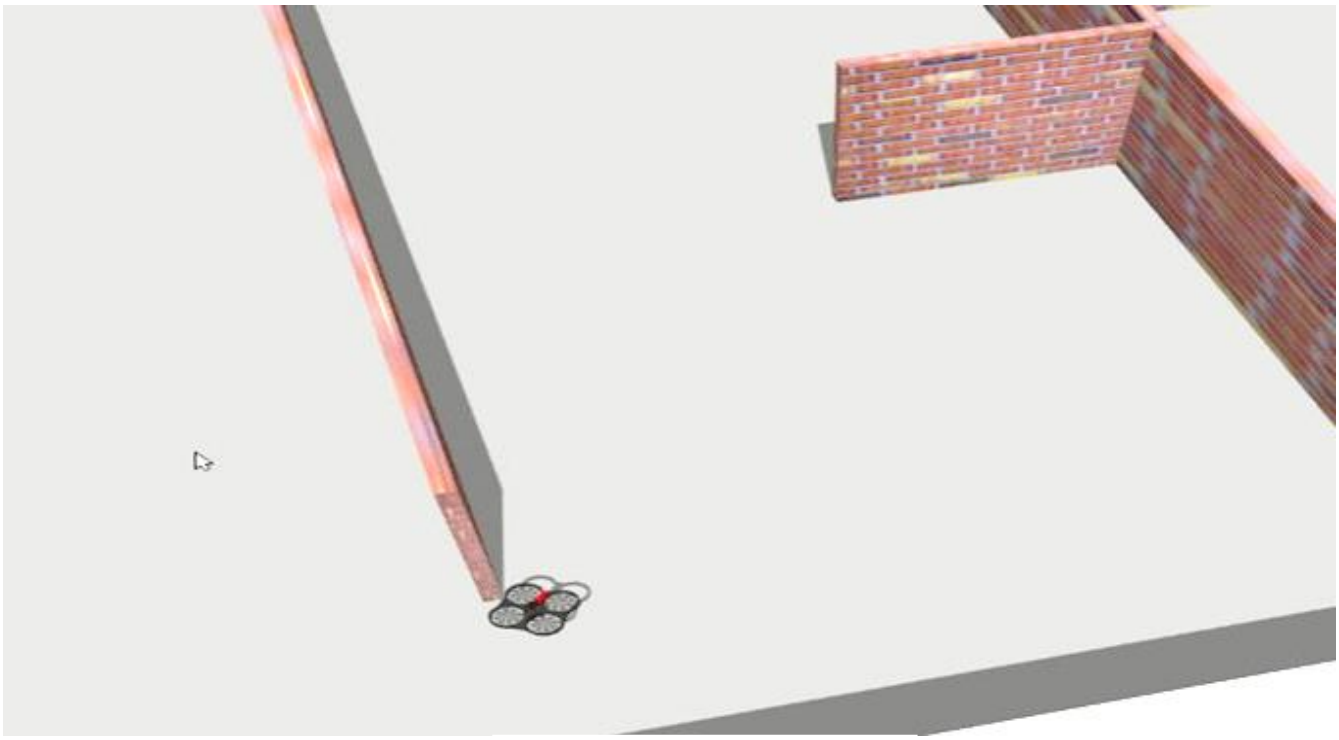

Figure (15) second obstacle

Figure 16 shows the 3rd obstacle

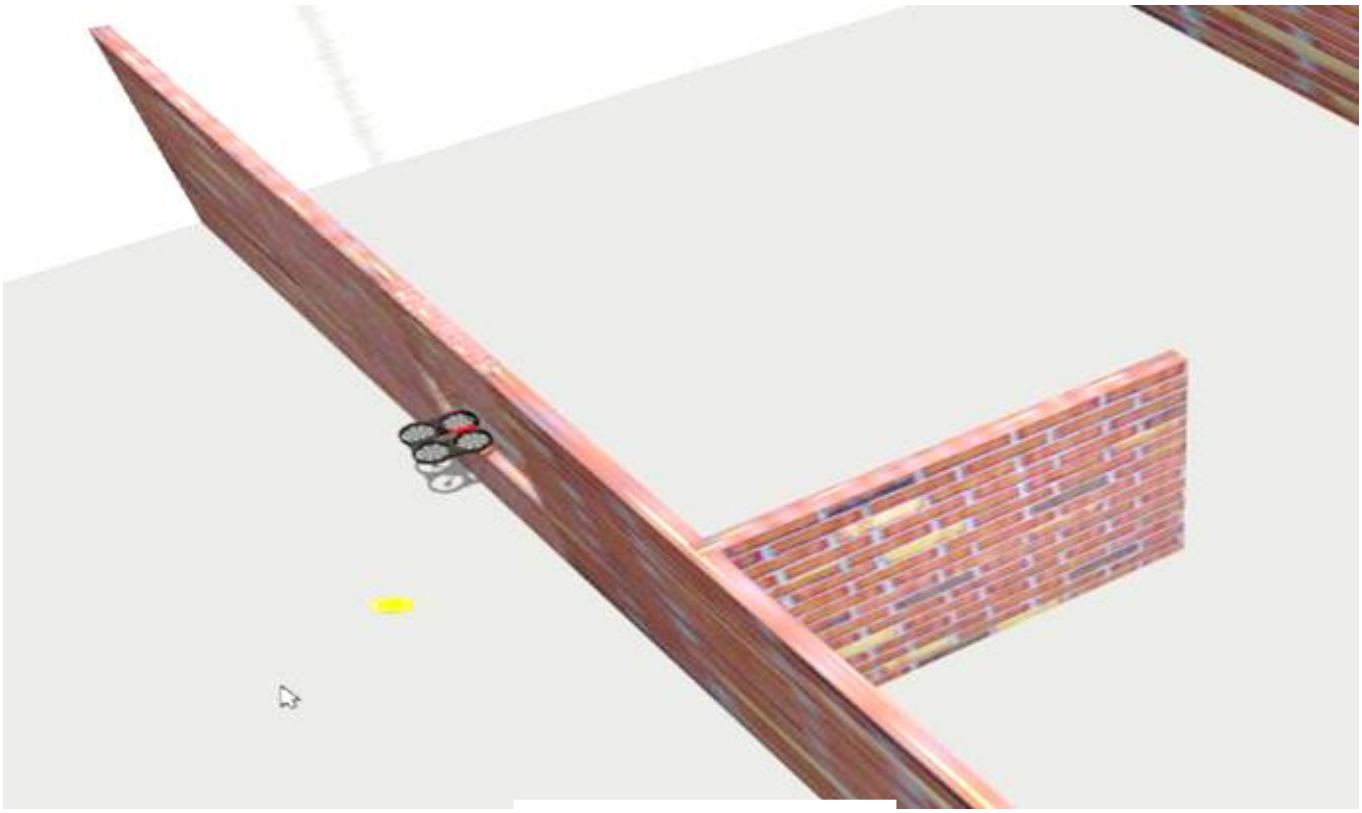

Figure (16) third obstacle

Figure 17 shows the 4th obstacle

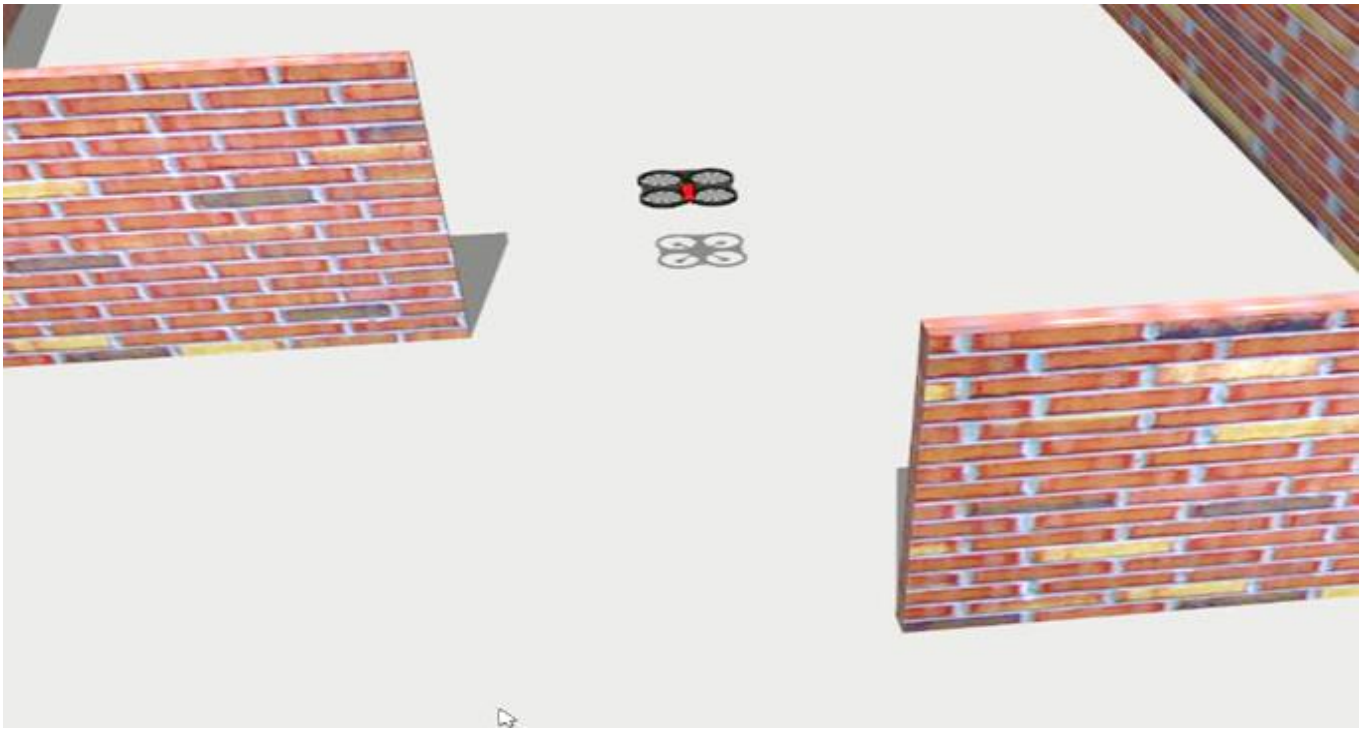

Figure (17) fourth obstacle

Figure 18 shows Reaching the goal

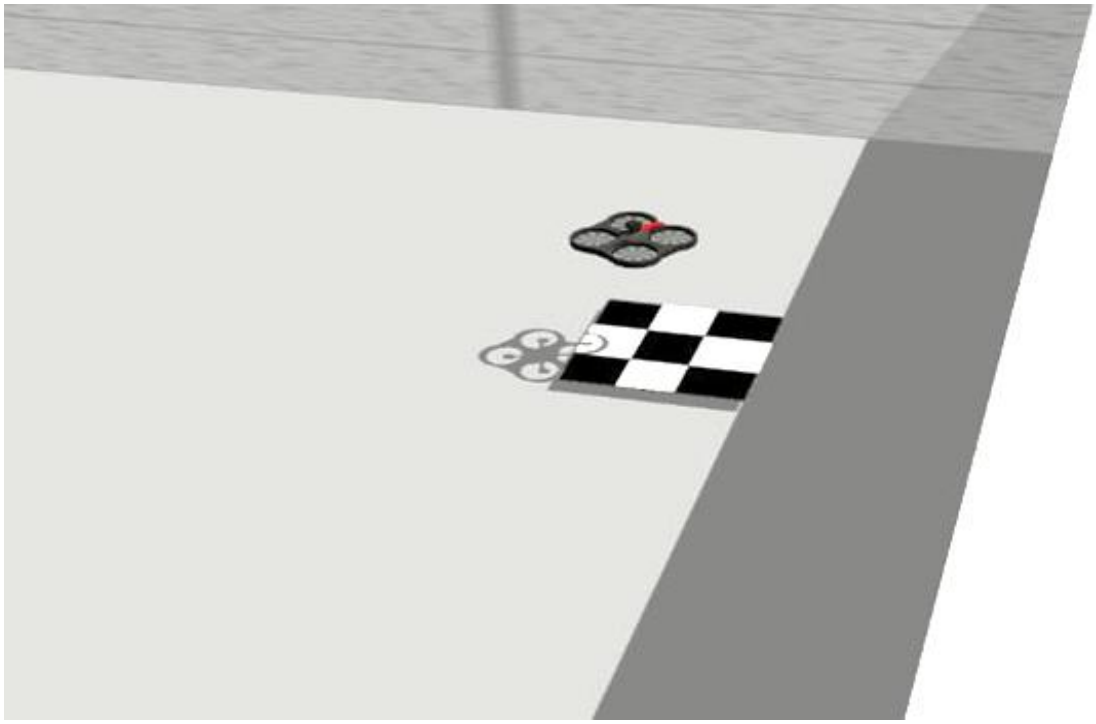

Figure (18) reaching goal

The two below figures showing the path comparison of using the new strategy verses the victor field histogram. Figure 19 show the path of path following like obstacle avoidance algorithm (PFLOA)

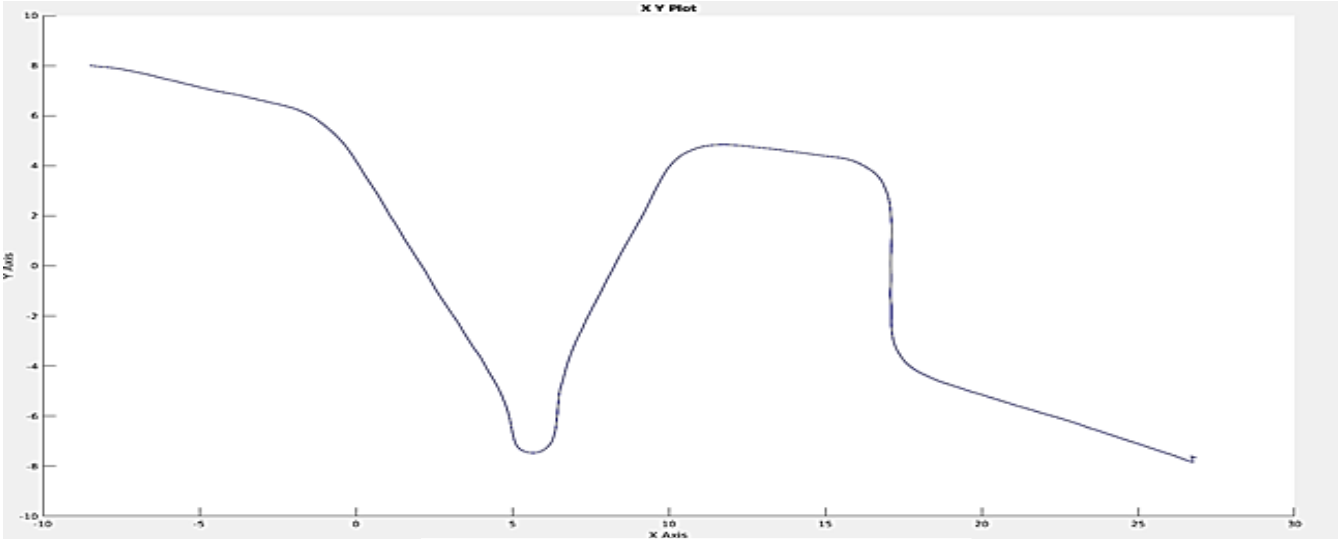

Figure (19) PFLOA path

Figure 20 shows the VFH path

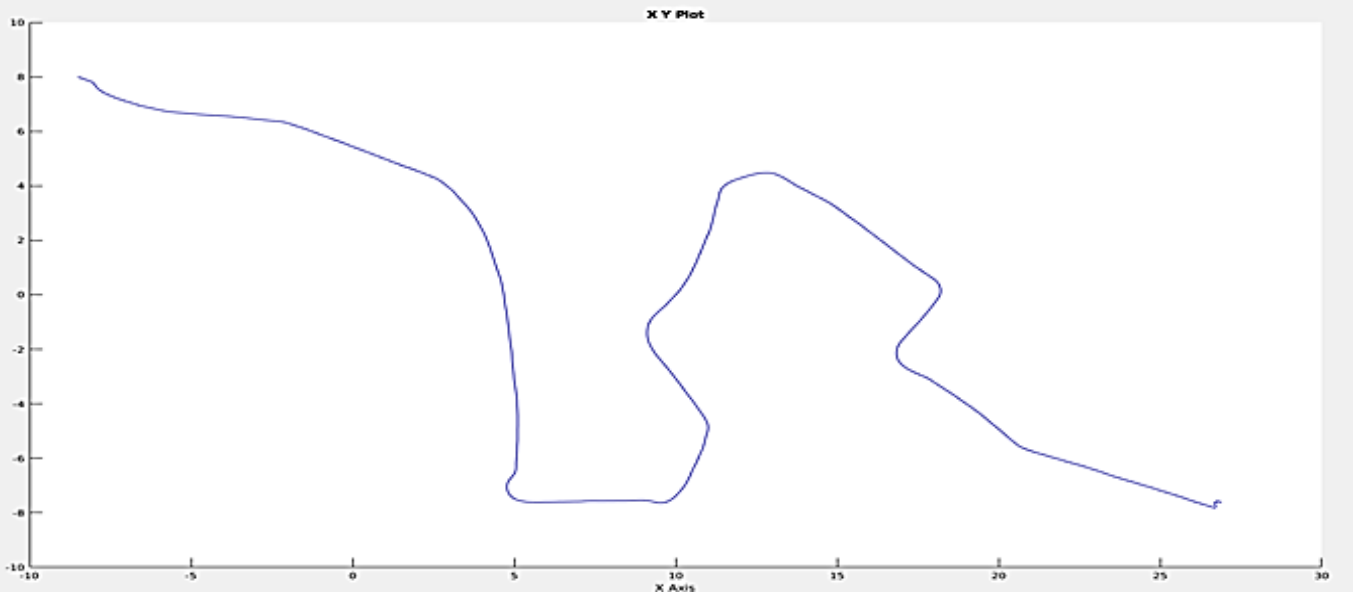

Figure (20) VFH path

The table (1) below showing the comparison between VFH and the new strategy (PFLOA) in terms of time, speed, distance and arrival safety

Algorithm	**Time**	**Distance**	**speed**	**Safety**
VFH	large	long	Same	Same
PFLOA	less	short		

Table (1) algorithm comparison

CONCLUSION

Quadrotor used widely last few years because of simple stricture and suitable for many applications, it is now a very successful market. quadrotor movements need an algorithm for path following and obstacle avoidance. Many paths following and obstacle avoidance algorithms has been suggested and submitted in the field of robotics. In this work Pure pursuit algorithm PPA introduced to map the quadrotor between a start point and the goal point in desired path .Two scenarios have been suggested , and implemented using MATLAB with the aid of 3D gazebo simulator via ROS.The first one was quadrotor outdoor reaching different goals mission in a simulated city by reaching multi targets successfully. The second one was a new strategy of using only path following like obstacle avoidance algorithm in well-known environment with obstacles. In well-known interment it can be calculate the position of obstacles , then you can choose the best path to reach the target This strategy based on an idea of using only a pure pursuit algorithm (PPA) without using any known obstacle avoidance algorithm by following a waypoint to guide the quadrotor to the final destination. The simulation results showed for the first scenario that the quadrotor complete the task and arrive to different target accurately. For the second one the result showed that the suggested strategy faster and reach goal with short distance compared to VFH this is because of no extra weight for sensors to avoid obstacle also less processing time to get information to fed to the Simulink

REFERENCES

[1] Castillo P., Dzul A. and Lozano R. (2004) Real-time stabilization and tracking of a four-rotor mini rotorcraft. *IEEE Trans. Control Syst. Tech*. Vol. 12(4), pp.510-516.

[2] Xu R. and Ozguner U. (2008) Sliding mode control of a class of under actuated systems. *Automatica.* Vol. 44(1), pp. 233-241.

[3] Zuo Z. (2010) Trajectory tracking control design with command-filtered compensation for a quadrotor. *IET Control Theory Applied*. Vol. 4(11), pp. 2343-2355.

[4]] Hoffmann G., Rajnarayan D. Waslander S. Dostal D. Jang T. and Tomlin C. 2004 The Stanford testbed of autonomous rotorcraft for multi agent control (STARMAC)," in Proc. 23rd Digit. Avionics Syst. Conf. pp.

[5] Nils G. Paul B. and Sergio M. 2015 Obstacle Detection and Collision Avoidance for a UAV With Complementary Low-Cost Sensors Digital Object Identifier IEEE Access Vol 3, pp. 599609.

[6]] Xin-Zhong P., uei-Yung L. and Jyun-Min D. 2016 Path Planning and Obstacle Avoidance for Vision Guided QuadrotorUAV Navigation 12th IEEE International Conference on Control & Automation.

[7] Prathamesh S. Saee P. Jagdish R. and Arish S. 2014 Quadcopter – Obstacle Detection and Collision Avoidance International Journal of Engineering Trends and Technology (IJETT) Vol 17 No 2 pp. 84-87.

[8] Zhixiang L. Youmin Z. Chi Y. Laurent C. Didier T. 2019 Collision Avoidance and Path Following Control of Unmanned Aerial Vehicle in Hazardous Environment Journal of Intelligent & Robotic Systems Vol 95, Issue 1, pp. 193-210.

[9] Neerendra Kumar, Zoltan Vamossy .- Robot navigation with obstacle avoidance in unknown environment InternationalJournalofEngineering&Technology , 15,Nov,2018

[10] Quiñonez Y., Barrera F., Bugueño I., Bekios-Calfa J. 2018 Simulation and path planning for quadcopter obstacle avoidance in indoor environments using the ROS framework. In: Mejia J., Muñoz M., Rocha Á., Quiñonez Y., Calvo-Manzano J. (eds) Trends and Applications in Software Engineering. CIMPS 2017. Advances in Intelligent Systems and Computing, vol 688. Springer, Cham

[11] Ícaro V. Igor A. Davi S. Luiz G. 2015 Trajectory Tracking Control of an Aerial Robot with Obstacle Avoidance IFAC Vol. 48, Issue 19, pp. 81-86.

[12] Sohan Suvarna , Dibyayan Sengupta , Simulation of Autonomous Airship on ROS-Gazebo Framework " 2019 Fifth Indian Control Conference (ICC) IIT Delhi, India, January 9-11, 2019 , pp-237-241.

[13] Yao, W., Dai, W., Xiao, J., Lu, H., & Zheng, Z. (2015). *A simulation system based on ROS and Gazebo for RoboCup Middle Size League. 2015 IEEE International Conference on Robotics and Biomimetics (ROBIO).*

[14] Claudio Sciortino, Adriano Fagiolini, Member, IEEE , ROS/Gazebo-based Simulation of Quadcopter Aircrafts , 978-1-5386-6282-3/18/$31.00 ©2018 IEEE .

DOI: 10.37917/ijeee.sceeer.3rd.2 (15-16) June 2020

Open Access

Iraqi Journal for Electrical and Electronic Engineering
Conference Article

Design of a Wide Dual-Band Coplanar Probe Feed Antenna for WLANs Applications

Nabil Eyad Abdulhussein*[1], Abdulkareem S. Abdullah [1]
[1] Electrical Engineering Department, University of Basrah, Basrah, Iraq

Correspondence
*Nabil Eyad Abdulhussein
Electrical Engineering Department,
University of Basrah, Basrah, Iraq
Email: nabil.almansory@gmail.com

Abstract
This paper presents a new design to obtain wide dual-band operation from a coplanar probe feed antenna loaded with two shorted walls. The lower band of proposed antenna has a 10 dB bandwidth of 611 MHz (24.18%) around the center frequency 2527MHz, and the upper band has a bandwidth of 1255 MHz (27.88%) around the center frequency 4501MHz. The obtained bandwidths cover WLANs operations on all bands. The bandwidth of the first operating frequency covers ISM band (2400-2483.5) MHz, which is required by IEEE 802.11b, g and Bluetooth standards, and the bandwidth of the second operating frequency covers U-NII1 (5150-5350) MHz band, which is required by IEEE 802.11a and HiperLAN2 standards, and also covers U-NII2 (5470-5725) MHz and U-NII3/ISM (5725-5825) MHz bands, which are required by IEEE 802.11a standard. A three dimensional finite-difference time-domain (3-D FDTD) method is employed to analyze the proposed structure and find its performance. The simulated results are compared with the experimental results.

KEYWORDS: microstrip antenna, dual-band antenna, wideband antenna, wireless local area network (WLAN), finite-difference time-domain (FDTD), conventional perfect match layer (CPML).

I. INTRODUCTION

Some applications such as satellite links, wireless local networks (WLAN), cellular telephones and global positioning system (GPS) require wideband dual-frequency antennas, and microstrip patch antennas can be used to satisfy these requirements due to their low profile structure, light weight, ease of integration with microwave integrated circuits (MICs), and capability of producing dual frequency operations [1,2].

Various methods have been used to achieve dual frequency operation such as excitation of orthogonal modes [3], using slots in the patch [4,5], loading the patch with shorting pins [6,7], using stacked patch [8,9] and using planar antennas with special geometries to create several resonance paths [10]. Using these methods achieves very narrow bandwidth, 0.5% - 1.5% (SWR=2), so it is necessary to use additional techniques to improve it.

In this paper, a new design of a broadband dual-frequency antenna with coplanar probe feed is presented. A two shorting walls between the patch and the ground plane are existed to control the two resonant frequencies. A full-wave method of a three dimensional finite- difference time-domain (3-D FDTD) method is employed to analyze the proposed structure and find its performance. The advantage of using the FDTD method is that the structures with complex geometry can be analyzed in this numerical technique. The obtained bandwidths cover WLANs operations on all bands. The first band covers ISM (2400-2483.5MHz) band, and the second band covers U-NII1 (5150-5350) MHz, U-NII2 (5470-5725) MHz, and U-NII3/ISM (5725-5825) MHz bands [11].

In Section 2 the details of the design considerations of the proposed antenna are described. The simulation and experimental results of the antennas performance are presented in Section 3 and Section 4. The conclusion is presented in section 5.

II. ANTENNA GEOMETRY

Fig. 1 shows the proposed antenna, where the radiating patch has dimensions of $(19\times40)\ mm^2$. The ground plane is L-shaped to facilitate the use of coplanar probe feed. In this design, the horizontal portion of L-shaped ground plane has dimensions of $(50\times60)\ mm^2$ and the vertical portion of L-shaped ground plane has a height of *10 mm* constituting an air-layer substrate to this antenna. The vertical portion of the ground plane is shifted a distance *2 mm* from edge of the horizontal portion of the ground plane. A two shorted walls with a width of *2 mm* are connected between the patch and the horizontal portion of the L-shaped ground plane and placed at distance *d* from the vertical portion of ground plane.

The inner edges of two shorted walls are separated by a distance *36 mm*.

The distance of two shorted walls from the patch edge d is varied to have a variable frequency ratio of the two resonant frequencies.

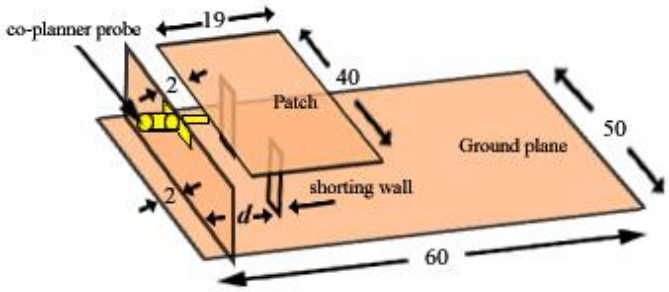

Fig. 1: Proposed configuration for dual-band coplanar probe feed antenna.

The 3-D FDTD method is used for the simulation of the complete structure of the antenna. The FDTD problem space is composed of cells with $\Delta x = 0.5mm$, $\Delta y = 0.5mm$ and $\Delta z = 2mm$ which are selected to be smaller than (1/20) wavelength of maximum frequency (6.5GHz) in order to ensure the accuracy of the computed results [12,13]. These cell sizes make the volume of object to be ($120\Delta x$, $100\Delta y$ and $5\ \Delta z$). The boundaries are terminated by 8 cells conventional perfect match layers (CPML) and 10 cells air gap is left between the object in the problem space and CPML boundaries. The calculated time step is $\Delta t = 1.045\ psec$ and the simulation is performed for 2200 time steps.

III. RESULTS AND DISCUSSION

The simulation is performed with different values of *d*, and Fig. 2 shows the simulated return losses for different values of *d*. The two resonant frequencies (f_{r1} and f_{r2}) and the frequency ratio (f_{r2}/f_{r1}) variations against *d* variations are shown in Fig. 3, and the corresponding antenna performance is listed in Table I.

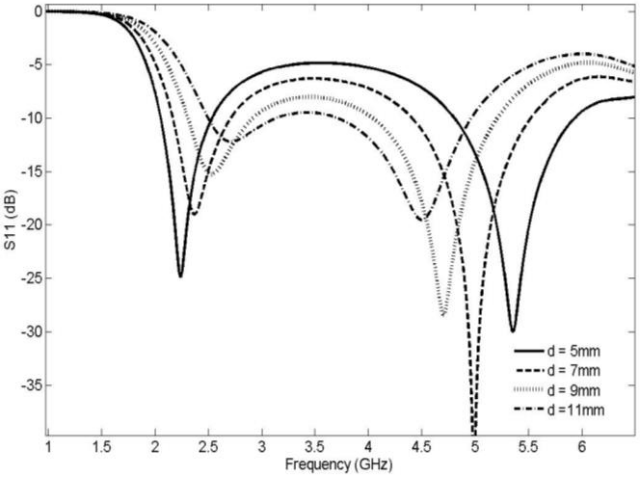

Fig. 2: Calculated Return losses for different value of d.

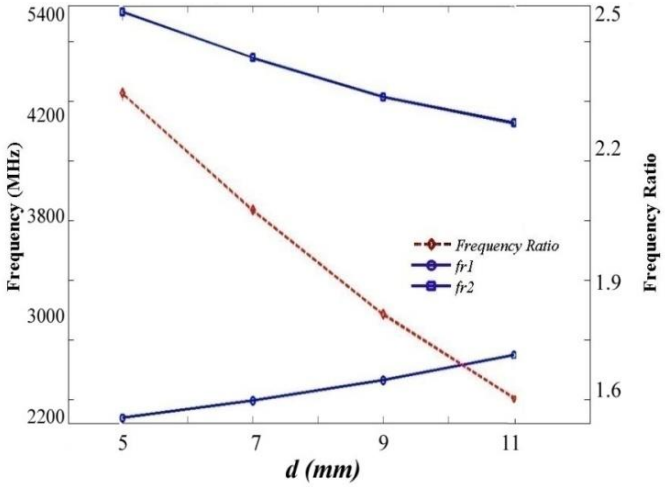

Fig. 3: Resonant frequencies f_{r1} and f_{r2} and frequency ratio (f_{r2}/f_{r1}) against d.

TABLE I
PERFORMANCE OF THE ANTENNA FOR DIFFERENT VALUE OF *d*

d *mm*	f_{r1} *MHz*	BW_1 *MHz, %*	f_{r2} *MHz*	BW_2 *MHz, %*	(f_2/f_1)
5	2239	482, 21.53	5354	1127, 21.05	2.39
7	2371	545, 22.99	5002	1111, 22.21	2.11
9	2527	611, 24.18	4701	1164, 24.76	1.86
11	2719	639, 23.50	4501	1255, 27.88	1.66

From the above results, it is clear that the increasing in the distance *d* causes the lower frequency f_{r1} to increase and the higher frequency f_{r2} to decrease, so that the frequency ratio decreased. It is also clear that, the 10 dB bandwidth at the first resonant frequency reaches 24.18% and 27.88% at the second resonant frequency. These are large values of bandwidth compared with the other structures.

From Table I, it is shown that, by setting d = 5 *mm* the lower frequency of the proposed design has a bandwidth of 482 MHz (2054-2536) MHz, and the upper frequency has a bandwidth of 1127 MHz (4804-5931) MHz. These obtained bandwidths cover WLAN operations in all bands. The bandwidth of the first operating frequency covers ISM band (2400-2483.5) MHz, which is required by IEEE 802.11b,g and Bluetooth standards, and the bandwidth of the second operating frequency covers U-NII1 (5150-5350) MHz band, which is required by IEEE 802.11a and HiperLAN2 standards, and also covers U-NII2 (5470-5725) MHz and U-NII3/ISM (5725-5825) MHz bands, which are required by IEEE 802.11a standard.

The proposed antenna with *d=5 mm* has been constructed and shown in Fig. 4. The measured and simulated return losses of designed antenna are shown in Fig. 5. There is a good agreement between simulated and measured results.

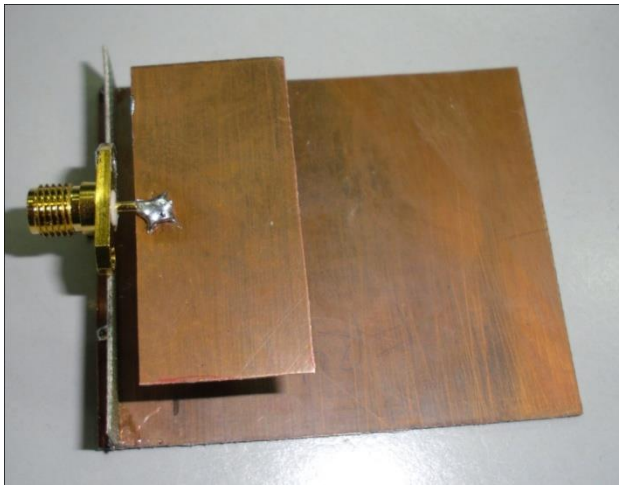

Fig. 4: A photograph of co-planner microstrip antenna.

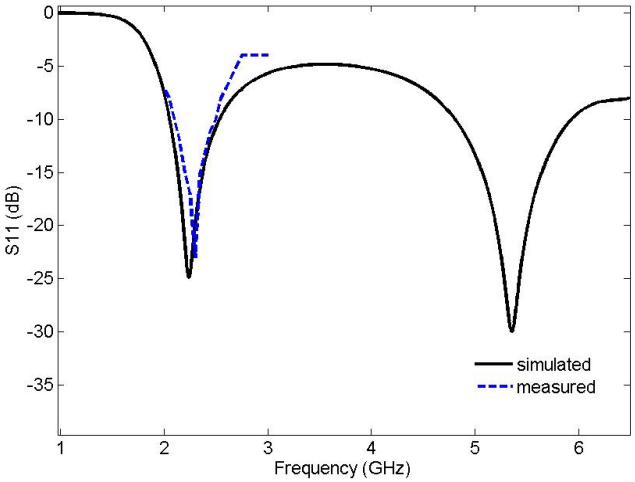

Fig. 5: Measured (2-3GHz) and simulated return losses for d =5 mm.

Note: It is worth to mention that the measurements that have been done on the fabricated antenna are considered in the frequency range (2-3) GHz. This is due to the practical limit of the RF generator available at our lab.

IV. FAR-FIELDS CALCULATIONS

With the FDTD technique, the direct evaluation of the far field calls for an excessively large computational domain, which is not practical. Instead, the far-zone electromagnetic fields are computed from the near-field FDTD data through a near-field to far-field transformation technique [14].

The directivity patterns are calculated in the *xy*, *xz*, and *yz* plane cuts at 2.45 GHz and 5.6 GHz for *d=5 mm*. These patterns are plotted in Fig. 6, Fig. 7, and Fig. 8, respectively. A three dimensional patterns for the two resonant frequencies are calculated and plotted in Fig. 9.

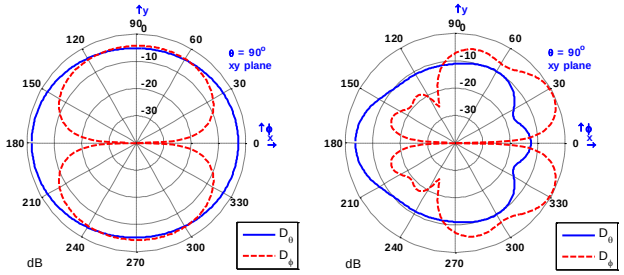

(a) 2.45 GHz (b) 5.6 GHz

Fig. 6: Radiation pattern in the xy plane cut.

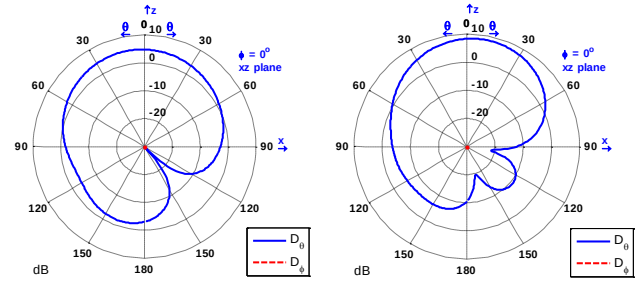

(a) 2.45 GHz (b) 5.6 GHz

Fig. 7: Radiation pattern in the xz plane cut.

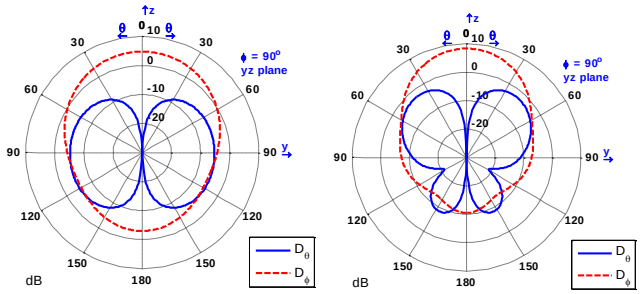

(a) 2.45 GHz (b) 5.6 GHz

Fig. 8: Radiation pattern in the yz plane cut.

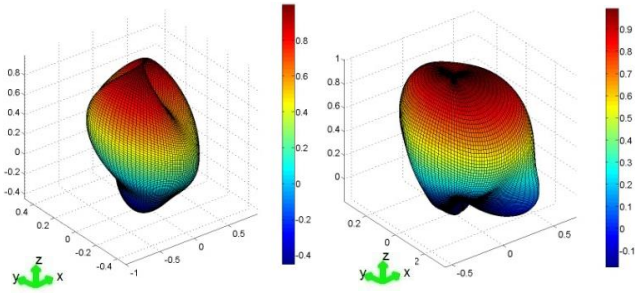

(a) 5.45 GHz *(b) 5.6 GHz*

Fig. 9: Three dimensional radiation patterns of the proposed antenna.

V. CONCLUSION

A new coplanar probe feed antenna is proposed in this paper to obtain a wide-band dual-band operation. The proposed antenna is loaded by two shorting walls existed between patch and ground plane. The distance of two shorted walls from the patches edge *d* is varied to obtain the effect of them on the two resonant frequencies and their bandwidths. The proposed structure is analyzed by the 3D-FDTD method and the calculated results of the proposed antenna agree well with experimental results. The first band of proposed antenna has a 10 dB bandwidth of 24.18% at the center frequency 2527MHz, and the second band has a bandwidth of 27.88% at the center frequency 4501MHz. The first band covers ISM (2400-2483.5MHz) band, and the second band covers U-NII1 (5150-5350) MHz, U-NII2 (5470-5725) MHz, and U-NII3/ISM (5725-5825) MHz bands.

REFERENCES

[1] R. Garg, P. Bhrtia, I. Bahl and A. Ittipitoon, *Microstrip Antenna Handbook*, Artech House, 2001.

[2] C. A. Balanis, *Antenna Theory: Analysis and Design*, Second Edition, New York, Wiley, 1997.

[3] K. L. Wong, *Compact and Broadband Microstrip Antennas*, New York, John Wiley & Sons, 2002.

[4] S. Maci, G. B. Gentili, P. Piazzesi, and C. Salvador, *"Dual Band Slot Loaded Patch Antenna,"* Proc. Inst. Elect. Eng. Microw. Antennas Propagation, Vol. 142, Jun. 1995, PP. 225-232.

[5] B. F. Wang and Y. T. Lo, *"Microstrip Antennas for Dual Frequency Operation,"* IEEE Transactions on Antenna and Propagation, Vol. 32, Sep. 1984, pp. 938-943.

[6] K. L. Wong and W. S. Chen, *"Compact Micostrip Antenna with Dual Frequency Operation,"* IEEE Electronic Letters, Vol. 33, No. 8, Apr. 1997, pp. 646-647.

[7] S. C. Pan and K. L. Wand, *"Dual Frequency Triangular Microstrip Antenna with Shorting Pin,"* IEEE Transactions on Antenna and Propagation, Vol. 45, Dec. 1997, pp. 1889-1891.

[8] C. S. Lee, V. Nalbandian, and F. Schwering, *"Planner Dual-Band Microstrip Antenna,"* IEEE Transactions on Antenna and Propagation, Vol.43, No.8,Aug. 1995, pp. 892-894.

[9] J. Anguera, C. Puente, C. Borga, and J. Soler, *"Dual-frequency broadband-stacked microstrip antenna using a reactive loading and a fractal-shaped radiating edge,"* IEEE Antenna and Wireless Propagation Letters, Vol. 6, 2007, pp. 309-312.

[10] Z. N. Chen and M. Y. W. Chia, *Broadband Planar Antennas: Design and Applications*, New York, John Wily & Sons, 2006.

[11] C. A. Balanis, *Modern Antenna Handbook*, New York, John Wiley & Sons, 2008.

[12] H. R. Chuang and L. C. Kuo, *"3-D FDTD Design Analysis of a 2.4 GHZ Polarization-Diversity Printed Dipole Antenna With Integrated Balun and Polarization – Switching Circuit for WLAN and Wireless Communication Application,"* IEEE Transactions on Microwave Theory and Technology, Vol.51, No.2, February 2003, pp. 374-381.

[13] D. M. Sullivan, *Electromagnetic Simulation Using the FDTD Method*, New York, IEEE Press series on RF and Microwave Technology, 2000.

[14] A. Elsherbeni and V. Demir, *The Finite Difference Time Domain Method for Electromagnetics with Matlab Simulations*, United States of America, SciTech Publishing, 2009.

DOI: 10.37917/ijeee.sceeer.3rd.3 (15-16) June 2020

Open Access

Iraqi Journal for Electrical and Electronic Engineering
Conference Article

Encrypted Vehicular Communication Using Wireless Controller Area Network

Mohammed Al-Qaraghuli[1], Saadaldeen Rashid Ahmed Ahmed[*2], Muhammad Ilyas [3]
[1] Electrical and Computer Engineering, Altinbas University, Istanbul, Turkey
[2] Computer Science, Tikrit University, Baghdad, Iraq
[3] Electrical and Electronics Engineering, Altinbas University, Istanbul, Turkey

Correspondence
*Saadaldeen Rashid Ahmed Ahmed
Computer Science, Tikrit University,
Baghdad, Iraq
Email: Saadaljanabi95@gmail.com

Abstract
In this paper, we focus on ensuring encrypted vehicular communication using wireless controller area network performance at high node densities, by means of Dedicated Short-Range Communication (DSRC) algorithms. We analyses the effect of the vehicular communication parameters, message-rate, data-rate, transmission power and carrier sensing threshold, on the application performance. After a state-of-the-art analysis, we propose a data-rate DSRC algorithm. Simulation studies show that DSRC performs better than other decentralized vehicular communication algorithms for a wide range of application requirements and densities. Vehicular communication plays one of the most important roles for future autonomous vehicle. We have systematically investigated the impact of vehicular communication using the MATLAB© application platform and achieved an accuracy of 93.74% after encrypting all the communications between the vehicles and securing them by applying the encryption on V2V communication in comparison with the existing system of Sensor Networks which stands at 92.97%. The transmission time for the encryption is 165 seconds while the rate of encryption is as low as 120 Mbps for the proposed awareness range of vehicles to vehicle using DSRC algorithm in Wireless-Controller Area Network for communication. Experimental results show that our proposed method performs 3% better than the recently developed algorithms.

KEYWORDS: Controller area network; Dedicated short-range communication; Encryption; Transmission; V2V; communication;

I. INTRODUCTION

In this paper, we have formulated and developed an encrypted vehicular communication using wireless controller area network with introduction of Dedicated Short-Range Communication (DSRC) algorithms. Every year, road traffic accidents kill about 1.3 million people worldwide, and severely injure another 50 million [1]. Nearly 33,000 [2] and 27,000 [3] deaths happen every year due to road traffic accidents in US and Europe respectively. There were around 3500 road fatalities in Turkey in 2015 [4]. The estimated economic loss due to road traffic accidents for the Turkey is over 7 billion euros every year.

Encrypted and Advanced Driver Assistance Systems (EADAS) have been developed, to alleviate the burden on drivers and improve driving safety [5]. EADAS makes the driver aware of potentially hazardous situations in the environment and instruct the driver to take corrective actions. In some cases, corrective actions are taken automatically, i.e., without any assistance from the driver. These are known as automation systems [6]. EADAS and self-driving cars can use the surrounding connected vehicles to sense the environment. Connected vehicles add the following benefits to systems that only rely on sensors [7]. Connected vehicles provide an extended field of perception, beyond line-of-sight, and hence, allow the detection of threats invisible to on-board sensors.

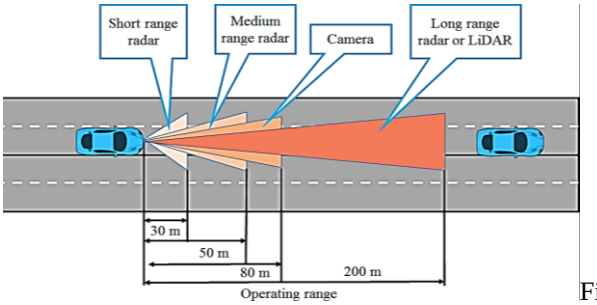

Fig. 1. Sensor operation range and line-of-sight detection [7]

The sensing encrypted range of a vehicle is defined as the range around a vehicle within which the vehicle senses the channel busy if other vehicles in the range transmit the

message [8]. Vehicles sense each other message transmissions to avoid message collisions. Hidden nodes of a vehicle (node) are vehicles that do not sense each other message transmissions but they can sense the transmissions of the vehicle [9]. Hidden nodes may lead to message collisions, as they cannot sense each other's transmissions. The hidden node problem is common in carrier sensing mechanism based wireless networks. Capture effect can reduce the hidden node problem in V2X communication.

A. *Problem Statement*

Vehicular Safety applications track the neighbor vehicles to predict and avoid dangerous situations. There are different problems and challenges that must need an attention to be solved in the first place. Some of the problems and challenges are given by:

- The effects of unreliable communication on application reliability
- Less secure communication
- Limited channel capacity
- Dynamic vehicular environment
- Broadcast transmission
- Low sensing range of vehicle

B. *Research Contribution*

Optimizing the usage of the encrypted channel so that vehicular communication applications are sustained even at large vehicular densities, is crucial. The objective of this paper is to develop an encrypted vehicular communication system using wireless CAN with DSRC algorithm and to ensure reliable safety application performance at high vehicular densities by means of DSRC algorithms. Specifically, data-rate adaptation techniques are explored to make DSRC algorithms scalable to high vehicular densities. The specific questions we address in this paper are the following:

R1: To what extent communication parameters influence vehicular communication performance?

R2: To what extent various DSRC algorithms with wireless CAN influence application performance?

R3: To what extent does the data-rate DSRC with wireless CAN improve the application performance compared to DSRC algorithms reported in the literature?

R4: To what extent coexistence of new DSRC algorithms with the already deployed DSRC affects the application performance?

R5: Can we experimentally validate the results of DSRC algorithms for encrypted vehicular communication?

The positioning of vehicles is performed using Global Navigation Satellite Systems (GNSS) such as GPS (Global Positioning System) and Galileo [10]. Accurate positioning of the vehicles is necessary for reliable TTC estimation [11]. The VSC-A project [12] by USDOT identified two different levels of GPS accuracy, for different classes of safety applications: road-level and lane-level. Applications such as EEBL require a road-level accuracy of less than 5m and applications such as FCW require a lane-level accuracy of less than 1.5 m [13]. Vehicular communication has investigated GPS accuracy and availability at various urban, rural, and highway environments. It concluded that GPS is adequate in most of the environments [14]. Although GPS outage may appear in deep urban environments [15], techniques that estimate the position of a vehicle based on in-vehicle sensors information such as speed and yaw rate can be utilized. Research is ongoing to improve the availability and accuracy of GPS.

C. *Runtime adaptation of DSRC based on channel quality*

Due to the highly dynamic vehicular environment the channel quality changes due to shadowing and scenarios such as rural and urban affecting the packet reception ratio PRR, i.e., probability of beacon message delivery [16]. Changes in PRR may affect the application performance. Thus, to ensure the reliability of applications DSRC algorithms should adapt parameters, such as the minimum required message-rate of the application, based on the channel quality on runtime [17]. DSRC algorithms such as SAE [18] use PRR as channel quality indicator and generate additional beacon messages when the PRR decreases below a threshold to ensure reliability [19]. We recommend the investigation of such DSRC adaptation mechanisms further. Accurate positioning of the vehicles is necessary for reliable DSRC estimation. The PRC project for vehicles [20] by USDOT identified two different levels of GPS accuracy.

D. *Data transmit rate of DSRC*

The benefit of DSRC is that it guarantees the awareness range requirement of the application. DSRC tries to maximize the awareness range for a fixed transmit power. However, applications have a minimum awareness range requirement [21]. Thus, tuning the transmit power to guarantee the desired awareness range along with message-rate and data-rate might further increase the application performance [22]. The required transmit power for a desired awareness range changes with data-rate. Further studies are necessary to analyze the impact of tuning the data-rate on the selection of the transmit power and vice-versa. We recommend the investigation of DSRC algorithms that tune multiple times the same parameters as they can improve the maximum vehicular density supported by the channel.

$$T_D = \left\{\exp\left[\frac{v - v_{max}}{v_{max}}\right]\right\}, for\ v \le v_{max} \quad (1)$$

Where T_D is the data transmission rate, 'v' represents the velocity of vehicle and v_{max} represents the maximum velocity of vehicle with respect to the data transmission as they are taken from [22]. We have discussed ways to

measure the application reliability, which reflects the effect of unreliable wireless communication on the reliability of the application [23]. The application requirements have been mapped to communication parameter requirements, in particular, the minimum message-rate, and PRR to ensure reliable safety applications [24]. We have shown that increasing the message-rate can increase the application reliability [25]. The analysis of this chapter will be utilized in the forthcoming chapters to design an efficient congestion control algorithm that can guarantee the reliable operation of safety applications [26].

We presented a preliminary model to analyze the effect of the PRR and message-rate on application reliability. Further analysis of the application reliability considering the mobility of vehicles, channel characteristics and scenarios should be part of a future study [27].

E. V2X Communication Reliability

V2X safety application reliability is determined by several subsystems as shown in Fig 2 [28]. The sensor subsystem gathers sensor information such as position, velocity and acceleration. The communication subsystem transmits its neighbor vehicles sensor information to an application controller using V2X communication. The application controller computes the safety metric such as TTC to decide the necessary actions, which are then performed by the actuator subsystem. In awareness warning phase the warnings are provided to the driver to decide the necessary actions; however, in automatic pre/post-crash the system decides the necessary actions such as automatic braking, steering and safety system deployment such as air bags. We have analyzed the time delay for propagating the transmission messages represented by '*d*' which is defined as the difference between the timestamps of message reception t_{Rx} and transmission t_{Tx} respectively by equation (2) taken from [25].

$$d = t_{Rx} - t_{Tx} \quad (2)$$

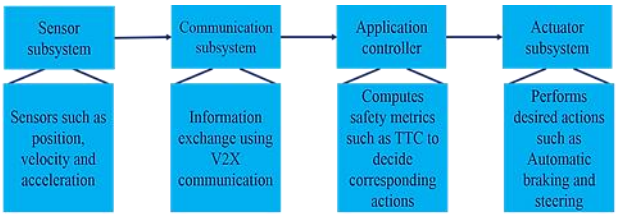

Fig. 2. Function sequence of V2X safety application [28].

F. V2X Communication Application

Tuning the communication parameters may affect the application reliability and awareness range of the application. Message-rate based DSRC algorithms in CAN network may decrease the message-rate below the minimum required message-rate to avoid congestion affecting the application reliability [29]. Transmit power and carrier sensing threshold DSRC algorithms limit the transmission and sensing range respectively which may conflict with the awareness range requirements of the application. Similarly, data-rate DSRC algorithms with wireless CAN limit the communication range which may affect the awareness range requirements of the application

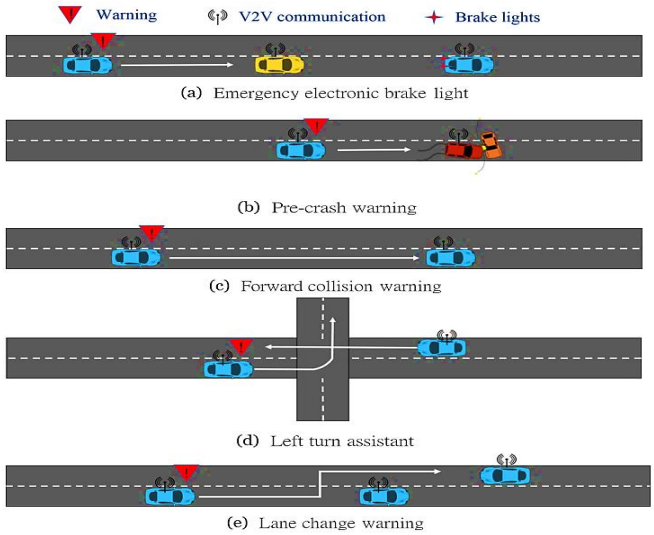

Fig. 3. Different types of V2X communication with warnings. [30]

The general principle of V2X safety applications, e.g. encrypted V2V applications suggested by the USDOT VSC project as shown in Fig. 3 [30], is to use the exchanged information among vehicles to compute a safety metrics. DSRC algorithms should choose the appropriate communication parameters such that they avoid congestion and simultaneously satisfy the minimum application reliability and awareness range requirements of the application.

II METHODOLOGY

In this research work, to encrypt the communication of vehicles we proposed a DSRC algorithm in wireless CAN network for a large number of vehicles, we would need a large number of wireless CAN networks in the open-source dataset as well as vehicular communication data present in dataset. In order to encrypt the communication of vehicles, we utilize an emulation platform MATLAB where each wireless CAN emulates multiple vehicles.

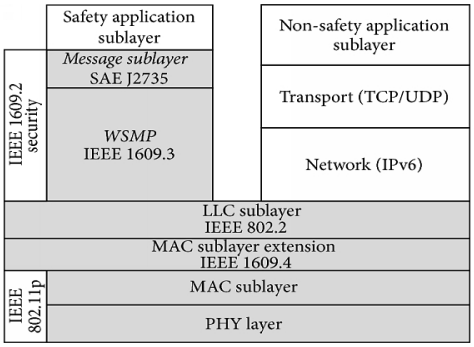

Fig. 4. DSRC architecture specified by Network.

We are interested in the behavior of the DSRC algorithms for large vehicular densities. Since in reality each vehicle has its own CAN network operating independently from other CAN network, we would, in principle, need a number of CAN network in the order of three thousand. Since this is infeasible due to cost reasons, we chose to emulate multiple virtual CAN networks on one physical CAN network. We call a physical CAN network an Emulation Node (EN), i.e., a device that emulates the behavior of multiple CAN networks. The number of physical layer devices we had available was four. Each EN generates and transmits several beacon messages as if generated by many CAN network (several hundred vehicles). Of course, our emulation approach deviates from the behavior of CAN networks in real traffic scenarios. We examine what this means, and consequently what the system limitations are of the emulation platform and the impact on the behavior of wireless CAN networks, while leaving this out has no influence on the performance aspects of DSRC we are present the propagation delay in equation (3) however the we propose finding the respective coordinates of vehicles in equation (4). In a similar way, we define message delivery time for V2V communications as:

$$d = d + \Delta T \quad (3)$$

where d [s] is the propagation time delay within a cluster, as defined by [31], and ΔT [s] is the minimum time interval

$$D_{SD} = \sqrt{(y_D - y_S)^2 + (X_D - X_S)^2} \quad (4)$$

where (xS, yS) and (xD, yD) are the respective coordinates of vehicle S and vehicle D [30].

C. DSRC Algorithm in Wireless CAN

Many devices support wireless CAN and have a DSRC architecture specified by Network [31]. We adopt this DSRC architecture, shown in Fig. 4, where the interaction between the DSRC algorithm and the protocol layers in network are shown. This is similar to the network architecture. The PHY, MAC and LLC layers of IEEE 802.11p in wireless CAN network are accessed via the Logical Link Control Application Programming Interface (LLC-API). The application and facilities layer of network are accessed using the Application Facilities Layer Application Programming Interface (AF-API) in MATLAB. The application layer runs a pseudo application to generate the beacon

Messages. The facilities layer controls the message-rate as determined by the DSRC algorithm. The focus of the experiments is on the broadcast transmission of beacon messages and DSRC algorithms in which the network and transport layers are not involved, hence, these are not considered in our implementation. Note that in our implementation, we leave out security and privacy of beacon messages. Implementing this would require a lot of processing by the safety devices, which would seriously restrict the number of OBUs [32] that can be emulated by an EN, while leaving this out has no influence on the performance aspects of DSRC we are interested in. The DSRC algorithms obtain the channel load information, CAN network and packet count, sensed by the physical layer via the MATLAB and they adjust the message-rate, data-rate, and transmit power accordingly.

TABLE I
PROPOSED AWARENESS RANGE OF DIFFERENT VEHICLES USING DSRC ALGORITHM IN WIRELESS CAN FOR COMMUNICATION IN COMPARISON WITH DIFFERENT TECHNIQUES

Parameters	Approach awareness range (m)				
	Wireless CAN	IP-SEC [23]	Sensor Networks [23]	PDR-DCC [23]	LIMERIC [23]
Encryption Transmission Time (Overall)	165	180	175	195	175
Rate of Encryption (Overall)	120	145	140	155	125

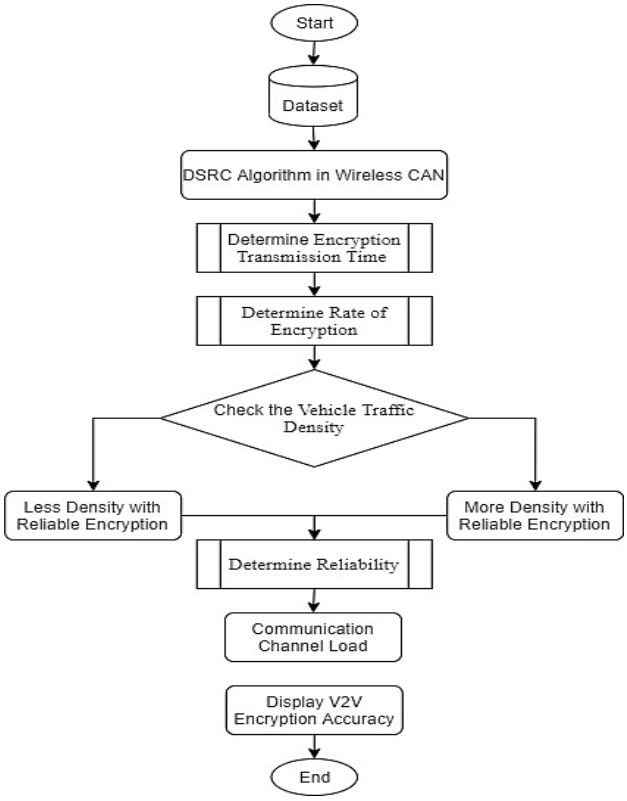

Fig. 5. The pictorial representation of followed approach.

D. Encryption in Wireless Controller Area Network (CAN)

An encrypted vehicular communication emulates multiple wireless CAN networks; however, it has a single PHY and MAC protocol entity. In reality, the wireless CAN's belonging to different vehicles generate their messages independently and use their own MAC entity to access the

channel, competing with the other wireless CANs. Since, in case of contention, the MAC protocol uses random back-off, the order in which messages finally access the channel is also random [33]. In our new emulation experiments, however, messages generated by multiple wireless CANs, emulated by the same DSRC algorithm for encryption, queue up in the same MAC layer queue, and hence try to access the channel one after the other, in the order in which they were generated. The implications of this are:

1. There is no contention between messages generated by the same DSRC algorithm emulating several wireless CAN networks. Thus, there are no collisions between the messages from wireless CAN emulated by the same DSRC algorithm. In reality encryption occur. On the other hand, messages generated by different wireless CAN, still compete. In brief, the packet reception ratio (PRR) experienced by the emulated vehicles is better than in reality. Further study is necessary to quantify the effect of the emulation platform on DSRC performance.
2. Since the encryption messages emulated by the same wireless CAN access the channel sequentially, the channel access time is increased. This effect is discussed in detail in [34]. The study concludes that the increased channel access time limits the maximum channel load that can be created by the emulation platform. Furthermore, the study shows that augmenting the beacon size increases the maximum channel load attainable by the emulation platform.

TABLE II

PROPOSED AWARENESS RANGE OF DIFFERENT VEHICLES USING DSRC ALGORITHM IN WIRELESS CAN FOR COMMUNICATION WITH DENSITY.

Parameters	Vehicle Traffic Density	Approach awareness range (m)		
		Wireless CAN	IP-SEC [23]	Sensor Networks [23]
Encryption Transmission Time	Less Density	78	160	150
	More Density	126	150	100
Rate of Encryption	Less Density	1	5	3
	More Density	1	8	5

C. Encrypting the Communication

In vehicular communication networks, the elapsed time in receiving the controller area network (CAN) bus information from the CAN network of the vehicle should be taken into consideration, prior to the transmission of data to the other vehicle. Once the data is transmitted either by IEEE802.11p or LTE, Time of Flight (TOF) comes into picture [35]. To estimate the overall performance of vehicular communication network these two-time factors need to be considered. A mobile service can be used to provide the live updates of the traffic situation on the road to the users. To get the live updates, the users need to transmit and receive the data from the remote server when they are driving on the road. We determine the performance of IEEE802.11p and LTE as vehicular networks in real time. Each wireless CAN network emulates a quarter of the total number of vehicles. In our preliminary experiments, the wireless CAN transmit at the default 10 Hz message-rate without any DSRC algorithm. The maximum data-rate of the emulation platform is fixed at 18 Mbps. For each vehicular communication and data-rate, we run the experiment for 60s on MATLAB. We average measurements of all four wireless CAN networks using DSRC algorithm

Table III

PARAMETERS OF DIFFERENT MEASUREMENTS FOR ENCRYPTED VEHICULAR COMMUNICATION.

Parameters	Measurements
Encrypted Data Size (Payload)	500 bytes
Channel load threshold (CBPT)	60 %
Vehicle transmit power	0 dBm
Peak antenna gain	4.6 dBi
Vehicle carrier sensing threshold	-95 dBm
Message-rate	1 to 10 Hz
Data-rate [11]	3, 4.5, 6, 9, 12, and 18 Mbps
Total Vehicular Communication	5.9 GHz

1) Collecting the vehicle information in real time and transmitting the information to a remote TCP (Transmission Control Protocol) server or UDP (User Datagram Protocol) server.
2) Calculating the time elapsed to receive controller area network (CAN) data from the CAN network and transmitting to the server at different traffic situations and driving speeds. The elapsed time in transmitting the user data to the server is an essential challenge to estimate the overall performance of the vehicular networks.

III RESULTS

Encrypted vehicular communications System utilizes dynamics information provided by the vehicle to estimate the driver's intended future path. The estimate is provided without dependence on future road geometry information obtained from outside sources (e.g., map databases, vehicle probes). In order to determine if the LTE can meet the minimum vehicular communication requirement, the first step that has been considered to determine the latency. The MATLAB is being used for the simulation purpose with several built-in libraries. Due to mobility, vehicles move in and out of the observing zone. Thus, the vehicles and the links (sender-receiver pairs) on which the data is encrypted change over time.

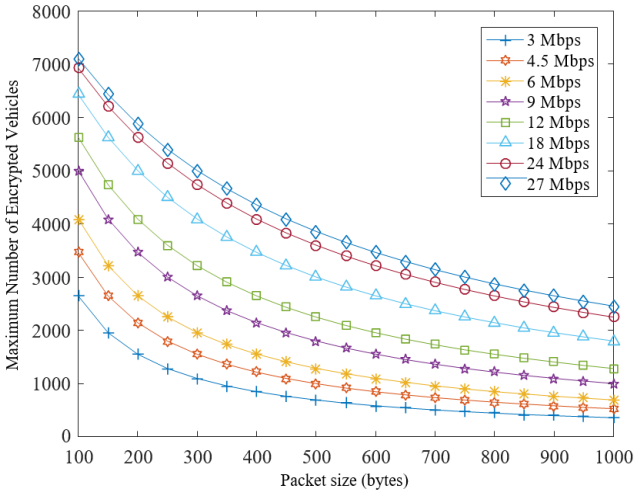

Fig. 6. Encrypted transmission time as a function of packet size for different data-rates during communication using DSRC algorithm.

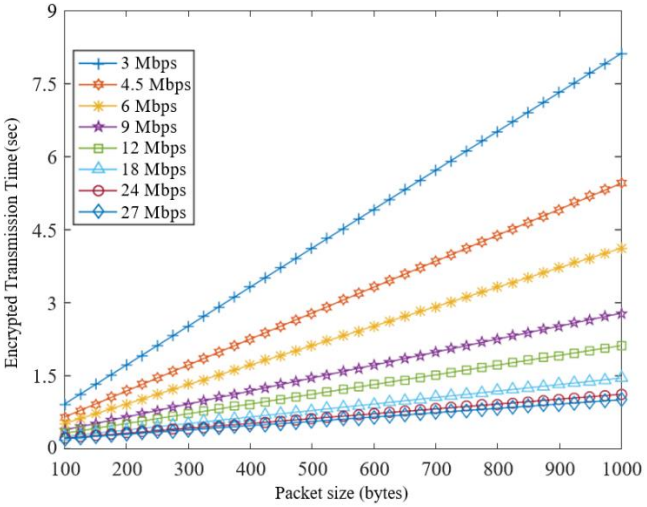

Fig. 7. Maximum number of encrypted vehicles per second in the channel for different data-rates and packet sizes for secure communication using DSRC algorithm

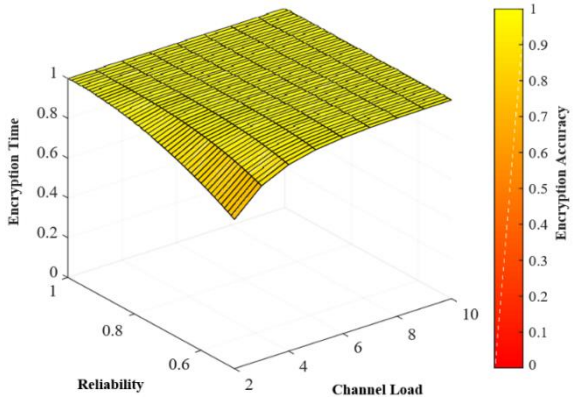

Fig. 8. For best case vehicular communication encryption, the encryption time with reliability on y-axis however the encryption accuracy with channel load stands at 93.74%.

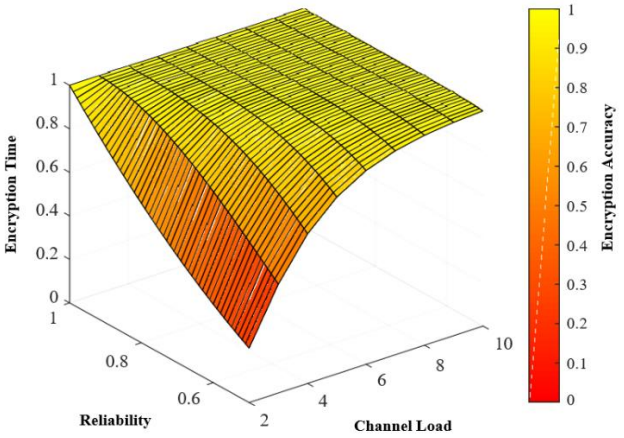

Fig. 9. For worst case vehicular communication encryption, the encryption time with reliability on y-axis however the encryption accuracy with channel load stands at 47.89%.

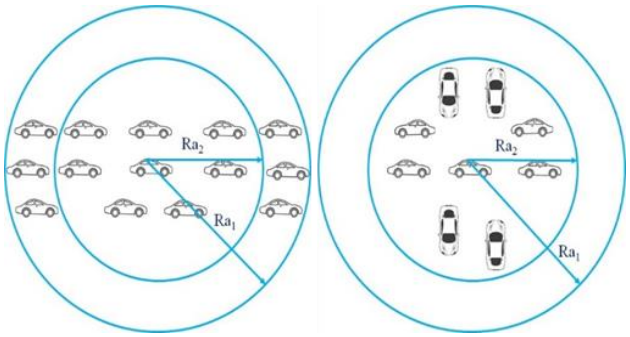

(a) Best Case Encryption (b) Worst Case Encryption

Fig. 10: Pictorial demonstration of encrypting the vehicular communication in both best and worst case.

Over a simulation time of 60s, we collect data on 600 to 800 vehicles and 900,000 to 1,500,000 links presents in dataset passing in the MATLAB as library were encrypted for communication. The specific number of vehicles and links depends on the vehicular density and the DSRC algorithm.

IV DISCUSSION

Vehicular communication plays one of the important roles for future autonomous vehicle. Current vehicular communication is more directed towards DSRC (Dedicated Short-Range Communications). The DSRC law is not enforced and some other technology such as D2D (Device to Device) based on LTE (Long Term Evolution) will provide good results and become possible alternative using the wireless controller area network for communication. The scope of this paper is to have an encryption based DSRC algorithm with wireless CAN network that has the capability to process transmit and receive the data and could able to interface all of the following devices for vehicular communication. And also, to have a capability to help in the future of autonomous vehicles. We have compared the accuracy of wireless controller area network that encrypts vehicle-to-

vehicle communication with existing techniques that are being used for encryption of communication in [23].

TABLE IV

THE COMPARISON OF WIRELESS CAN NETWORK WITH OTHER EXISTING DEVELOPED SYSTEMS FOR ENCRYPTION

LIMERIC [23]		PDR-DCC [23]	
Message-rate	1 to 10 Hz	Message-rate	10 Hz
Data-rate	6 Mbps	Data-rate	3, 4.5, 6, 9, 12 and 18 Mbps
Encryption Accuracy	92.45%	Encryption Accuracy	79.56%

Sensor Networks [23]		Wireless CAN	
Message-rate	1 to 10 Hz	Message-rate	1 to 10 Hz
Data-rate	3, 4.5, 6, 9, 12 and 18 Mbps	Data-rate	6 Mbps
Encryption Accuracy	89.56%	Encryption Accuracy	93.74%

This research paper explains the research study, done for one of the performance evaluations of encrypted vehicular communication using wireless controller area network. It can be further continued to develop a device and a server with more functionalities for encrypted vehicular communication.

V CONCLUSION

In this paper, we have developed an encrypted vehicular communication using wireless controller area network with the help of DSRC encryption algorithm. Vehicular communication-based safety applications rely on exchange of messages between vehicles, to inform their environment, and, foresee and avoid hazardous situations. We focused on ensuring a desirable encryption performance at high vehicular densities by means of Dedicated Short-Range Communication (DSRC) algorithms. Channel load is the major cause for degradation of the encryption performance at high vehicular densities. DSRC algorithms optimize the usage of the channel to avoid load which is crucial for a desirable encryption performance at high vehicular communication. We have systematically investigated the effect of vehicular communication on the MATLAB application platform and achieved an accuracy of 93.74% for encrypting all the communications between the vehicles and making them secure in symmetry. The encryption transmission time for the encryption recorded at 165 seconds while the rate of encryption recorded as low as 120 Mbps for the proposed awareness range of different vehicles using DSRC algorithm in wireless CAN for secure vehicular communication.

REFERENCES

[1] E. Halawany, B.M.; Jameel, F.; Da Costa, D.B.; Dias, U.S.; Wu, K. Performance Analysis of Downlink NOMA Systems over κ-μ Shadowed Fading Channels. IEEE Trans. Veh. Technol. 2019, 69, 1046–1050

[2] K. Anwar, W.; Franchi, N.; Fettweis, G. Performance Evaluation of Next Generation V2X Communication Technologies: 5G NR-V2V vs. IEEE 802.11bd. In Proceedings of the IEEE 90th Vehicular Technology Conference Vehicular Technology Conference (VTC-Fall 2019), At Honolulu, HI, USA, 22–25 September 2019

[3] L. Magueta, R.; Teodoro, S.; Castanheira, D.; Silva, A.; Dinis, R.; Gameiro, A. Multiuser Equalizer for Hybrid Massive MIMO mmWave CE-OFDM Systems. Appl. Sci. 2019, 9, 3363

[4] L. Magueta, R.; Castanheira, D.; Silva, A.; Dinis, R.; Gameiro, A. Hybrid multi-user equalizer for massive MIMO millimeter-wave dynamic subconnected architecture. IEEE Access 2019, 7, 79017–79029.

[5] D. Castanheira, D.; Lopes, P.; Silva, A.; Gameiro, A. Hybrid beamforming designs for massive MIMO millimeter-wave heterogeneous systems. IEEE Access 2017, 5, 21806–21817

[6] F. Magueta, R.; Castanheira, D.; Silva, A.; Dinis, R.; Gameiro, A. EADAS iterative space-time equalization for multi-user mmW massive MIMO systems. IEEE Trans. Commun. 2016, 65, 608–620

[7] L. Jameel, F.; Haider, M.A.A.; Butt, A.A. Second order fading statistics of UAV networks. In Proceedings of the 2017 Fifth International Conference on Aerospace Science & Engineering (ICASE), Islamabad, Pakistan, 14–16 November 2017; pp. 1–6

[8] L. Jameel, F.; Jabeen, F.; Hamid, Z. Analysis of co-channel interference in VANETs under nakagami-m fading. In Proceedings of the 2016 International Conference on Frontiers of Information Technology (FIT), Islamabad, Pakistan, 19–21 December 2016; pp. 153–158

[9] M. Khan, F.; Pi, Z. mmWave mobile broadband (MMB): Unleashing the 3–300 GHz spectrum. In Proceedings of the 34th IEEE Sarnoff Symposium, Princeton, NJ, USA, 3–4 May 2011; pp. 1–6

[10] L. Jameel, F.; Haider, M.A.A.; Butt, A.A. Robust localization in wireless sensor networks using RSSI. In Proceedings of the 2017 13th International Conference on Emerging Technologies (ICET), Islamabad, Pakistan, 27–28 December 2017; pp. 1–6

[11] L. Giordani, M.; Mezzavilla, M.; Dhananjay, A.; Rangan, S.; Zorzi, M. Channel Dynamics and SNR Tracking in Millimeter Wave Cellular Systems. In Proceedings of the 22th European Wireless Conference, VDE Association, Oulu, Finland, 18–20 May 2016; pp. 306–313

[12] E. Verdone, R. Outage probability analysis for short-range communication systems at 60 GHz in ATT urban environments. IEEE Trans. Veh. Technol. 2017, 46, 1027–1039

[13] Y. Wang, Y.; Venugopal, K.; Heath, R.W.; Molisch,

A.F. MmWave vehicle-to-infrastructure communication: Analysis of urban microcellular networks. IEEE Trans. Veh. Technol. 2018
[14] M. Petrov, V.; Kokkoniemi, J.; Moltchanov, D.; Lehtomaki, J.; Juntti, M.; Koucheryavy, Y. The Impact of Interference from the Side Lanes on mmWave/THz Band V2V Communication Systems with Directional Antennas. IEEE Trans. Veh. Technol. 2018, 67, 5028–5041
[15] [15] L. Milanés, V.; Shladover, S.E.; Spring, J.; Nowakowski, C.; Kawazoe, H.; Nakamura, M. Cooperative Adaptive Cruise Control in Real Traffic Situations. IEEE Trans. IEEE Trans. Intell. Transp. Syst. 2014, 15, 296–305.
[16] K. Karagiannis, G.; Altintas, O.; Ekici, E.; Heijenk, G.; Jarupan, B.; Lin, K.; Weil, T. Vehicular Networking: A Survey and Tutorial on Requirements, Architectures, Challenges, Standards and Solutions. IEEE Commun. Surv. Tutorials 2016, 13, 584–616
[17] P. Kim, B.; Yi, K.; Yoo, H.-J.; Chong, H.-J.; Ko, B. An IMM/EKF Approach for Enhanced Multitarget State Estimation for Application to Integrated Risk Management System. IEEE Trans. Veh. Technol. 2015, 64, 876–889
[18] F. Zingoni, A.; Diani, M.; Corsini, G. A Flexible Algorithm for Detecting Challenging Moving Objects in Real-Time within IR Video Sequences. Remote Sens. 2017, 9, 1128
[19] D. Ponte Müller, F.; Diaz, E.M.; Rashdan, I. Cooperative Positioning and Radar Sensor Fusion for Relative Localization of Vehicles. In Proceedings of the 2016 Intelligent Vehicles Symposium (IV), Gothenburg, Sweden, 19–22 June 2016; pp. 1060–1065
[20] R. Kloiber, B.; Strang, T.; Röckl, M.; de Ponte Müller, F. Performance of CAM Based Safety Applications Using ITS-G5A MAC in High Dense Scenarios. In Proceedings of the 2011 Intelligent Vehicles Symposium (IV), Baden-Baden, Germany, 5–9 June 2016; pp. 654–660
[21] E. Liu, J.; Wan, J.; Wang, Q. A survey on position-based routing for vehicular ad hoc networks. J. Telecommun. Syst. Arch. 2016, 62, 15–30.
[22] J. Lin, Y.W.; Chen, Y.S.; Lee, S.L. Routing Protocols in Vehicular Ad Hoc Networks: A Survey and Future Perspectives. J. Inf. Sci. Eng. 2010, 26, 913–932
[23] Y. Lee; M. Müller. Survey of Routing Protocols in Vehicular Ad Hoc Network Communication for Encryption. In Advances in Vehicular Ad-Hoc Networks: Developments and Challenges; Information Science Reference (an Imprint of IGI Global); United States of America: New York, NY, USA, 2009; pp. 113–175
[24] Y. Bilal, S.M.; Khan, A.R.; Ali, S. Review and performance analysis of position-based routing protocols. Wirel. Pers. Area Commun. 2016, 1, 559–578
[25] E. Halawany, B.M.; Jameel, F.; Da Costa, D.B.; Dias, U.S.; Wu, K. Performance Analysis of Downlink NOMA Systems over κ-μ Shadowed Fading Channels. IEEE Trans. Veh. Technol. 2019, 69, 1046–1050
[26] T. Anwar, W.; Franchi, N.; Fettweis, G. Performance Evaluation of Next Generation V2X Communication Technologies: 5G NR-V2V vs. IEEE 802.11bd. In Proceedings of the IEEE 90th Vehicular Technology Conference (VTC-Fall 2019), At Honolulu, HI, USA, 22–25 September 2019.
[27] R. Magueta, R.; Teodoro, S.; Castanheira, D.; Silva, A.; Dinis, R.; Gameiro, A. Multiuser Equalizer for Hybrid Massive MIMO mmWave CE-OFDM Systems. Appl. Sci. 2019, 9, 3363
[28] R. Magueta, R.; Castanheira, D.; Silva, A.; Dinis, R.; Gameiro, A. Hybrid multi-user equalizer for massive MIMO millimeter-wave dynamic subconnected architecture. IEEE Access 2019, 7, 79017–79029
[29] E. Castanheira, D.; Lopes, P.; Silva, A.; Gameiro, A. Hybrid beamforming designs for massive MIMO millimeter-wave heterogeneous systems. IEEE Access 2017, 5, 21806–21817
[30] T. Magueta, R.; Castanheira, D.; Silva, A.; Dinis, R.; Gameiro, A. Hybrid iterative space-time equalization for multi-user mmW massive MIMO systems. IEEE Trans. Commun. 2016, 65, 608–620
[31] U. Jameel, F.; Haider, M.A.A.; Butt, A.A. Second order fading statistics of UAV networks. In Proceedings of the 2017 Fifth International Conference on Aerospace Science & Engineering (ICASE), Islamabad, Pakistan, 14–16 November 2017; pp. 1–6
[32] U. Jameel, F.; Jabeen, F.; Hamid, Z. Analysis of co-channel interference in VANETs under nakagami-m fading. In Proceedings of the 2016 International Conference on Frontiers of Information Technology (FIT), Islamabad, Pakistan, 19–21 December 2016; pp. 153–158
[33] P. Khan, F.; Pi, Z. mmWave mobile broadband (MMB): Unleashing the GHz spectrum. In Proceedings of the 34th IEEE Sarnoff Symposium, Princeton, NJ, USA, 3–4 May 2011; pp. 1–6.
[34] M. Jameel, F.; Haider, M.A.A.; Butt, A.A. Robust localization in wireless sensor networks using RSSI. In Proceedings of the 2017 13th International Conference on Emerging Technologies (ICET), Islamabad, Pakistan, 27–28 December 2017; pp. 1–6

DOI: 10.37917/ijeee.sceeer.3rd.4 *(15-16) June 2020*

Open Access

Iraqi Journal for Electrical and Electronic Engineering
Conference Article

The Design and Implementation of a Single-Actuator Soft Robot Arm for Lower Back Pain Reduction

Alaa Al-Ibadi*
Computer Engineering Department, Basrah University, Basrah, Iraq

Correspondence
*Alaa Al-Ibadi
61004 Basrah University, Basrah, Iraq
Email: alaa.abdulhassan@uobasrah.edu.iq

Abstract
This paper presents a simple and fast design and implementation for a soft robot arm. The proposed continuum arm has been built by a single self-bending contraction actuator (SBCA) with two-fingers soft gripper. Because of the valuable advantages of the pneumatic artificial muscle (PAM), this continuum arm provides a high degree of safety to individuals. The proposed soft robot arm has a bending behaviour of more 180° at 3.5 kg, while, its weight is 0.7 kg. Moreover, it is designed to assist the people by reducing the number of backbends and that leads to a decrease in the possibility of lower back pain.

KEYWORDS: Pneumatic artificial muscle (PAM), Bending actuator, Lower back pain, Continuum arm, Human-robot interaction.

I. INTRODUCTION

The major cause of disabilities for a long period in life is the lower back pain (LBP) [1]. While more than 90% of LBP symptoms are unknown, clinical researchers are still developing structural anatomical and the mathematical biomechanical model [2]. On the other hand, the majority of work types require body bend to pick up tools and objects. This process causes medical back problems.

The high probability of injury risks is the major significant aspect of human-robot collaboration. The soft robotics represent substantial alternatives for rigid robots due to its softness and low weight. The soft pneumatic actuators that inspired by a human's muscle, such as the pneumatic artificial muscle (PAM), are widely utilised to build such forms of robotic systems. Numerous advantages are known for the PAM, such as the high force to weight ratio, multiple degrees of freedom (DoF), variable stiffness, low cost and it is safe for human-robot collaboration [3][4][5][6]. Thus, soft robots are safe for individuals and can work together with a human in the same workspace.

The bending pneumatic air muscles have been developed by numerous researchers. Among them is that presented by [7] using two chambers instead of one inner tube to create a bending actuator. The authors in [8] proposed a PneuNet actuator by utilising various thicknesses for the inner tube. The implementation of the PneuNet is easy, however, it lacks in the ratio of the elasticity. To overcome this restriction, a polymer fibre is used in the PneuFlex actuator to support the rubber substrate, as proposed by [9]. In comparison with the silicone, the polyethylene terephthalate (PET) material is three to four times less elastic. [10] utilised the strain limiting layer on one side of the extension actuator to prevent elongation from this side and to make the other side free to extend. This method is used by [11] but adapted by using a high tension thread to partially fix the extensor PAM length. [12] utilised the impact of the braided angle by using two different braided angles of the braided mesh for the contractor muscle actuator to develop the bending performance. [13] used two integrated jamming actuators in parallel to create a bending performance. The jamming technique is used by [14] to control the bending stiffness.

[15] used tendons to establish the bending behaviour for the soft gripper. The PAM can be used in various engineering areas including humanoid robots, wearable robots for medical applications, industrial and airspace applications, and mobile robots [16]. On the other hand, bending muscle can be implemented by 3D printing, this technology provides fast prototyping, flexible design, and an easy way to implement the actuators and sensors that have the complex structure [17]. Furthermore, 3D printing offers an efficient way to build an actuator by using different materials and layout at the same time [18]. A fused deposition modelling (FDM) technology has been used by [19] to develop a 3D printed pneumatic muscle. Inserting soft sensors during the fabrication of the pneumatic actuators by the 3D technology is called 4D printing methods and it provides a valuable technique to manufacture such types of actuators [20].

In this paper, a proposal of a soft robot arm with a proper soft gripper is presented by using the techniques of the SBCA. The experiment to identify the performance of the proposed

robot arm is explained together with several uses to assist the workers or lower back pain people.

II. Materials and Methods

In this paper, the self-bending contraction actuator (SBCA) by Al-Ibadi, et al. [21] is used to design a single actuator continuum robot arm. The specifications for this actuator are listed in Table 1. The small size of the SBCA is used to design a two-finger soft gripper and it is mounted to the end of the soft robot arm.

A. Fabrication of the continuum arm

The simple type of the contraction pneumatic soft muscle is built by using inner rubber tube surrounded by braided mesh, then closed by two solid ends with a small air inlet [22] [23]. On the other hand, the SBCA is a modified version of the contraction actuator with an inserting flexible reinforcement road to prevent the contraction from the rod side and establishes the bending behaviour [24]. Fig. 1 shows the construction procedure of the continuum arm.

TABLE. 1.
The material specification of the robot continuum arm

L_0 (m)	0.6
Rubber thickness (m)	0.0011
Braided thickness (m)	0.0005
Rubber diameter (m)	0.00265
Rubber stiffness(N/m)	545
Rod length (m)	0.6
Rod thickness (m)	0.003
Rod width (m)	0.025

L_0 is the length of the SBCA at a relaxed condition (no pressure).

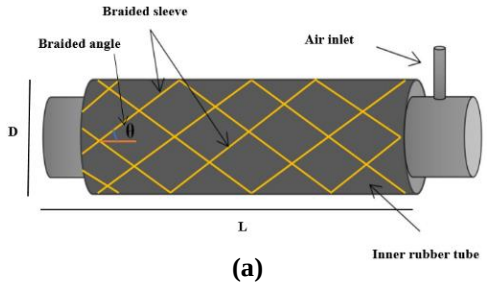

(a)

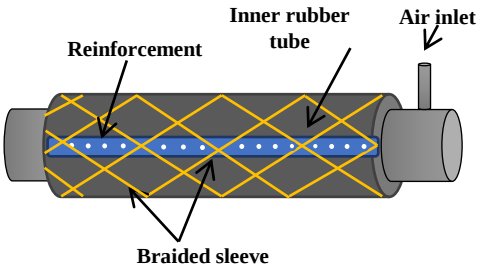

(b)

(c)

Fig. 1. The structure procedure of the continuum arm [21].

The end effector is made from two small size bending actuators. In order to maximise the grasping volume, the soft fingers are pulled by an elastomer ribbon as illustrated in Fig. 2.

The soft gripper offers highly efficient grasping performance due to its soft texture, compliance, high grasping force, low weight, and low cost. The end effector has been designed to be mounted at the end of the soft robot arm to grasp different types of objects and tools may the workers need to reduce the number of their back bending.

(a)

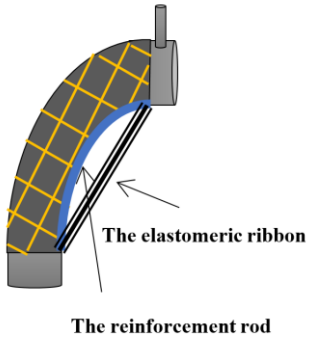

(b)

Fig. 2. The two fingers soft gripper based on SBCA. (a) The soft gripper at different air pressures. (b) The schematic design for the soft finger.

Fig. 3. Shows the continuum arm and the soft gripper at several actuating conditions. To verify the softness, compliance, and safety for human-robot interaction.

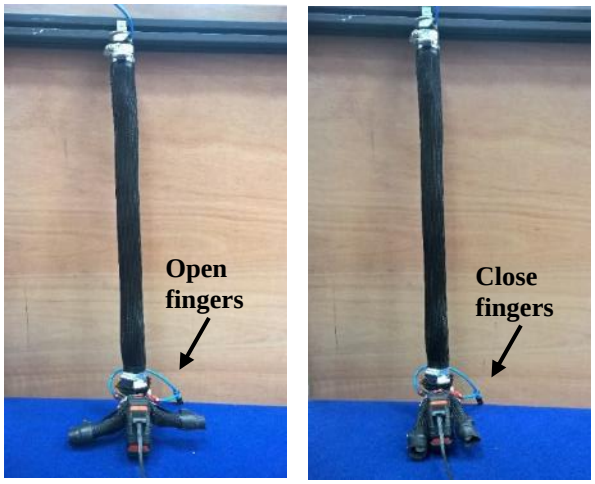

(a) **(b)**

(c)

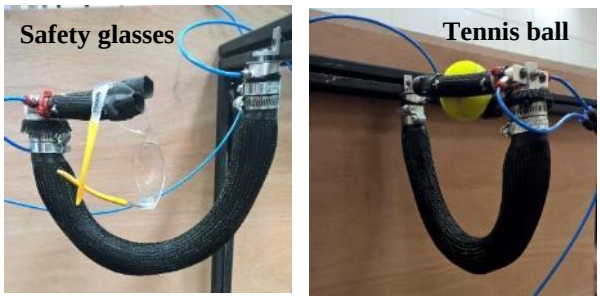

(d)

Fig. 3. The entire continuum arm and several actuations and grasping examples.

III. Experiments and Results

An experiment has been done to evaluate the maximum bending force for the proposed arm. The continuum arm is fixed from the inlet end to the frame vertically, then air pressure is applied via three stages solenoid valve gradually. At each step, the soft arm bends to a specific bending angle (see Table. 2 For a 30 cm SBCA). To reduce the bending angle to its initial value (zero degrees), a load is attached to the free end. At each time the pressure is increasing, the load is rising to maintain zero bending angles. The maximum tested air pressure for safety work is 500 kPa. Fig. 4 shows an example of this procedure.

The proposed soft arm is tested at a maximum bending force of 9.2 kg and 3.5 kg at 180°. The weight of the proposed arm together with the two-fingers soft gripper is 0.7 kg and this gives about a "13" force to weight ratio.

TABLE. 2.
The maximum bending angle at different loads for the 30 cm SBCA

Load (kg)	*Bending angle (degree)*
0.0	213.1
0.5	136.2
1.0	73.0
1.5	49.3
2.0	34.1

Fig. 4. A 30 cm SBCA at 300 kPa and loaded by 1.0 kg.

IV. Conclusion

Using the soft robot arm close to humans is safe due to the softness and the lightweight of its material.
The proposed robot arm provides significant assistance to humans to prevent or reduce the pain caused by bending the human back.
The pneumatic muscle actuator provides numerous advantages over the rigid types, Specially for the human-robot interaction.
This paper presented a single SBCA of 50 cm in length to design a robot arm that can be used close to humans to pick up objects and tools from the ground and lift them to the individuals to help them reduce the number of back bending. This leads to reducing back pain.

Acknowledgment

Many thanks to the computer engineering department of the university of Basrah for their support and providing the required lab facilities.

References

[1] D. Hoy *et al.*, "The global burden of low back pain: Estimates from the Global Burden of Disease 2010 study," *Ann. Rheum. Dis.*, 2014, doi: 10.1136/annrheumdis-2013-204428.
[2] R. A. Deyo, S. K. Mirza, J. A. Turner, and B. I. Martin, "Overtreating Chronic Back Pain: Time to Back Off?," *J. Am. Board Fam. Med.*, vol. 22, no. 1, pp. 62–68, Jan. 2009, doi: 10.3122/jabfm.2009.01.080102.
[3] A. Al-Ibadi, S. Nefti-Meziani, and S. Davis, "The Design, Kinematics and Torque Analysis of the Self-Bending Soft Contraction Actuator," *Actuators*, vol. 9, no. 2, p. 33, Apr. 2020, doi: 10.3390/act9020033.
[4] K. Asaka and H. Okuzaki, *Soft Actuators*. Tokyo: Springer Japan, 2014.
[5] H. D. Yang, B. T. Greczek, and A. T. Asbeck, "Modeling and analysis of a high-displacement pneumatic artificial muscle with integrated sensing," *Front. Robot. AI*, 2019, doi: 10.3389/frobt.2018.00136.
[6] A. Al-Ibadi, S. Nefti-Meziani, and S. Davis, "Design, Kinematics and Controlling a Novel Soft Robot Arm with Parallel Motion," *Robotics*, vol. 7, no. 2, p. 19, May 2018, doi: 10.3390/robotics7020019.
[7] M. R. M. Razif, A. A. M. Faudzi, M. Bavandi, I. N. A. M. Nordin, E. Natarajan, and O. Yaakob, "Two chambers soft actuator realizing robotic gymnotiform swimmers fin," in *2014 IEEE International Conference on Robotics and Biomimetics (ROBIO 2014)*, 2014, pp. 15–20, doi: 10.1109/ROBIO.2014.7090300.
[8] F. Ilievski, A. D. Mazzeo, R. F. Shepherd, X. Chen, and G. M. Whitesides, "Soft robotics for chemists," *Angew. Chemie - Int. Ed.*, 2011, doi: 10.1002/anie.201006464.
[9] R. Deimel and O. Brock, "A compliant hand based on a novel pneumatic actuator," in *2013 IEEE International Conference on Robotics and Automation*, 2013, pp. 2047–2053, doi: 10.1109/ICRA.2013.6630851.
[10] G. Miron, B. Bédard, and J.-S. Plante, "Sleeved Bending Actuators for Soft Grippers: A Durable Solution for High Force-to-Weight Applications," *Actuators*, vol. 7, no. 3, p. 40, Jul. 2018, doi: 10.3390/act7030040.
[11] B. Tondu and P. Lopez, "Modeling and control of McKibben artificial muscle robot actuators," *IEEE Control Syst.*, vol. 20, no. 2, pp. 15–38, Apr. 2000, doi: 10.1109/37.833638.
[12] A. A. M. Faudzi, M. R. M. Razif, I. N. A. M. Nordin, K. Suzumori, S. Wakimoto, and D. Hirooka, "Development of bending soft actuator with different braided angles," in *IEEE/ASME International Conference on Advanced Intelligent Mechatronics, AIM*, 2012, doi: 10.1109/AIM.2012.6266037.
[13] A. Jiang, S. Adejokun, A. Faragasso, K. Althoefer, T. Nanayakkara, and P. Dasgupta, "The granular jamming integrated actuator," in *2014 International Conference on Advanced Robotics and Intelligent Systems (ARIS)*, 2014, pp. 12–17, doi: 10.1109/ARIS.2014.6871512.
[14] T. Wang, J. Zhang, Y. Li, J. Hong, and M. Y. Wang, "Electrostatic Layer Jamming Variable Stiffness for Soft Robotics," *IEEE/ASME Trans. Mechatronics*, vol. 24, no. 2, pp. 424–433, Apr. 2019, doi: 10.1109/TMECH.2019.2893480.
[15] M. Manti, T. Hassan, G. Passetti, N. D'Elia, C. Laschi, and M. Cianchetti, "A Bioinspired Soft Robotic Gripper for Adaptable and Effective Grasping," *Soft Robot.*, vol. 2, no. 3, pp. 107–116, Sep. 2015, doi: 10.1089/soro.2015.0009.
[16] G. Andrikopoulos, G. Nikolakopoulos, and S. Manesis, "A Survey on applications of Pneumatic Artificial Muscles," in *2011 19th Mediterranean Conference on Control and Automation, MED 2011*, 2011, doi: 10.1109/MED.2011.5982983.
[17] A. Zolfagharian, A. Z. Kouzani, S. Y. Khoo, A. A. A. Moghadam, I. Gibson, and A. Kaynak, "Evolution of 3D printed soft actuators," *Sensors Actuators A Phys.*, vol. 250, pp. 258–272, Oct. 2016, doi: 10.1016/j.sna.2016.09.028.
[18] J. Z. Gul *et al.*, "3D printing for soft robotics – a review," *Sci. Technol. Adv. Mater.*, vol. 19, no. 1, pp. 243–262, Dec. 2018, doi: 10.1080/14686996.2018.1431862.
[19] H. K. Yap, H. Y. Ng, and C. H. Yeow, "High-Force Soft Printable Pneumatics for Soft Robotic Applications," *Soft Robot.*, 2016, doi: 10.1089/soro.2016.0030.
[20] A. Zolfagharian, A. Kaynak, and A. Kouzani, "Closed-loop 4D-printed soft robots," *Mater. Des.*, vol. 188, p. 108411, Mar. 2020, doi: 10.1016/j.matdes.2019.108411.
[21] A. Al-Ibadi, S. Nefti-Meziani, and S. Davis, "Active Soft End Effectors for Efficient Grasping and Safe Handling," *IEEE Access*, vol. 6, pp. 23591–23601, 2018, doi: 10.1109/ACCESS.2018.2829351.
[22] A. Al-Ibadi, S. Nefti-Meziani, and S. Davis, "Efficient Structure-Based Models for the McKibben Contraction Pneumatic Muscle Actuator: The Full Description of the Behaviour of the Contraction PMA," *Actuators*, vol. 6, no. 4, p. 32, Oct. 2017, doi: 10.3390/act6040032.

[23] S. Neppalli and B. A. Jones, “Design, construction, and analysis of a continuum robot,” in *2007 IEEE/RSJ International Conference on Intelligent Robots and Systems*, 2007, pp. 1503–1507, doi: 10.1109/IROS.2007.4399275.

[24] A. Al-Ibadi, S. Nefti-Meziani, S. Davis, and T. Theodoridis, “Novel Design and Position Control Strategy of a Soft Robot Arm,” *Robotics*, vol. 7, no. 4, p. 72, Nov. 2018, doi: 10.3390/robotics7040072.

Open Access

Iraqi Journal for Electrical and Electronic Engineering
Conference Article

Healthcare Monitoring and Analytic System Based Internet of Thing

Bahaa S. Mostafa*[1], Abbas Hussain Miry[2], Tariq M. Salman[3]
[1] Electrical Engineering Department, Al-Mustansiriyah University, Baghdad, Iraq

Correspondence
* Bahaa. S. Mostafa
Electrical Engineering Department,
Al-Mustansiriyah University, Baghdad, Iraq
Email: bahaaaldeen31@gmail.com

Abstract
In this work, a healthcare monitoring system-based Internet of Medical Things (IoMT) is proposed, implemented, analyze it by artificial intelligence using fuzzy logic. Atmega microcontroller was used to achieve the function of the proposed work and provide the area for monitoring and Analytic(decision) to the caretakers or doctors through putting the results in the platform. In this paper, the heart rate pulse sensor and infrared temperature sensor are chosen, which give skin temperature and room temperature to provide their results to the caretaker. The decision that gives the patient is in a normal state, or the fuzzy logic does an abnormal state or risk state. The fuzzy logic is used for it accurate and fast in processing data and gives a result very closer to the reality in smart health services. IoMT enables the doctors and caretakers to monitor the patient easily at any time and any place by using their intelligent laptops, tablets, and phones. Finally, the proposed system can contribute to the construction of a wide healthcare monitoring system in the unit or in the department that follows on for the hospital. Therefore, Doctors can improve the accuracy of the diagnosis, as they receive all the patient data necessary.

KEYWORDS: Atmega microcontroller board; Cloud Computing; Internet of Things; Pulse rate; Temperature sensor.

I. INTRODUCTION

Increasing mortality cases for the patient, elderly, and people with chronic diseases because it don't exist for enough healthcare monitoring, thus, the attention of researchers towards the benefits of the internet especially after appear supposedly Internet of Things (IoT) and specifically the Internet of Medical Things (IoMT). In the last decade, the large expansion of IoT makes all things to be correlated. Some of IoT's applications include smart city, home automation, intelligent climate, smart shopping, automated transportation, and health care. IoMT allows for sustained development in the health care sector, in the field of patient treatment and communication. The major benefits of IoMT in health-care organizations are improved outcomes of treatment, Reduced costs, enhanced patient care, better risk control, better disease detection, and reduced errors. The key feature of the health care system is checking vital signs of the patient, such as skin temperature, Electrogradigram (ECG), respiration, percentage of oxygen saturation, blood pressure, motion and heart rate [1].
On the subject of IoMT, several studies have been proposed, analyzed, and investigated (related work), for example, Healthcare Monitoring System Based on Pulse Sensor [2],

Healthcare based on loT using Raspberry Pi [3], An Intelligent Sensor Based System for Real Time Heart Rate Monitoring (HRM)[4], Neuro Fuzzy based Healthcare System using IoT [5], A SMART PATIENT HEALTH MONITORING SYSTEM USING IOT [6], Healthcare IoT-Based Affective State Mining Using a Deep Convolutional Neural Network[7] and Fuzzy-based Driver Monitoring System (FDMS): Implementation of two intelligent FDMSs and a testbed for safe driving in VANETs [8]. Each study in the previous works has a different way to realize the function of the IoMT, a different number of sensors, different types of vital signs, different types of machine learning used, different microcontrollers used, different ages of patient, and different platforms.
In this paper, the skin temperature, room temperature, heartbeat rate is measured, then analyze it by using fuzzy logic with many rules to decide the degree of risk, and put the results of measurements and decision in the platform. The microcontroller that uses in this paper is Atmega microcontroller.
In the future, the proposed system could lead to the development of a comprehensive healthcare monitoring system in the hospital unit or department. This project would also support ICU patients, and It can also facilitate the monitoring of the elderly in nursing homes.
The organization of this paper is as follows: Sec.2 internet of things and cloud (upidots). Sec.3contains the designed system, theoretical operation concepts, and implementation.

In Sec. 4, the results of the developed system are presented, demonstrated, and discussed. Finally, the conclusion of the proposed system is presented in Sec. 5.

II. Internet of Things (IOT)

The Internet of Things (IoT) refers to the process of using computer networks to build and shape Internet-connected objects. IoT means that, rather than have a few numbers of efficient electronic devices such as computers, laptops and tablets, it is easier to have a vast number of low-powered gadgets such as air conditioners, wristbands, fridges and umbrellas. Such objects mesmerize in IoT have the power of creative reasoning to perform the assigned task without the need for a personality and a name [9].

The "Thing" or entity present in the physical world, for data collection and processing, will obtain data from person or a living thing and turn those inputs into the Internet. This is made possible by using sensors to save during the specified time the value provided by the thought. "Actuators" may be used by linking items in the universe to show the outputs to the human body. Some of these outputs are triggered by the collected data and are processed with the Internet [9, 10].

IoT and cloud computing, by integrating two technologies, are equally involved in similar ways. The tracking system that is advanced by integrating these two systems to accurately monitor patient records even at the remote site, which is helpful to doctors. IoT technology is continuously sponsored to boost the performance of the Cloud in terms of high resource availability, usage, energy computational capability and energy. In addition, cloud computing is gaining support from IoT technology by improving the domain to manage the real environment and dynamically and distributed transition of the many new services. However, the IoT-based cloud platform should be comprehensive to build new technologies and applications in the smart world [9, 11]. The combination of IoT and cloud based online applications works well in terms of performance as opposed to ordinary web-based applications. Those combinations can be used by emerging applications such as military, banking, and medical applications. The cloud-based IoT technique in particular would support the efficient provision of services in medical applications for monitoring and remotely accessing the records. IoT Based Healthcare systems use the requisite data to capture on time such as regular adjustments in health parameters and update the risk of medical parameters within a standard time period. Additionally, IoT apps and the sensor readings relevant to medical parameters can be used effectively to detect the disease in good time before the dangerous state is reached [9, 11].

The essential advantages of IoT in healthcare systems are [12]:

1) Treatment outcomes: As the tracking is constant, reliable and automatic, all data is processed in the cloud and sent to the doctor in an orderly manner; the care processes have moved correctly. Using this technique will ensure prompt medical attention for estimating recovery.

2) Costs reduction: With the opportunity to meet patients and view them remotely, the cost of inpatient visits can be reduced. In addition, many patients may be treated and stabilized at their homes with the introduction of home care equipment.

3) Errors reduction: Comprehensive and reliable data obtained automatically and without human error will significantly reduce the incidence of medical errors and the associated financial and vital costs.

4) Disease management: If signs of a patient's health are registered and documented, the disease can be detected and treated prior to its progression.

5) Medication management: IoT allows people to avoid drug abuse through the exact use of medications as well as hospitals and health centers.

6) Patient's satisfaction: The focus on patient needs, prompt care, accuracy of data, reduction of frequent visits, cost savings, recording of recovery processes, and the most importantly is the active participation of patients in the treatment process, all of which have a positive effect on them.

III. System Design, Theoretical Concepts and Implementation

A. System Architecture

The designed system architecture for the proposed IoMT based healthcare monitoring system using Fuzzy logic as shown in Fig 1. The designed system works in an IoMT environment. Room temperature sensor, skin temperature sensor and heart rate sensor will be putted on and near to the patient. With the aid of the sensors that placed on and about the patient, healthcare condition for the patients can be gotten and then can be transfer the information of these sensors records to the target device through ethernet shield that connect on the Atmega microcontroller. The collected data from the microcontroller is sent to cloud using cable in ethernet shield for visualization the analysis data. The collected data can be accessed through upidots IoMT platform.

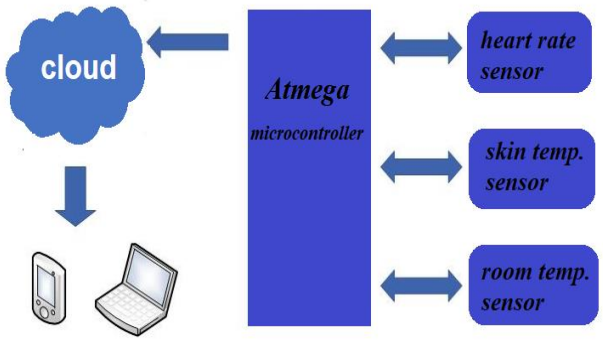

Fig1. System architecture

B. Theoretical concepts

1. Fuzzy logic basics

The Fuzzy logic (FL) approach have utilized. It was introduced by Lotfi Zadeh in 1965. The (FL)-based methodology focuses on the decision-making purpose. It is mainly used to get deficient data to take decision with the concepts called true or false and degrees of truth. The fuzzy set fully include the classical set. The membership function property is utilized for implementing the fuzziness of elements in the set that will have the solution based on the experiment in spite of knowledge. The weighted rate methodology is used to implement the membership function inside the fuzzy interference system[13-14].
In our work, the collected data form the sensors is analyzed by fuzzy logic. The graphs based on the inferences made using fuzzy logic is generated. The advantage of using fuzzy logic is that we do not require many data sets to analyze the newly data collected. Another advantage of Fuzzy logic is its power of interpretability and simplicity [15]. Mamdani Inference Method is used as a Fuzzy methodology that is a commonly used methodology and simplest method because its structure depending on min-max operations. The Mamdani fuzzy inference method have also chosen because of its wide spread acceptance and it is well suited for human inputs. The output from the Mamdani method can also be sufficiently transferred to a linguistic form[14].
The fuzzy rule base system is utilized to produce the outputs according to the offered input for the system. In this paper, 2 input parameters will be entered to the system. The first (skin temperature) consist of 2 membership functions and the second (heart rate) consist of 3 membership functions. The output (degree of risk) consist of 3 membership functions. The number of rules is calculated based on each given parameter's membership function. The whole number of rules framed is 6 as shown in (Table **1**). The membership function values and the fuzzy rules are introduced by researcher's proposition based on the fuzzy inference concept.

	Input		Output
	Skin temperature	Heart pulse rate	Degree of risk
1	Hyper thermal	Normal	Low
2	Hypo thermal	Normal	Low
3	Hyper thermal	Tacky cardia	Med
4	Hypo thermal	Tacky cardia	High
5	Hyper thermal	Brady cardia	High
6	Hypo thermal	Brady cardia	High

Table 1. The fuzzy rule table with different categories of the input and output parameters

Fig. **2** demonstrates the Fuzzy Inference System in which the heart pulse rate and skin temperature are the input values.

After finish Fuzzification, Defuzzification methodology is used for producing the output for degree of risk.

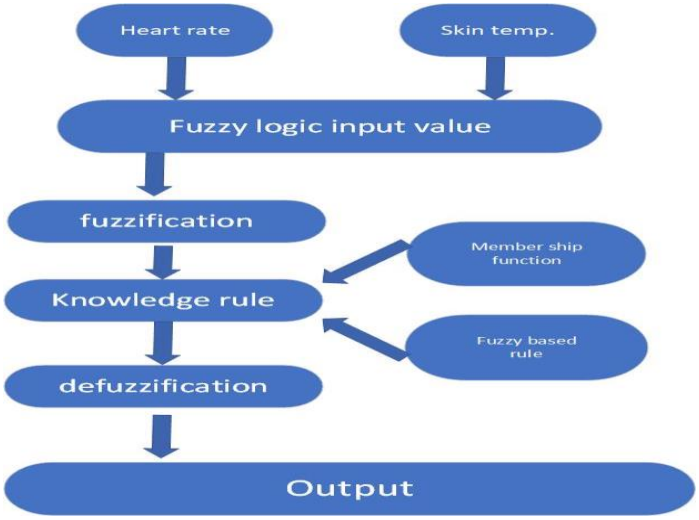

Fig. 2. Fuzzy Inference System

The input membership functions are formulated using the trapezoidal function, and the output
membership function is formulated using the trapezoidal membership function. Fig. **3**
demonstrates the membership function for heart rate whose parameters for analyzing heart rate are brady, normal and tacky.
Fig. **4** show the membership function for skin temperature whose parameters for analyzing skin temperature are hypo and hyper.
Fig. **5** show the membership function for output whose parameters for analyzing output are low, medium and high.

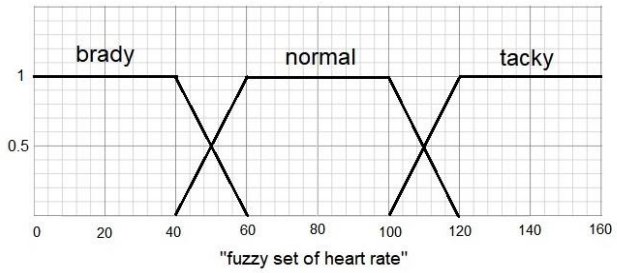

Fig.3 membership function for heart rate

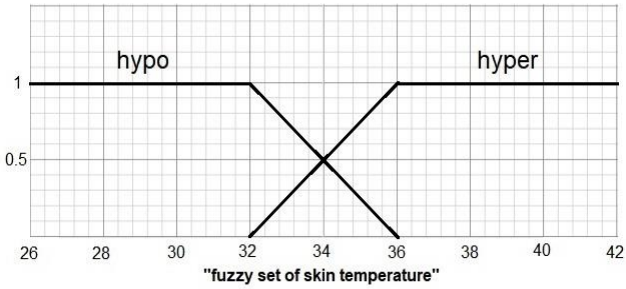

Fig.4 membership function for skin temperature

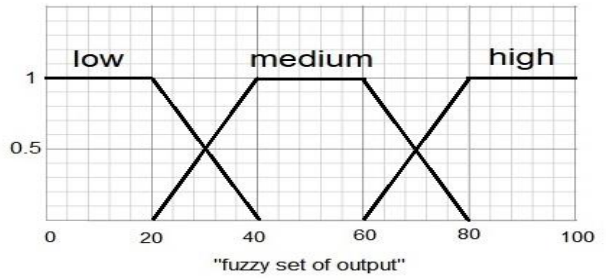

Fig.5 membership function for output

2. Arduino Uno

It is a microcontroller board which used the 8-bit ATmega328P microcontroller from Atmel. It has 6 analog inputs,14 digital input/output, a 16 MHz crystal, a power jack, reset button and a USB connection. easy connecting it to a computer with a USB cable or battery is enough to get it started or powering it with an AC-to-DC adapter. Uno Software (IDE) gives simply application development on windows platform [16-17].

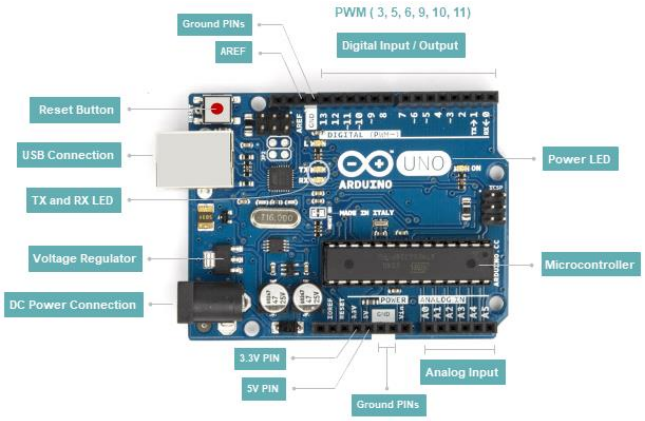

Fig 6. Arduino Uno

3- Temperature IR Sensor

The MLX90614 is an Infra-Red Thermometer which is non-contact temperature monitoring. The MLX90614 integrates a low-noise amplifier, 17-bit ADC and an effective DSP package while achieving high thermometer accuracy and resolution.

The thermometer comes in a factory fitted with a digital SMBus output that gives full access to the temperature measured in the 0.02 ° C maximum temperature range(s).

Fig 7. Temperature IR Sensor

4-Grove - Ear-clip Heart Rate Sensor

Heart rate ear clip kit includes an ear clip and a module receiver. The system to calculate heart rate can be used to track patient and athlete heart rate. The whole device is highly adaptive, low power consumption and very portable.

Fig 8. Ear-clip Heart Rate Sensor

C. Implementation

The following figures show the installation of the Ethernet Shield directly on the Atmega microcontroller board through the corresponding blocks, and also shows how to supply the sensors connected to the power (5v) by red wire and ground by black wire through mini board. Where the information transfer wire of the heartbeat sensor was connected to one of the analog blocks and the information wire of the skin temperature sensor was connected by green wire to the two blocks, or lines are called Serial Clock (or SCL) and Serial Data (or SDA).

The power of the microcontroller can be supplied in several ways, the first by laptop from the USB port and the second by an external adapter that connects to its power jack in the controller and the third by batteries that connect to the port (Vin).

The shield provides a standard RJ45 ethernet jack, reset button on the shield resets both the shield and the Atmega microcontroller, and the number of informational LEDs.

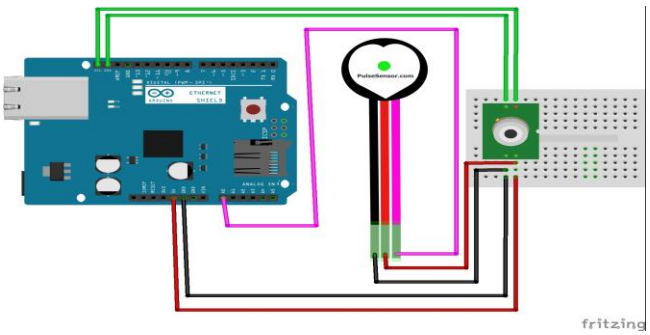

Fig 9. Installation of circuit

IV. RESULTS AND DISCUSSION

A. Mechanism Operating

The department's connections to the installation and testing phase of the smart health metering system are shown as in the following figure after mentioning the steps of installing the device.

STEP.1: The sensor Pulse is set at the patient's ear. This involves an IR-sensor. Get pulse from the sensor in every pumping. This sensor output from the signal conditioning unit for amplification is provided to the Atmega microcontroller.

STEP 2: The patient places his finger over the opening underneath the skin temperature sensor, so the sensor takes the value of the skin temperature through the IR and then goes to the Arduino Uno.

Figure 10. Experimental environment

B. Testing and findings health care unit

The developed Patient Health Monitoring System is checked to use different people from normal to uncommon states of health. The different tests and results give minimum error rate and the findings are described below.

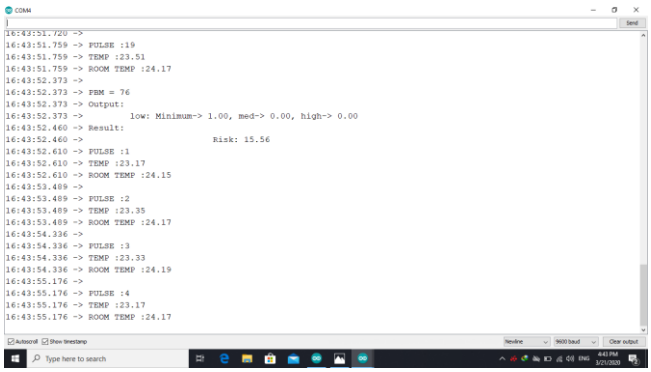

Fig 11. Screenshot: degree of risk

Through the tests that I conducted on several people, especially the elderly and shown in the photos above, I notice when the vital signs of the body (heartbeat and skin temperature) are within the normal range, the smart system gives a low risk ratio, unlike if one of the vital signs out of the normal range, the smart system It will give a risk ratio that is appropriate to these data, so caregivers will be able to know how dangerous the observer is, with ease and speed, to take the necessary measures.

In the Fig 12 graph of the green heart rate sensor signal repeats every 15 seconds and the red skin temperature sensor signal repeats every two seconds depending on the delay specified in the program. Whereas, the x axis represents the time and the y axis represents the amplitude.

In addition, the system gives room temperature in order to prevent the influence of temperature changes on the health condition of the observer.

C. Data display in the cloud

Regular vital parameters such as heart rate, body temperature, EEG signals can be shown in a laptop or cell phone and the same can be sent to the doctor in emergencies. In the above picture, the information of the person watching is shown on the cloud, where the skin temperature, room temperature, and the number of heartbeats appeared. The Fuzzy logic system gave the patient's risk level directly. It was high because the skin temperature was lower than the normal limit, and the number of heartbeats was lower than the normal limit, and this condition is considered Very dangerous from a medical point of view.

This can be achieved using our program, the results of which are put online and can be seen from anywhere in the world. Since this is a concept model, our framework displays the almost real-time values of various health parameters.

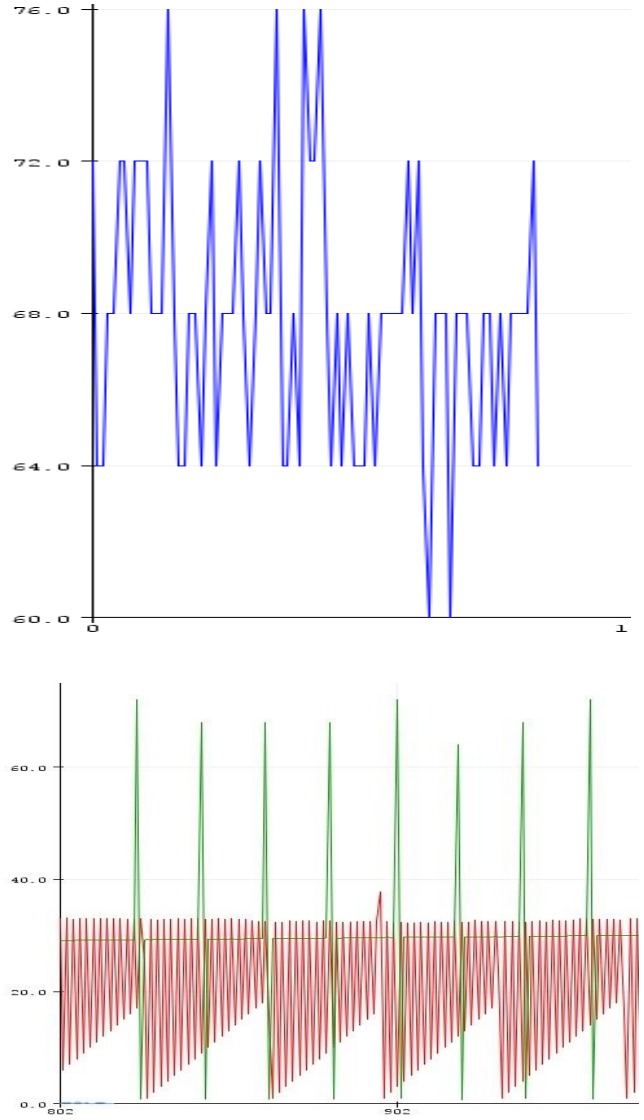

Fig 12. Screenshot: sensing signals in plotter

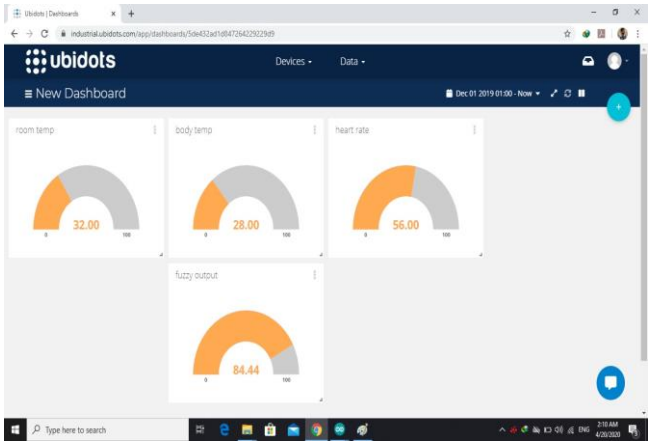

Fig 13. Screenshot: parameter on cloud

V Conclusion and Future Work

The Use of Internet of Things technology in healthcare with an intelligent system (fuzzy logic) can reduce the need for hospitals, and thus fewer deaths, especially among the elderly. IoT protocols enable easy integration with caregiver devices and applications and make the solution very much scalable. This paper proposes and explains a very easy-to-use device and uses the fuzzy logic system found in the Arduino libraries to analyze the recorded values from the sensors, and then give the risks ratio directly. It found through the experiment that using this system provides good results that can be relied upon easily, quickly, and accurately, even though some of the components used are not original. As for using an original and well-made component company, this system can be used throughout the day for monitoring without any problems, as it is easy to use and suitable for the elderly.

The IOT platform will be paired with cloud computing in the future so that the information can be accessible for diagnosis and intensive care in all hospitals.

References

[1] C. Krishna and N. Sampath, "Healthcare Monitoring System Based on IoT," in *2017 2nd International Conference on Computational Systems and Information Technology for Sustainable Solution (CSITSS)*, 2017, pp. 1-5.

[2] Suryawanshi, Chandani, and Bhakti Kurhade. "Healthcare Monitoring System Based On Pulse Sensor." Ijsr. Net 4.4 (2013): 2946-2949.

[3] M. S. D. Gupta, V. Patchava, and V. Menezes, "Healthcare based on iot using raspberry pi," in 2015 International Conference on Green Computing and Internet of Things (ICGCIoT), 2015, pp. 796-799.

[4] Farin, Nusrat J., S. M. A. Sharif, and Iftekharul Mobin. "An intelligent sensor-based system for real time heart rate monitoring (HRM)." (2016).

[5] S. Mumtaj and A. Umamakeswari, "Neuro fuzzy based healthcare system using iot," in 2017 International Conference on Energy, Communication, Data Analytics and Soft Computing (ICECDS), 2017, pp. 2299-2303.

[6] C. Senthamilarasi, J. J. Rani, B. Vidhya, and H. Aritha, "A smart patient health monitoring system using IoT," International Journal of Pure and Applied Mathematics, vol. 119, pp. 59-70, 2018.

[7] M. G. R. Alam, S. F. Abedin, S. I. Moon, A. Talukder, and C. S. Hong, "Healthcare IoT-Based Affective State Mining Using a Deep Convolutional Neural Network," IEEE Access, vol. 7, pp. 75189-75202, 2019.

[8] K. Bylykbashi, E. Qafzezi, M. Ikeda, K. Matsuo, and L. Barolli, "Fuzzy-based Driver Monitoring System (FDMS): Implementation of two intelligent FDMSs and a testbed for safe driving in VANETs," *Future Generation Computer Systems*, vol. 105, pp. 665-674, 2020.

[9] P. M. Kumar, S. Lokesh, R. Varatharajan, G. C. Babu, and P. Parthasarathy, "Cloud and IoT based disease prediction and diagnosis system for healthcare using Fuzzy

neural classifier," *Future Generation Computer Systems*, vol. 86, pp. 527-534, 2018.
[10] K. Shankar, M. Ilayaraja, and K. S. Kumar, "Technological Solutions for Health Care Protection and Services Through Internet Of Things (IoT)," *International Journal of Pure and Applied Mathematics*, vol. 118, pp. 277-283, 2018.
[11] M. Bansal and B. Gandhi, "IoT Based Development Boards for Smart Healthcare Applications," in *2018 4th International Conference on Computing Communication and Automation (ICCCA)*, 2018, pp. 1-7.
[12] Z. Alansari, N. B. Anuar, A. Kamsin, S. Soomro, and M. R. Belgaum, "The Internet of Things adoption in healthcare applications," in *2017 IEEE 3rd International Conference on Engineering Technologies and Social Sciences (ICETSS)*, 2017, pp. 1-5.
[13] K. Vani and R. R. Neeralagi, "IoT based health monitoring using fuzzy logic," *International Journal of Computational Intelligence Research*, vol. 13, pp. 2419-2429, 2017.
[14] A.H. Mary, Tolgay Kara, and A.H. Miry, "Inverse kinematics solution for robotic manipulators based on fuzzy logic and PD control," *Al-Sadiq International Conference on Multidisciplinary in IT and Communication Techniques Science and Applications*, IEEE, pp. 1-6, 2016.
[15] R. S. Krishnan, E. G. Julie, Y. H. Robinson, S. Raja, R. Kumar, and P. H. Thong, "Fuzzy Logic based Smart Irrigation System using Internet of Things," *Journal of Cleaner Production*, vol. 252, p. 119902, 2020.
[16] H. N. Saha, D. Paul, S. Chaudhury, S. Haldar, and R. Mukherjee, "Internet of Thing based healthcare monitoring system," *,IEEE Annual Information Technology, Electronics and Mobile Communication Conference (IEMCON)*, 2017, pp. 531-535.
[17] A. H. Miry, G. A.Aramice ," Water monitoring and analytic based ThingSpeak ", *International Journal of Electrical and Computer Engineering* , Vol. 10, No. 4, pp. 3588~3595 ,2020.

DOI: 10.37917/ijeee.sceeer.3rd.6 (15-16) June 2020

Open Access

Iraqi Journal for Electrical and Electronic Engineering
Conference Article

WSNs and IoT Their Challenges and applications for Healthcare and Agriculture: A Survey

Mohammed Mehdi Saleh
Education College – Qaim, University of Anbar, AL-Anbar, Iraq

Correspondence
*Mohammed Mehdi Saleh
Qaim, Anbar, Iraq
Email: mohammedmhedi@uoanbar.edu.iq

Abstract
Nowadays, the Wireless Sensor Network (WSN) has materialized its working areas, including environmental engineering, agriculture sector, industrial, business applications, military, intelligent buildings, etc. Sensor networks emerge as an attractive technology with great promise for the future. Indeed, issues remain to be resolved in the areas of coverage and deployment, scalability, service quality, size, energy consumption and security. The purpose of this paper is to present the integration of WSNs for IoT networks with the intention of exchanging information, applying security and configuration. These aspects are the challenges of network construction in which authentication, confidentiality, availability, integrity, network development. This review sheds some light on the potential integration challenges imposed by the integration of WSNs for IoT, which are reflected in the difference in traffic features.

KEYWORDS: IoT, Wireless sensor networks, Healthcare, Agricultural, Wireless Body Area Networks, Wireless Biomedical Sensors.

I. INTRODUCTION

The advancement in computer networks, wireless communication technology and microelectronic mechanical systems have allowed WSNs to be one of fastest growing technologies. WSNs have gained massive attention for their prospective applications in a different area such as surveillance, environmental monitoring, safety, health care, border and others [1]. WSNs use autonomous low-energy sensors which can monitor and track the environmental conditions surrounding them. Usually each sensor includes a power unit, a micro-controller, a wireless communication unit and a number of environmental sensors (i.e. humidity, pressure and temperature) [2]. In accordance with the latest ICT developments, WSNs for internet of things (IoT) can build ever more sophisticated, integrated infrastructure that can gathered and processed massive quantities of data [3]. These heterogeneous technologies, along with artificial intelligence technologies, could be used to set up the next generation disaster management systems. WSNs have an active role in the IoT, as they are the core building elements of the concept [4]. During this year, an approximate 50 billion devices are expected to connect to the network [5] and Most of them are fitted with sensors.

One of the primary advantages of WSNs is their ability to operate in harsh and uninhabited environments such as deserts, hills and war zones. Where deployment of sensors and human tracking of the networks in such areas is dangerous and often impossible [6]. This type of deployment increases costs or even energy consumption over all the network compared to manual deployment. This strategy needs huge numbers of sensor nodes to be deployed to cover the region required Sensor nodes have limited sensing, processing and communication capacities along with non-replaceable battery. Furthermore, in several applications, it is impossible to substitute the sensor nodes when stop functioning due to external environment or their power is totally exhausted [7],[8]. However, the imbalance in energy consumption still affects sensor performance efficiency.

The paper falls into six sections. Section one is an introductory one. The second section discusses the design challenges of WSNs. Section three discusses the security requirements in WSNs. While section four reviews hierarchical architecture of WSNs. In the fifth section, the researcher presents some potential applications and recent deployments. The last section concludes the whole paper.

II. DESIGN CHALLENGES OF WSNS

There are different challenges facing the design of WSNs. Most WSNs have different applications and application requirements that is why still not possible to handle all of the design challenges in a single network. Now let us bring up in detail some design challenges [9],[10],[11].

Scalability: Scalability is known as the capacity to support growing numbers of network users. Based on WSN applications, the number of sensors can reach one hundred thousand and sometime there is a need to increase or

decrease the number of sensors. A synchronization scheme should scale well with rising number of nodes and/or elevated network density. The system should support the addition of new sensors or devices at runtime, to adjust the system over time with increasing disabilities. Software platforms and distributed services will be needed to integrate hardware and application level seamlessly, and interoperability between them will be essential [12].

Fault tolerance: Sensor nodes are vulnerable to failure due to a variety of factors, such as environmental hazards, hardware issues, physical damage and energy loss. Therefore, WSN protocols should be able to identify errors to be corrected immediately to maintain WSNs running within the required limits.

Hardware constraints: The primary objective of the WSN designer is to produce small, active sensors that can be fitted with actuators and other components such as a global positioning system. Any additional characteristics increase the physical size of the sensor and the power usage. There needs to be a balance between hardware limitations and software development (algorithms and protocols) and the sensors need to be cheaper and more efficient. Designing and developing wearable sensors without unobtrusiveness is still a big obstacle for healthcare applications. As in the PATHS [13] sensor units, the need to integrate multiple sensors into one system makes it harder. Such wearable sensors are often heavy and highly obtrusive devices, so several publications study the integration of sensor devices with the fabric [14],[15]. In relation to the above, the sensitivity of sensor devices is especially significant when users wear sensors in harsh conditions such as fire or exercise situations. The sweat can negatively affect the action of the sensors, resulting in decreased sensitivity of the wearable sensors or requiring recalibration of the sensors. Et al.[16] proposes an automated triaxle accelerometer self-calibration algorithm.

Energy consumption: Energy is still the most serious design challenge for a WSN, as sensor nodes operate on a limited battery[17]. It is important that energy is used wisely and effectively to significantly extend the network's lifespan. The energy source could be replenished, in other instances, by solar and other means. Solar cells that can produce up to 15 mW / cm2 under direct sunlight, but cannot be used with wearable wireless sensors because sensors are preferred to be placed under clothing. Motion[18] and body heat[19] based energy scavenging techniques for healthcare systems should be studied for such applications. WSNs operate in harsh and uninhabited environments, making it difficult to replenish the power source, which could lead to the complete disposition of the sensor nodes [20]. The major cause of power consumption in sensor nodes can be allocated in three practical areas: sensing, communication, and processing, each requiring optimization.

III. SECURITY REQUIREMENTS IN WSNS

Data confidentiality, data integrity, data authentication, data availability and data refreshment are currently the security requirements of WSN explained below[21].

Data confidentiality: Typically, WSNs collect confidential data as required in military or healthcare applications. These deployed sensors require security aspects to keep the data secret from unauthorized parties as data confidentiality.

Data integrity: Data integrity is a fundamental requirement for accurate sensor data in WSN. Adversaries may alter the data during transmission, so that false or malicious data would result in incorrect decisions and potential financial losses. Data integrity ensures the user that the obtained data is not modified by the attacker during transit.

Data authentication: Authentication of origin and validity of data is critical in WSN. Some administrative responsibilities (e.g. modifying the network or monitoring the service cycle of sensor nodes) require authentication. The opponent may simply insert messages into the network so the receiver must be confident that the data used in every decision taking phase come from the right source. The authentication scenarios in WSN are as follows: First sensor node authentication guarantees the confidentiality and validity of the data gathered by the node. Then the user authentication ensures that only licensed users access data from the sensor node.

Data availability: WSN services should still be available all the time, especially in case of system upgrades, hardware failures, power outage disruptions or security attacks. Some research papers have proposed various solutions towards this goal. Some solutions include using additional node communication and the introduction of a central access control system to ensure efficient delivery of services to users.

Data freshness: Even in the case authentication and confidentiality are guaranteed, it is required to ensure that the data obtained is fresh and no attacker can retransmit old data. Data freshness is particularly important when using shared-keys to transmit data between WSN nodes.

IV. HIERARCHICAL ARCHITECTURE OF WSNS

WSNs consists of a number of tiny, cost-effective and low-power sensor nodes that are deployed manually or may be randomly in or very close to the phenomenon of interest. Sensor nodes continuously collect data, process and then transfer data to a base station (BS) named a sink, either through single-hop or multi-hop communications. The sensor node network configurations are done manually by network administrator or dynamically by dynamic routing protocol, depending on the route created [11]. Sensor nodes in WSNs are continually changing their locations during run time. Sensor nodes can change their positions during runtime and can leave and dynamically join the network, so it is a complex task to organize a communication scheme for them. Therefore, the clustering algorithms used to resolve the issue of organizing communication and provide organized communication methods for the unstructured WSN. It organizes the nodes into groups called as clusters, then assigns a cluster head (CH) for each group that performs data collecting and processing tasks for the whole cluster [11],[22].

In the hierarchical architecture, nodes with higher residual energy are assigned as CH, and low-energy nodes sense local

data and then send it to their corresponding CH. The CH will collect, process and transmit the data directly or through another CH to the BS [23],[24]. Figure 1 shows the cluster-based WSNs architecture with single-hop and multi-hop communication between CHs and BS [22]. CHs can manage bandwidth communication to avoid data redundancy when each node collects and transmits information because only CHs can communicate with other CHs and BS [18]. Data are aggregated at the CH to discard redundant and non-correlated data this reduces the energy consumption of the network by stopping the transmission of redundant data. Clustering reduces size of the table save at the nodes, makes it much easier to handle by localizing the route set up within the CH [11],[19]. However, the CHs can die quickly because of the additional workload. However, because of extra workload, CHs may die quickly. Several researchers had suggested using specific nodes called relay or gateways nodes. They act as CHs and had the same features and can be supplied with extra energy to extend their lifetime.

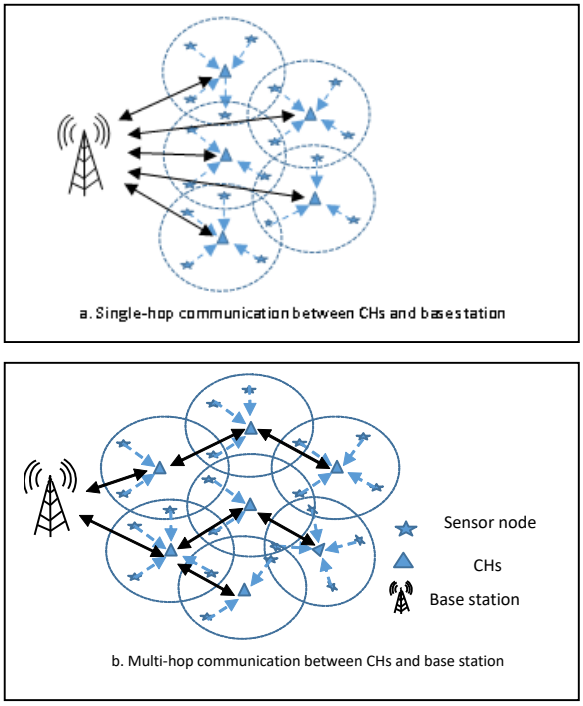

Fig. 1: Cluster-based WSNs architecture [22].

The small dashed arrows indicate the communication between the sensor nodes and their respective CHs, and the large arrows for communication between CH with CH or CHs with BS.

V. APPLICATION OF WIRELESS SENSOR NETWORK

A. *Agricultural applications*

Technologies such as WSNs for IoT leveraged growth and introduced more robots and artificial intelligence into agriculture[25]. Advancements in wireless communication, sensor network technology and massive data analytics software have created sensors more efficient. These sensors are low-cost, low-power, multi-functional, small in size and interact at short distances used in agriculture to maximize the returns with reduced cost[11]. Sensors collect data on physical attributes such as weather, crop, temperature, humidity and soil information. The data collected give farmers detailed guidance on planting, fertilizers, irrigation, safety, and harvesting. In addition, the data collected can promote the forecasting of the future state of the land and enhance management results by correctly evaluating and reacting to variability in each field [26]. It helps minimize the usage of fertilizers, soil, pesticides and fuel and lowers the cost of production [11], [25] .

In Greenhouses: Modern Greenhouse technologies are quickly being developed and expanded. The environmental conditions of the greenhouse have a direct impact on the growth of crops and it is important to track and control this type of environment in real time [27],[28]. In modern greenhouses the active use of environmental automatic control technologies is an appropriate way of enhancing the greenhouse control technologies. A WSN is a group of small sensing devices or nodes that collect data in a given location about climate elements such as light, temperature, carbon dioxide, and humidity [29]. Then, these nodes send the data gathered to the BS, which transmits the data to a central computer that analyzes and extracts meaningful information. This system will help farmers to effectively monitor climate change changes in real time through a network monitoring platform. Most greenhouse sensors would be designed within the standard limitations [27]. Table 1 shows some examples of wireless sensors and their characteristics used in real-time greenhouse monitoring systems.

TABLE1:
Examples of sensors used in greenhouse monitoring system and their characteristics.

Sensor	Types	Features			
		Range	Accuracy	Power consumption	Operating Temperature
Humidity	Global Water WE600 [30]	0 ~100 % RH	±2% RH	30mW	-10°C ~ 50°C
	CHS series [31]	5 ~ 95% RH	±5% RH	3.15mW	0°C ~ 50°C
	Durable [32]	0 ~ 95% RH	± 5%RH in -50°C, ± 2%RH in -25°C	4mW	0°C ~ 50°C
Temperature	Global Water WE600 [30]	-50 ~ +50° C	±0.1°C	40mW	-50°C ~100°C
	Durable [32]	0°C ~ 50°C	± 0.2°C in -25°C, ± 0.5°C in 50°C	4mW	-10°C ~ 50°C

The greenhouse climate-controlling model is developed by Pahuja et al., in 2013 and deployed in India [29]. This model measures and analyzes the environmental parameters for plant growth. For improvising and developing technology, they incorporated and integrated a system that automatically monitors, analyzes and solves issues related to their problems [29]. The intelligent monitoring system established by Liu et al. in 2016 to monitor grape planting in

the greenhouse [33]. They incorporated parameters which have a direct effect on grape growing. The system or process might be monitored online. Furthermore, each and every single development stage was captured by sensors using a video and image capturing technique. The data which was gathered via the sensors, provided an active database for further investigation and analysis [33],[29].

In the field: The rapid evolution of sensing and communication technologies has reduced agricultural cost considerably. Wireless sensors have been fully developed for intelligent, low power and low data rates sensors using in agriculture. Irrigation, pesticide management and fertilization are now regulated using WSNs provide real-time feedback between crops and local weather conditions to ensure secure crop growth and reduce the quantity of chemicals and water needed [34]. The sensors are inexpensive, allowing wide-ranging deployment and robust communication through redundant propagation paths for accurate information.

The Italian company Netsens has developed a new monitoring system called VineSense shown in figure 2(a) based on WSNs IoT technology [35]. The sensors deployed in the area are constantly monitoring and sending data measurements to the remote base station. Finally, end users analyze the received data through the VineSense web interface [35]. MeteoSense represents the fresh generation of professional weather stations developed by the Netsens company as shown in figure 2(b) [36]. Real-time information collected from sensors is transferred by using reliable GPRS technology. The MeteoSense is smaller, more economical, more robust, more fault-tolerant, easier to install and more energy efficient. It also uses a lithium battery that can operate up to 50 days without recharging and low power use of less than 1W while connected to GPRS [36].

a. Vinesense b. weather station (MeteoSense)

Fig. 2: weather stations for agriculture.

B. Healthcare

WSNs are used effectively in several prototypes and commercial applications for general health monitoring for the elderly, children and chronically ill. The major categories of health applications include activity monitoring, physiological monitoring, location monitoring, drug intake monitoring and medical status monitoring. Some of the existing WSNs applications and related proposals are included in Table 2.

Wireless Body Area Networks (WBANs): They are special wireless devices for healthcare systems[37]. WBANs Monitor the physical condition of the body then provide feedback via connectivity to patients or doctors. WBANs are primarily used to observe physiological parameters such as heartbeat, stress, oxygen, temperature and blood glucose monitoring [37]. A typical wireless body area network is showed in Figure 3 [38]. Health issues that may arise from diabetes include blood pressure, heart disease, stroke, blindness, kidney disease, and amputation. Wireless Biomedical Sensors (WBS) can be a more active way of treating diabetes by providing a more reliable and accurate glucose monitoring technique [37]. Wearable biosensors for IoT, are becoming highly interesting techniques that are commonly used to monitor changes in the body's biological data [39]. The main categories of biosensors are suitable for health, sport, military and other purposes. The rapid development of Wearable Biosensors offers advantages such as ease of use, low price and reliable real-time information which satisfies all clinical requirements [39]. Typically, wearable biosensors depend on wireless sensors that are included in bandage, bracelets and wearable products. The data collected by using these technologies are processed to identify occurrences predicting possible worsening of the clinical circumstances of the patient then send details to the patients or physicians through the wireless network[37],[40].

At-home Healthcare: When people age, they face a range of cognitive, physical and social changes that affect their health, independence and quality of life [41]. It is difficult to monitor and treat diseases such as diabetes, heart failure, congestive and asthma. WBANs address the social burden of aging populations and associated diseases. WSNs carried on or installed in human living areas can gather information on physiological patterns and behavioral conditions in real time and everywhere. From such living records, important conclusions can be made about the health of elderly [42].

TABLE 2:
Overview of WSNs applications for pervasive healthcare monitoring.

Category	Name	Hard ware design	Software design	GUI design	Sensing modality	Routing	Obtrusive	Context aware	machine learning	Loc. track.	RFID use
Activity monitoring	AICO[51]	Yes	Yes	Yes	Multi	Single	Low	High	Yes	yes	Passive
	Caregiver's Ast.[52]	No	Yes	Yes	Single	Single	Low	Medium	No	No	Passive
At-home Healthcare	ITALH [43]	Yes	No	Yes	Multi	Single	High	Medium	Yes	GPS	No
	HipGuard [45]	Yes	No	No	Multi	Single	High	High	No	No	No
Physiological monitoring	CodeBlue [46]	Yes	Yes	Yes	Multi	Multi	High	High	No	RF	No
	MEDiSN [47]	Yes	Yes	Yes	Multi	Multi	High	High	No	RF	No
	PATHS [13]	Yes	No	Yes	Multi	Single	High	Low	No	No	No

The IT for Home Assisted Living (ITALH) project [43] proposes the use of mobile phone-activated video camera only in emergency situations. In this system, the sensor node processor analyzes the accelerometer data in real time and identifies events such as falls or other common and abnormal events [44]. HipGuard [45] is a posture monitoring system designed for recovery durations of approximately 8 to 12 weeks after hip replacement surgery. The system has seven sensor nodes on the waist, thighs and shins edges that collect data and the processor analyzes them to monitor the condition of the hip [44].

Physiological monitoring: In physiological monitoring systems, WSN monitors and examines important human signs like respiratory rate, temperature, pulse oximetry [44]. WBANs can be deployed and applied in a variety of contexts, including disaster response, in-hospital patient surveillance and remote continuous monitoring for the elderly. Furthermore, technologies that automate clinical monitoring have the capability to enhance the healthcare quality in both the disaster and therapeutic environments [44]. Devices like the CodeBlue [46] and MEDiSN [47] target these application scenarios. Where, CodeBlue focuses on re-enhancing the process of triage during disasters with the help of WSNs comprising motes with IEEE 802.15.4 radios. CodeBlue integrated a variety of wearable health sensors such as ECG, oxygen saturation (SpO2) measurement and electromyography (EMG) pulse rate [48]. MEDIAN is used to enhance the monitoring process for hospitalized patients and disaster victims. MEDiAN has similar objectives to CodeBlue, but unlike the ad-hoc network used in Code Blue, MEDiUM utilizes a wireless backbone network of easily deployable relay points (RPs) [47]. The PATHS [13] is an ECG-measuring system that includes a wearable biosensor with two-axis accelerometer sensors, and a Bluetooth handheld device for collecting data from the wearable unit [44].

Activity Monitoring and Motion: The monitoring of activity levels and movement is another area of healthcare technology for WSNs. Wearable sensors can monitor limb movement and muscle function and are suitable for various clinical practice such as gait analysis activity classification, athletic performance [48],[42]. In the usual scenario, the patient wears up to eight gyroscopes and accelerometers (one on each limb segment) equipped with a micro-electromechanical system (MEMS) [49], [50]. The base station collects data from the network via a computer-class device in the patient's home.

The data analysis can be conducted to recover the patient's motor coordination and activity level, which is then used to monitor the patient response to treatment. In such tests, wearable sensor weight and size must be reduced to prevent encumbering the movement of a patient [53]. Lu and Fu [51]introduce an activity recognition approach with location-awareness by using various multi-modal and unobtrusive wireless sensors. Such wireless sensors are built into ambient intelligence-compliant objects (AICOs) which are ordinary household items protected by a virtual layer. Based on the data collected, AICOs generate explicit and implicit features empowered by location information and merge them generate more reliable estimates. The aim of the AICO project is to collect data naturally so they have prototyped the AICO floor, which collects data naturally in a way not altering the previous interaction [44]. The Caregiver's Assistant [52] is another behavior monitoring system which is built to monitor elderly people at home. The system works essentially by equipping different items in the user's home with RFID tags. Along with the Tag in the hand of the user, these tags help monitor what products they choose in real time. This system can be helpful for elderly with cognitive disabilities [44].

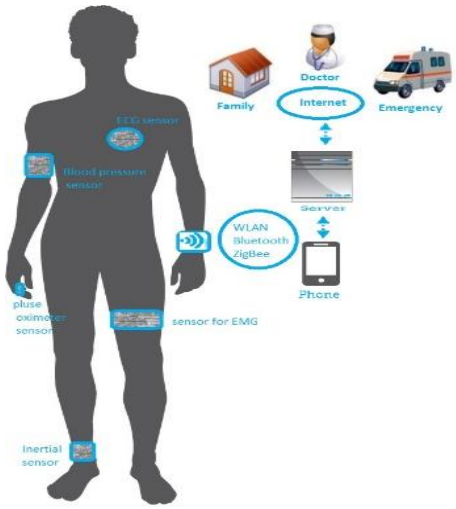

Fig. 3: Wearable Biosensors Network (WBS) architecture.

VI. Conclusion

The IoT smart sensors in healthcare applications allow the precise measurement, monitoring and analysis of a range of critical indicators of health status. This approach enables real-time access to patient health condition data and provides clinicians with feedback about the patient reaction to treatment. Concerning agriculture, water issues, irrigation methods and reducing the use of fertilizers, pesticides and fuel play a significant role in reducing cost of production. WSNs will help farmers by predict of the future state of the land and enhance management results by correctly evaluating and reacting to variability in each field. Despite the great promise of WSNs for the future, problems remain to be addressed in the areas of coverage and deployment, scalability, quality of service, size, energy consumption and security. This survey primarily identifies the different sides of WSNs for IoT and how IoT will be the main focus of future technologies. It also discusses the different problems which need to be resolved when using WSNs for IoT and security requirements. It also proposes a general overview of the WSNs for IoT technology and its various recent applications in agriculture and healthcare.

REFERENCES

[1] I. F. Akyildiz and M. Can Vuran, Wireless Sensor Networks. 2010.

[2] D. Chen, Z. Liu, L. Wang, M. Dou, J. Chen, and H. Li, "Natural disaster monitoring with wireless sensor networks: A case study of data-intensive applications upon low-cost scalable systems," Mob. Networks Appl., 2013, doi: 10.1007/s11036-013-0456-9.

[3] E. Asimakopoulou and N. Bessis, "Buildings and crowds: Forming smart cities for more effective disaster management," in Proceedings - 2011 5th International Conference on Innovative Mobile and Internet Services in Ubiquitous Computing, IMIS 2011, 2011, doi: 10.1109/IMIS.2011.129.

[4] M. Jacobsson and C. Orfanidis, "Using Software-defined Networking Principles for Wireless Sensor Networks," Proc. 11th Swedish Natl. Comput. Netw. Work. (SNCNW 2015) Karlstad, May 28-29, 2015, 2015.

[5] Cisco Systems, "Fog Computing and the Internet of Things: Extend the Cloud to Where the Things Are," Www.Cisco.Com, 2016.

[6] M. Rebai, M. Le Berre, H. Snoussi, F. Hnaien, and L. Khoukhi, "Sensor deployment optimization methods to achieve both coverage and connectivity in wireless sensor networks," Comput. Oper. Res., 2015, doi: 10.1016/j.cor.2014.11.002.

[7] G. Anastasi, M. Conti, M. Di Francesco, and A. Passarella, "Energy conservation in wireless sensor networks: A survey," Ad Hoc Networks, 2009, doi: 10.1016/j.adhoc.2008.06.003.

[8] E. Lattanzi, E. Regini, A. Acquaviva, and A. Bogliolo, "Energetic sustainability of routing algorithms for energy-harvesting wireless sensor networks," Comput. Commun., 2007, doi: 10.1016/j.comcom.2007.05.035.

[9] I. F. Akyildiz, W. Su, Y. Sankarasubramaniam, and E. Cayirci, "Wireless sensor networks: A survey," Comput. Networks, 2002, doi: 10.1016/S1389-1286(01)00302-4.

[10] M. Azharuddin, P. Kuila, P. K. Jana, and S. Thampi, "Energy efficient fault tolerant clustering and routing algorithms for wireless sensor networks," in Computers and Electrical Engineering, 2015, doi: 10.1016/j.compeleceng.2014.07.019.

[11] P. Kuila and P. K. Jana, "Energy efficient clustering and routing algorithms for wireless sensor networks: Particle swarm optimization approach," Eng. Appl. Artif. Intell., 2014, doi: 10.1016/j.engappai.2014.04.009.

[12] T. Gao, D. Greenspan, M. Welsh, R. R. Juang, and A. Alm, "Vital signs monitoring and patient tracking over a wireless network," in Annual International Conference of the IEEE Engineering in Medicine and Biology - Proceedings, 2005.

[13] Z. Li and G. Zhang, "A physical activities healthcare system based on wireless sensing technology," in Proceedings - 13th IEEE International Conference on Embedded and Real-Time Computing Systems and Applications, RTCSA 2007, 2007, doi: 10.1109/RTCSA.2007.10.

[14] R. Paradiso, G. Loriga, and N. Taccini, "A wearable health care system based on knitted integrated sensors," IEEE Trans. Inf. Technol. Biomed., 2005, doi: 10.1109/TITB.2005.854512.

[15] L. M. Borges, N. Barroca, F. J. Velez, and A. S. Lebres, "Smart-clothing wireless flex sensor belt network for foetal health monitoring," in 2009 3rd International Conference on Pervasive Computing Technologies for Healthcare - Pervasive Health 2009, PCTHealth 2009, 2009, doi: 10.4108/ICST.PERVASIVEHEALTH2009.6028.

[16] M. Gietzelt, K. H. Wolf, M. Marschollek, and R. Haux, "Automatic self-calibration of body worn triaxial-accelerometers for application in healthcare," in Proceedings of the 2nd International Conference on Pervasive Computing Technologies for Healthcare 2008, PervasiveHealth, 2008, doi: 10.1109/PCTHEALTH.2008.4571063.

[17] C. Gherbi, Z. Aliouat, and M. Benmohammed, "A survey on clustering routing protocols in wireless sensor networks," Sensor Review. 2017, doi: 10.1108/SR-06-2016-0104.

[18] M. Renaud, K. Karakaya, T. Sterken, P. Fiorini, C. Van Hoof, and R. Puers, "Fabrication, modelling and characterization of MEMS piezoelectric vibration harvesters," Sensors Actuators, A Phys., 2008, doi: 10.1016/j.sna.2007.11.005.

[19] V. Leonov, P. Fiorini, S. Sedky, T. Torfs, and C. Van Hoof, "Thermoelectric MEMS generators as a power supply for a body area network," in Digest of Technical Papers - International Conference on Solid State Sensors and Actuators and Microsystems, TRANSDUCERS '05, 2005, doi: 10.1109/SENSOR.2005.1496414.

[20] P. Baronti, P. Pillai, V. W. C. Chook, S. Chessa, A. Gotta, and Y. F. Hu, "Wireless sensor networks: A survey on the state of the art and the 802.15.4 and ZigBee standards," Computer Communications. 2007, doi: 10.1016/j.comcom.2006.12.020.

[21] A. Jain, K. Kant, and M. R. Tripathy, "Security solutions for wireless sensor networks," in Proceedings - 2012 2nd International Conference on Advanced Computing and Communication Technologies, ACCT 2012, 2012, doi: 10.1109/ACCT.2012.102.

[22] P. Kuila, S. K. Gupta, and P. K. Jana, "A novel evolutionary approach for load balanced clustering problem for wireless sensor networks," Swarm Evol. Comput., 2013, doi: 10.1016/j.swevo.2013.04.002.

[23] W. R. Heinzelman, A. Chandrakasan, and H. Balakrishnan, "Energy-efficient communication protocol for wireless microsensor networks," in Proceedings of the Hawaii International Conference on System Sciences, 2000, doi: 10.1109/hicss.2000.926982.

[24] V. Kumar, S. Jain, and S. Tiwari, "Energy Efficient Clustering Algorithms in Wireless Sensor Networks: A Survey.," Int. J. Comput. Sci. Issues, 2011.

[25] J. Gubbi, R. Buyya, S. Marusic, and M. Palaniswami, "Internet of Things (IoT): A vision, architectural elements, and future directions," Futur. Gener. Comput. Syst., 2013, doi: 10.1016/j.future.2013.01.010.

[26] O. Elijah, T. A. Rahman, I. Orikumhi, C. Y. Leow, and M. N. Hindia, "An Overview of Internet of Things (IoT) and Data Analytics in Agriculture: Benefits and

Challenges," IEEE Internet Things J., 2018, doi: 10.1109/JIOT.2018.2844296.
[27] D. Liu, X. Cao, C. Huang, and L. Ji, "Intelligent agriculture greenhouse environment monitoring system based on IOT technology," in Proceedings - 2015 International Conference on Intelligent Transportation, Big Data and Smart City, ICITBS 2015, 2016, doi: 10.1109/ICITBS.2015.126.
[28] Y. E. M. Hamouda and B. H. Y. Elhabil, "Precision Agriculture for Greenhouses Using a Wireless Sensor Network," in Proceedings - 2017 Palestinian International Conference on Information and Communication Technology, PICICT 2017, 2017, doi: 10.1109/PICICT.2017.20.
[29] R. Pahuja, H. K. Verma, and M. Uddin, "A wireless sensor network for greenhouse climate control," IEEE Pervasive Comput., 2013, doi: 10.1109/MPRV.2013.26.
[30] W. Measure and R. Humidity, "WE600-700-01 0213 Humidity & Temperature Sensors," pp. 1–2.
[31] H. Sensor, "Humidity Sensor CHS series Overview of the CHS series," no. June, 2016.
[32] Aosong, CM2301 temperature and humidity sensor. 2018.
[33] A. Ali, Y. Ming, S. Chakraborty, and S. Iram, "A comprehensive survey on real-time applications of WSN," Future Internet. 2017, doi: 10.3390/fi9040077.
[34] N. Wang, N. Zhang, and M. Wang, "Wireless sensors in agriculture and food industry - Recent development and future perspective," Computers and Electronics in Agriculture. 2006, doi: 10.1016/j.compag.2005.09.003.
[35] W. P. Iot, "the Iof2020 Use Case Architectures and Overview of the Related Iot Systems," no. 731884, pp. 1–221, 2020.
[36] K. F. Meteosense and M. Unit, "MeteoSense 2.0 main unit," pp. 1–3.
[37] S. Patel, H. Park, P. Bonato, L. Chan, and M. Rodgers, "A review of wearable sensors and systems with application in rehabilitation," Journal of NeuroEngineering and Rehabilitation. 2012, doi: 10.1186/1743-0003-9-21.
[38] J. Sun, Y. Fang, and X. Zhu, "Privacy and emergency response in e-healthcare leveraging wireless body sensor networks," IEEE Wirel. Commun., 2010, doi: 10.1109/MWC.2010.5416352.
[39] F. Firouzi et al., "Internet-of-Things and big data for smarter healthcare: From device to architecture, applications and analytics," Future Generation Computer Systems. 2018, doi: 10.1016/j.future.2017.09.016.
[40] Sensors in Medicine and Health Care. 2004.
[41] A. D. Wood et al., "Context-aware wireless sensor networks for assisted living and residential monitoring," IEEE Netw., 2008, doi: 10.1109/MNET.2008.4579768.
[42] A. Minaie, A. Sanati-Mehrizy, P. Sanati-Mehrizy, and R. Sanati-Mehrizy, "Application ofwireless sensor networks in health care system," in ASEE Annual Conference and Exposition, Conference Proceedings, 2013.
[43] T. R. Hansen, J. M. Eklund, J. Sprinkle, R. Bajcsy, and S. Sastry, "Using smart sensors and a camera phone to detect and verify the fall of elderly persons," Eur. Med. Biol. Eng. Conf., 2005, doi: 10.1.1.135.5331.
[44] H. Alemdar and C. Ersoy, "Wireless sensor networks for healthcare: A survey," Comput. Networks, 2010, doi: 10.1016/j.comnet.2010.05.003.
[45] P. Iso-Ketola, T. Karinsalo, and J. Vanhala, "HipGuard: A wearable measurement system for patients recovering from a hip operation," in Proceedings of the 2nd International Conference on Pervasive Computing Technologies for Healthcare 2008, PervasiveHealth, 2008, doi: 10.1109/PCTHEALTH.2008.4571068.
[46] D. Malan, T. Fulford-Jones, M. Welsh, and S. Moulton, "Codeblue: An ad hoc sensor network infrastructure for emergency medical care," … Implant. Body Sens. …, 2004.
[47] J. G. Ko et al., "MEDiSN: Medical emergency detection in sensor networks," in SenSys'08 - Proceedings of the 6th ACM Conference on Embedded Networked Sensor Systems, 2008, doi: 10.1145/1460412.1460452.
[48] B. R. Chen, K. K. Muniswamy-Reddy, and M. Welsh, "Ad-hoc multicast routing on resource-limited sensor nodes," in REALMAN 2006 - Proceedings of Second International Workshop on Multi-hop Ad Hoc Networks: from Theory to Reality, 2006, doi: 10.1145/1132983.1132998.
[49] J. W. Judy, "Microelectromechanical systems (MEMS): Fabrication, design and applications," Smart Mater. Struct., 2001, doi: 10.1088/0964-1726/10/6/301.
[50] M. Staples, K. Daniel, M. J. Cima, and R. Langer, "Application of micro- and nano-electromechanical devices to drug delivery," Pharmaceutical Research. 2006, doi: 10.1007/s11095-006-9906-4.
[51] C. H. Lu and L. C. Fu, "Robust location-aware activity recognition using wireless sensor network in an attentive home," IEEE Trans. Autom. Sci. Eng., 2009, doi: 10.1109/TASE.2009.2021981.
[52] M. Philipose, S. Consolvo, and I. Smith, "Fast, Detailed Inference of Diverse Daily Human Activities," 17th Annu. Symp. User Interface Softw. Technol., 2004.
[53] F. Michahelles and B. Schiele, "Sensing and monitoring professional skiers," IEEE Pervasive Computing. 2005, doi: 10.1109/MPRV.2005.66.

Open Access

Iraqi Journal for Electrical and Electronic Engineering
Conference Article

Robotics Path Planning Algorithms using Low-Cost IR Sensor

Israa Sabri A. AL-Forati *, Abdulmuttalib T. Rashid,
Electrical Engineering Department, University of Basrah, Basrah, Iraq

Correspondence
* Israa Sabri A. AL-Forati
Electrical Engineering Department,
University of Basrah, Basrah, Iraq.
Email: israa.subri.1@gmail.com

Abstract
A robot is a smart machine that can help people in their daily lives and keep everyone safe. the three general sequences to accomplish any robot task is mapping the environment, the localization, and the navigation (path planning with obstacle avoidance). Since the goal of the robot is to reach its target without colliding, the most important and challenging task of the mobile robot is the navigation. In this paper, the robot navigation problem is solved by proposed two algorithms using low-cost IR receiver sensors arranged as an array, and a robot has been equipped with one IR transmitter. Firstly, the shortest orientation algorithm is proposed, the robot direction is corrected at each step of movement depending on the angle calculation. secondly, an Active orientation algorithm is presented to solve the weakness in the preceding algorithm. A chain of the active sensors in the environment within the sensing range of the virtual path is activated to be scan through the robot movement. In each algorithm, the initial position of the robot is detected using the modified binary search algorithm, various stages are used to avoid obstacles through suitable equations focusing on finding the shortest and the safer path of the robot. Simulation results with multi-resolution environment explained the efficiency of the algorithms, they are compatible with the designed environment, it provides safe movements (without hitting obstacles) and a good system control performance. A Comparison table is also provided.

KEYWORDS: IR Sensors, obstacle avoidance, path planning Algorithms, Robotics.

I. INTRODUCTION

Robots are computer programmable devices that can automate certain actions. Much attention is paid to being able to replace a person with some tasks such as physical activity, decision making, and Special with the dangerous application. In the robotics field, one of the most important requirements is autonomous navigation. Robotic navigation is a strategic approach to the target position. this process includes four main components [1]: firstly is perception.it Extracts profit-related information via robots using sensors, the localization is the secondly, it is the process of locating the robot position in the employed environment; thirdly is the path planning, The robot achieves its goal by defining how to drive; finally is the motion control, The robot realizes the desired path by adjusting its movement. Nowadays, with the rapid increase in information technologies and multimedia facilities, localization and path planning techniques have improved greatly [2]. clearly in indoor environment, such as supermarkets, airport lobbies, exposition rooms, garages, etc. Robots are currently performing various tasks. The most basic requirement is localization technique. It is used to estimate the position and orientation of the robot depending on the environment and previous knowledge of the system such as the original position chart. Localization Techniques It is important because it is difficult to accomplish autonomous tasks without precise information about the location in an indoor environment. Path planning technique is defined as an organized sequence of transformation and alternation after the current position of the robot to the destination in the whole environment. however, there are two techniques: global and local path planning [3,4]. Typically, a global path developer creates a complex path that is built with low resolution on a specific environmental map on the other hand, the local path planning algorithm creates low-level paths and does not need to know the existing environment in advance based on the information obtained from the sensors. Works well in a dynamic environment range. However, this method is not suitable if the target location is identified. In general, mixing both approaches can remove some of their weaknesses and improve the benefits of mixing [5–7]. Robot systems can use sensors for communication, obstacle detection, distance measurement, etc. [8, 9]. Localization and path planning were the most important issues in choosing the right sensor for distance

measurement in an automaton system [10]. Sensors such as infrared sensors, laser scanners and ultrasonic can be prepared by mobile robots for telemetry. [11-13]. As an alternative to expensive sensors such as cameras and laser scanners, low cost sensors in many applications are used to determine distance [14-16]. However, not only the design of the distance diagram is required for localization; the identity of the source and recipient of the localization algorithms is required to estimate contract locations and depends on the communication between the nodes. Still the main challenge is to looking for cheap internal system sensors to achieve communication between nodes which are the infrared sensors [17]. Some types of sensors have been used for the localization and path planning systems, such as LRFs, WiFi positioning, the RFID, ultrasonic positioning, Bluetooth technology, vision sensors, an infrared IR transmitter and receiver, and VLC visible light communication technology. Although the hardware required Bluetooth [18, 19] and WiFi [20] it is simply combined into mobile policies, both Bluetooth localization Systems and WiFi are simply disturbed because interfering with extra signals disturbs their precision. LRF [21] positioning and Ultrasonic [22] systems have the benefit of high precision and simple system construction. Even now, the two categories of sensors are still unable to detect indoor mobile robots correctly when the robot is surrounded by certain influences. LRF is limited by the transparent walls in the environment and is used in indoor environments. An accurate localization can be obtained using an RFID radio frequency identification system with dense and IC tags [23] in a reasonable configuration. In this paper, two algorithms were proposed to solved the path planning system using low-cost IR sensors. First of all, the robot position is detected using the modified binary search algorithm then two algorithms where proposed: Shortest orientation algorithm and active orientation algorithm to move the robot safely from its original place over its trajectory to the target. The paper is ordered as follows: Section (II) path planning algorithms using IR sensor system, Simulation results are presented in section (III) To finish, in (IV) conclusions are conferred.

II. PATH PLANNING ALGORITHMS USING AN IR SYSTEM

This section introduces a proposed algorithm for indoor path planning structure built on the activation of IR receiver sensors that are regularly distributed in the work environment. These IR sensors are used to locate the robot's position through the robot moving towards the target. The robot's primary location is detected by scanning the environment using a modified binary search algorithm. Virtual trajectories represent the paths that a robot follows to scope a target. As a result, the IR receiver sensor within the detection range of the virtual orbit becomes active. The robot follows the trajectory represented by these activated IR sensors and scans only these activated IR receiver sensors to calculate the position at each step of the move.

A. *The Initial Position of The Mobile Robot*

The planned system consists of a 2-D environment with several holes distributed regularly. In Fig. 1, each hole is equipped with one IR receiver sensor. The IR sensors in this system arranged into two groups. The first represents one IR transmitter sensor equipped with the base of the mobile robot, and the second represents an array of IR receiver sensors of various sizes regularly placed in the environment. The central unit scans rows of IR receiver sensors row by row to identify signals from IR transmitters on the robot.

Fig. 1: Environment of (16*16) array of holes.

Only IR receiver sensors that are within range of the IR transmitter are identified. The identified sensors are then instantiated as a group and the centroid algorithm is used to detect the robot's position from the identified receiver sensor scene. The first localization process relies on scanning every column of the IR receiver array using a modified binary search algorithm. It works in logarithmic time, it is a simple calculator technique and can be improved. Search development is good at splitting a cluster many times. The search limited the exhibit to the lower part if the search volume value was less than the middle entry in the array. Others were limited to the higher parts. It will be checked continuously until the required number is encountered or the array is filled. At each stage of the algorithm procedure, the beginning and end of the last part of the array must be recalled. This calculation is multifaceted and depends on the logarithm of the exhibit size [24]. In this paper, the localization process relies on the use of a modified binary search algorithm to find the initial position of the mobile robot. The differences between the proposed algorithm and the binary search algorithm are summarized in the resulting steps.

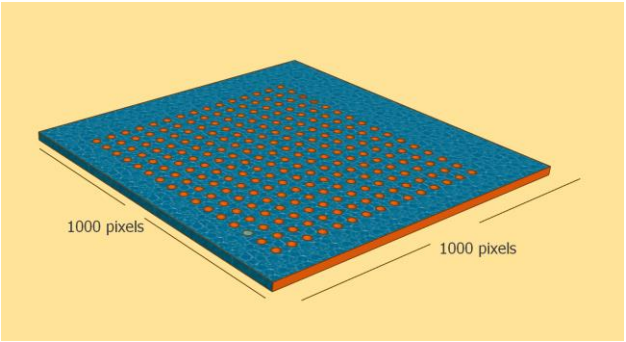

B. *The Modified Binary Search Algorithm*

In this paper, the localization process relies on the use of a modified binary search algorithm to find the initial position of the mobile robot. The differences between the proposed algorithm and the binary search algorithm are summarized in the resulting steps.

1) The Binary Search Algorithm: is built using decimal numbers, so the sort order is the first period of the algorithm. However, this system uses two logical principle states. One

is for the active IR receiver sensor, 0 is inactive. As a result, no sorting sequence is needed at this stage. The (Infrared sensor) IR receiver sensor is arranged in the 2D array; consequently, the matrix search algorithm is applied to each row and the column of this array.

2) In This Environment: several IR receiver sensors are used later and the search procedure is a convention for multiple values at once. Since the position of each IR receiver sensor is known, it can be used to estimate the position of the information robot, which consists of the robot IR transmitter sensor.

3) The Progress of the Localization Process: begins with a modified binary search algorithm, crossing the rows of the IR receiver sensor array. The IR receiver sensor symbolizes each column within the sensing range, one by one, plus zero. This technique is repeated until each IR is labeled. A sensor within the detection range with a value of 1. As a result, the information from the active IR receiver sensor is sent to the microcontroller to detect the robot's position.

C. *The Robot Orientation Estimation*

The robot's current orientation is very important for drawing the line follower path. To do that, the robot will take a step forward which is shown in Fig. 2, Use the modified binary search algorithm to compute the proposed location of the robot. By knowing the last and the current location we can estimate the robot orientation according to (1).

$$\Theta = \tan^{-1}((y_R^1 - y_R^o) / (x_R^1 - x_R^o)) \quad (1)$$

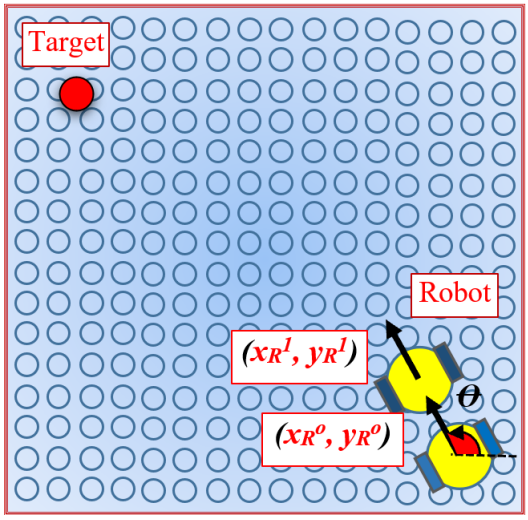

Fig. 2: Estimate the robot orientation.

Where Θ is the robot orientation. (xRo, yRo) is the coordinate axis for the robot at position o and (xR1, yR1) is the coordinate axis for the robot at position 1.

D. *The Robot Path Planning Algorithms*

This section proposed two algorithms for the robot path planning of the mobile robot toward the target.

1) *Shortest Orientation Algorithm*

This algorithm distinguishes the active IR receiver sensors that need to be scanned, estimates the robot's current position, calculates the direction of the straight line between the robot's and the target's position, and finally detected the direction of the straight line. The flow chart that describe the algorithm is shown in Fig.3.

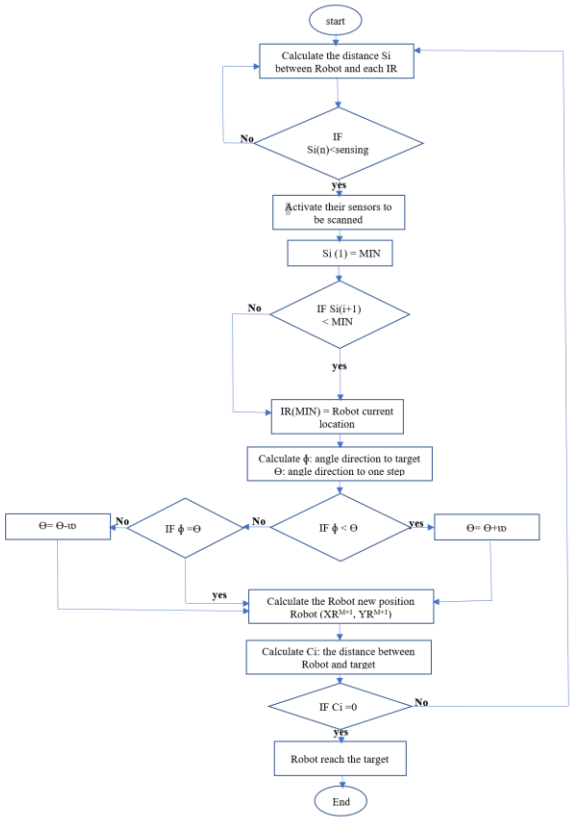

Fig. 3: The flow chart describes Shortest Orientation Algorithm

This algorithm requires some steps to compare with Robot orientation or adjustment to determine robot orientation. The following steps describe the robot orientation adjustment.

Step1: First, identify the active IR receiver sensor that needs to be scanned. This process is accomplished by measuring the distance between the robot's current position and the position of all IR receiver sensors using (2).

$$S_i = \text{Sqrt}((y_{ir}^N - y_R^M)^2 - (x_{ir}^N - x_R^M)^2) \quad (2)$$

Where Si is the distance between the IR sensor N and the robot at position M. (xirN, yirN) is the coordinate axis for the IR sensor N and (xRM, yRM) is the coordinate axis for the robot at position M. The IR sensor with distance less than it in the sensing range must be activated as shown in Fig. 4.

Step2: In this step, we need to estimate the current status of the mobile robot. This process is performed using a linear search algorithm. The algorithm may check the active infrared sensor and treat the nearest infrared sensor as a current position of the mobile robot that is shown in Fig. 5.

Step3: The orientation of the direct line between the current

location of the mobile robot and the target location must be computed using (3).

$$\phi = \tan^{-1}((y_g - y_R^M) / (x_g - x_R^M)) \quad (3)$$

Where ϕ is the direct line orientation between the target position and the robot in position j as shown in Fig. 6. (xg, yg) is the coordinate axis for the target.

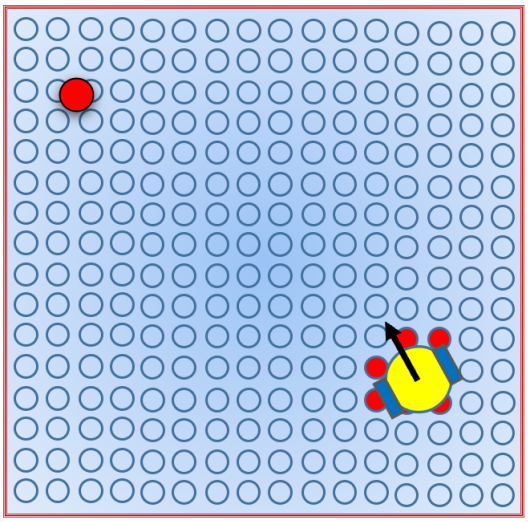

Fig. 4: Estimate the active IR receiver sensors.

Step4: This step is used to adjust the orientation of the mobile robot when it moves toward the target position. The adjustment depends on the comparison between the current orientation of the mobile robot and the direction of the path between the robot and the target locations. The decision of adjustment is dependent on (4) and (5).

$$\Theta = \Theta + \omega \quad \{ \Theta < \phi \} \quad (4)$$
$$\Theta = \Theta - \omega \quad \{ \Theta > \phi \} \quad (5)$$

where ω is the magnitude of changing in the direction of the robot at each step of the movement.

Step5: Dependent on the current position and orientation of the mobile robot, the next position is computed using (6) and (7).

$$x_R^{M+1} = x_R^{M+1} + L * \text{Cos}(\Theta) \quad (6)$$
$$y_R^{M+1} = y_R^{M+1} + L * \text{Sin}(\Theta) \quad (7)$$

Where L is the increment distance at each step of the robot movement. (xRM+1, yRM+1) is the coordinate axis of the mobile robot at the next movement.

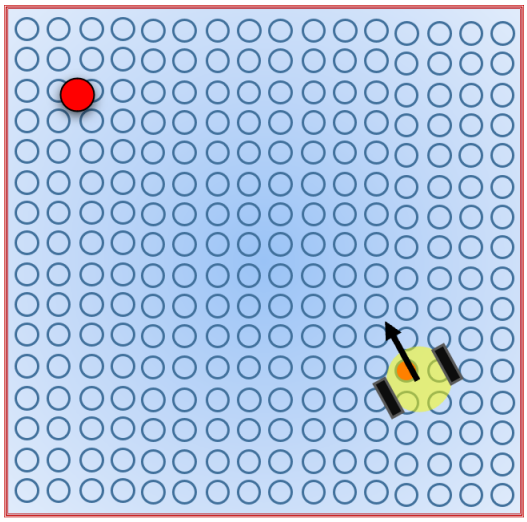

Fig. 5: Estimate the current location of the mobile robot.

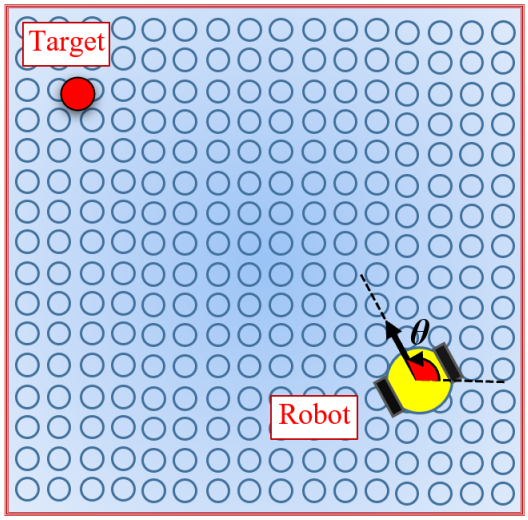

Fig. 6: The orientation of the direct path between the robot and the target.

Step6: In this step, the proposed orientation of the robot calculated in the previous section and the calculation of the next location (step 1) are repeated until the robot reaches the target. (8) is used for this proposal.

$$C_i = \text{Sqrt}((y_t - y_R^M)^2 - (x_t - x_R^M)^2) \quad (8)$$

Where Ci is the current distance between the robot and the target position.

2) Active Orientation Algorithm

This algorithm defines the phases for construction a virtual trajectory from the initial position to the destination for the mobile robot using the algorithm of a tangent visibility graph. The flow chart that describe the algorithm is shown in Fig.7.

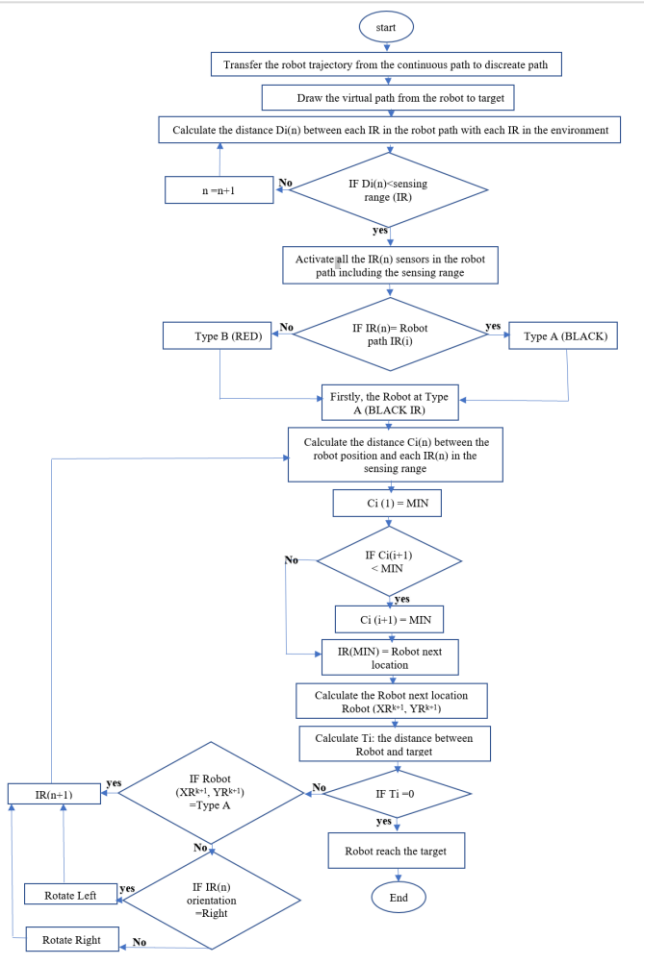

Fig. 7: The flow chart describes Active Orientation Algorithm

The process is summarized by searching for the shortest path for the mobile robot by assuming the shortest path between the robot trajectory path to the destination. The investigation of this method is characterized:

Step 1: First, the trajectory of the robot is transferred from the continuous path to the discrete path. This discrete path simplifies the process of distinguishing adjacent IR receiver sensors.

Step 2: Activate the IR receiver within the detection range of the individual arguments of the robot trajectory described in Fig.8. This process helps reduce localization time by reducing the number of IR receiver sensors that are scanned.

Step 3: classified two types of active infrared receiver sensors: The infrared sensor (black) on the robot path is marked as type A, and the infrared sensor (red) near the robot path is marked as type B. Fig. 9. This arrangement helps control the robot orientation during the moving process.

Step 4: At first, the robot location is at the first A-type IR receiver sensors. Use equation 1 to compute the orientation of the line between the first and the second A-type of IR sensors. If the orientation of this line is greater than the robot orientation then the robot orientation must be enlarged to its first step movement, else it must be decreased.

Step 5: At the current position, if the closeness active IR sensor is from A-type then the robot must repeat step one. If the closeness active IR sensor is from B type and located at the right side of the A-type active IR sensor that is shown in Fig. 10, the robot must turn left at it is next movement step else it must rotate right.

Step 6: Repeat Step one and step two until the robot scopes the target point.

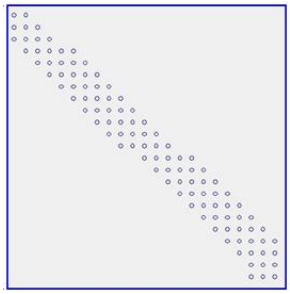

Fig. 8: Discretion the robot trajectory.

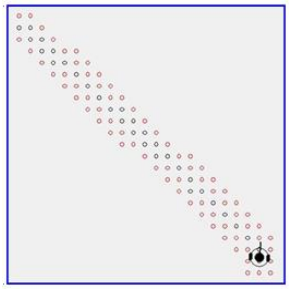

Fig. 9: Separate The active IR sensors into two types.

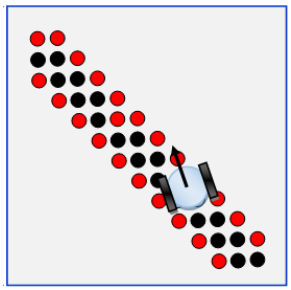

Fig. 10: Control the robot's orientation.

III. THE SIMULATION RESULTS

The proposed indoor path planning algorithms are simulated using the VB programming language. The simulated environment consists of various (8*8, 16*16, 32*32 and 64*64) IR receiver sensors with (1000*1000) pixels dimensions which distributed regularly in the environment, the first step in this procedure is to find the robot position by using the scan process using a proposed algorithm called the modified binary search algorithm.

A proposed path planning algorithm called the shortest orientation and the active orientation algorithms are used to determine the path planning from the robot source to the target location. An active IR receiver sensor are distinguished to reduce the processing time of localization proposed techniques. The simulations are repetitive for changed topologies illustrative a different robot position, by changing the dimensionally for the IR receiver sensors. The parameters used in this scheme are:

1) The Various Number of IR Receiver Sensors in the Environment.

2) The Execution Time (second) for the Robot to Reach the Target for Different Sensing Rang and Different Environments.

Table.1. shows the comparison in the path distance and the time of arrival between the active orientation algorithm and the shortest orientation algorithm, each of them wok in a multi-resolution environment without obstacle colliding their path.
the shortest orientation algorithm is the best because it has a minimum distance path with low arrival time in comparison with the active orientation algorithm through the path trajectory from source to target.Fig.11, and Fig. 12, shows the snapshot for robot path planning in a 32*32 Pixels environment using the shortest orientation and the active orientation algorithms. The goal of these simulations is to show the different path planning execution times in different types of environments.

TABLE I

PERFORMANCE COMPARISON WITH DIFFERENT TARGET LOCATIONS FOR BOTH THE ACTIVE ORIENTATION ALGORITHM AND THE SHORTEST ORIENTATION ALGORITHMS.

Target location (pixels)	active orientation algorithm		shortest orientation algorithm	
	The shortest path (Pixels)	Time of arrival (Sec)	The shortest path (Pixels)	Time of arrival (Sec)
(360,650)	279	2.741	253	2.013
(650,570)	503	5.533	430	4.21
(800,410)	634	7.32	520	5.442
(690,130)	598	6.617	407	5.79

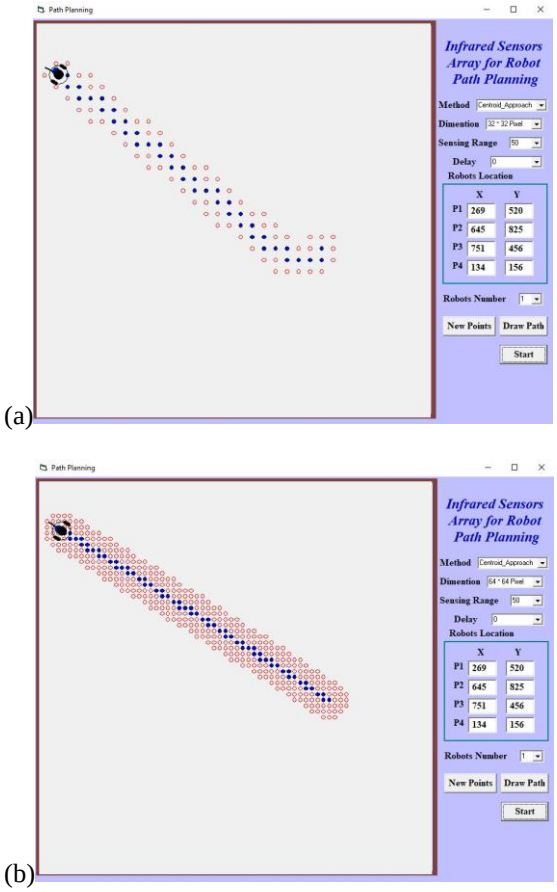

Fig. 11: Shortest orientation path planning algorithm in 32*32 and 64*64 Pixels

Fig. 13, shows the robot path planning comparison among different types of the environment and different path planning algorithms. The execution time is increased as the number of the IR sensors increase and also, the shortest orientation algorithm has less execution time than the other algorithm. the second simulation shown in Fig. 14, and Fig. 15, shows the complete robot path planning for different dimensional environments. Fig. 16, shows that the (64*64) IR sensors environment produces a more accurate path planning than the other types of the environment. Also, the shortest orientation algorithm has more accuracy than the other algorithm.

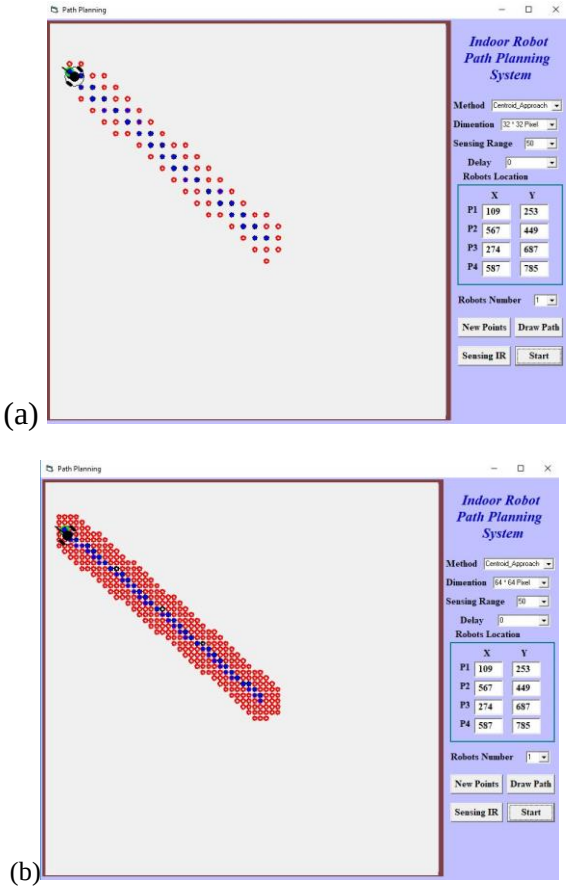

Fig. 12: Active orientation path planning algorithm in 32*32 and 64*64 Pixels environment.

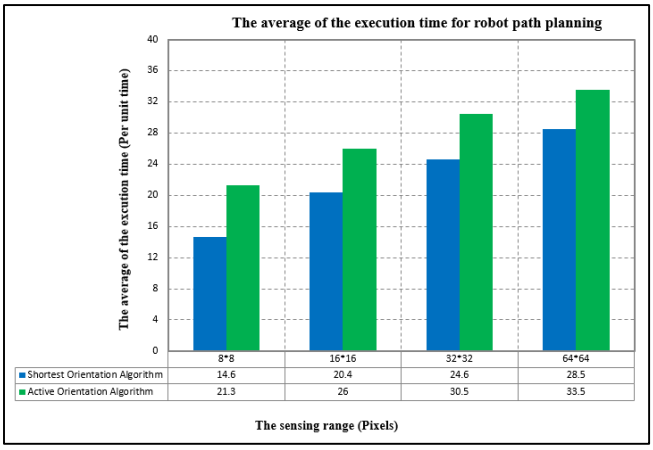

Fig. 13: The execution time comparison for different environments.

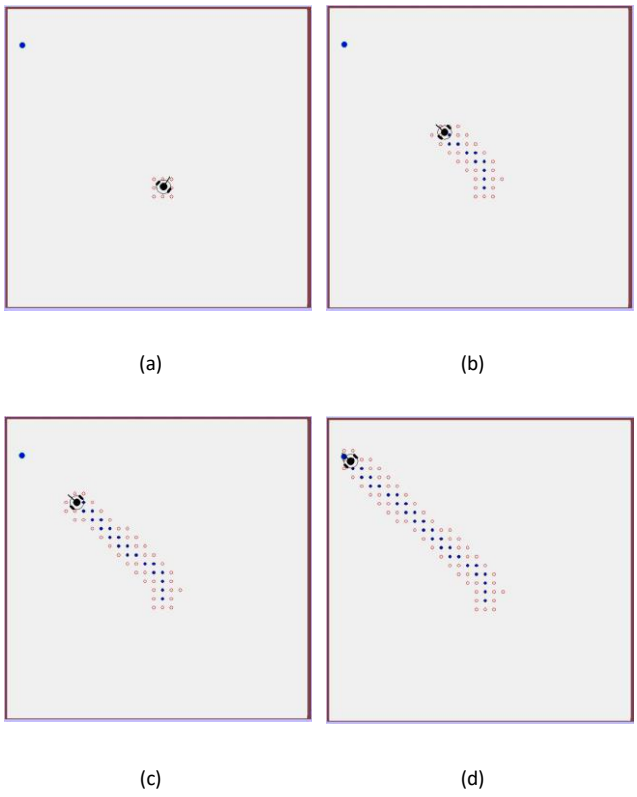

Fig. 14: The snapshot for the shortest orientation path planning algorithm.

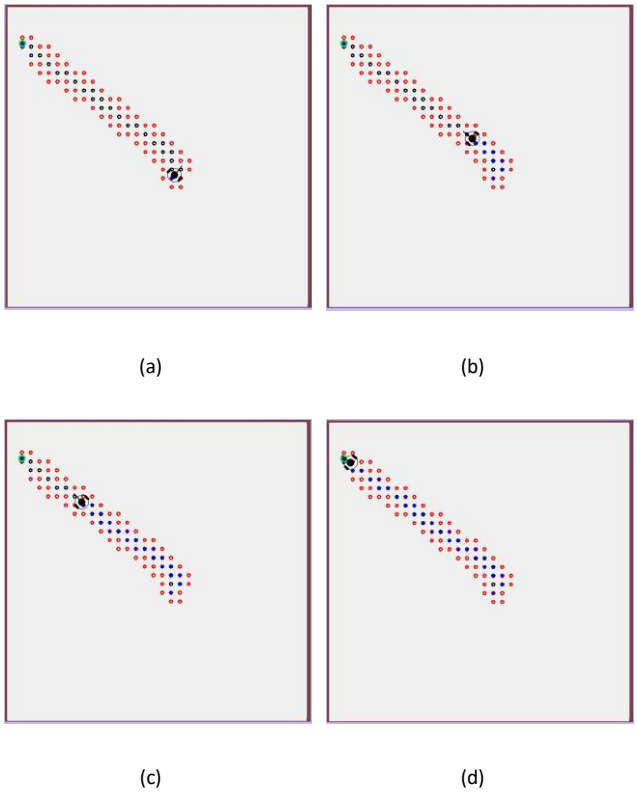

Fig. 15: The snapshot for active orientation path planning algorithm.

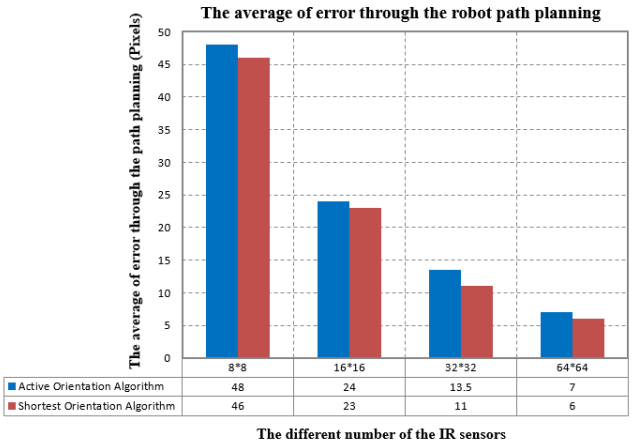

Fig. 16: The average of the error comparison between the shortest orientation and the active orientation algorithm.

IV Conclusion

This paper proposed a new technology using low-cost transmitters and receivers for path planning of an internal mobile robot system. The IR transmitter is installed on the robot and the IR receivers are uniformly distributed in the environment in various dimensions. Two simulation results are discussed in this paper: The execution time for the path planning and the error estimation through the path planning process. Table of comparison also applied. In general, the results show that as the sensing range of the IR receive sensor increased, the execution time is increased and when the dimension of the environment increases the execution time also increases. This happens because the larger number of IR sensors means higher computation time. The second simulation results show that as the IR receiver sensing range rises the average of estimated error is reduced. Also, increasing the dimensional of the environment leads to increase the accuracy in path planning. furthermore, the shortest orientation algorithm is the best in comparison with the active orientation algorithm, which has less execution time and less average errors in a different environment during the robot simulation.

References

[1] Siegwart and I.R. Nourbakhsh, "Introduction to Autonomous Mobile Robot," Massachusetts Institute of Technology Press, *Cambridge*, USA, Vol. 1, pp. 13-36, 2004.

[2] Y. GU, A .Lo, S. Member, and I. Niemegeers, "A Survey of Indoor Positioning Systems for Wireless Personal Networks," *IEEE Communications Surveys & Tutorials*, Vol. 11, No. 1, pp. 13 – 32, 2009.

[3] Y.Q. Qin, D.B. Sun, N. Li, Y.G. Cen, "Path planning for mobile robot using the particle swarm optimization with mutation operator," In Proceedings of the international conference on machine learning and cybernetics (*IEEE Cat*. No. 04EX826), Shanghai, China, Vol. 4, pp. 2473-2478, 2004.

[4] I. S. Alfurati and Abdulmuttalib T. Rashid, "Shortest Distance Orientation Algorithm for Robot Path Planning using Low-Cost IR Sensor System," . Proc. of the 2nd *International Conference on Electrical, Communication and Computer Engineering* (ICECCE) 14-15 April 2020, Istanbul, Turkey, inpress.

[5] H. Zhang, J. Butzke, and M. Likhachev, "Combining global and local planning with guarantees on the completeness," *International Conference on Robotics and Automation*, USA, pp. 4500–4506, 2012.

[6] I. S. Alfurati and Abdulmuttalib T. Rashid, "An Efficient Mathematical Approach for an Indoor Robot Localization System," *Iraqi Journal of Electrical and Electronic Engineering*, vol. 15, Issue 2, pp. 61-70, 2019.

[7] Z. Bi, Y. Yimin and Y. Wei, "Hierarchical path planning approach for mobile robot navigation under the dynamic environment," *6th International Conference on Industrial Informatics*, Korea, pp. 372–376, 2008.

[8] F. Wu, and J. Williams, "Design and implementation of a multi-sensor based object detecting and removing autonomous robot exploration system," *Journal of Computer and Communications*, vol. 2, pp. 8-16, 2014.

[9] S. Rathod, V. Bansal, and K. T. Patil, "Real-time speed based obstacle detection with path planning," *International Journal of Advance Foundation and Research in Science & Engineering*, vol. 2, no.10, pp. 32- 41, 2016.

[10] J. I. Bangash, A. Abdullah, and A. Khan, "Issues and challenges in localization of wireless sensor networks," Sci.Int (Lahore), pp. 595-603, 2014.

[11] I. S. Alfurati and Abdulmuttalib T. Rashid, "Performance Comparison of Three Types of Sensor Matrices for Indoor Multi-Robot Localization," *International Journal of Computer Applications* (0975 – 8887), vol.181, Issue 26, pp. 22-29, 2018.

[12] O. A. Hasan, R. S. Ali, A. T. Rashid, "Centralized approach for multi-node localization and identification," *Iraq J. Electrical and Electronic Engineering*, vol.12, no 2, pp. 178-187, 2016.

[13] I. S. Alfurati and Abdulmuttalib T. Rashid, "Practical Implementation of an Indoor Robot Localization and Identification System using an Array of Anchor Nodes," *Iraqi Journal of Electrical and Electronic Engineering*, DOI: 10.37917/ijeee.16.1.2.

[14] J. Guivant, E. Nebot, and S. Baiker, "Localization and map building using laser range sensors in outdoor applications," *Journal of Robotic Systems*, vol.17, no.10, pp. 565-583, 2000.

[15] R. J. Guivant, F. Masson, and E. Nebot, " Simultaneous localization and map building using natural features and absolute information," *Robotics and Autonomous Systems*, vol.40, pp. 79–90, 2002.

[16] I. S. Alfurati and Abdulmuttalib T. Rashid, "Multi-Robot localization system using an array of LEDs and LDR sensors," *International Journal of Computer Applications* (0975 – 8887), Vol. 176, no. 10, April 2020.

[17] V. Jungnickel, V. Pohl, S. Nönnig, and C. V. Helmolt, "A Physical Model of the Wireless Infrared

Communication Channel," *IEEE Journal On Selected Areas In Communications,* vol. 20, no. 3, pp.159-209, 2002.

[18] C. Galvan, I. G. Tejada, and R. Brena, "Wifi Bluetooth based combined positioning algorithm," *Procedia Engineering* 35, pp.101–108, 2012.

[19] Raghavan AN, Ananthapadmanaban H, Sivamurugan MS, Ravindran B, "Accurate mobile robot localization in indoor environments using Bluetooth," *International conference on robotics and automation,* pp 4391–4396, 2010.

[20] G. Jekabsons, and V. Kairish, "An analysis of wi-fi based indoor positioning accuracy," *Appl Comput Syst*., vol. 44, pp.131–137, 2011.

[21] G. Cho SH and Hong S, "Map-based indoor robot navigation and localization using a laser range finder," *11th international conference on control automation robotics vision,* pp 1559–1564, 2010.

[22] Yayan U, Yucel H, and Yazıcı A, "A low cost ultrasonic based positioning system for the indoor navigation of mobile robots," *J Intell Robot Syst*., vol. 78, no. 3, pp. 541–552, 2015.

[23] G. Mi J and Takahashi Y, "Performance analysis of mobile robot self-localization based on different configurations of the RFID system," *International conference on advanced intelligent mechatronics* (AIM), Busan, Korea, pp 1591–1596, July 2015.

[24] I. S. Alfurati and Abdulmuttalib T. Rashid, "Design and Implementation an Indoor Robot Localization System Using Minimum Bounded Circle Algorithm," The 8th *International Conference on Modeling, Simulation and Applied Optimization* (ICMSAO'2019), 2019.

Open Access
Iraqi Journal for Electrical and Electronic Engineering
Conference Article

Two Algorithms For Static Polygon Shape Formation Control

Bayadir A. Issa*, Abdulmuttalib T. Rashid
Electrical Engineering Department, University of Basrah, Basrah, Iraq

Correspondence
*Bayadir A. Issa
Electrical Engineering Department,
University of Basrah, Basrah, Iraq
Email: bayader.phd@gmail.com

Abstract
This paper provides a two algorithms for designing robust formation control of multiple robots called Leader- Neighbor algorithm and Neighbor-Leader algorithm in unknown environment. The main function of the robot group is to use the RP lidar sensor attached to each robot to form a static geometric polygon. The algorithms consist of two phases implemented to investigate the formation of polygon shape. In the leading- neighbor algorithm, the first stage is the leader alignment and the adjacent alignment is the second stage. The first step uses the information gathered by the main RP Lidar sensor to determine and compute the direction of each adjacent robot. The adjacent RP Lidar sensors are used to align the adjacent robots of the leader by transferring these adjacent robots to the leader. By performing this stage, the neighboring robots will be far from the leader. The second stage uses the information gathered by adjacent RP sensors to reposition the robots so that the distance between them is equal. On the other hand, in the neighbor-leader algorithm, the adjacent robots are rearranged in a regular distribution by moving in a circular path around the leader, with equal angles between each of the two neighbor robots. A new distribution will be generated in this paper by using one leader and four adjacent robots to approve the suggested leader neighbor algorithm and neighbor-leader algorithm .

KEYWORDS: Mobile robot, RP lidar sensor, polygon shape formation, leader- neighbor.

I INTRODUCTION

Mobile robots formation control has many applications such as transportation, observation and search tasks. Therefore, it has been considered by many researchers [1-5]. Formation control means the problem of maintaining the relative position and orientation of robots in a cluster while at the same time enabling the cluster to travel in general. The utilization of formation control allows one to accomplish complex missions as every specific task can be achieved in one robot navigation [6,7]. Fundamental formation control issue includes maintaining required geometric movements of adjusting shapes and sizes such as triangular, square, polygon or section. Numerous types of control methods have been proposed to control the formation such as support issues [8, 9] including a virtual-structure approach, behavior-based approaches, and Leader-follower approaches [10]. Behavior based approach is decentralized control method used to control one or more robots in a group; note that the decentralized control method means there is no planning or reasoning to generate the responses [11-13]. Means there is no central part mange the system. So, its implemented with less communication, behavior based approach make the robots drive the controls for multiple computing objects at the same time. Also, in behavior based approach several states are prescribed for each robot and the final control is derived from a weighting of relative importance of each state [14-16]. In virtual structure approach the entire formation is regarded as a single structure where each robot is given a set of control to follow the desired trajectory of formation as rigid body. The main advantages of this approach is that a single mathematical rule translate the entire sensory input space into the actuator output space without the need of multiple rules or behaviors [17]. While the leader-follower methodology is that one robot goes about as a leader whose movement characterizes the way for the whole gathering. All follower robots will utilize the characterized way to accomplish a specific objective or to accomplish a characterized task. Follower robots should situate themselves as per the position and direction of the leader[18]. By and large, a few sorts of methodologies are presented in the writing for keeping up formation dependent on the leader-follower approach. The followers ought to keep up an ideal relative posture concerning the facilitate outline fixed on the leader and now and again, it is essential for every robots to pursue more than single guided robot to accomplish a particular formation along these lines, high correspondence cost is required. The authors in [19] have suggested a Leader-follower formation that is implemented based on the relative

movement states to shape and preserve the formation of multi-robots. The main idea of this strategy is to locate an objective and accurate speed to change the robot's present state. In [20], a virtual leader-follower technique and potential capacities for the formation control and hindrance shirking issue for multi-robot systems. Moreover, in [21] self-ruling ground vehicles have been intended with the end goal that depends on running and bearing data that has been obtained from a forward-looking camera on the Formation control. A visual direction control calculation is planned where continuous picture preparing is utilized to give input signals.

The goal of this paper is to provide a simple explanation of low-cost high accuracy formation control algorithms for a multi-robot system, suitable for unknown areas called leader-neighbor algorithm and neighboring of the leader algorithm. In which a single leader robot controls the formation of the neighbors robots which they are neighbors to it and distributed randomly in unknown environments. The Simulation of navigation multi mobile robots in unknown environments is done by using Visual Basic language. Simulation results show that the mobile robots follows the shortest path and reaches the target. The leader robot localize the other robots by obtaining the lidar signals of each robot and then controlling the distance between each two neighbor robots to obtain a static polygon shape formation. We consider one leader robot and four follower robots each of which is equipped with one RP lidar sensor. The proposed algorithms is described in Section II and III. Simulations results are explained in Section IV. and the conclusions are discussed finally.

II PROPOSED LEADER NEIGHBOR ALGORITHMS

A. *Leader-neighbor algorithm*

Typically, control over the formation algorithm expects configurable robots to access ideal grading data. In multi-robot systems where it is important to maintain the shape of the formation, the required shape strength will only demonstrate the formation of the group if the neighboring robots have sensors that are perfectly tuned. The leader-follower formation leads to a directed topology that describes the relationships between neighboring robots and analyzes the main characteristics of formation control algorithms such as stability, gravity, and proximity time. When analyzing the distribution of responsibilities between adjacent robots, we find that increasing the number of robots in the team requires additional costs to coordinate all sensor pairs of neighboring robots. This section introduces a new algorithm that controls the formation of multiple robots called the Leader-Neighbor algorithm. This method uses a distance-based algorithm in which the distances between the robots are actively constrained and fixed, and they can be considered recorded together, so the robots are transformed, localized and directed by previous robots. It is imposed in an environment and determines the distance between them. In addition, the next robot direction is restricted according to the rotation of the leader. The investigations of the leader-neighbor algorithm explained in the following steps:

Step1: Leader's alignment stage:

Firstly, in this stage, the robots are distributed randomly. The coordinate axis and the orientation are computed for each robot with respect to the leader one. This posture information can be obtained from the RP lidar sensor which is equipped on each robot. The leader RP lidar sensor will give the orientation and distance information of each robot with respect to the leader position and orientation.

Step2: Circular path drawing for leader's alignment:

In this step we use the orientation of the neighbor robots with respect to the leader one and their orientation to draw the first circular path as described below and shown in Fig1. The neighbors robots scan the environment using their RP lidar sensors and compute their new orientation with respect to the leader one according to the following conditions

If $0 < u_i \leq \pi$ then,

$$u_i = u_i - j \quad (1)$$

Else if $\pi < u_i \leq 2\pi$ then,

$$u_i = u_i - j \quad (2)$$

-End if.

Step3: Neighbor's alignment stage:

Neighboring robots are placed in uneven circular tracks in the distance around the leader robot. Initially, a uniform distribution is achieved by changing the direction of the neighboring robots. Then, these robots have to move in a circular path until they are evenly distributed.

Step4: Rearranged the distances among the neighbor robots: A uniform formation of adjacent robots occurs when the angle between any two adjacent robots in relation to the leading robot is the same value. This process is accomplished by calculating the angle ρ between each two adjacent robots and with respect to the leader.

$$\rho = 2\pi / n \quad (3)$$

$$\gamma_i = \tan\text{-}1((y_i - y_o) / (x_i - x_o)) \quad (4)$$

where n is the number of the neighbor robots.

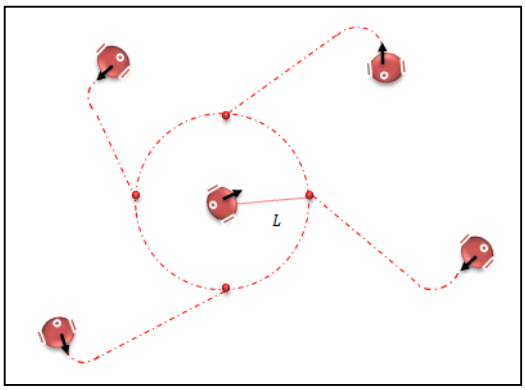

Fig.1 The leader's alignment by the neighbor robots.

Step5: Rearranged the angles between the neighbor robots and the leader one in ascending manner by:

1- Compute the orientation angle between each two neighbor robots.

$$\vartheta_i = \gamma_i + 1 - \gamma_i \quad (5)$$

where ϑ_i is the angle between the robots i and i+1.

2- If the angle ϑ_i is less than the angle ρ then increase the angle γ_i.

$$\gamma_i = \gamma_i + j \quad (6)$$

3- Compute the new position of neighbor robot i.

$$x_{i+1}=x_i+ m*\cos(\gamma_i) \quad (7)$$

$$y_{i+1} = y_i + m*\sin(\gamma_i) \quad (8)$$

4- Repeat for current neighbor robot and for all robots until all the angles between the neighbor robots and the leader one are equal and have the value ρ.

5- Compute the new orientation for the neighbor i and the new position of the neighbor robot i

$$\beta_i = \pi\text{-}u_i + \varphi i \quad (9)$$

$$x_{i+1}=x_i + m*\cos(\beta_i) \quad (10)$$

$$y_{i+1}= y_i + m * \sin(\beta_i) \quad (11)$$

6- Repeat 1, 2 and 3 until $R_i = L$ as shown in Fig. 2. Where L represents the formation distance between the neighbors robots and the leader. Where the distance Ri must be computed from the following equation.

$$R_i= \text{sqrt}((y_i - y_o)2+(x_i- x_o)^2) \quad (12)$$

Where j is the increment angle at each step that taken by the robot to reach to the target point. Fig.3 shows the uniform formation of the neighbor robots.

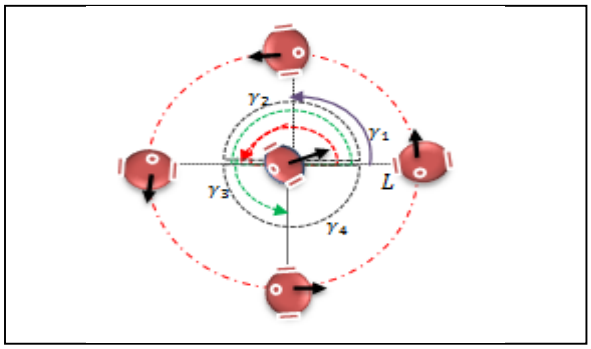

Fig2. neighbor robot i with respect to the leader one.

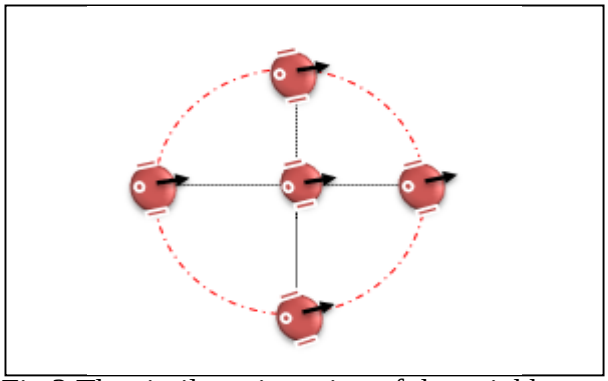

Fig.3 The similar orientation of the neighbor robots with leader.

B. Neighboring of leader algorithm

This section introduces the neighboring of leader algorithm to form a static polygon shape formation. This algorithm is used to predict the paths of neighboring robots depending on the leader's location. It takes into account the monitoring location of the mobile leader robot. First, the positions and orientations of adjacent robots are calculated according to the position of the leader, and in each step of the neighboring robots, the length of the move step increases by a factor (l) until the distance between the neighboring robots equal to the radius of the circle around which the target of each robot around the leader will form a static polygon.

III SIMULATION RESULTS

The new two algorithms (leader–neighbor and neighboring of leader) are simulated to investigate the formation of multi mobile robots using visual basic programming language and tested in Windows environment using an Intel core i5. The different strategies of polygon shape formation are simulated by considering the effect of the connectivity between the neighbor robots and the leader one. Two types of the simulations are implemented on different distribution representing different number of neighbor robots (n) ranging from 3 to 7 robots. The robots were randomly placed on a 500x500 pixels area. For a measureable analysis of this algorithm, we used the following performance metrics:

1. Number of neighbors robots (n): this metric is used to measure the time required to complete the static polygon formation when increasing the number of robots.
2. The formation completing time (t): this metric is used to measure the percentage of the completing time with respect to the number of the neighbor robots.

Fig. 4 (a)–(d) represent the Screenshots of the simulation at different time steps. Fig.4.d represents the final static formation shape in global knowledge environment. The main goal of this simulation is to show the relation between the number of robots and the accomplishment percentage. Fig. 5 shows the second simulation strategy which implemented on different number of neighbor robots (3 to 7 robots) as shown in fig 6,7,8. Fig. 8 shows the comparison between the number of the neighbor robots and the accomplishment percentage. As the number of the robots increase in the environment, the accomplishment percentage is increase. The purpose of these simulation is to compute the time required to complete the formation for different number of neighbor robots. From Fig. 9 we found that as the number of the neighbor robots increase the execution time is increase.

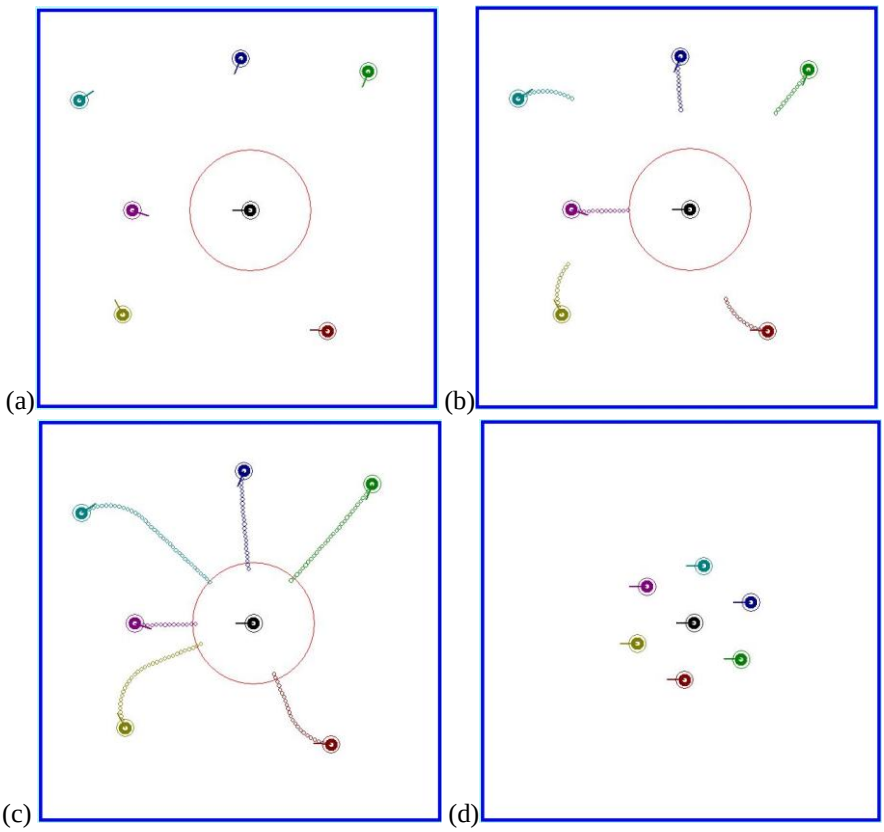

Fig.4 The formation of the robots. (a-d) Screenshots at different time steps using leader-neighbor algorithm.

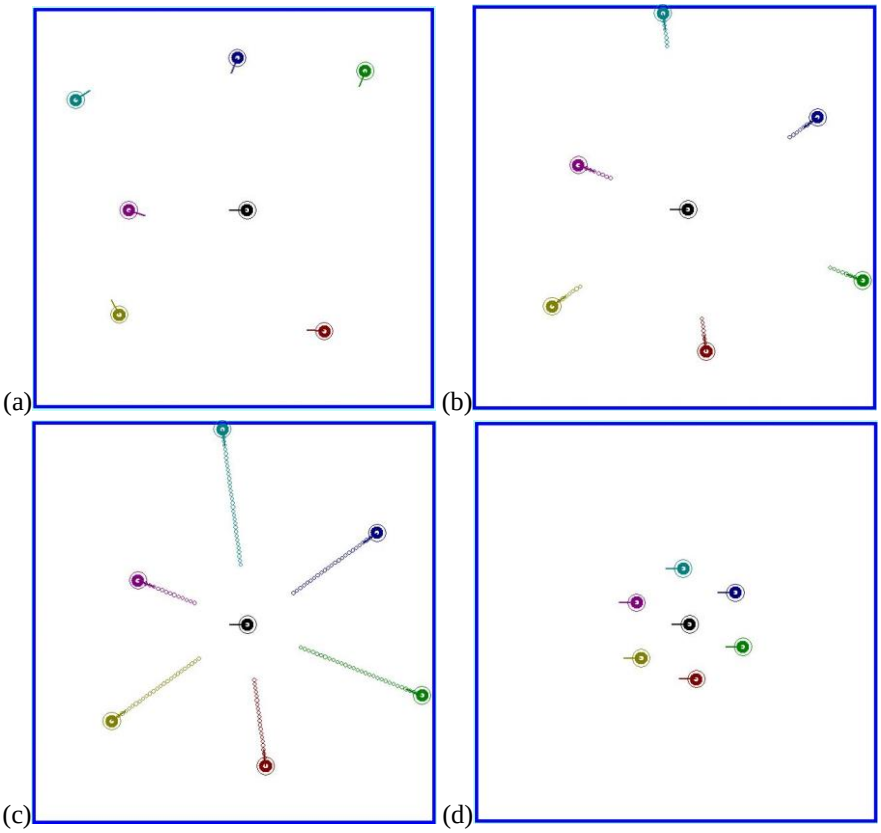

Fig.5 The formation of the robots. (a-d) Screenshots at different time steps using the neighbor-leader algorithm.

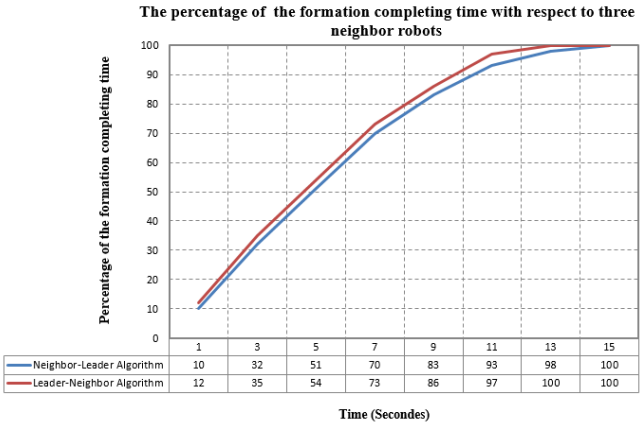

Fig. 6 Polygon formation for three neighbor robots.

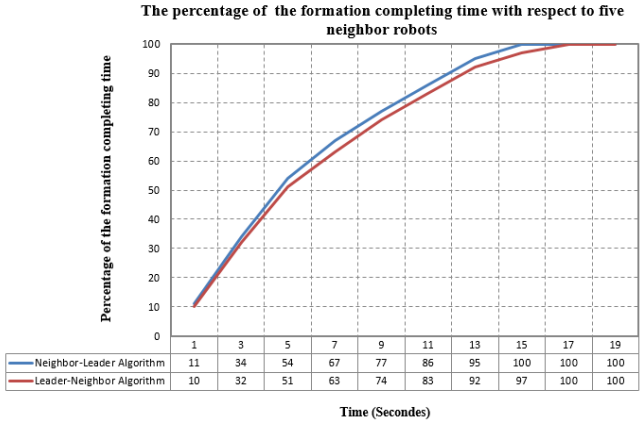

Fig. 7 Polygon formation for five neighbor robots.

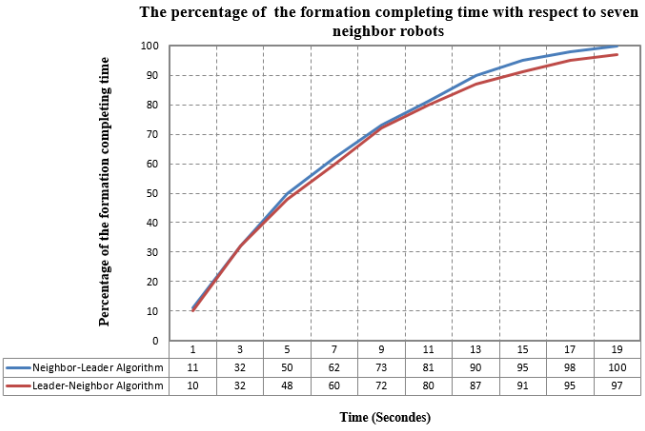

Fig. 8 Polygon formation for seven neighbor robots.

IV CONCLUSIONS

In this paper, two novel algorithms are proposed to control the a static polygon shape formation in an unknown environment called leader neighbor algorithm and neighboring of the leader algorithm by using several numbers of mobile robots localized and distributed randomly. Simulation results are implemented in an environment with a different number (3 to 7) of robots. The results show that the algorithm have a better efficiency to complete the formation. From results we found that the accomplishment percentage is increases as the number of the neighbor robots increase. Also, as the number of the robots increase the execution time is increase.

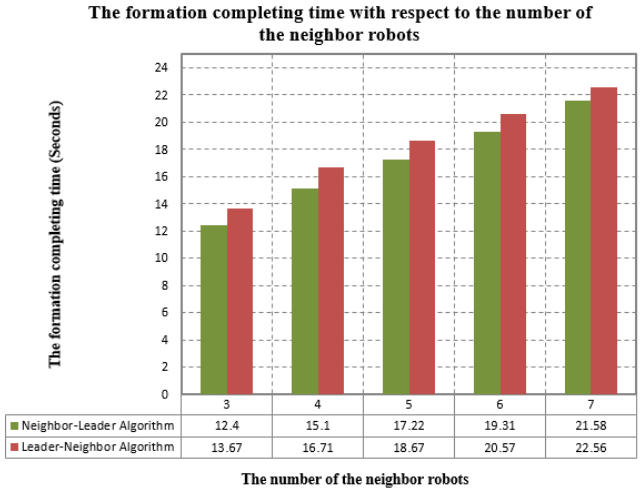

Fig. 9 Comparison the time of formation for the two suggested algorithms.

REFERENCES

[1] B. Issa, A. Rashid " RP Lidar Sensor for Multi-Robot Localization using Leader Follower Algorithm" *Iraqi Journal of Electrical and Electronic Engineering*, vol. 15, no.2 ,PP. 2019.

[2] A. Rashid, A. Ali and M. Frasca " Polygon Shape Formation for Multi-Mobile Robots in a Global Knowledge Environment" *Iraqi Journal of Electrical and Electronic Engineering* Vol. 15, No.1, 2019.

[3] A. Rashid and A. Ali, " Polygon Shape Formation for Multi-Mobile Robots in a Local Knowledge Environment" *Basrah Journal of Engineering Scinces* Vol. 19, No.2 – 2019.

[4] Guo,J.; Lin, Z.; M. Cao, Z. et.al. Adaptive Leader-Follower Formation Control for Autonomous Mobile Robots" *American Control Conference, Marriott Waterfront*, Baltimore, MD, USA, July 02, 2010.

[5] A. Tews, M. Matari, G.Sukhatme, "Avoiding Detection in a Dynamic Environment" *The International Conference on Intelligent Robots and Systems*, Sendai, Japan, 2004.

[6] J. Toibero, F. Roberti, R. Carelli, P. Fiorini "Formation Control for Non-Holonomic Mobile Robots: A Hybrid Approach" *Multi-Robot, Systems Tech Education and Publishing in Vienna*, Austria, pp. 326, May 2008.

[7] R. Zhao, H. Lee, "Fuzzy-based Path Planning for Multiple Mobile Robots in Unknown Dynamic Environment" *JEET*, Vol. 12,No. 2, PP. 918-925 2017.

[8] J. Mora, E. Montijanoy, et.al "Distributed Multi-Robot Formation Control among Obstacles" *A Geometric and Optimization Approach with Consensus the MIT-Singapore Alliance for Research and Technology*.2013.

[9] H. Yang, X. Bao, et al. "A Multi-Robot Formation Platform based on an Indoor Global Positioning System" *Appl. Sci*. 2019.

[10]T. Nascimento, F. Fontes, "Leader Following Formation Control For Omnidirectional Mobile Robots" *The International Conference on Informatics in Control, Automation and Robotics ICINCO*, PP.135-144, 2011.

[11]G. Gamage, G. Mann, R. Gosine, "Leader follower based formation control strategies for non-holonomic mobile robots Design" *Implementation and Experimental Validation American Control Conference*, Marriott Waterfront, Baltimore, MD, USA June 30-July 02, 2010.

[12]O. Hachour "The proposed path finding strategy in static unknown environments" *International Journal Of Systems Applications" Engineering & Development*, no 4, vol. 3, 2009.

[13]Wang, Yuanzhe "Multi-robot formation control in obstacle environments" This document is downloaded from *DR-NTU, Nanyang Technological University Library*, Singapore, 2019-02-19.

[14]A. Solot, A. Ferlini " Leader-Follower Formations on Real Terrestrial Robots" *Association for Computing Machinery*, Beijing, China,19 August, 2019.

[15]T. Soleyman and F. Saghafi "Behavior-based acceleration commanded formation flight control", *International Conference on Control, Automation and Systems* IEEE, 17 December 2010.

[16]J. R T. Lawton, R.W. Beard and B.J. Young "A decentralized approach to formation maneuvers", *IEEE Transactions on Robotics and Automation*, Vol. 19, No. 6 , Dec. 2003.

[17]L. Barnes, M.David Fields, and K. P. Valavanis "Unmanned ground vehicle swarm formation control using potential field" *Mediterranean Conference on Control* 2007.

[18]Y. Zhao, Y. Zhang, and J. Lee "Lyapunov and Sliding Mode Based Leader-follower Formation Control for Multiple Mobile Robots with an Augmented Distance-angle Strategy" *International Journal of Control, Automation and Systems* vol.17, no.5, PP. 1314-1321, 2019.

[19]Y. Dai, V. Tran, et al "Leader-Follower Formation Control of Multi-robots by Using a Stable Tracking Control Method" *Conference Paper· Springer-Verlag Berlin Heidelberg* June 2010.

[20]J. Yan, X. Guan, et al "Formation Control and Obstacle Avoidance for Multi-Agent System-Based Virtual Leader-Follower Strategy" International journal of Information Technology and Decision Making. Vol.16,No.03,PP. 865-880 in 2017.

[21]S. He, M. Wang, et al "Leader–Follower Formation Control of USVs With Prescribed Performance and Collision Avoidance" *Journals & Magazines: IEEE Transactions on Industrial* vol. 15, PP. 572 – 581, 23 May 2018.

Open Access

Iraqi Journal for Electrical and Electronic Engineering
Conference Article

Enhancing Reading Advancement Using Eye Gaze Tracking

Saadaldeen Ahmed*, Mustafa latif fadhil, Salwa Khalid Abdulateef
College of Computer Science and Mathematics, Tikrit University, Salah Aldin, Iraq

Correspondence
*Saadaldeen Ahmed
College of Computer science and Mathematics,
Tikrit University, Salah Aldin, Iraq
Email: Saadaljanabi78@gmail.com

Abstract
This research aims to understand the enhancing reading advancement using eye gaze tracking in regards to pull the increase of time interacting with such devices along. In order to realize that, user should have a good understanding of the reading process and of the eye gaze tracking systems; as well as a good understanding of the issues existing while using eye gaze tracking system for reading process. Some issues are very common, so our proposed implementation algorithm compensate these issues. To obtain the best results possible, two mains algorithm have been implemented: the baseline algorithm and the algorithm to smooth the data. The tracking error rate is calculated based on changing points and missed changing points. In [21], a previous implementation on the same data was done and the final tracking error rate value was of 126%. The tracking error rate value seems to be abnormally high but this value is actually useful as described in [21]. For this system, all the algorithms used give a final tracking error rate value of 114.6%. Three main origins of the accuracy of the eye gaze reading were normal fixation, regression, skip fixation; and accuracies are displayed by the tracking rate value obtained. The three main sources of errors are the calibration drift, the quality of the setup and the physical characteristics of the eyes. For the tests, the graphical interface uses characters with an average height of 24 pixels for the text. By considering that the subject was approximately at 60 centimeters of the tracker. The character on the screen represents an angle of ±0.88◦; which is just above the threshold of ±0.5◦ imposed by the physical characteristics of the eyeball for the advancement of reading using eye gaze tracking.

Keywords: User interface, human computer interaction, detection and tracking, reading, models, intelligent systems

I. INTRODUCTION

Using eye gaze interaction for reading advancement, it would allow to free the hands and by consequence not to overstress the hand muscles. Plus, it would not add some load to the eye muscles because eyes move anyway without any interaction constraint. A simple example shows that when using the mouse to click on a button, the eyes follow the movement of the mouse on the screen in any case. Eye movements are fast and using them to interact would be fast as well. But nowadays most of the interactions with eye gaze, as eye typing systems for instance, is slower than with ordinary inputs (keyboard for example). Combining eye gaze and another modality would allow to speed-up the interaction and reading process.

There has been a point by point survey of works on visualization made over the final few a long time such as [17], [18] and [19] that tended to later improvements in following strategies, comparing distinctive procedures of estimation, setup, application and challenges included utilizing center as input factors. Hansen [18] gives an in-depth survey on diverse eye models, eye discovery methods and eye calibration models, and a rundown of eye utilize. To talk about mistakes within the follow of the highlights from the models of the eye show, jitter and redistribution due to the client wearing glasses. In any case, our work contrasts for a few reasons in this survey. To begin with, our survey is pointed particularly at highlighting issues that influence the evaluation of the execution of perceptual following frameworks, such as measurements and exactness precision and the sources of blunder checks. In [11], a study is made on measuring and improving the parent-child joint attention for reading. It is really important for social learning activities. The study is made on one of these social learning activities that is storybook reading. The point of this study is to give to the mother a feedback of where the child looks and to give to the child a feedback of where the mother looks. Most of the time, when reading storybook, the child and the mother are not paying attention to the same things at the same time. The mother is reading the text and the child is mostly looking at images. Learning print-related skills is done when there is a real joint attention. Giving them real-time

feedbacks allows the mother to know what the child is looking at and to adapt her reading; it also allows the child to know which word his mother is reading and the pronunciation of the word.

Inquire about on eye tracking created by the 1960s and follow-up observing was begun within the 1970s with a specific center on making strides exactness and decreasing issues for clients. The application's center on accomplishing the common purpose of human-computer interaction implied small. This changed within the 1990s as the optical eye obtained the input and computer applications [23]. Post 2000, the fast improvement of computer speed, advanced video processing and moo taken a toll has brought us following apparatuses closer to clients, utilizing gaming, virtual reality and web promoting [24].

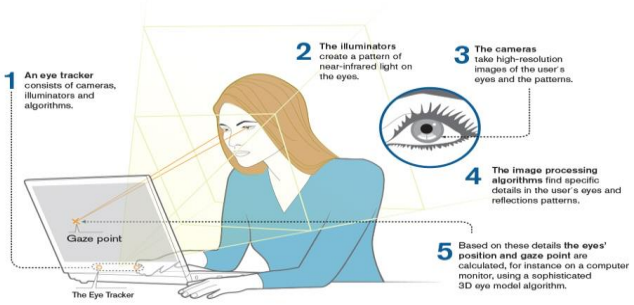

Fig.1: Relation between head front and gaze path

Real-time tracking and tracking of traffic on vehicle platforms are utilized in driver bolster programs to screen caution and driving levels. These set up an eye-tracking setup that is placed on the car dashboard in conjunction with the computer algorithms of the computer using algorithms. On handheld gadgets such as phones or tablets, the front camera is utilized to screen user's consideration to perform assignments such as locking / opening phones, visual present, raise lights, or impede sensors [15] [16]

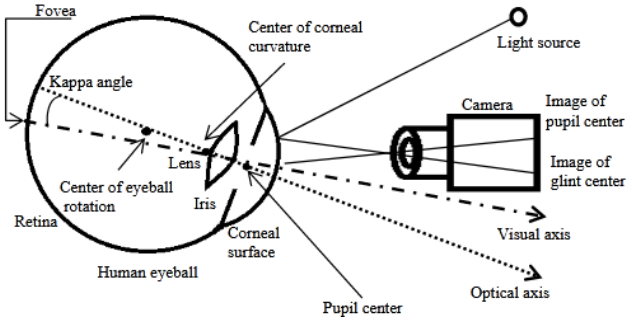

Fig.2: A. Human eye ball model

Eye parameters and setup resources used in 3D eye tracking [21] [22]. The light axis is exposed as a line combination the center of the mass decomposition and the center of student. The vertical axis passes during the fovea and the medial area of the corneal curvature. Kappa angle is the angular deviation between the visual and visual axis.

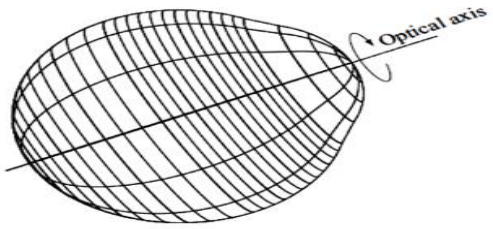

Fig.2: B. aspherical form of the corner

An aspherical model of the cornea, as a surface of revolution about the optical axis of the eye [20]

A. **Hygienic interaction:** Another advantage of eye gaze tracking system is their hygienic interface. Because of the absence of contact needed with such systems, it would fit perfectly in environments with high hygienic requirements [8]. For example, in an operation room for surgery, eye gaze systems would fill the requirements; there is indeed no need of touch interaction with the systems. It can also be useful for public interfaces when there is epidemic menace and when there is a need for hygienic interaction.

B. **Remote control**: Nowadays, with the technology, it is possible to have remote control with eye gaze tracking systems. Detecting the eyes over meters of distance is now possible with the lenses of the camera and its high resolution. It is even possible to detect the eyes at one meter with low cost eye gaze tracking systems [11].

C. **Interaction certified**: Using eye gaze interaction certifies the presence of a user in front of the webcam as well as the attention of this user. Eye gaze interaction can require some specific behavior of the user; for instance, for the user to go on with further features, it can be asked to read a warning text [4].

D. **User's activity detailed**: The eyes reveal a lot about someone activities; tracking them gives useful information about what the user is doing. Without further data analysis, an eye gaze tracking system provides information about what the eyes are looking at, and this is already of big potential for context-aware systems. With simple data analysis, it is possible to detect whether a user is reading or doing other activities for example. With further data analysis, it is possible to detect emotional or physical condition of the user, as their level of literacy and their age [9].

II. METHODOLOGY

The usability testing is another field of commercial interest for eye gaze tracking. As seen previously, the first use of eye gaze trackers has been for military research to find out the best location of instruments in aircraft cockpits. It is an advantage to be able to track the direction of the eye when

introducing a new device to someone. This way, it is possible to see where the user is looking when searching for the control to solve a specific task. Nowadays, internet is also a commercial platform and it is important to find out the usability of web pages as in [2].

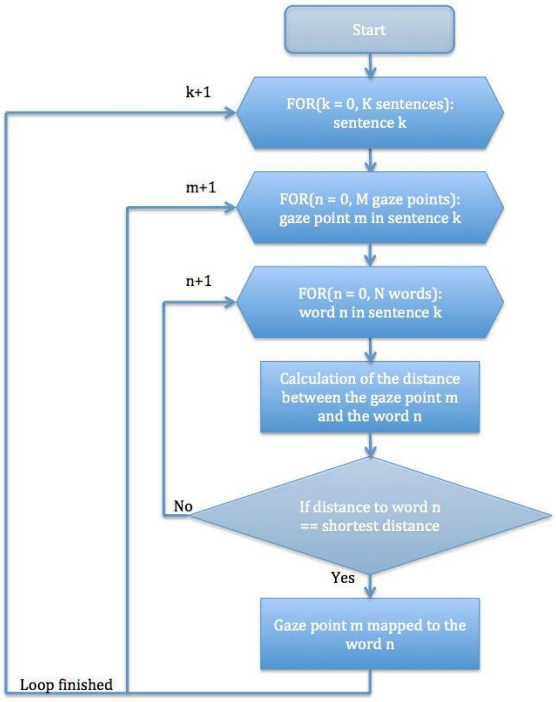

Fig. 3: Implementation flowchart.

We look at the gaze points in the list containing the gaze information. And we check if for a gaze point, the previous gaze point is equal to the following and if the time elapsed is less than 200 milliseconds. If for a gaze point all the conditions are gathered, the gaze point is removed from the list.

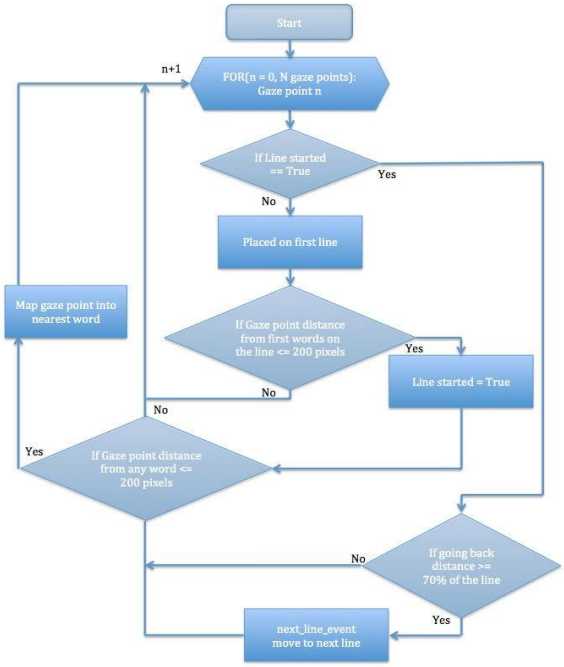

Fig. 4: Baseline algorithm flowchart.

The other kind of contact lenses is the magnetic one. The contact lenses have a coal that is integrated in it. This coal allows to detect the change in the magnetic field. It is very useful because when eyes rotate, an electric field is produced.

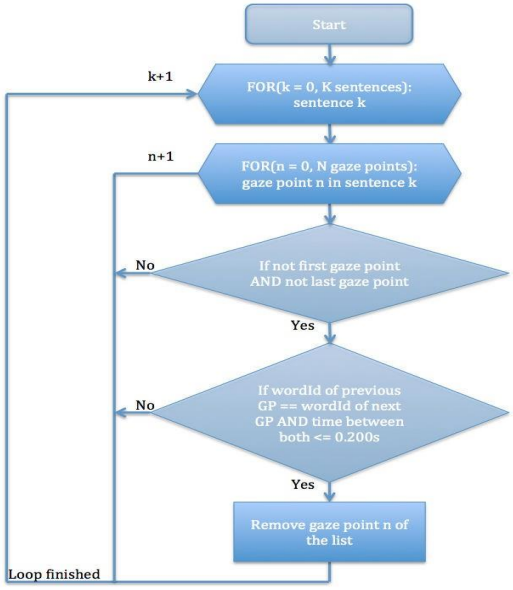

Fig. 5: Smoothing algorithm flowchart.

For each gaze point, we look if the line is started; it means that we look at the gaze point to see if it is mapped onto one of the first words of the line. If it is, we consider the line started and we can follow the reading path to detect the next line event. Then we map the gaze points into the corresponding words on the first line. It uses the same principle. First, we check if the gaze point falls directly onto a word and if not, we calculate the nearest distance to the word. The gaze point is mapped only if the distance is less than 200 pixels.

The data from the lenses, there is a thin wire connected to the measuring device that is uncomfortable for the user [7]. This method is used anyway because it has a really high accuracy and a nearly unlimited resolution. Magnetic contact lenses are found in the field of psychological and medical researches [2]. The principle of video-based eye gaze tracking is to detect the eye and the pupil from video sequences to find out the gaze direction. Because the method is unobtrusive, it is the one that is the most used. The purpose of video-based eye gaze tracking is to estimate the gaze direction based on video sequences [6]. One way of doing this is to detect the iris using the contrast between the white of the eyeball and the dark of the iris. Concerning the horizontal estimation of the gaze direction [10].

All the video-based methods require the detection of the pupil. To do that, image processing is mandatory. In image processing, what is called edge detection is typically what is needed to detect the elliptical contour of the pupil [13]. A method is to calculate the characteristics of the ellipse formed by the shape of the pupil to estimate the gaze direction. Another method tracks the rotational movements of the eyes but this kind of systems are not very spread. The eye gaze tracking systems based on video do not need

interaction or contact: that is why maintenance is not mandatory. Unlike mice and keyboards, the eye tracking devices do not need to be cleaned, which becomes a real problem for mice and keyboards. The camera centered eye positioning system is focusing on the center axis is shown in fig. 6.

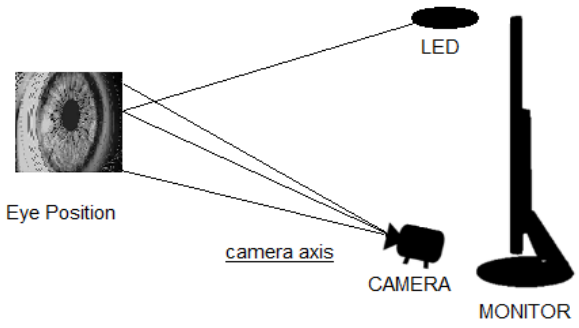

Fig. 6: Image projection plane [12]

III. RESULTS

A. Results with no processing

The results obtained in this section are obtained directly from the raw data. The tracking error rate is calculated directly from the data with no processing and algorithms. These results are presented in the Table 1.

TABLE 1:
No processing results.

Subjects	Tracking error rate
Subject 01	1.288
Subject 02	1.387
Subject 03	1.383
Subject 04	1.522
Average	***1.395***

B. Results with the baseline processing

The results obtained in this section are obtained by extracting information from the raw data. The tracking error rate is calculated on the processed data. The baseline algorithm presented in methodology. These results are presented in the Table 2.

Subjects	Tracking error rate	Improvement
Subject 01	1.317	−2.21%
Subject 02	1.246	10.15%
Subject 03	1.233	10.83%
Subject 04	0.935	38.57%
Average	***1.183***	***14.33 %***

Table 2: Baseline processing results

C. Results with the processing to smooth the data

The results obtained in this section are obtained by applying the smoothing algorithm to the previous processed data. The tracking error rate is calculated on this new processed data. The smoothing algorithm presented methodology is applied. These results are presented in the Table 3.

TABLE 3:
Smoothing processing results.

Subjects	Tracking error rate	Improvement (basic processing)	Improvement (raw data)
Subject 01	1.260	4.48%	2.21%
Subject 02	1.211	2.76%	12.69%
Subject 03	1.195	3.40%	13.60%
Subject 04	0.918	3.72%	39.69%
Average	***1.146***	***3.02%***	***17.05 %***

The tracking errors have been clustered based on the type of the fixations of the errors. Three groups have been made: normal fixation, regression and skip fixation (between the previous fixation and the actual fixation, one or more words have been skipped). The corresponding percentages are given in the Table 4.

TABLE 4:
Errors cluster percentages.

Subjects	Normal fixation	Regression	Skip fixation
Subject 01	23.60%	11.80%	64.60%
Subject 02	11.41%	7.51%	81.08%
Subject 03	15.90%	10.70%	73.39%
Subject 04	20.89%	16.03%	62.98%
Average	***17.98 %***	***11.51 %***	***70.51 %***

The main source of errors is the skip fixation. Most of the time, we do not find hypothesis changes that correspond to reference changes. That is why this cluster has a high percentage. The percentage of the errors caused by the regressions is quite high. When reading, regressions happen but at a low frequency. Here, the percentage is close to the percentage of the errors caused by normal fixations, fixations which happen at a higher frequency.

D. Good tracking ability: The eye gaze trackers are able to enhance the advancement track of the gaze of any person, regardless of their ethnicity, the wear of glasses or contact lenses, and their age. There is also a good tolerance to lightning; the trackers are able to work even with large differences in light conditions.

E. Tracking optimization: The methods of dark and bright pupil are both used while tracking. The most suitable method is automatically calculated and used. Both methods are optimized; it is thus possible to get better tracking quality and better ability to track a wider range of population.

F. High accuracy: High accuracy of the trackers provides precise and reliable data about the position of the gaze of the user. The ability to move the head and the possibility of having changes in lightning allow to have a natural environment for the user.

H. Validity measures: The eye gaze trackers provide a tracking status meter and numerical validity measures for each data point, that are built-in and in real time. Thanks to it, it is possible to specify the correctness of the data that are recorded. With this validity information, it is possible to filter the data recorded in order to remove the corrupted one and to have a better data quality. Because the model can have a data rate of 120Hz, it is possible to use it for research in the field of neurological processes where it is valuable to have a higher quantity of detailed measures.

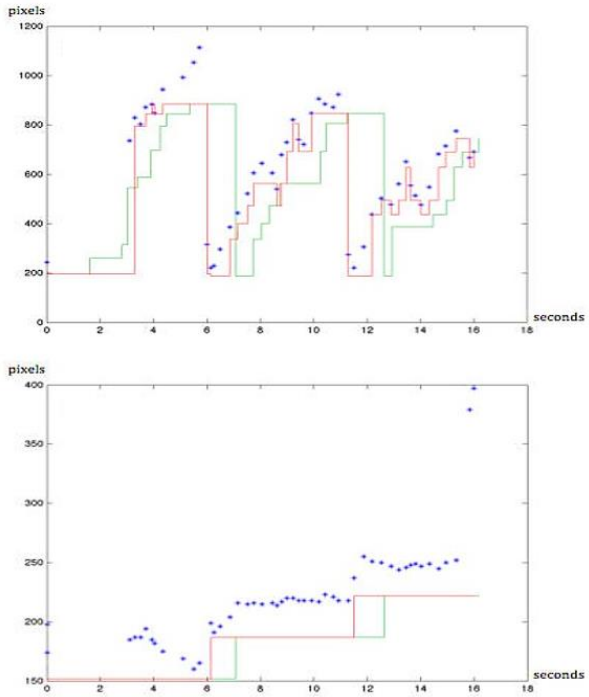

Fig. 7: Gaze data plots for sentence for all subjects.

IV. CONCLUSION

The purpose of this work is to understand reading process and enhance it in order to be able to follow this process with an eye gaze tracker. This way, mapping gaze points into corresponding words would be possible without too many errors. As a consequence, the fusion of eye gaze tracking and speech recognition would give better results than only speech recognition. During tests carried out to collect the data, an eye gaze tracker was used with different subjects. While recording the subjects reading the texts, the eye gaze tracker recorded the gaze point's location of the subjects. The information obtained from manual transcription are used as reference and the information from the eye gaze tracker are the hypothesis. The evaluation is performed by calculating the tracking error rate. The goal is to have the lowest tracking error rate while using only the hypothesis data.

REFERENCES

[1] David Beymer and Daniel M. Russell. Webgazeanalyzer: a system for capturing and analyzing web reading behavior using eye gaze. In CHI '05 Extended Abstracts on Human Factors in Computing Systems, pages 1913–1916, 2015.

[2] Richard A. Bolt. Eyes at the interface. Proceedings of the 1982 Conference on Human Factors in Computing Systems, pages 360–362, 2017.

[3] Hannah Faye Chua, Julie E. Boland, and Richard E. Nisbett. Cultural variation in eye movements during scene perception. Proceedings of the National Academy of Sciences, PNAS, 102(35):12629–12633, 2015.

[4] Q. Ji and Z. Zhu, Eye and Gaze Tracking for Interactive Graphic Display, Proc. Second Intl Symp. Smart Graphics, pp. 79-85, 2002

[5] K. Krafka, A. Khosla, P. Kellnhofer, H. Kannan, S. Bhandarkar, W. Matusik," Eye tracking for everyone," in Proc. IEEE Conf. Comput. Vis. Pattern Recognit., pp. 21762184, Jun. 2016.

[6] Q. He, X. Hong, X. Chai, J. Holappa, G. Zhao, X. Chen, and M. Pietikinen," Omeg: Oulu multi-pose eye gaze dataset," in Proc. Image Anal., pp. 418-427, 2015.

[7] Q. Huang, A. Veeraraghavan, and A. Sabharwal, "Tabletgaze: Dataset and analysis for unconstrained appearance-based gaze estimation in mobile tablets," Mach. Vis. Appl., vol. 28, no. 5, pp. 445-461, 2017.

[8] K. A. Funes Mora, F. Monay, and J.M. Odobez," EYEDIAP: A database for the development and evaluation of gaze estimation algorithms from RGB and RGB-D cameras," in Proc. ACM Symp. Eye Tracking Res., pp. 255-258, 2014.

[9] K. A. Funes Mora and J.-M. Odobez," Person independent 3d gaze estimation from remote RGB-D cameras," in Proc. IEEE Int. Conf. Image Process., pp. 2787-2791, 2013.

[10] T. Schneider, B. Schauerte, and R. Stiefelhagen," Manifold alignment for person independent appearance-based gaze estimation," in Proc. Int. Conf. Pattern Recognit., pp. 1167-1172, 2014.

[11] E. Wood, T. Baltrusaitis, L.P. Morency, P. Robinson, and A. Bulling," Learning an appearance-based gaze estimator from one million synthesised images," in Proc. ACM Symp. Eye Tracking Res., pp. 131- 138, 2016.

[12] E. Wood, T. Baltrusaitis, X. Zhang, Y. Sugano, P. Robinson, and A. Bulling," Rendering of eyes for eye-shape registration and gaze estimation," Proc. IEEE Int. Conf. Comput. Vis., pp. 3756-3764, 2015.

[13] A. Shrivastava, T. Pfister, O. Tuzel, J. Susskind, W. Wang, R. Webb," Learning from simulated and unsupervised images through adversarial training", Proc. IEEE Conf. Comput. Vis. Pattern Recognit., pp. 2242-2251, Jun. 2016.

[14] K. He, X. Zhang, S. Ren, and J. Sun," Deep residual learning for image recogni-tion," Proc. IEEE Conf. Comput. Vis. Pattern Recognit., pp. 770778, June 2016.

[15] S. Wyder, and P.C. Cattin," Eye tracker accuracy: quantitative evaluation of the invisible eye center location," International Journal of Computer Assisted Radiology and Surgery, vol. 13, pp. 1651-1660, 2017.

[16] A. Plopski, J. Orlosky, Y. Itoh, C. Nitschke, K. Kiyokawa, and G. Klinker, Automated spatial calibration of HMD systems with unconstrained eye-cameras, Proc. Int. Symp. Mixed Augmented Reality, pp. 9499, 2016.

[17] Y. Zhang, Z. Qiu, T. Yao, D. Liu, and T. Mei," Fully Convolutional Adaptation Networks for Semantic Segmentation," 2018 IEEE/CVF Conference on Computer Vision and Pattern Recognition, pp. 6810-6818, 2018.

[18] [28] Y. Sugano, Y. Matsushita, and Y. Sato," Learning-by-synthesis for appearance-based 3d gaze estimation," in Proc. IEEE Conf. Comput. Vis. Pat-tern Recognit., pp. 1821-1828, 2014.

[19] X. Zhang, Y. Sugano, M. Fritz, and A. Bulling," MPIIGaze: RealWorld Dataset and Deep Appearance-Based Gaze Estimation," IEEE Transactions on Pattern Analysis and Machine Intelligence, vol. 41, pp. 162-175, 2017.

[20] R. Valenti and T. Gevers," Accurate Eye Center Location and Tracking Using Isophote Curvature," Proc. IEEE Conf. Computer Vision and Pattern Recognition, pp. 1-8, 2018.

[21] Morten Hojfeldt Rasmussen and Zheng-Hua Tan. Fusing eye-gaze and speech recognition for tracking in an automatic reading tutor - a step in the right direction? submitted to SLATE 2013, France, 2013.

[22] T. Joda, G. O. Gallucci, D. Wismeijerc, and N. U. Zitzmann, Augmented and virtual reality in dental medicine: A systematic review, Computers in Biology and Medicine, vol. 108, pp. 93-100, May. 2019.

[23] J. Lasse, and F. Konradsen, A review of the use of virtual reality head-mounted displays in education and training, Education and Information Technologies, vol. 23, pp. 1515-1529, 2017

[24] K. Fujii, G. Gras, A. Salerno, and G. Yang, Gaze gesture based human robot interaction for laparoscopic surgery. Medical image analysis, vol. 44, pp. 196-214, 2018.

Open Access
Iraqi Journal for Electrical and Electronic Engineering
Conference Article

Two Dimensional Path Planning with Static Polygon Obstacles Avoidance

Duaa Ahmed Ramadhan*[1], Abdulmuttalib T. Rashid[2], Osama T. Rashid[3]
[1] Electrical Engineering Department, University of Basrah, Basrah, Iraq
[2] Electrical Engineering Department, University of Basrah, Basrah, Iraq
[3] Computer Engineering Department, Iraq University Collage, Basrah, Iraq

Correspondence
* Duaa Ahmed Ramadhan
Electrical Engineering Department,
University of Basrah, Basrah, Iraq
Email: duaa.eng.coe1992@gmail.com

Abstract
This paper presents the designing of path planning system in an environment contains a set of static polygon obstacles localized and distributed randomly by using differential drive mobile robot. In this paper the designed algorithm (two dimensional path planning algorithm) is proposed in order of investigate the path planning of mobile robot with free collision using the visibility binary tree algorithm. The suggested algorithm is compared with the virtual circles tangents algorithm in the time of arrival and the longest of the path to the target. The aim of this paper is to get an algorithm has better performance than the other algorithms and get less time of arrival and shortest path with free collision.

KEYWORDS: Mobile robot, path planning, polygon obstacle.

I. INTRODUCTION

Path planning concept is a way of moving robot from the initial point to the destination point with free collision and less time arrival, and shortest path [1]. It has a wide number of applications in games [2], logistics [3], and robotics [4]. Path planning of mobile robot is one of the most challenges in robotics because it is applied in different applications such as routing transportation, organizing allocation of machines in factories, controlling robots, intelligent agents [5] and also in military applications [6]. Path planning algorithms can be implemented in static, dynamic, and real time different environments, therefore it suffers from number of problems such as single agent path planning, multi agent path planning, adversarial path planning, and changes in dynamic environments that require pre-processing operation which makes path planning complex in real time [7]. There are many algorithms used for path planning system construction. Path planning algorithms classified into two types: on-line and off-line path planning. On-line path planning suitable for a partially known environment with a static target, since the robot uses its sensors to know about the environment but not all they can be solve moving target problem [8-10]. On-line path planning depends on the current environment information to select the current optimal path [11]. Off-line path planning was not suitable for the large dynamic environment and moving target problem handling because it consumes time since the complete path from start to the target is computed at the start position [12]. Off-line path planning algorithms converted to incremental algorithms in order to be more efficient [13, 14]. Incremental algorithms suitable for a partially known environment but not solve moving target problem. In this paper, differential-drive mobile robot is used in an environment contains fixed polygon obstacles. Visibility binary search algorithm [15], Minimum bounding circle algorithm [16, 17] are used to draw tree of paths which is contacts with obstacles then choose a good path from this tree. Also use virtual circles tangents algorithm then compare between them to get algorithm with good performance.

II TWO DIMENSIONAL PATH PLANNING ALGORITHM

In this section of research, it will design path planning system in an environment contains a set of static polygon obstacles by using differential drive mobile robot. Method of algorithm is based on obstacle avoidance by drawing paths in contact with obstacles to configure a tree of paths using visibility binary algorithm [15]. The shortest path is chosen of this tree for moving a robot to the target point.

A. Compute the centriod of each obstacle

In this section, it will represent every obstacle with a circle contains all of polygon obstacle heads and then find a center of this circle to use it for exploration if this obstacle block the way of robot or not. For this purpose, algorithm is chosen is Minimum bounding circle algorithm [16, 17], this algorithm depends on using Chan's algorithm in Fig.1 and 2.

```
Chan's Algorithm (p)
1. For t=1; 2; …
2.  Let m=min (2^ (2^t), n)
3.  Let r=ceil (n/m)
4.  Divide stage
5.      For k =1 to r do
6.          For i =1 to m do
7.              Compute sub hull P (m) using Graham's scan and
store the vertices in an ordered array S in CCW oriented.
8.  End
9.  Jarvis stage
10.   Find leftmost vertex S0 from all sub hulls that resulted
from Graham scan algorithm
11.   Compute final convex hull ch (h) using Jarvis March
algorithm
12.   End
```

Fig. 1 Chan's algorithm

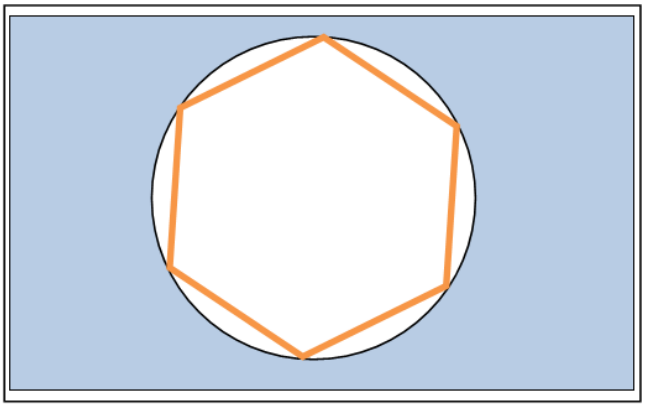

Fig. 2 Minimum bounding circle algorithm

B. Binary tree paths construction algorithm

In this section, it will construct a tree of paths for a robot according to the following steps:

Step 1: Direct path to the target: In this step, a direct path is drawing for moving robot from initial point to target point as in Fig. 3.

Step 2: Testing the collision with an obstacle: In this step, it will test an interception of one of obstacles for path of robot. At first, it will determine distance between every obstacle and path that connect between robot and target using the following relations [19] as in Fig. 4

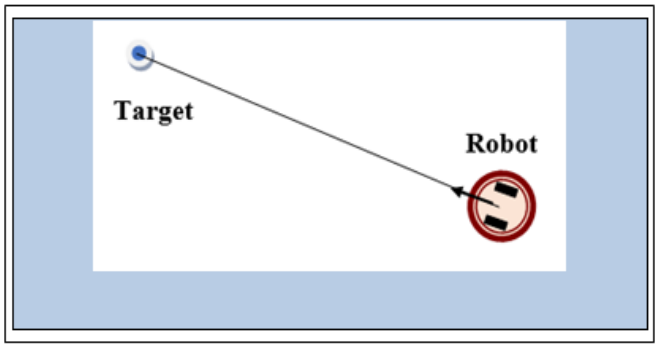

Fig. 3 Direct path

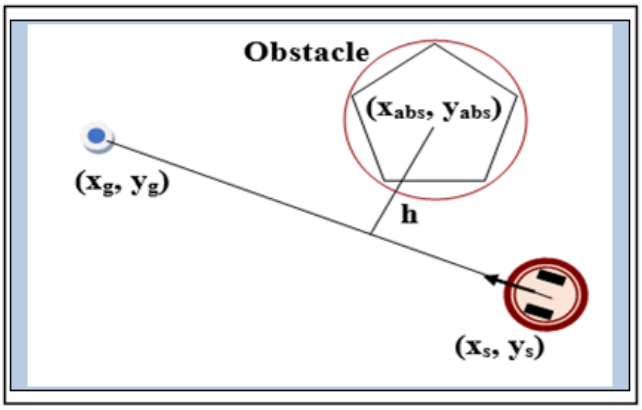

Fig. 4 Detection the collision with the obstacle

$$a = (yg - ys) / (xg - xs) \quad (1)$$
$$b = -1 \quad (2)$$
$$c = ys - a * xs \quad (3)$$
$$h = Abs(a * xabs + b * yabs + c) / Sqrt(a\ 2 + b\ 2)) \quad (4)$$

Step 3: Choose the nearest collision

In this step, it will choose obstacles that far away from the path that connect between robot and target with shortest distance from the radius of circle that surrounding obstacle. The obstacle that having minimum value of distance about robot it will be the first obstacle that intercept path of robot. The following relation determined distance between obstacle and robot:

$$Dis = ((x_s - x_{abs})^2 + (y_s - y_{abs})^2)^{0.5} \quad (5)$$

Step 4: Estimate the outer and inner tangent points: In this step, it will determine the outer and inner tangent points for tangent contacts from robot to obstacle. In order to deflect direction of robot to prevent collision between it and obstacle. Estimation of tangent points by the following steps:

1. Determine distance between every head in polygon obstacle and the direct path from robot to target as in Fig. 5.
2. 2. Vertices of the polygon obstacle that having largest distance for path between robot and target represent tangent points.

Step 5: Draw the outer and inner tangent lines: In this step, it will draw lines that contacts with obstacle from robot as in Fig. 6.

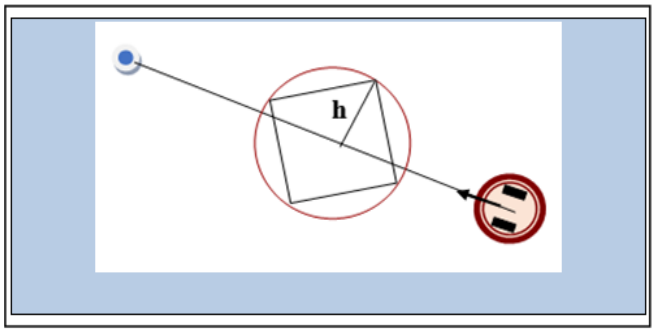

Fig. 5 Estimate the two tangent points

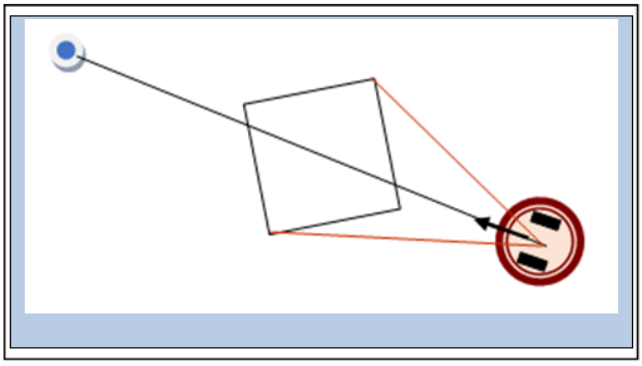

Fig. 6 The two tangent lines

Step 6: Complete the binary tree construction: Repeat the previous steps starting with every tangent point to target in order to repeat drawing tangents for obstacles that interception path of robot until the tree of tangents is complete as in Fig. 7.

C. Optimal paths estimation

In this part, it will choose the shortest path of a set of paths from robot and target using algorithm called visibility binary search algorithm [15] as in Fig.8.

D. Low level path planning

In this part, it will determine the way of moving robot from source to target. Robot that used in this research is differential drive mobile robot as in Fig. 9. The way of moving depends on dynamic motion for this robot.

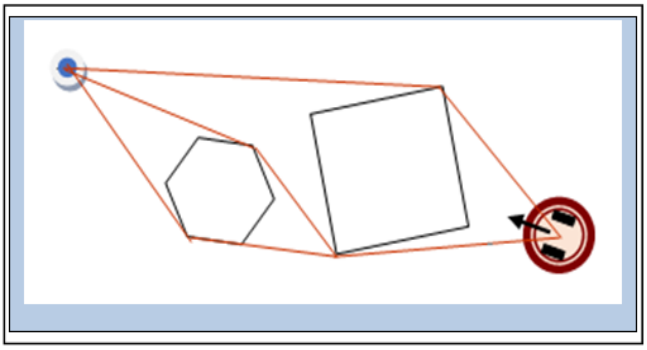

Fig. 7 Complete binary tree construction

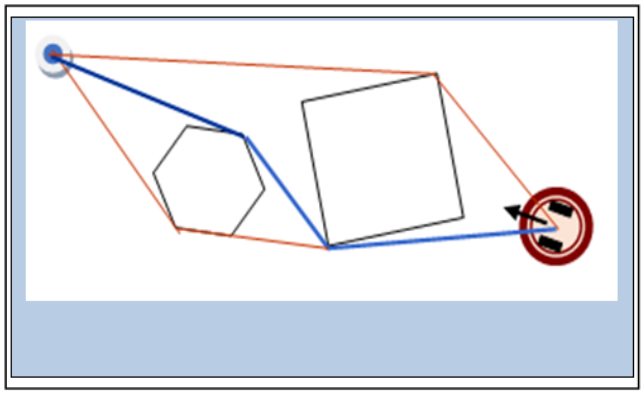

Fig.8 Optimal path from robot to the target

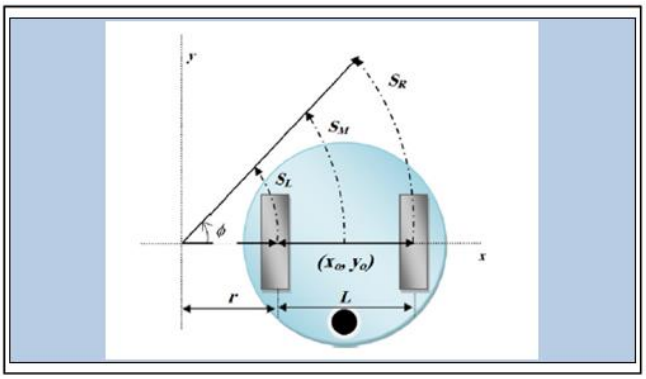

Fig. 9 Differential drive mobile robot.

Let the coordinates (X_0, Y_0) represent the global position of the center of the robot in a fixed reference frame. It will consider a line is vertical to the wheel axis and goes through the point (X_0, Y_0) as an orientation reference for the robot. This line make an angle Θ with the positive x axis represents the direction of the robot. The displacement for the left and right wheels is called *SL*, *SR* respectively, *r* is the turn radius for the inner (left) wheel, *L* represent the distance between the wheels, and Θ represent the angle of the turn in radians. SM represent the displacement at the center point on the main axle. To be suitable for small robot applications where on-board computing power is limited, the approximated equations for the robot movement as follows:

$$xc(t) = s\cos\Theta + x_0 \quad (6)$$

$$yc(t) = s\sin\Theta + y_0 \quad (7)$$

Where

$$s = (SR + SL)/2 \quad (8)$$

III Simulation Results

The new algorithm (two dimensional path planning algorithm) is simulated to investigate the path planning of mobile robot using Visual basic programming language and tested in Windows environment using an Intel core i5. The different distributed of polygon shape obstacles are simulated by considering the effect of the time of arrival and the shortest distance to complete the path planning with free collision. The suggested algorithm is compared with virtual circles tangents algorithm in the time of arrival and the longest of the path to the target. Fig. 10 (a)-(f) represent the Screenshots of the simulation at different time steps for the two dimensional path planning algorithm. Fig. 11 (a)-(f) represent the Screenshots of the simulation at different time steps for the virtual circles tangent algorithm. Fig. 12 (a)-(c) represent the path planning with zero, one and two obstacles using the two dimensional path planning algorithm. Fig. 12 (d)-(f) represent the path planning with zero, one and two obstacles using the virtual circles tangent algorithm.

The main goal of this simulation is to show the relation between the number of obstacles and the time of arrival and the long the path to the goal.

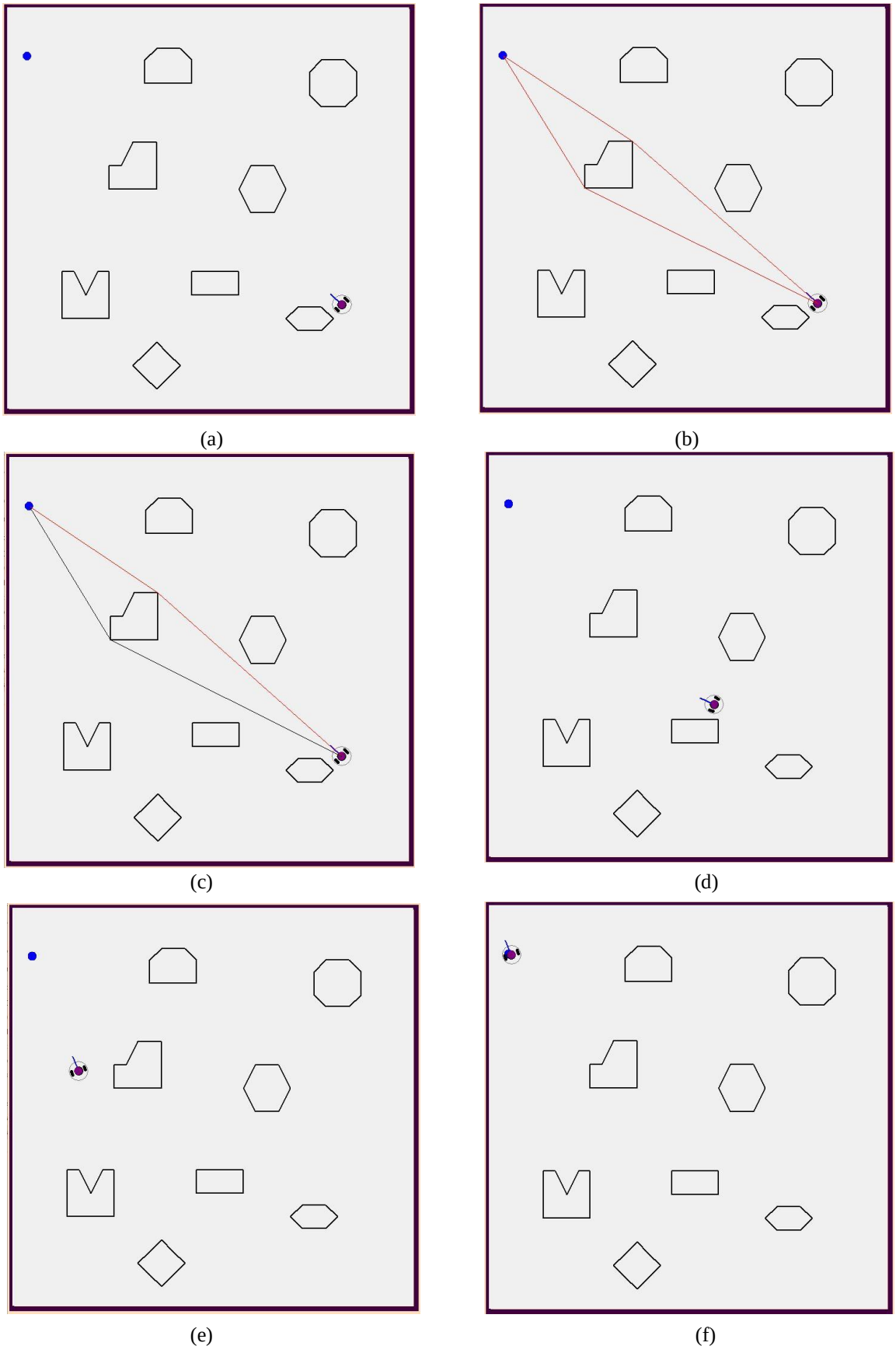

Fig.10 The two dimensional path planning algorithm. (a-f) Screenshots at different time steps trajectory planning.

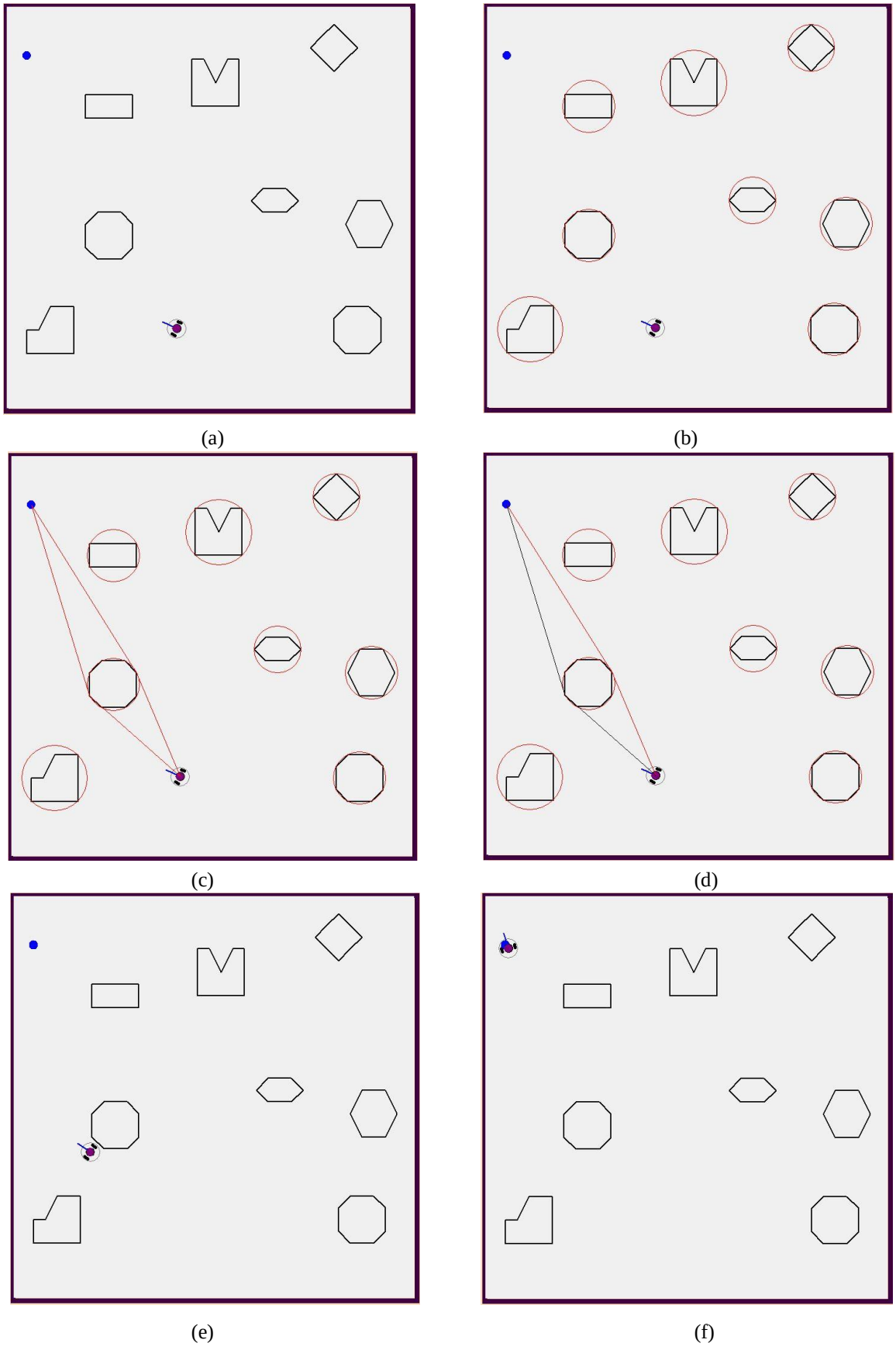

Fig.11 The virtual circles tangent algorithm. (a-f) Screenshots at different time steps trajectory planning.

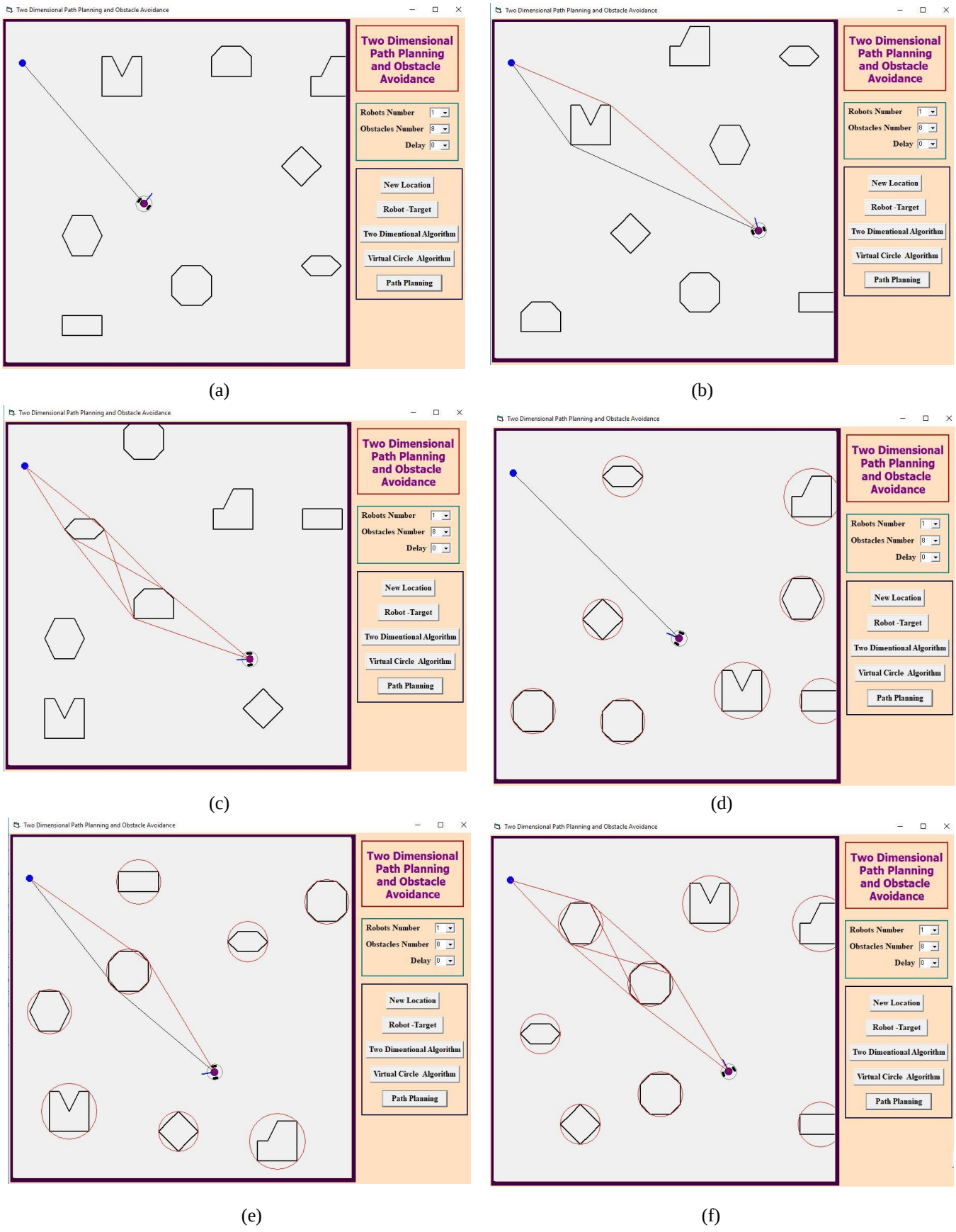

Fig.12 Path planning with different number of obstacles. (a-c) The two dimensional path planning algorithm (d-f) the virtual circles tangent algorithm.

Fig. 13 shows the comparison between the number of obstacles and the time of arrival between the 2D path planning algorithm and the virtual circles tangent algorithm. As the number of the obstacles increase in the environment, the time of arrival increase for both algorithm but the two dimensional produced best performance than the virtual circles tangent algorithm. Fig. 14 shows the second comparison between the two dimensional path planning algorithm and the virtual circles tangent algorithm in computing the length of the path to the target. As the number of the obstacles increase in the environment, the length of the path for both algorithm is also increased. The two dimensional path planning algorithm produced best performance than the virtual circles tangent algorithm.

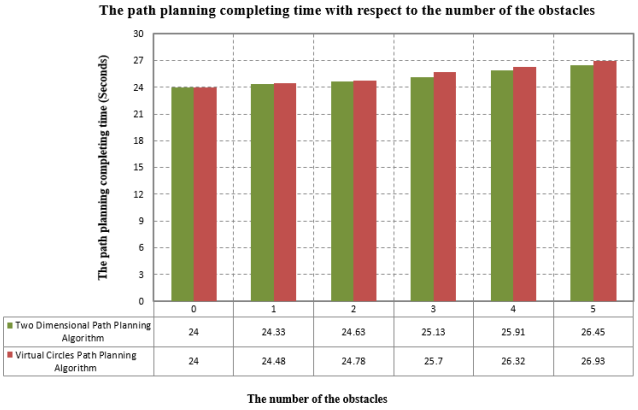

Fig. 13 Comparison the time of arrival for both the two dimensional path planning algorithm and the virtual circles tangent algorithm.

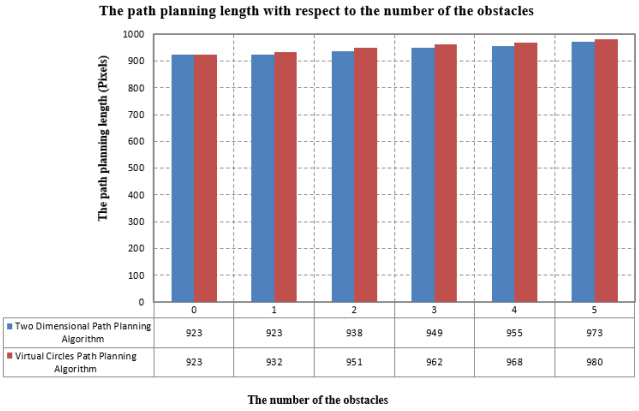

Fig. 14 Comparison the length of the path for both the two dimensional path planning algorithm and the virtual circles tangent algorithm.

IV. Conclusion

In this paper, a novel two dimensional path planning algorithm in a global knowledge environment by using several numbers of obstacles localized and distributed randomly. Simulation results are implemented in an environment with a different number (0 to 8) of obstacles using both the two dimensional path planning algorithm and the virtual circles tangent algorithm. The results show that both the algorithm have less time of arrival as the number of the obstacles decrease. The same results are obtained when we measure the length of the path to the target point. The suggested algorithm has better performance than the virtual circles tangent in both the time of arrival and the length of the path.

References

[1] Z. Y. Ibrahim, A. T. Rashid and A. F. Marhoon (2016). Prediction-Based Path Planning with Obstacle Avoidance in Dynamic Target Environment. Basrah Journal of Engineering Science, 16(2), 48-60.

[2] N.R. Sturtevant, and R. Geisberger, "Ä Comparison of High-Level Approaches for speeding Up Path finding", As-sociation for the advancement of artificial Intelligence, pp.76-82, 2010.

[3] B. Bonet, and H. Geffner, "Planning as heuristic search", Artificial Intelligence-journal Elsevier, vol. 129, No.1-2, pp.5-33, 2001.

[4] J. Van den Berg, R.shah, A. Huang, and K. Goldberg, "ANA*: Anytime Nonparametric A*", Association for the advancement of artificial Intelligence, pp.105-111, 2011.

[5] B.coppin, Artifital Intelligent Illuminated, 2004.

[6] J.Kaur, V. K. Banga and G.Singh, "Robotic Path Planning Using the Intelligent Control", International Conference on Advances in Electrical and Electronics Engineering (ICAEE'2011).

[7] R. Graham, H. McCabe, and S. Sheridan, "Path finding in Computer Games", The IBT journal, Vol.4, pp.57-81, 2003.

[8] A.T. Rashid, A. A. Ali, M. Frasca, and L. Fortuna," An algorithm for multi-robot collision-free navigation based on shortest distance", Robotics and Autonomous Systems, Vol. 75, p.p. 119-128, 2016.

[9] Z. Y. Ibrahim, A. T. Rashid and A. F. Marhoon (2016). Path planning algorithm for mobile robot navigation in a dynamic environment based on motion prediction and tangency graph. 2017 IEEE First International Conference on Recent Trends of Engineering Science and Sustainability.

[10] C.Undeger, and F.polat," Real-Time Edge Follow: A Real-Time Path Search Approach", IEEE Transactions on Systems Man and Cybernetics Part C. October 2007.

[11] M. Shahab Alam, M. Usman Rafique, and M. Umer Khan, "Mobile Robot Path Planning in Static Environments using Particle Swarm Optimization" , International journal of computer science and electronics engineering (IJCSEE) ,vol.3, pp. 253-257,2015.

[12] J.F. Canny, J.M. Malik, D.D. Edwards" Artificial Intelligence A Modern Approach", 1995.

[13] S. Koenig, and M. Likhachev," Fast Replanning for Navigation in Unknown Terrain", IEEE TRANSACTIONS ON ROBOTICS, VOL.21, NO.3, JUNE 2005.

[14] A.Stentz," The Focussed D* Algorithm for Real-Time Replanning", International Joint Conference on Artificial Intelligence, August 1995.

[15] A. T. Rashid, A. A. Ali, M. Frasca, and L. Fortuna," Path planning with obstacle avoidance based on visibility binary tree algorithm", Robotics and Autonomous Systems, vol. 61, p.p1440–1449, 2013.

[16] Z. Y. Ibrahim, A. T. Rashid and A. F. Marhoon (2016). An algorithm for Path planning with polygon obstacle avoidance based on the virtual circle tangents. Iraq Journal Electrical and Electronic Engineering, 12(2), 221-234.

[17] I. S. Alfurati and A. T. Rashid (2019),” Design and Implementation an Indoor Robot Localization System Using Minimum Bounded Circle Algorithm”, 2019 8th International Conference on Modeling Simulation and Applied Optimization (ICMSAO).

[18] A. T. Rashid, A. A. Ali, M. Frasca , and L. Fortuna," Path planning and obstacle avoidance based on shortest distance algorithm", 2017 Second Al-Sadiq International Conference on Multidisciplinary in IT and Communication Science and Applications (2nd-AIC-MITC’17), Iraq, 2017.

[19] A. T. Rashid, A. A. Ali, M. Frasca, and L. Fortuna," Multi-robot collision-free navigation based on reciprocal orientation", Robotics and Autonomous Systems, vol. 60, p.p1221–1230, 2012.

Open Access

Iraqi Journal for Electrical and Electronic Engineering
Conference Article

Adaptive Energy Management System for Smart Hybrid Microgrids

Bilal Naji Alhasnawi*, Basil H. Jasim
Electrical Engineering Department, University of Basrah, Basrah, Iraq

Correspondence
*Bilal Naji Alhasnawi
Electrical Engineering Department,
University of Basrah, Basrah, Iraq
Email: bilalnaji11@yahoo.com

Abstract
The energy management will play an important role in the future smart grid by managing loads in an intelligent way. Energy management programs, realized via House Energy Management systems (HEMS) for smart cities, provide many benefits; consumers enjoy electricity price savings, and utility operates at reduced peak demand. This paper proposed an adaptive energy management system for islanded mode and grid-connected mode. In this paper, a hybrid system that includes distribution electric grid, photovoltaics, and batteries are employed as energy sources in the residential of the consumer in order to meet the demand. The proposed system permits coordinated operation of distributed energy resources to concede necessary active power and additional service whenever required. This paper uses home energy management system which switches between the distributed energy and the grid power sources. The home energy management system incorporates controllers for maximum power point tracking, battery charge and discharge and inverter for effective control between different sources depending upon load requirement and availability of sources at maximum powerpoint. Also, in this paper, the Maximum Power Point Tracking (MPPT) technique is applied to the photovoltaic station to extract the maximum power from hybrid power system during variation of the environmental conditions. The operation strategy of energy storage systems is proposed to solve the power changes from photovoltaics and houses loads fluctuations locally, instead of reflecting those disturbances to the utility grid. Furthermore, the energy storage systems energy management scheme will help to achieve the peak reduction of the houses daily electrical load demand. The simulation results have verified the effectiveness and feasibility of the introduced strategy and the capability of the proposed controller for a hybrid microgrid operating in different modes.

KEYWORDS: Inverters, Converters, Micro-grid, Photovoltaics, Batteries, Utility Grid, House loads.

I. INTRODUCTION

The influence of renewable energy resources and units of energy storage in distribution systems can greatly alter the performance of the network grid [1], and integration in the distribution grid has positive effects such as improvement of reliability, bus voltage profile, and reduce grid losses. In addition to the benefits, unwanted management of simultaneous network operations can shorten its life. Therefore, an optimal management schedule is required for the proper operation of these units. One of the main goals of a distribution grid operator is to reduce operating costs, to reduces electricity bills [2]. Moreover, reliability is another important goal in studying power distribution networks, which play an important role in distribution studies that play a significant role in improving system performance especially in reducing subscriber blackouts and any operational program is not acceptable regardless of reliability indicators in modern power systems [3].

The incorporation of different distributed energy resources, energy storage system and electrical loads distributed into the renewable energy system is called microgrid [4]. Recently, there has been a lot of interest in using microgrids in power systems as it is considered to be a flexible and smart active energy grid. In addition, it can improve system reliability, efficiency, and safety, and promote the integration of renewable energy sources [5]. The microgrid can be connected to the grid or distributed energy resources can be used to deliver the load without the network. Incorporation of distributed energy resources and controllable load into the distribution network creates unique challenges for managing the energy management system. The main role of microgrid energy management system is to determine the optimal transmission of microgrid and main network energy independently every hour to meet the demand demands of the load. The literature offers different proposals for microgrid energy management systems with different algorithms and different microgrids such as in

research [6]. The rest of this paper is organized as follows. Section II presents a description of the related works. Section III presents the overall energy management system. Section IV presents a description of the proposed system in this paper. Section V presents the mathematical model of the distributed hybrid generation system, section VI presents the control methods for photovoltaics and the battery system, section. Section VII presents the proposed houses energy management systems, the section VIII presents results of the proposed system, Finally, section IX concludes the paper.

II. Literature Review

The methods and models for implementing smart home energy management systems have recently received considerable attention. In this section, we review relevant research covering energy management strategies in the context of areas related to this work, namely: cost savings; load and PV generation forecasting; modeling complexity temporal resolution; and retail tariff settings, battery degradation, and computational feasibility. In [7] the authors propose optimal power management for grid-connected hybrid power generation systems, including photovoltaics, wind turbines, fuel cells, and electrolysis. The system trades electricity with the local network using real-time electricity pricing over a 24-hour horizon/period based on simulation results. The interior search algorithm was used to optimize energy management in the above case. In [8], the authors proposed a centralized system for energy management of microgrid in Island mode and grid-connected mode. In Island mode, the fuel cell will only work if the battery is less than 80%. grid connected mode requires a 60% threshold to ensure reliable operation. In [9], the authors suggested the energy management system to hybrid microgrid with wind-turbine, photovoltaics, and battery power. The control and data acquisition system work in real-time. The power management system is based on a set of rules that improve MG performance by controlling and monitoring power generation, loads, and storage items [10], the authors proposed an energy management system for the isolated microgrid. The isolated event was treated as a natural probability distribution of failure within the utility network. The aim was to reduce microgrid operating costs. This includes costs associated with running a small turbine, wind turbine, batteries, and loads. In [11], the authors proposed an energy management system to hybrid AC and DC Microgrid which guarantees economic transmission despite doubts associated with the use of renewable energy sources. the load control is on-demand, taking into account generators, controllable loads, and battery charge/discharge limits (thermal and electric vehicles).

III. Energy Management System Overview

The system of energy management can be defined as an automated, real-time, and comprehensive, automated system used for optimum scheduling and management of demand energy response and manageable load and operating within the distribution system. The power management system provides data management, monitoring, and network information, and controls all automatic energy storage system(ESS) and distributed generation systems(DGS) that compose the microgrids [12].

The main features of the energy management system are [13]:

1. Maximize energy availability for each customer and increase system reliability.
2. Reducing energy loss, operating cost.
3. Maximizing the usage of renewable energy resources.
4. Reduced energy purchased outside the microgrid.
5. Manage all distributed generators, energy storage systems, and controllable load when resynchronization with the utility grid.

The energy management system requires data input such as the forecast of the non-dispatchable generation unit, electrical/heat load forecast, energy price, the state of charge (SoC) of the energy storage system, energy prices, forecasts of the thermal or electrical loads, operational reliability and security constraints of the grid, and information about the PCC (common coupling point) operation with the utility grid [14]. All this data is collected by the energy management system and develops a series of control procedures. The purpose of these actions is to reduce the total operating cost of the microgrid network and the energy bill paid by consumers, while reducing the network losses and emissions, and increasing the energy quality and reliability experienced by consumers [15]. Therefore, the energy management system provides output level information on utility (export / import power to main network), DER level (disconnection / connection or dispatch scheduling), and to the loads level As illustrate in Figure 1 [16].

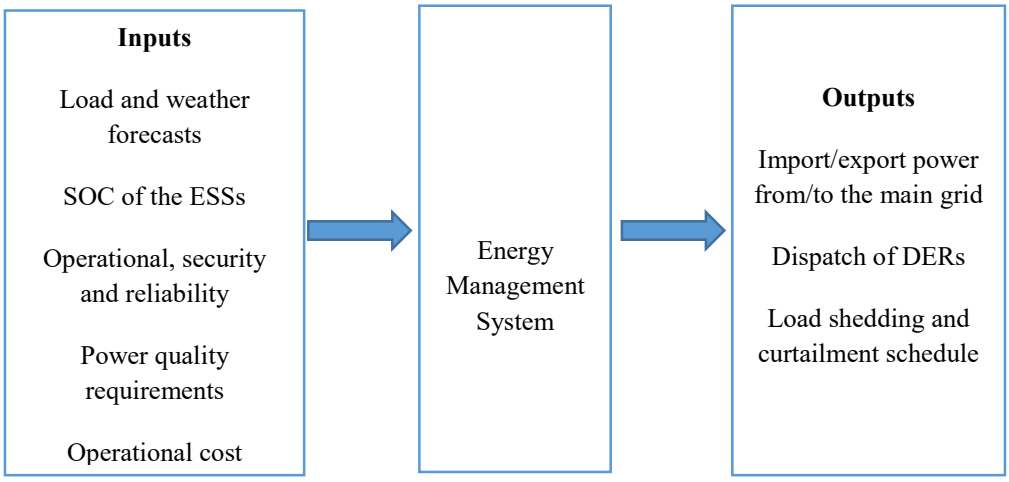

Figur.1: Input and output data in the energy management system

IV. PROPOSED SYSTEM DESCRIPTION

Figure.2 illustrates the overall configuration of the proposed system which includes a photovoltaic system with maximum power point tracking control, inverter and battery control, and control. The system integrates battery power as a backup unit to run critical loads and maintain voltage and frequency microgrid in emergency situations. The battery is usually placed in parallel with the photovoltaic system. The battery is usually placed parallel to the photovoltaic system. The batteries either absorbs or injects real power via a converter. The converter operates in boost mode when the battery supplies power to the network or load and operates in buck mode when the battery draws power from the photovoltaic. The battery injects or absorbs real power via a converter. The batteries are usually placed in parallel with the photovoltaics system. The converter operates in boost mode when the battery provides power for load or the grid and is on when the batteries feeds the power to load or grid and operates in buck mode when the batteries draws power from photovoltaic. The lead-acid batteries are commonly selected for photovoltaic application.

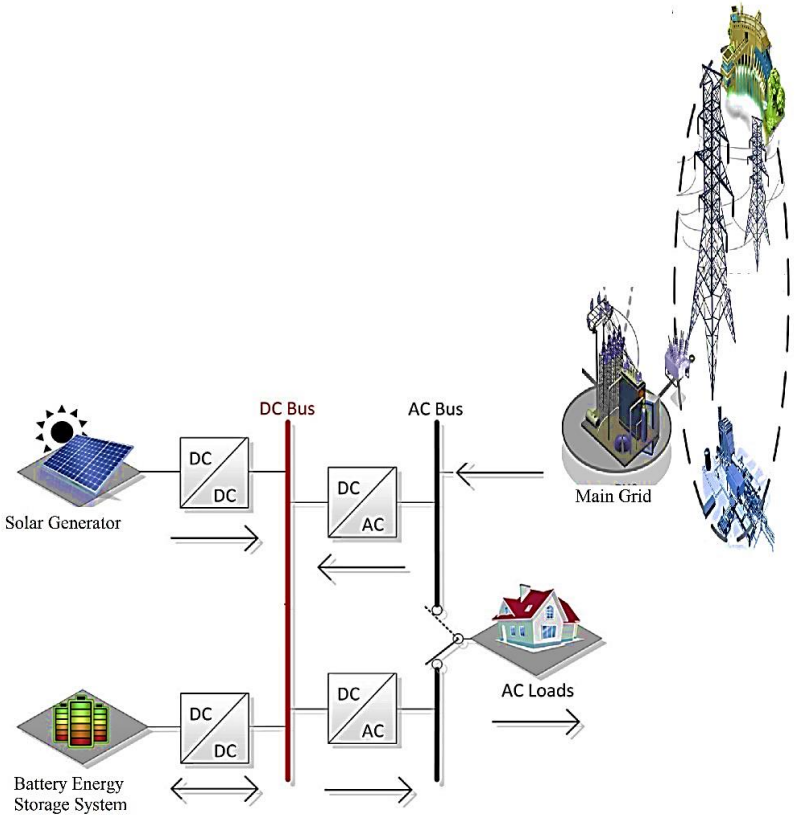

Figure.2: The proposed system structure

V. DISTRIBUTED HYBRID ENERGY GENERATION SYSTEM

A. Modeling of PV Cell

Figure.3 illustrates the equivalent circuit based on the single diode model of PV cell which can be represented as a current source, diode, series resistance, and parallel resistance. The I-V characteristics of PV cell are described by the mathematical standard equation which is [17]:

$$I = I_{ph;cell} - I_{0;cell}\left[\exp\left(\frac{q(V+IR_{s;cell}}{akT}\right) - 1\right] - \frac{V+IR_{s;cell}}{R_{p;cell}} \quad (1)$$

Where:

I_{PH}, *the cell* is the photocurrent (A) of the PV cell which represents the current source,

Id, the cell is the current (A) computed by the Shockley diode equation of PV cell,

I_o, *the cell* is reversed leakage or the saturation current of the PV cell diode,

q is the electron charge ($1.602 \times 10^{-19}\ C$),

k is the Boltzmann's constant ($1.38 \times 10^{-23}\ J/K$),

T is the temperature of the diode measured in Kelvin (K),

R_s, the cell is the series resistance of PV cell (Ω),

R_p , the cell is parallel resistance of PV cell (Ω) and

If the series and parallel resistances of PV cells are not taken into account, then the model of the PV cell is the ideal model. Figure 4 illustrates the I-V curve derived from Equation (1) for the ideal PV cell. It is noted that the net output cell current (I) results from the difference between I_{PH}, cell and I_d,cell of PV cell [18,19].

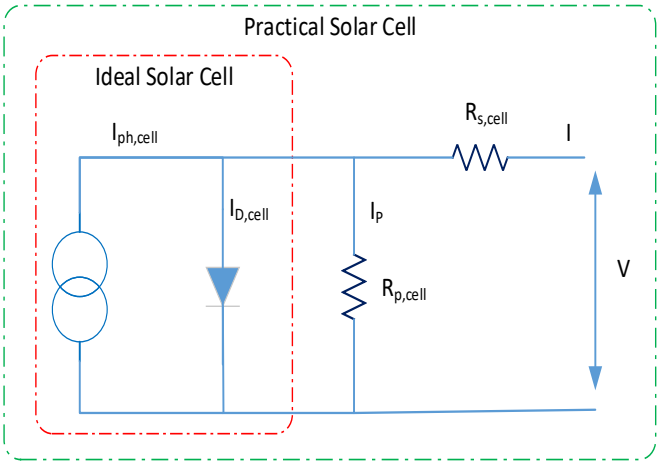

Figure 3: The equivalent circuit of the PV cell

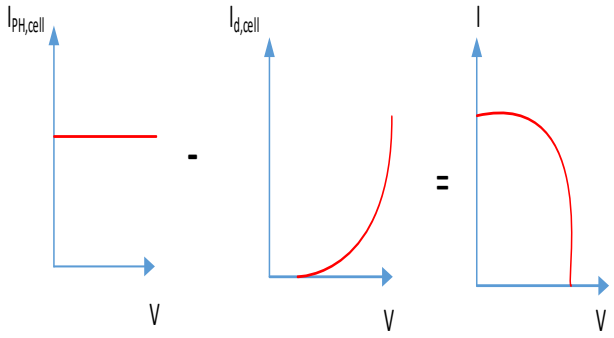

Figure 4: A typical I-V curve of PV cell

B. Modeling of PV Module

As stated earlier, a PV module is composed of PV cells jointed in a series and parallel forms. Therefore, the mathematical standard Equation is derived from Equation (1) and the description of the I-V characteristic of the PV module becomes [20]:

$$I = I_{PH} - I_O\left[exp\left(\frac{V+IR_S}{a\,Vt}\right) - 1\right] - \frac{V+IR_S}{Rp} \quad \ldots\ldots (2)$$

where:

I_{PH} is the photocurrent (A) of the module

Vt is the thermal voltage of the module which is equal to $NskT/q$ where *Ns* refers to the number of series-connected cells,

I_O is reverse leakage current of the module,

R_S is the series resistance of the module and

R_p is the parallel resistance.

Equation (2) produces the I-V curve as indicated in Figure 5, where three salient points are bolded:

1. Short circuit current point (0, I_{sc}).
2. Maximum power point (MPP) (V_{mpp}, I_{mpp}) located at the V-I curve.
3. Open circuit voltage point (V_{oc}, 0).

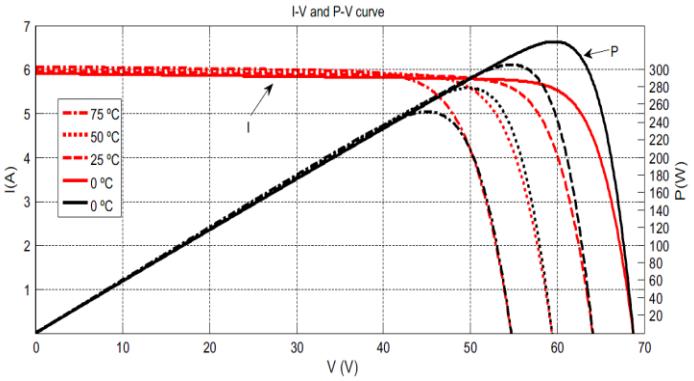

Figure 5: I -V, P - V curves of a practical photovoltaic module at different temperature levels and constant insolation

The photocurrent of a PV module (I_{PH}) depends on the amount of the solar irradiance falling on the module and the PV cell temperature corresponding to the below Equation [21]:

$$Iph = \frac{G}{Gn}(I_{ph;n} + Ki\Delta T) \quad \dots (3)$$

where:
$I_{PH.n}$ is the photocurrent under the nominal condition (usually $25C^O$ temperature and 1000W/m2 irradiance), ΔT is the difference between the actual temperature (T) and the nominal temperature (T_n) of the PV cell and they are measured in℃,
G_n is the nominal irradiance (1000 W/m2).
G is the solar irradiance measured in W/m2,
Ki is the temperature coefficient.
While the open voltage circuit (V_{oc}) depends on the cell temperature corresponding to the below Equation:

$$V_{oc} = V_{oc;n} + K_v\Delta T \quad \dots (4)$$

where:
K_v is the temperature coefficient of the open-circuit voltage and $V_{oc;n}$ is the open-circuit voltage under the nominal conditions. The diode saturation current (Io) can be obtained according to the below Equation:

$$I_o = \frac{I_{sc;n}+K_i\Delta T}{exp\left(\frac{V_{oc;n}+K_v\Delta T}{a\,V_t}\right)-1} \quad \dots (5)$$

where $I_{sc;n}$ is the short circuit current under the nominal conditions [19].

B. Battery Storage System

Battery storage systems store the extra energy generated by renewable energy generation systems. However, if there is a lack of energy from the renewable energy generation system, the battery bank will be discharged to meet the demand for the load. the model of the battery as follows [22]:

$$SOC_{bat} = 100\left[1 - \left(\frac{1}{Q_{bat}} * \int_0^t i_{bat}(t)dt\right)\right] \quad \dots (6)$$

$$B_{AH} = \frac{1}{3600}\int_0^t i_{bat}(t)dt \quad \dots (7)$$

where SoC_{bat} is the battery state of charge (%), Q_{bat} is the maximum battery capacity (Ah), i_{bat} is the battery current and B_{AH} is the battery ampere-hour. The battery's initial state-of-charge (SoC) is set to 80%. In this system, the battery is modeled according to the characteristics of deep-cycle lead-acid batteries with discharge efficiency assumed to be 90%.

C. Loads

The loads consist of residential and commercial loads. Commercial loads appear on asynchronous devices to show the effect of commercial inductive loads, such as air conditioning systems, on the Microgrids. Residential loads are designed according to the daily non-seasonal consumption profile of the resort island. Residential loads are simulated according to the actual difference in the specific load profile for the specified resort island.

VI. The Proposed Control Method for Photovoltaics and Battery System

To ensure a stable response in the hybrid microgrid network during normal operation, figure 6 and figure 7 illustrates two news proposed control methods. In this paper, the investigation is carried out to choose the state which has a major influence on the DC-link voltage state. This will lead to reducing the controller effort needed to limit the DC-link voltage and thus using a small controller gain, which preserves the stability.

A. The Control of the converter interfaced Photovoltaics

A single-phase boost phase is used to boost the voltage from the panel and maximum power point tracking. The input current (I_{PV}) is sensed before the input capacitance along with the panel voltage (V_{PV}). These two values are used in the maximum power point tracking algorithm. The maximum power point tracking algorithm calculates a reference point the panel input that needs to be maintained at to be at the maximum powerpoint. The maximum power point tracking is realized using an inner current loop and an outer voltage loop, as shown in Figure.6. Therefore, the sign for the outer voltage compensator reference and feedback are reversed. Note that the converter output has not been adjusted. To prevent the output voltage from rising higher than the rating of the components, the voltage feedback is mapped to the internal comparators, which can do a cycle by cycle trip of the PWM in the case of overvoltage.

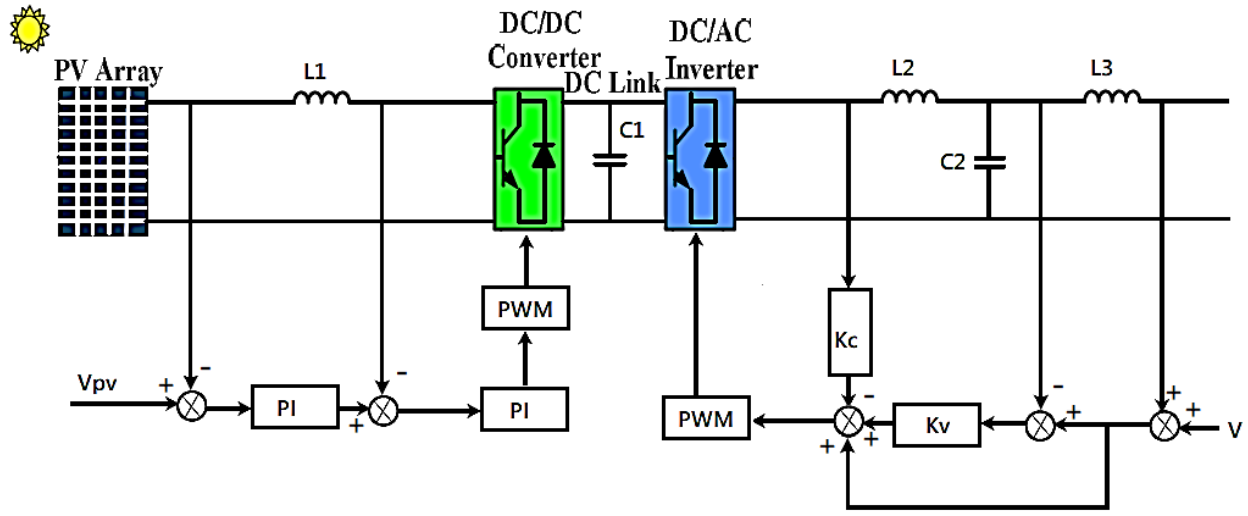

Figure.6: The proposed controller of the converter with maximum power point tracking

B. The Control of bidirectional-converter interfacing battery

In the proposed system, as shown in Fig.2, the bidirectional converter consists of the high-frequency inductor and the output filter capacitor and two switches that allow bidirectional current flow. In the power management method, there is a two-voltage controller with adequate limitation blocks to achieve the required power flow under different conditions. These controllers produce a reference current for energy storage. The first control unit is to regulate the DC-Bus voltage, and the second controller is to control the battery voltage. In order to improve the power management in the hybrid microgrid, backup energy storage is included. It consists of a battery connected to a DC bus with a bidirectional converter. This converter performs multiple functions: it acts as a battery charge regulator in grid-connected operation, and a boost converter to deliver energy from the batteries to the microgrid when the fuel cell and photovoltaics sources have insufficient power to feed the loads (AC loads and DC loads) in islanded operation. In island mode operation, the most favorable operating conditions occur when the load energy and the photoelectric extracted power agree, that is when the converter does not process power. Figure.7 shows a simplified phase of the converter power and its bidirectional control structure.

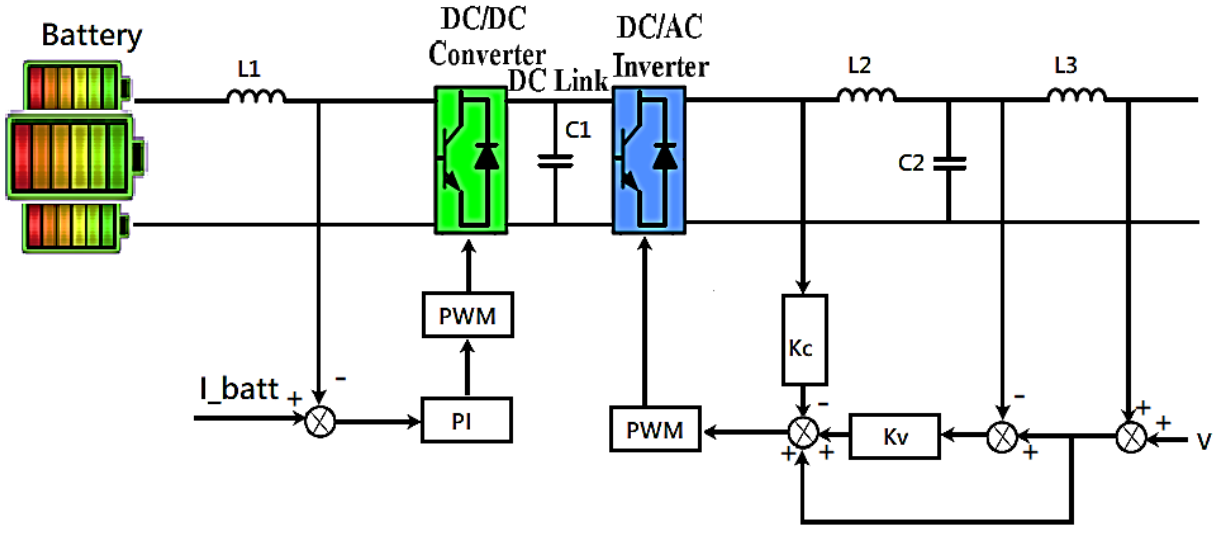

Figure.7: The proposed controller of battery storage

VII. The Proposed Home Energy Management System

In islanded mode, the battery is used as a backup power source when the photovoltaic generated power is less than the customer's energy demand. In this mode, when the photovoltaic source produces more power than that of connected loads, then the excess power is stored in the battery. The energy stored in a battery is used whenever the power demand of consumption exceeds the actual photovoltaic power generation. In the mode of grid-connected operation, the battery is enabled to charge from utility power and photovoltaic. In this operating mode, the energy generated by the photovoltaic cells is delivered to the batteries at a constant rate. At the time of beginning, photovoltaic array produces lower power from which the battery can't charge. During this condition, grid power is taken by the inverter as supplementary energy. As soon as the battery charge power reduces, the inverter begins to supply power into the grid. Once the battery gets fully charged, all the generated power from photovoltaic delivered to the grid.

The hybrid microgrid real power exchanged with the grid $P_{grid}(t)$ is the sum of the photovoltaic generation system P_{PV} , the $P_{Batt}(t)$ and loads (Figure.2).

$$P_{grid}(t) = P_{PV}(t) + P_{Batt}(t) - P_{Load}(t) \quad \ldots(8)$$

During such a long time, the fast power variations exchanged with the battery $P_{Batt}(t)$ can be neglected. Equation (8) is expressed over a long range of time as follows:

$$\{P_{grid}\}T = \{P_{PV} - P_{Load}\}T \quad \ldots(9)$$

During such a short time, the batteries masters the power flow thanks to its fast response time. The power reference of the battery $P_{Batt}(t)$ can be calculated by the inversion of the Equation (8) as:

$$P_{Batt}(t) = P_{grid}(t) - P_{PV}(t) + P_{Load}(t) \quad \ldots(10)$$

The battery has an extremely fast charging and discharge response, and so in this study, Batteries are used for the DC-Bus voltage control of the hybrid microgrid. The storage capacity of battery is subject to the following constraints:

$$E_{Batt\,min} \leq E_{Batt}(t) \leq E_{Batt\,max} \quad \ldots(11)$$

where $E_{Batt\,min}$ and $E_{Batt\,max}$ are the minimum and maximum allowable storage capacities of batteries. $E_{Batt\ min}$ is determined according to the following equation.:

$$E_{Batt\,min} = SOC_{Batt} \times E_{Batt\,max} \quad \ldots(12)$$

The houses microgrid can exchange power with local grid. The surplus produced power of the photovoltaic after charging batteries is sold to the grid. If the total produced power of the hybrid microgrid cannot satisfy the demand, power will be purchased from the utility grid.

VIII. The Results of the Proposed System

To show the effectiveness of the proposed control method, a proposed microgrid is simulated using Matlab/Simulink to validate the performance. This microgrid consists of photovoltaic and battery units. The parameters are listed in Table I. The performance has been tested in both grid-connected and island mode during unintentional islanding. In grid-connected mode, the photovoltaic generates MPPT reference and the battery generates reference sent by control. At first, the batteries are assumed to be fully charged and the load is not connected to the system yet. The power grid is connected to domestic from the distribution transformer. The surplus power from the home energy management system is fed into the power grid. Also, it can supply power to the home energy management system in the case of a shortage of power generation in the photovoltaic system. This transfer of power between home energy management system and power grid takes place with the help of a bidirectional DC to AC inverter. The photovoltaic is allowed to operate at its standard test condition with an operating $1000\,W/m2$ Irradiation and $25C^o$ temperature. The simulation is carried out for 80 seconds. The total power generated by the photovoltaic is maintained constant at 6 kW by the MPPT controller. Figure 8 shows the output current and voltage for the photovoltaic power generation.

Table 1: Simulation Parameters

Parameter	Value
k_p	25
k_i	60
ω	$2\pi \times f$
f	*50*
V	220 V
X	1 mH
R	0.08Ω

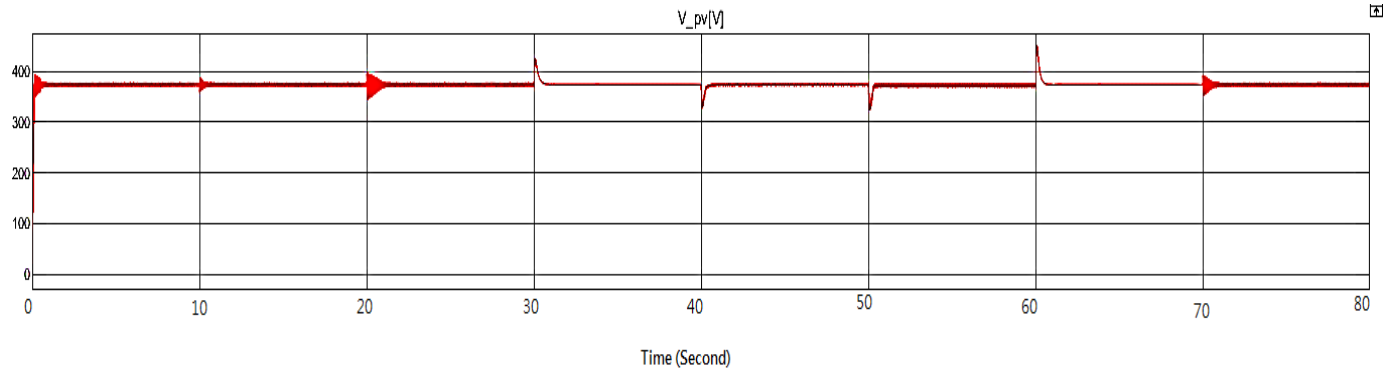

(a)

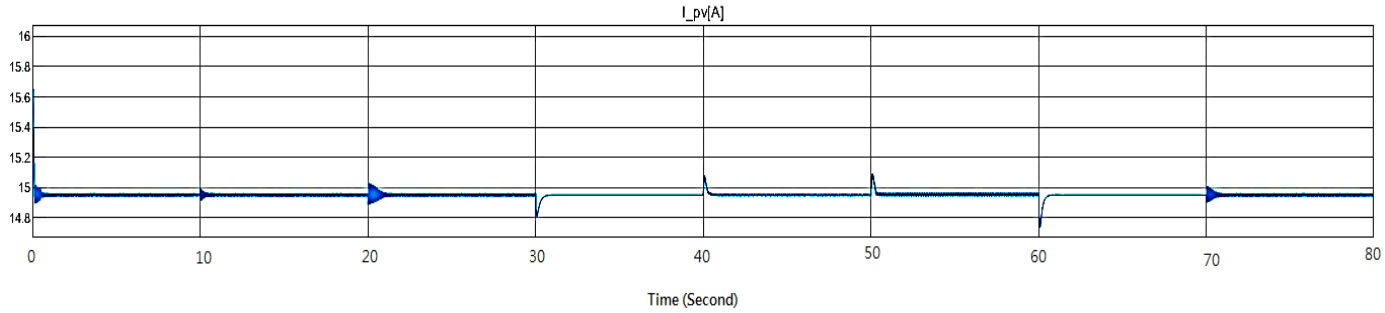

(b)

Figure.8: (a) the photovoltaic voltage at MPPT and (b) the photovoltaic current at MPPT

System load will take effect at the specified time interval. In this study, two rated PQ loads with the real power of 4 kW and 100 AVR are connected to the home energy management system. Figure 9 shows the time interval when loads are being connected to the home management system

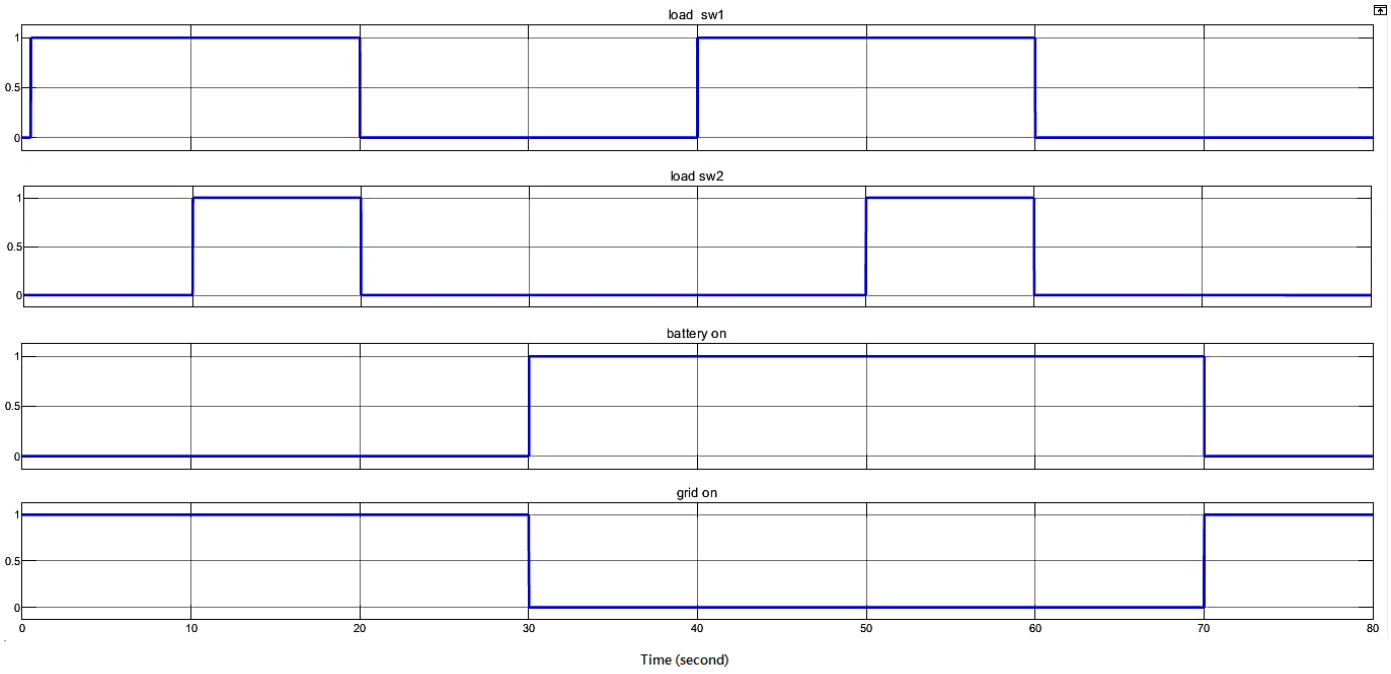

Figure.9: Switching between island, grid operations modes and loads

Consider operating in grid-connected mode, where the first load of 4KW is connected at time t=0.75 second. The load consumes more than half the power generated from the photovoltaic, and the remaining power is returned to the power grid. At time t = 10 seconds, second load (also 4KW) is connected. Currently, the system has a total system load of 8,000 watts (4kw+4Kw), which is more than the power generated by the photovoltaic system. Hence, the shortage of power is supplied to the consumer by the utility power. Therefore, the grid will help to balance the power demand of consumers along with the photovoltaic system. Figure 10 shows the residential load at different times.

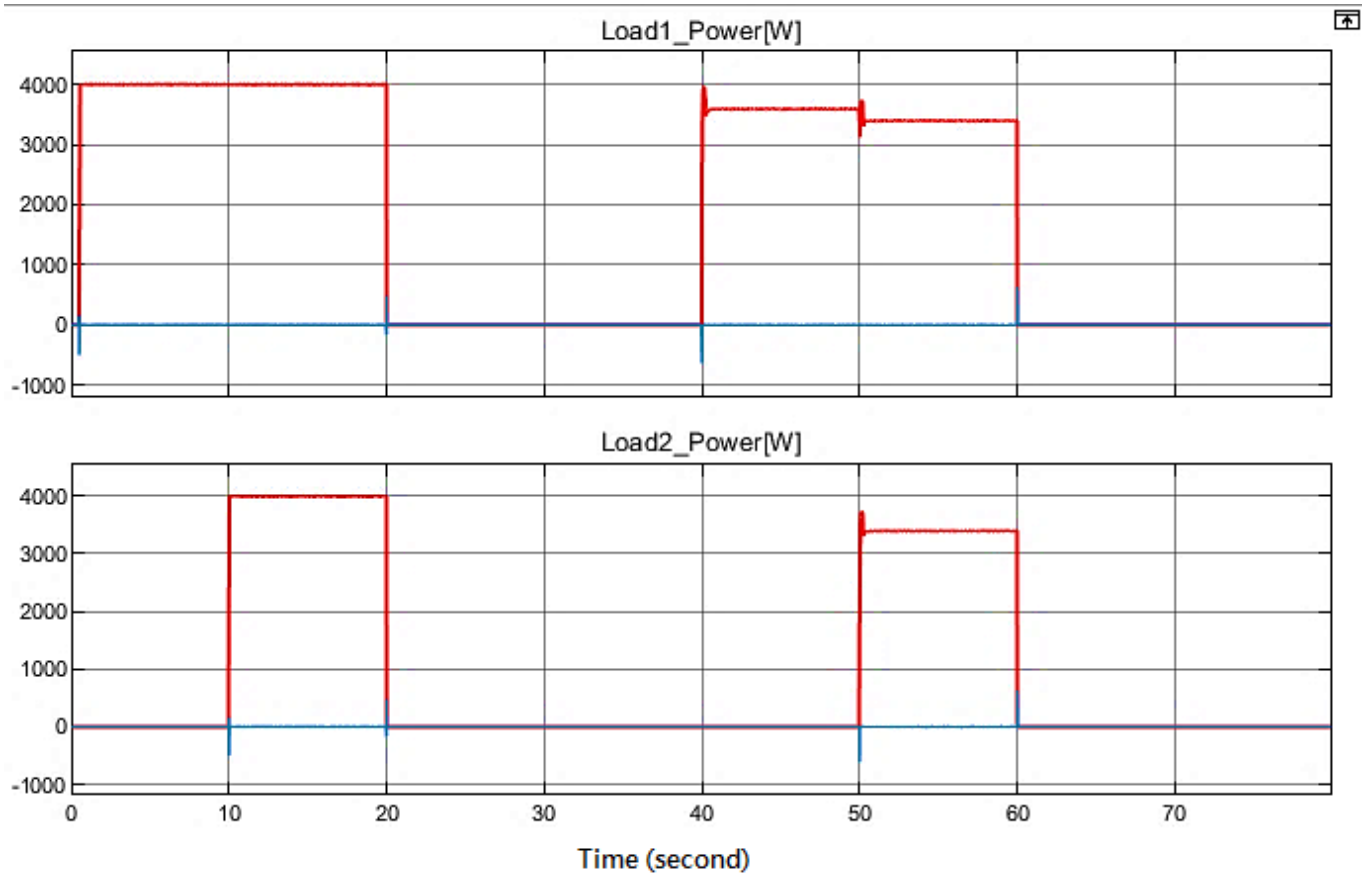

Figure.10: Load variation at home for many time

Then, to test the proposed system behavior in the transition condition, the grid is now disabled at time t=30 seconds. Now the microgrid operates in an island mode of operation. Figure 9 shows the system's response to loading changes from 4 kW to 8 kW. In this mode, the photovoltaic system is allowed to generate its maximum power of 6 kW. The battery operates in the islanded mode. The battery will supply the complementary power required to meet consumer power demand. The output of inverter decreases or increases based on the requirement of load power, while the DC-link voltage is kept constant. The maximum power point tracking controller provides the reference value for DC link voltage and is maintained constant by the battery DC to DC converter by absorbing or delivering adequate power.

Figure 9 shows the transition from the grid to the island operating mode. Here again, the first load and second load of capacity 4 kW each is connected to the home energy management system at time t=40 second and t=50 second respectively. During the connection of the first load, the photovoltaic supplies the required power as the power demand is below the photovoltaic generated power. When the second load is connected to the home energy management system, the total load becomes 8 kW is higher than the photovoltaic generated power. The battery power is enabled to provide this power difference to make power balance. The following Figures illustrate the various parameters home energy management system in the grid-connected and islanded mode of operation.

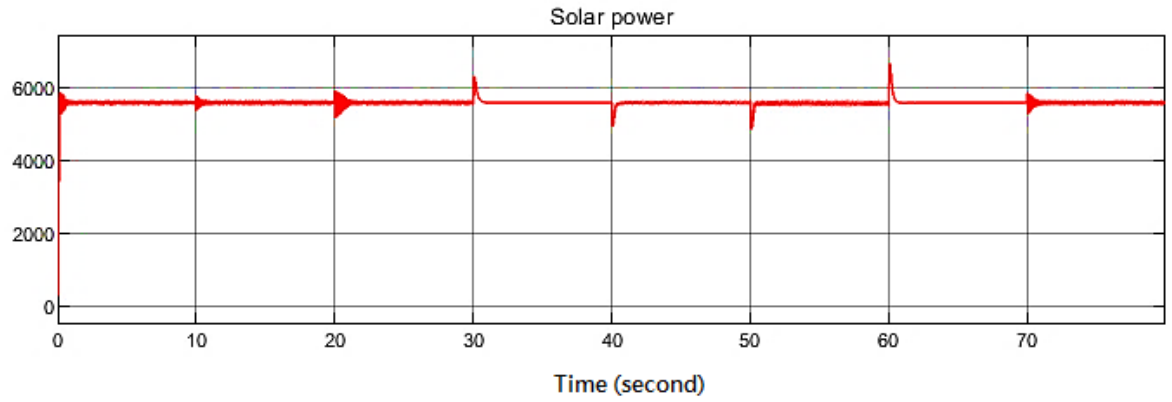

Figure.11: The photovoltaic power during island and grid modes

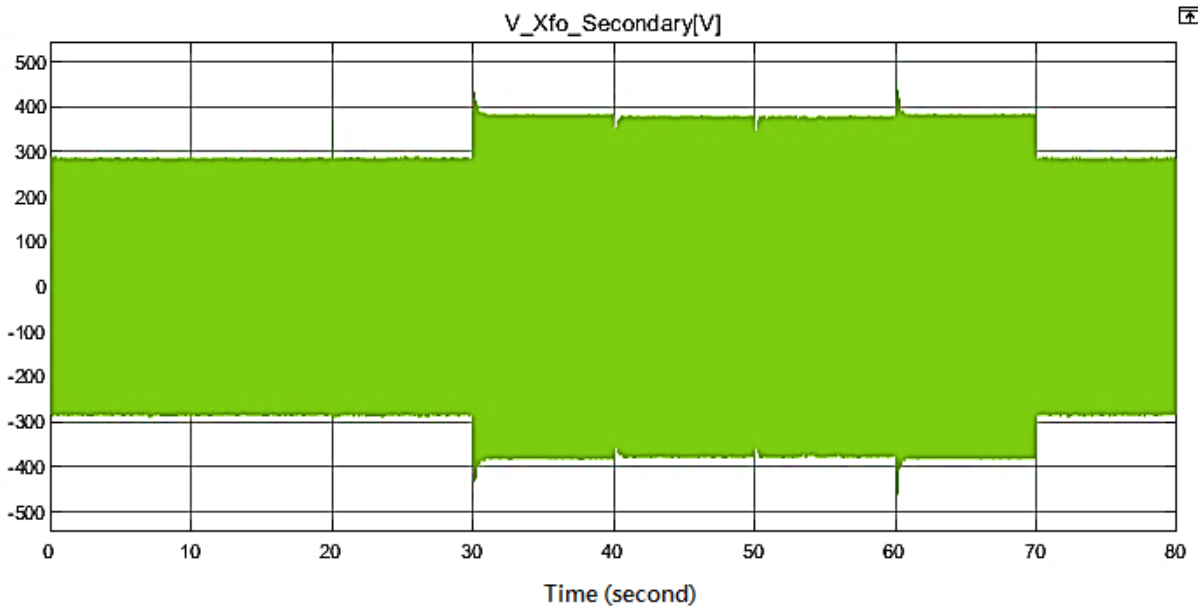

Figure.12: Load voltage during both island and grid modes of operation

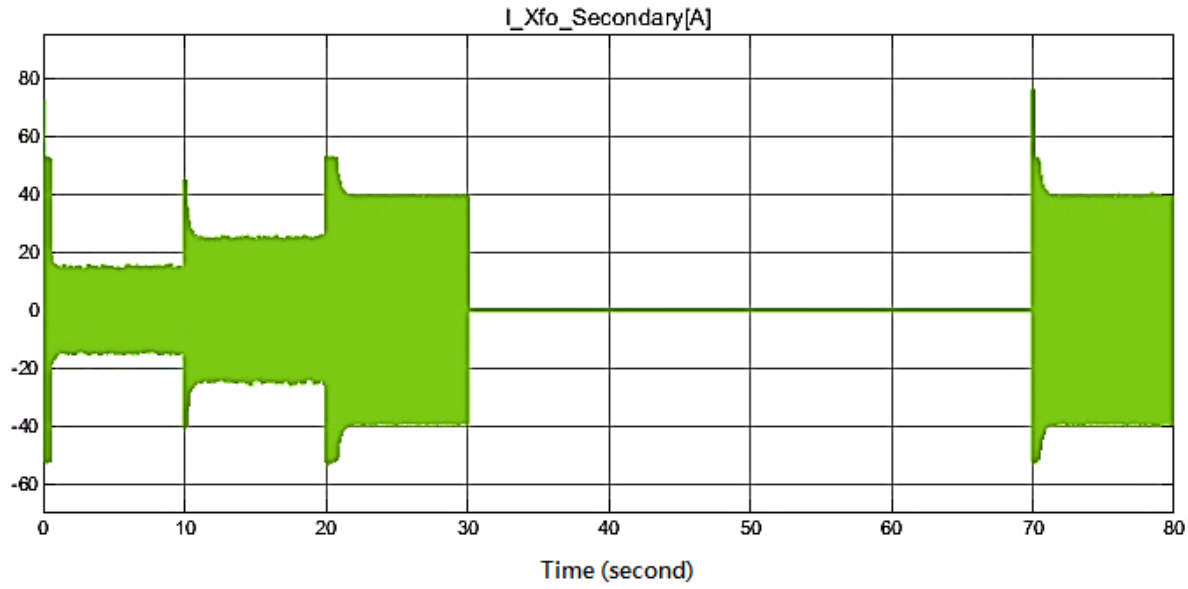

Figure.13: The contributed via the grid for island and grid modes

Figure.11 shows the power generated by the photovoltaics. The total power generated remained almost constant at 6 kW throughout the simulation. Figure.12 illustrates the load voltage during grid operated mode and islanded mode of operation. Obviously, for the time interval from t=0 second to 30 seconds, the system operated in grid-connected mode drawing power from both grid and photovoltaic systems. From time interval t=30 second to 70 seconds, the grid is disabled and now the system is operated in islanded mode feeding power to loads from both photovoltaic system and battery. Figure 13shows the current drawn from the utility grid. It is evident that the grid does not contribute to load during the interval of time t=30 to 70 seconds, as the grid is disabled. Figure14 replicates the power drawn from the grid to meet the demand power of residential homes. The Figure15 shows the battery parameters, state of charge, voltage, current and power during island operating mode at the time of transfer from the grid to island mode, the battery starts to discharge energy into an inverter for meeting the insufficient power that is not been ably met by the photovoltaic system.

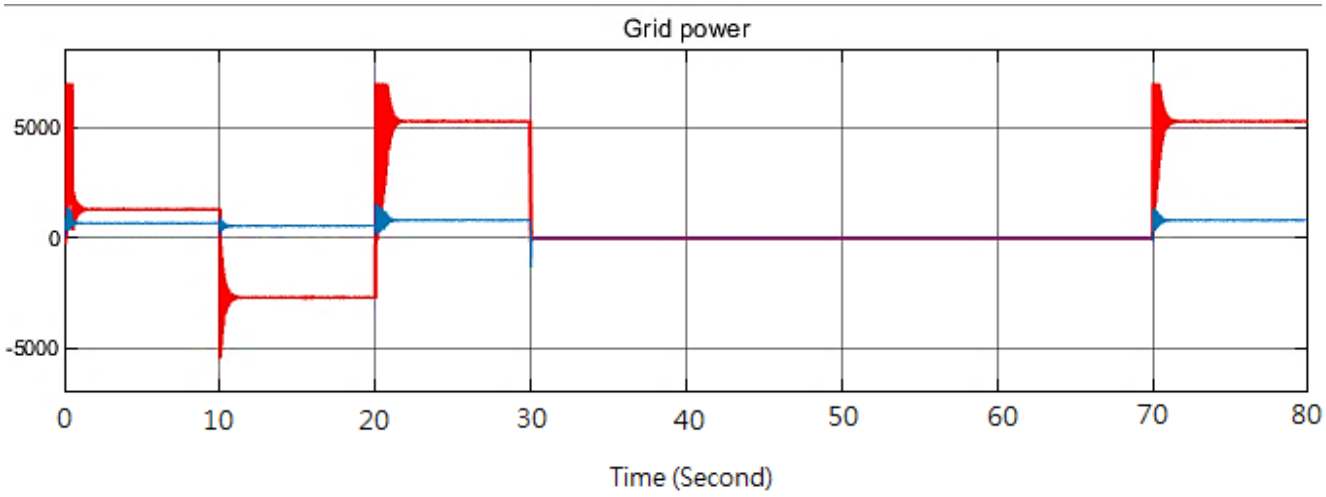

Fig.14. The active and reactive power of utility grid

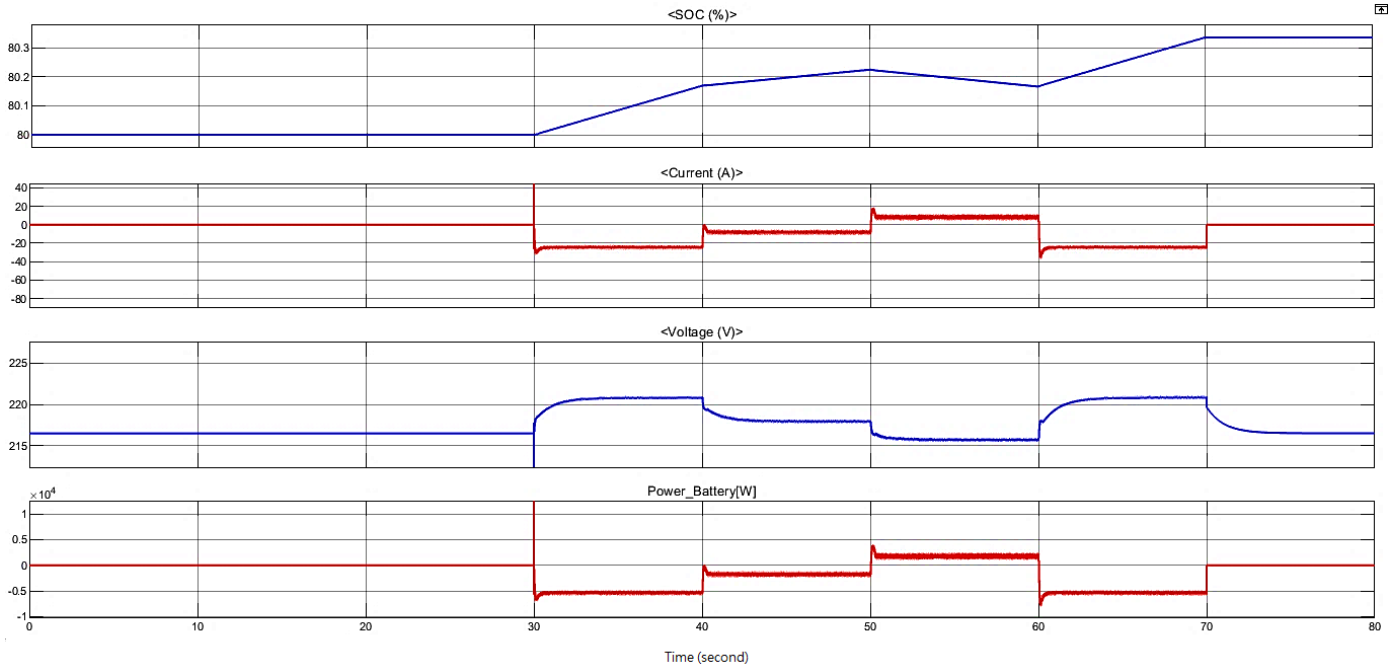

Fig.15. Battery discharge and charging during the transfer of grid to island operation

IX. CONCLUSIONS

In this work, a home management system shows the effectiveness of such a technique to deliver uninterrupted power to the consumer through various controller designs. Also, this paper proposes an effective control strategy for smooth transition from grid-connected to islanding mode due to unintentional islanding. Using the energy management system as part of the control design of a grid-connected microgrid can minimize the total operating cost. The supervisory control has been added to the control model to adjust any deviation between the main grid power and the scheduled reference power by modifying the reference set-point of the battery power given by the energy management system. The results show that the proposed adaptive energy management system for smart hybrid microgrids based on green energy supports the minimal use of power of utility grid. The proposed strategy is able to share the power among the distributed generator units even under unbalanced conditions. Also, results reveal that the incremental conductance method collects more daily energy than the constant voltage method when the ambient temperature is high. However, the irradiation and load variations tests show that the incremental conductance method is more oscillation, less dynamic response, and less stable about the maximum power point than conventional methods. Hence, the proposed method is more responsive and efficient than the conventional method.

REFERENCES

[1] M. H. Kapourchali and M. Sepehry, "Fault Detector and Switch Placement in Cyber-Enabled Power Distribution Network," IEEE Transactions on Smart Grid, Vol.9, No.2, pp-980-992, 2018.

[2] M. Tabari, A. Yazdani, "An Energy Management Strategy for A DC Distribution System For Power System Integration of Plugin Electric Vehicles". IEEE Transaction on Smart Grid, Vol.7, pp. 659- 668, 2016.

[3] A. Rajabi, L. Li, J. Zhang, and J. Zhu, "Aggregation of Small Loads for Demand Response Programs—Implementation And Challenges: A Review", 2017 IEEE International Conference on Environment and Electrical Engineering and 2017 IEEE Industrial and Commercial Power Systems Europe (EEEIC / I&CPS Europe), pp. 1-6,2017.

[4] Ma Xiandong, Wang Yifei, Qin Jianrong, "Generic model of a community-based microgrid integrating wind turbines, photovoltaic and CHP generations", Appl energy, vol.112, pp.147-582, 2013.

[5] Alonso Monica, Amaris Hortensia, Alvarez-Ortega Carlos. "Integration of Renewable Energy Sources In Smart Grids By Means Of Evolutionary Optimization Algorithms", Expert Systems with Applications, vol.39, pp.22-55, 2015.

[6] Zhang Yu, Gatsis N, Giannakis GB, "Robust Energy Management For Microgrid With High-Penetration Renewables". IEEE Transactions on Sustainable Energy, vol.4, pp.45-53, 2015.

[7] Rouholamini, M.; Mohammadian, M. "Heuristic-Based Power Management of A Grid-Connected Hybrid Energy System Combined With Hydrogen Storage", Journal of Renewable Energy, vol.89, pp.12-24, 2016.

[8] Almada, J.B.; Leão, R.P.S.; Sampaio, R.F.; Barroso, G.C. A Centralized and Heuristic Approach For Energy Management of an AC Microgrid " , Journal of Renewable Sustainable Energy Review, vol.45, pp.67-87, 2016.

[9] Merabet, A.; Tawfique Ahmed, K.; Ibrahim, H.; Beguenane, R.; Ghias, A.M.Y.M, "Energy Management and Control System for Laboratory Scale Microgrid BasedWind-PV-Battery", IEEE Transactions on Sustainable Energy, vol.8, 2017.

[10] Farzin, H.; Fotuhi-Firuzabad, M.; Moeini-Aghtaie, M. "Stochastic Energy Management of Microgrids during Unscheduled Islanding Period", IEEE Transactions on Industrial Informatics, vol.13, pp.1079 - 1087, 2017.

[11] Battistelli, C.; Agalgaonkar, Y.P.; Pal, B.C. "Probabilistic Dispatch of Remote Hybrid Microgrids Including Battery Storage and Load Management" IEEE Transactions on Smart Grid, vol.8, pp.1305 - 1317, 2017.

[12] Basu, A. K., Chowdhury, S. P., Chowdhury, S, & Paul, "Microgrids: Energy Management by Strategic Deployment of DERs—A Comprehensive Survey", Renewable and Sustainable Energy Reviews, vol.15, pp. 4348–4356, 2011.

[13] Molderink, A., Bakker, V., Bosman, M. G. C., Hurink, J. L., & Smit, G. J. M, "Management and Control of Domestic Smart Grid Technology", IEEE Transactions on Smart Grid, vol. 2, pp. 109–119, 2010.

[14] Chen, C., Duan, S., Cai, T., Liu, B., & Hu, G. (2011). "Smart Energy Management System for Optimal Microgrid Economic Operation" IET Renewable Power Generation, vol.5, pp. 258-265, 2012.

[15] Lujano-Rojas, J. M., Monteiro, C., Dufo-López, R., & Bernal-Agustín, J. L, "Optimum Load Management Strategy for Wind/Diesel/Battery Hybrid Power Systems", Journal of Renewable Energy, vol. 44, pp. 288–295, 2013.

[16] Palma-Behnke, R., Benavides, C., Lanas, F., Severino, B., Reyes, L., Llanos, J., & Saez, D , "A Microgrid Energy Management System Based On The Rolling Horizon Strategy", IEEE Transactions on Smart Grid, vol. 4, pp. 996–1006, 2013.

[17] S. Jamalaldin, S.Hakim and H.Razak, "Damage Identification Using Experimental Modal Analysis and Adaptive Neuro-Fuzzy Interface System (ANFIS)", Topics in Modal Analysis, Conference Proceedings of the Society for Experimental Mechanics Series 30, Vol.5, pp.399-405, 2012.

[18] B. Tarek, D. Said, and M.Benbouzid, "Maximum Power Point Tracking Control for Photovoltaic System Using Adaptive Neuro-Fuzzy", IEEE, 8th International Conference and Exhibition on Ecological Vehicles and Renewable Energies (EVER), pp. 1-7, 2013.

[19] M. Mahdavi, Li Li, J. Zhu and S.Mekhilef, "An Adaptive Neuro-Fuzzy Controller for Maximum Power Point Tracking of Photovoltaic Systems", IEEE, 2015, TENCON 2015-2015 IEEE Region10 Conference, pp.1-6, 2015.

[20] M. Villalva, J. Gazoli, E. Ruppert, "Modeling and Circuit-Based Simulation of Photovoltaic Arrays", Brazilian Journal of Power Electronics, Vol. 14, No. 1, pp. 35-45, 2009.

[21] K.ElNounou, "Design of GASugeno Fuzzy Controller for Maximum Power Point and Sun Tracking in Solar Array Systems", Master Thesis, The Islamic University, Gaza, 2013.

[22] Fathima AH, Palanisamy K. "Optimization in Microgrids with Hybrid Energy Systems – A Review". Renewable & Sustainable Energy Reviews, Vol.45, pp. 431–46, 2015.

Bilal Naji Alhasnawi was born in Al Samawah, Iraq in 1993. he received the B.S. in Electrical engineering from the University of Kufa, in 2015. he received the M.S. degrees in Electrical engineering from the University of Basrah, in 2018. he is also working toward his Ph.D. degree within the Electrical Engineering Department, College of Engineering, University of Basrah, Basrah, Iraq. His research interests Smart Grid Engineering, Control Theory, Renewable Energy Technologies, Electrical Power Engineering, Power Systems Analysis, Power Electronics, Power Converters, Isolated Microgrids, Droop control, hierarchical control, Microgrids Optimization, Energy Management, Photovoltaics, Distributed Generation, Wireless Sensor Network, Information and Communication Technology, and Computer Engineering. He is an Active Reviewer of the IEEE ACCESS.

Dr. Basil H. Jasim. was born in Basrah, Iraq in 1973. He received the B.Sc and M.Sc degrees in Electrical Engineering and Control & Computers Engineering from the University of Basrah, Basrah, Iraq in 1995 and 1999 respectively. He also received his PhD degree in the field of Control and Systems from the Basrah University, Iraq in 2007. He is currently an Professor at the University of Basrah. His teaching interests covering wide areas of modules across the department of Electrical Engineering, University of Basrah, include Intelligent Control Systems, Robust Control Systems, Microprocessor & Microcontrollers and Industrial Automation. He currently serves as a co-editor of the Basrah Journal for Engineering Sciences. His research interests include Intelligent Control of Robotics, Computational Intelligence, Chaos & Nonlinear dynamics, Renewable electrical energy systems, and PLC applications in industrial and engineering education. Dr. Basil is a Senior Member of the IEEE.

Open Access

Iraqi Journal for Electrical and Electronic Engineering
Conference Article

Robotic Glove for Rehabilitation Purpose: Review

Yahya Salim Ahmed*[1], Auns Q. Al-Neami [2], Saleem Lateef [3]
[1]Medicine College, Mosul University, Mosul, Iraq
alhaleemay@gmail.com
[2] Department of Biomedical Engineering, College of Engineering, Al-Nahrain University, Baghdad, Iraq
uns_alneami@yahoo.com
[3] Department of Medical Instrumentation Techniques Engineering, Electrical Engineering, Technical College, Middle Technical University, Baghdad, Iraq
Saleem_lateef_mohammed@mtu.edu.iq

Correspondence
* Yahya salim ahmed
Medicine College, Mosul University, Mosul, Iraq
Email: alhaleemay@gmail.com

Abstract
Rehabilitation robots have become one of the main technical instruments that Treat disorder patients in the biomedical engineering field. The robotic glove for the rehabilitation is basically made of specialized materials which can be designed to help the post-stroke patients. In this paper, a review of the different types of robotic glove for Rehabilitation have been discussed and summarized. This study reviews a different mechanical system of robotic gloves in previous years. The selected studies have been classified into four types according to the Mechanical Design: The first type is a tendon-driven robotic glove. The second type of robotic glove works with a soft actuator as a pneumatic which is operated by air pressure that passes through a plastic pipe, pressure valves, and air compressor. The third type is the exoskeleton robotic gloves this type consists of a wearable mechanical design that can used a finger-based sensor to measure grip strength or is used in interactive video applications. And the fourth type is the robotic glove with a liner actuator this type consists of a tape placed on the fingers and connected to linear actuators to open and close the fingers during the rehabilitation process.

KEYWORDS: Robots, Actuator, Glove, Rehabilitation.

I. INTRODUCTION

Several types of rehabilitation robots have been developed for different purposes. These robots can provide additional or superior tasks to patients which can be used to help patients to do various tasks [1-2]. The patient with stroke is suffer from a constriction or discontinue of the blood flow in the brain which make a damage in the nervous system so to communicate with the remnant parts of the body will be reduce. Which causes damage on one side of the body by damaging the upper and lower limbs of this side and also weaken a human functional process as thinking and speech. Rehabilitation robots is use to help in rehabilitate this damage in acting as physical therapy [3]. The construction of the hand robotic glove is individual finger can be moved by servo motors which controlled by Arduino microcontroller and multi sensors to determine the hand clipper [4]. Another mechanical design for a rehabilitation robotic is the tendon actuator robotic exoskeleton for hand rehabilitation, can be classify as two types of design for the upper limb researched in the field of robotic gloves. The first one is a external robot which is inserts on the patient hand and robotically assisted him or a pre-determined tasks model and the second is a portable rigid to rehabilitate with another structure [5]. The soft actuators are based on use elastomeric materials because for its flexible use when wearing as gloves. The pressure amount of hydraulic for the soft actuators are used to control the finger flexion/extension [6,8]. The soft actuator can be also used with motion capture system to be used as task specific training (TST) for a post stroke rehabilitation [7]. Another soft robotic glove as hand rehabilitation device designed to assist for hand opening during the rehabilitation by inflatable plastic actuators [8,9]. There are some steps to develop a rehabilitation system to increase patient assistance for acquiring, one of these developments has been used to control the system through the EMG signal generated from the muscles [10]. Another development of the systems by connecting a smart phone device to control the system through it by five servo motors connected to the fingers [11,20]. It is also possible to control the smart robotic glove by analyzing the movement of the hand through image processing or a tele-operation and it is considered one of the methods used with certain cases of stroke patients [12]. Although there are several types of raw materials for glove production, as Fabric, rubber and plastic, there is a glove made by silicon for easy sterilization and use in hospitals for more than one patient [13]. It is possible to add an electrical stimulus to the glove when manufacturing to develop it to

reveal the intention of the patient to move his affected hand. This stimulation is through electrical currents to activate the affected nerves [14,15]. Other type of robotic glove control in addition to controlling by means of the EMG signal can also be controlled by sound instructions to control the process of opening and closing the glove during rehabilitation [16]. In some type of gloves, Bowden cables can be used during design as a means of transmitting movement from the glove to the motor. To reduce the additional weight carried by the patient's arm, which causes an obstacle to the design and an additional weight carried by the patient [17]. One of the modern developments of the robotic glove is the integration of a virtual – reality with the main design of the glove to stimulate the damaged brain area and enhance the relationship between the brain and the affected hand [18]. Another development could be added to the design, which is the possibility to monitor the patient remotely through the Internet during operations of rehabilitation [19]. One of the robotic glove designs is the X-Glove which is used for operations of rehabilitation [21]. The addition of virtual reality (VR) development to the pneumatic glove, to make the rehabilitation process of stroke patients more active [22]. Finally, most of the robotic gloves used for rehabilitation are designed to be suitable for the patient in terms of light weight, cheap and mobile so that the patient can use them easily without the need for a physical therapist and the possibility of combining easy methods of control.

II. Mechanical Design According Actuator

It is important to show the principle of mechanical design of a robotic glove and select the commensurate with the actual need of the patient. There are several types of design depending on the type of Actuator used in the design and can be divided as shown in the (Fig. 1). Then the review will be present these designs with mentioning specifications.

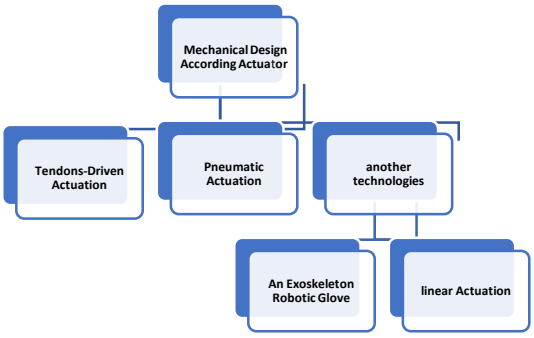

Fig. 1: Block diagram for several type of mechanical designs

A. Robotic Glove Based on Tendons-Driven Actuation

These robotic gloves are work on the principle of tendons. This design is simulating the installation of the tendons of the human hand by transient the movement of muscles to the upper and lower limbs of the human body. The rehabilitation process mainly depends on the repetition the exercises and the results of this process are clearly shown by comparing these results with the effectiveness of the hand before the exercises [37]. One of the most important characteristics of robotic glove when manufacturing is that it is low cost and light in weight [38]. Some robotic gloves Comprehension virtual reality technology to help stroke patients increase focus with the rehabilitation process [39]. The robotic glove should be arm fit so that it does not affect the patient's daily stroke activities [40]. After developing this glove, it is possible to send hand movement information to a(VR) program to determine if the rehabilitation movements are correct [41]. Tendons are rigidly attached to the glove to ensure safe opening and closing of the patient's hands during rehabilitation [42]. The parts needed to secure the tendons to the glove are designed by 3D printers [43]. The glove is controlled by attaching the Arduino processor to the actuators that perform the hand movement [44].

In 2013 Hyunki In et al. [23] Analyzed and discussed the force applied at the finger joints that produced by the force obtained from by the SNU Exo-Glove. By use a joint-less wearable robotic hand with fingers were driven by the tendons attached directly on the glove. The glove was operated by three motors the first to move the thumb, the second to move the index finger, and the third to move the middle finger, the movement is transfer from the actuators to the fingers by the tendons that similar to the action of the tendons in the human hand. The force generated at the human hand is analyzed before using the glove because the force applied to the joints of the fingers of the hand must be determined for the disable because it is weaker than the joints of the healthy fingers. The glove is shown in (Fig. 2a).

In 2015 Nycz et al. [5] proposed a technology has been rehabilitative and assist individuals has a hemi paresis in their upper limbs by a therapy outside of the clinic. The robotic glove has (6 DC actuators), five actuators attributed to five finger and the sixth for elbow. The actuators were located on the wrist to avoid burdened affected limb with heavy weights. Motors were located remotely in an external block, the glove's weight (2.75 kg) and size (260X200X85mm) dimension. Therefore, this robotic glove is light weight for the patient and is available with low cost and can be used outside the clinic for patients who need the rehabilitation and elbow rehabilitation has also been added in this system to become more useful it can be seen in (Fig. 2b).

In 2016 Kang et al. [13] presented a robotic glove based on tendon driven and used the silicone as a raw material in manufacturing so that more than one person can use it because it is sterile. The glove is driven by two actuators, one for thumb and the other for the index and middle fingers, in addition to pressure sensors for control the limit of the fling's movement. This is a new Exo-glove system that uses silicone instead of fabric in the glove design. The glove manufactured by a molding process using a silicone (KE-1300or KE-1300T, Shinetsu). In order to reduce the friction of wires in the glove a tube of Teflon was placed on the silicone glove to pass the tendons throw it. The glove actuators unit consists of two actuators (DCX22, 24V,20W, Maxon). The results show that the glove is capable of holding weight between (1 to 1.5 kg). The glove shown in (Fig. 2c).

In 2016, Bigger et al. [3] presented a novel design for a rehabilitative wearable glove depending on the principle of tendons to move three fingers through a system consisting of pieces like cups and tendons with the following specifications. The motors of the glove have the following parameter as rated torque (60mNm), speed (51rpm) and power (588mW). The extension process of the finger has been done by a elastic band which is implied on the glove. Various objects have been handled to calculate the angles of the finger's joints. The glove was developing an increase contribution to the metacarpophalyngeal joint (MCP) (from 11.21 to 42.09%) and decrease contribution to distal inter phalyngeal joint (DIP) (from 49.28 to 19.64%) increase motion has been increase the benefit of rehabilitation, the final structure of glove as shown in (Fig. 2d).
In 2017 Biggar et al. [10] proposed a systems development a glove will be treated with the physiotherapist during the rehabilitation process to be the recovery faster. The systems had been development was (J-Glove) and (X-Glove), this system works on principle of a cable-driven actuator that make it portable and wear by the patient. One of the most important specifications that must be considered when designing is the ease of movement of the finger joints, easy to wear, controllable and aesthetic properties. The glove is made by two layers of rubber material which the wires pass through a plastic piece that attached to the glove and the wires are connect to the actuators that move the fingers. The response rate of 35.14% for this glove. The protecting of patient in therapy was a factor should remain necessary consideration. Reductions in the weight of glove make it more comfortable to wear. The glove shown in (Fig. 2e). This type of robotic glove is used for post-stroke patients in the first weeks of injury to help them recover faster. One of the advantages of these gloves is the ability to open and close the patient's hand with a suitable force controlled by the actuators.

(a) (b) (c)

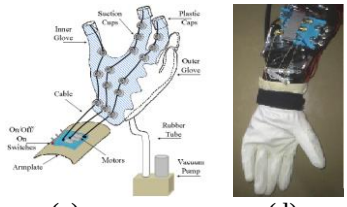

(e) (d)

Fig. 2: Robotic Glove Based on Tendon Driven Actuation (a): SNU Exo-Glove [23], (b): Tendon Driven Glove [5], (c) Silicone Glove [13], (d): Tendon Driven Glove [3] and (e) (J-Glove) and (X-Glove) [10]

B. Robotic Glove Based on Pneumatic Actuation

These types of robotic gloves are operated by the air pressure that passes through the air tubes and control by specific pressure valves and the source of this pressure is the air compressor. These pneumatic actuators are attached to the gloves to open and close the fingers. Glove can be designed to fit the size of the patient's fingers [23]. Pressure sensors are used with the glove to measure the grip strength of the glove used as a style of control [24]. From the design it is possible to control the glove via an interactive screen to specify the finger movements necessary for the rehabilitation process [25]. Most of these robotic gloves are operated by actuator that are controlled by the EMG signal after sensing it [26]. In this type of glove, the closing of the fingers is achieved by increasing the pressure inside the actuator and the opening is by reducing the pressure [27]. The bending value can be known by measuring the bending angles of the affected fingers to know the patient's recovery level [28]
In 2010 Connelly et al. [22] suggested a novel pneumatic glove (PneuGlove)which can provide independent extension assistance It can be used for rehabilitation with real or virtual items because the most common motor deficit was the fingers extension. The rehabilitation of hand gesture practices has been enhanced by incorporating virtual reality (VR) with robotic glove action and the glove can also be used with a wireless system that can measure joint movements using bending sensors. Some pressure parts used in the design as the servo valve that provides air pressure between (0–10 psi). The virtual reality (VR) application used the Head Mounted Display (HMD) as display device. The glove is permanently controlled by the VR program, which receives movement values via the shadow screen. As shown in (Fig. 3a).
In 2014 Polygerinos et al. [6] suggested a soft robotic glove consist of elastomeric chambers with fiber reinforcement under fluid pressure. The control system is designed with pressure sensors to control the outlet pressure of the pneumatic actuators and then regulated by a closed-loop controller. The robotic glove produces a great Features like: more freedom, safety, low cost, portability and be customizable depending on the hand anatomy. The Wight of glove must be less than (0.5 k gm). And the other controlling part less than (3 k gm (. A healthy person can generate a grip strength proximately (450 N) for a male and (300N) for a female. The components of the system are installed inside a bag and consist of (I) lithium polymer battery (5 Ah 14.8 V) with power regulator. (II) microcontroller (Arduino mega 2560R3), pressure sensors, and control boards managing. (III) Hydraulic pump with (9.6 W), volume of (250 ml), and (IV)other parts like: solenoid valves, mechanical switches, volt meter to show battery level. The sensors were used to monitor the pressure of actuator with a local feedback control loop is (150PGAA5, Honeywell, Morristown, NJ). That shown in (Fig. 3b).
In 2015 Polygerinos et al. [7] presented a robotic glove made by soft material to be safely on the length of the finger when it uses. The flexion of the glove is active and the extension of it is passive. The glove actuators are consisting of elastomeric bladders with a fiber reinforcement to give a

specific Features. Bending and extending depends upon the fluid pressure. A comparison was made between a patient with weak hand strength without using a glove and using a robotic glove. The rehabilitation process is applied to improve the hand function by repeating the exercise of rehabilitation tasks. Through the control box can move the fingers separately or implement a variety of preset finger movements. The cross section of the glove is (20 mm) wide and (7 mm) high to match the finger dimensions. The electrical and mechanical parts are placed inside the box (the electrical parts, pump and battery) necessary to operate the glove and are far from the glove. The actuation frequency must be 30flexing/extending hand cycles/minute. The glove shown in (Fig. 3c).

In 2015 Yap et al [1]. presented a soft pneumatic actuator and calculate its parameters as the radius of curvature and the output force produced by actuation to be suitable for hand rehabilitation use. It was finding by using two type of actuators (Eco flex 00-30) can be reach to (12.06 mm) of radius at (26 pa) and (Dragon skin 20) reach to (29.55mm) at (210 pa) .The relationships between the input pressure and the radius curvature was not linear but the relationship between input pressure and the linear displacement was linear .And the relationship between the output force and pressure similar to linear .Different type of silicone rubber give us different output characteristics. The requirement design was the bending actuator must can give suitable force to bend the finger joint. The actuator design was different from patient to another due to the complications of them diseases. The glove is shown in (Fig. 3d).

In 2016 Yap et al. [8] presented a robotic glove powered by inflatable actuators That is manufactured by the thermal bonding of flexible plastic sheets to be able to help patients open their fingers by generating a suitable force. The process of rehabilitating is done by repeating the exercise of tasks. The device can be designed to do opening the fingers by assist of the glove and the process of closing the fingers is voluntary by the patient. The air supply from the air compressor source to the actuator through a plastic tube. The total weight of this device was approximately (150 g) this type is lighter than other types. The control box can be carried away from the hand in order to minimize a weight on the hand and arm. The glove pneumatic system It consists of air compressor sensor, solenoid valves, small air compressor. A glove is shown in (Fig. 3e).

In 2018 Stilli et al. [17] presented an AirExGlove it was a light weight inflatable soft device combining the benefits of both pneumatic and tendon-driven. The glove consists of an external structure with pneumatic actuators that are placed on the back of the glove and tendons are installed along the glove from the inside to determine the amount of opening for the glove and the amount of closing force is by increasing the pressure applied by the actuators. The motors are placed inside a box away from the glove it may be fixed on the back or on belt. The tendons are connected to the motors through the Bowden cables and the air tubes transfer pressure from the air compressor to the motors installed inside the box. The weight of the envisioned actuation system is estimated to be less than (3 kg) as shown in (Fig. 3f). Patients are provided with this type of robotic glove for the purpose of soft rehabilitation in a manner that is intended for patients to open and close their hands in a soft manner, such as older patients, they are used for patients who need relatively little force to open and close compared to the Tendons-Driven Actuation type.

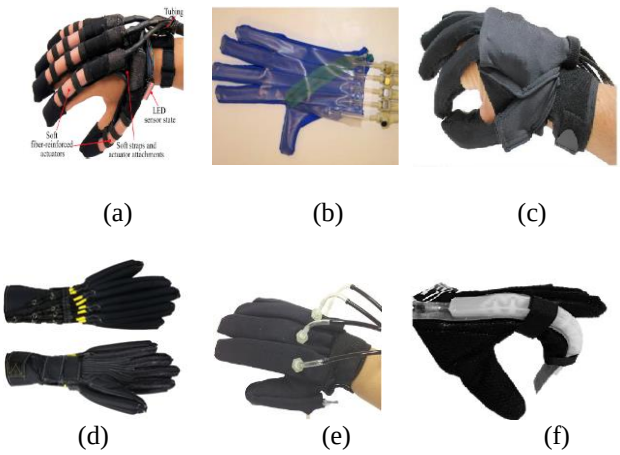

(a) (b) (c)

(d) (e) (f)

Fig. 3: Robotic Glove Based on Pneumatic Actuation (a): Penu Glove [1], (b): soft robotic glove [6], (c): Penu robotic glove [7], (d): soft pneumatic actuator [1], (e) inflatable actuators [8], (f): AirExGlove [17].

C. Robotic Glove Based on another technologies

There are other hybrids that are not included in the previous classifications. The use of myo arm band is one of the modern methods of glove controlling by sensing the EMG signal [29]. This type of glove is important because it provides the required amount of finger movements [30]. The glove can perform specific movement with animation and measure these movements to see the effectiveness of the hand [31]. It is possible to know the effectiveness of the hand by analyzing its movement through image processing [32]. One of the robotic glove Applications is the grab in addition to the rehabilitation process [33]. It is important in design to control holding objects to prevent slipping or falling from the glove [34]. Several experiments are performed to open and close the glove before starting to be used by the patient to ensure that the patient's hand is not harmed [35]. These gloves are designed for home use so they are uncomplicated, cheap and lightweight [36]

1. An Exoskeleton Robotic Glove

In 2015 Zhou Ma et al. [9] suggested a system was able to learn finger motion and force for move different objects to record and analyze the movements of hand function with grip and release patterns. Primary data have been collected from healthy hands and analyze to determine the glove's ability to effect on the hand. The actuator was a pneumatic piston located inside the glove; it can generate a force up to 16 N for each finger. The air compressor and the supporting devices were required to power and control the glove. The robotic glove was consisted of two main part: the forearm module and the glove module, control electronics, three

actuators, and a fabric cover were contained within the forearm module. The glove modules were including a glove, a conduit anchor and five FSR sensors Placed at the finger tips. The weights of the device were about 770 grams. The system components were: the demonstration procedure, the machine learning algorithm, the safe glove system, and a 3D GUI program, and the rehabilitation-assistive engineering procedure. The normal force had been controlled by the limitation of the force sensing resistors (FSR) sensor, the force measurement by Piezoresistive sensors. The surface electromyography (sEMG) can be used to determine the level of muscle activation (Fig.4a). This type of robotic glove is similar to the type of Tendon Drive but it is more complicated in terms of structure. It is usually used with interactive video systems that are used to enhance the mental ability of post- stroke patients in the rehabilitation process.

2. Robotic Glove Based on linear Actuation.

In 2015 Fischer et al. [21] presented a portable glove with linear actuator. the X-Glove was one of independently actuate each digit while also allowing free movement of each joint and cables serving as external extensor tendons run through cable guides attached to dorsal side of a modified batting acted with linear servo actuators (L12, Firgelli Technologies, Inc.) and Rabbit Core microcontroller (RCM 3410; Digi International, Inc.). After the used of the X-Glove there were an increase in grip and pinch strength. The initiation of treatment rather than over a longer period as the patient wished to start training as early as possible to maximize benefits (Fig. 3b). This type of robotic glove is suitable for treating patients who need rehabilitate the hand with characterized by accuracy in controlling the angles of opening and closing the fingers, but it is relatively heavy on the patient hand and is one of the undesirable features of the design.

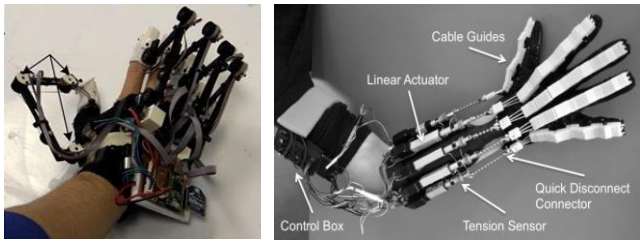

(a) (b)

Fig. 4: Exoskeleton Robotic Glove
(a): Exoskeleton Robotic Glove [9]. (b): linear Actuation Robotic Glove [21]

III. Discussion

Rehabilitation robots are usually used to help patients gain healing, such as stroke patients or spinal cord injuries, so these robots must have features that are appropriate for patients, and one of the most important is their effectiveness in the purpose of rehabilitation for the patient to benefit from them. In addition to being light weight so as not to be heavy on the affected limbs when used by the patient, by using materials with a low density in manufacturing and avoid using heavy materials as much as possible. And the cost of manufacturing it is not high, so that the patient can use it or acquire it, meaning that it is cheap.

It has also been shown that there are multiple models for designing this robotic glove to be appropriate for use by patients. Therefore, these smart gloves can be combined with certain systems such as virtual reality systems or certain video games that will help the patient to enhance communication between the brain and the affected limb and train the brain to restore the ability to control the affected limb. As for the patient's need for the stages of the rehabilitation process, this will be decided by the specialist doctor, according to the patient's age group and the level of injury. During the operation of the robotic glove for several hours during the rehabilitation process, it needs a suitable mobile power source to work for long periods and at the same time it is appropriate for the design for the system, like a rechargeable battery, it must be lightweight or it can be placed in a box away from the robotic glove and connected via wires to the glove.

IV. Conclusions

In this paper, various design models for the robotic gloves are presented for the purpose of rehabilitation. There are many types that have been reviewed, including those that are driven by tendons and actuators such as servo motors or with soft materials with pneumatic actuator or other types of actuator. Then explain the properties of parts and the work of these robotic gloves. Discussing future developments of these systems based on the patient's need for these developments. Each type of glove has certain operating properties, but all types must be uncomplicated to install and inexpensive and can be used at home by the patient himself without the need for anyone's help and at any convenient time.

Several systems can be combined after completing the robotic glove design in order to increase the patient's recovery speed and increase the patient's reaction interaction during the rehabilitation process. One of these systems is the Interactive Screen System (VR) which is used extensively in patients' rehabilitation operations to enhancing the robotic glove with patient. This technology makes it more interactive system.

The process of controlling the robotic glove is one of the important things during design it most of the control operations are through programmable microprocessors to control actuator that move the fingers. The EMG signal produce by the muscles is relied on to control the actuator and this signal is obtained by Mayowear sensors and it presented a muscle activity. It is considered one of the most common methods of control. It is also possible to control the grip strength of the robotic glove to make it able to carry and hold things without destroying or sliding them to be suitable for use by the patient.

This review may provide useful information for researchers within this specialty or for developing these systems in the future.

REFERENCES

[1] H. K. Yap, J. C. H. Goh, and R. C. H. Yeow, "Design and Characterization of Soft Actuator for Hand Rehabilitation Application," IFMBE Proc., vol. 45, pp. 367–370, 2015.

[2] U. Jeong, H. K. In, and K. J. Cho, "Implementation of various control algorithms for hand rehabilitation exercise using wearable robotic hand," Intell. Serv. Robot., vol. 6, no. 4, pp. 181–189, 2013.

[3] S. Biggar and W. Yao, "Design and Evaluation of a Soft and Wearable Robotic Glove for Hand Rehabilitation," IEEE Trans. Neural Syst. Rehabil. Eng., vol. 24, no. 10, pp. 1071–1080, 2016.

[4] A. M. M. Ali, R. Ambar, M. M. A. Jamil, and J. S. Pusu, "Via for," 2012.

[5] C. J. Nycz, M. A. Delph, and G. S. Fischer, "Modeling and design of a tendon actuated soft robotic exoskeleton for hemiparetic upper limb rehabilitation," Proc. Annu. Int. Conf. IEEE Eng. Med. Biol. Soc. EMBS, vol. 2015-Novem, no. July 2017, pp. 3889–3892, 2015.

[6] P. Polygerinos, Z. Wang, K. C. Galloway, R. J. Wood, and C. J. Walsh, "Soft robotic glove for combined assistance and at-home rehabilitation," Rob. Auton. Syst., vol. 73, pp. 135–143, 2015.

[7] P. Polygerinos, K. C. Galloway, E. Savage, M. Herman, K. O'Donnell, and C. J. Walsh, "Soft robotic glove for hand rehabilitation and task specific training," Proc. - IEEE Int. Conf. Robot. Autom., vol. 2015-June, no. June, pp. 2913–2919, 2015.

[8] H. K. Yap, J. H. Lim, J. C. H. Goh, and C. H. Yeow, "Design of a soft robotic glove for hand rehabilitation of stroke patients with clenched fist deformity using inflatable plastic actuators," J. Med. Devices, Trans. ASME, vol. 10, no. 4, 2016.

[9] Z. Ma, P. Ben-Tzvi, and J. Danoff, "Hand Rehabilitation Learning System with an Exoskeleton Robotic Glove," IEEE Trans. Neural Syst. Rehabil. Eng., vol. 24, no. 12, pp. 1323–1332, 2016.

[10] S. J. Biggar, W. Yao, L. Wang, and Y. Fan, "User-Centric Feedback for the Development and Review of a Unique Robotic Glove Prototype to Be Used in Therapy," J. Healthc. Eng., vol. 2017, 2017.

[11] D. Popescu, M. Ivanescu, R. Popescu, L. C. Popescu, A. Petrisor, and A. M. Bumbea, "Post-stroke assistive rehabilitation robotic gloves," Proc. 2016 Int. Conf. Expo. Electr. Power Eng. EPE 2016, no. Epe, pp. 360–365, 2016.

[12] D. Popescu, M. Ivanescu, S. Manoiu-Olaru, M. I. Burtea, and N. Popescu, "Robotic glove development with application in robotics rehabilitation," EPE 2014 - Proc. 2014 Int. Conf. Expo. Electr. Power Eng., no. Epe, pp. 168–173, 2014.

[13] B. B. Kang, H. Lee, H. In, U. Jeong, J. Chung, and K. Cho, "Conf 27_2016_Development of Polymer-Based Tendon-Driven Wearable Robotic Hand," pp. 3750–3755, 2016.

[14] S. Hartopanu and M. Poboroniuc, "New Issues on FES and Robotic Glove Device to Improve the Hand Rehabilitation in Stroke Patients," Nternational Conf. Mod. Power Syst., no. May, pp. 18–21, 2015.

[15] D. C. Irimia, M. S. Poboroniuc, S. Hartopanu, D. Sticea, G. Paicu, and B. E. Ignat, "Post-stroke hand rehabilitation using a hybrid FES-robotic glove," Proc. 2016 Int. Conf. Expo. Electr. Power Eng. EPE 2016, no. Epe, pp. 356–359, 2016.

[16] K. O. Thielbar et al., "Benefits of using a voice and EMG-driven actuated glove to support occupational therapy for stroke survivors," IEEE Trans. Neural Syst. Rehabil. Eng., pp. 1–10, 2016.

[17] A. Stilli et al., "AirExGlove-A novel pneumatic exoskeleton glove for adaptive hand rehabilitation in post-stroke patients," 2018 IEEE International Conference on Soft Robotics, RoboSoft 2018. pp. 579–584, 2018.

[18] C.-Y. Lina, Chia-MinTsaia, P.-C. Shihb, and H.-C. Wub, "Development of a novel haptic glove for improving finger dexterity in poststroke rehabilitation," Technol. Heal. Care, vol. 24, pp. 97–103, 2016.

[19] A. Karime, H. Al-Osman, W. Gueaieb, and A. El Saddik, "E-Glove: An electronic glove with vibro-tactile feedback for wrist rehabilitation of post-stroke patients," Proceedings - IEEE International Conference on Multimedia and Expo. 2011.

[20] A. A. Hidayat, Zainal Arief, and D. C. Happyanto, "Mobile Application With Simple Moving Average Filtering For Monitoring Finger Muscles Therapy Of Post-Stroke People," Int. Electron. Symp., pp. 1–6, 2015.

[21] H. C. Fischer et al., "Use of a Portable Assistive Glove to Facilitate Rehabilitation in Stroke Survivors with Severe Hand Impairment," IEEE Trans. Neural Syst. Rehabil. Eng. TNSRE-2015-00086.R2, pp. 1–9, 2015.

[22] L. Connelly, Y. Jia, M. L. Toro, M. E. Stoykov, R. V. Kenyon, and D. G. Kamper, "A pneumatic glove and immersive virtual reality environment for hand rehabilitative training after stroke," IEEE Transactions on Neural Systems and Rehabilitation Engineering, vol. 18, no. 5. pp. 551–559, 2010.

[23] Y. Guo, F. Xu, Y. Song, X. Cao, and F. Meng, A Soft Robotic Glove for Hand Rehabilitation Using Pneumatic Actuators with Variable Stiffness, vol. 2. Springer International Publishing, 2019.

[24] P. Polygerinos, Z. Wang, K. C. Galloway, R. J. Wood, and C. J. Walsh, "Soft robotic glove for combined assistance and at-home rehabilitation," Rob. Auton. Syst., vol. 73, pp. 135–143, 2015, doi: 10.1016/j.robot.2014.08.014.

[25] H. K. Yap et al., "A Fully Fabric-Based Bidirectional Soft Robotic Glove for Assistance and Rehabilitation of Hand Impaired Patients," IEEE Robot. Autom. Lett., vol. 2, no. 3, pp. 1383–1390, 2017, doi: 10.1109/LRA.2017.2669366.

[26] C. Dai and X. Hu, "Extracting and Classifying Spatial Muscle Activation Patterns in Forearm Flexor Muscles Using High-Density Electromyogram Recordings," Int. J. Neural Syst., vol. 29, no. 1, 2019, doi: 10.1142/S0129065718500259.

[27] Y. M. Zhou et al., "Soft robotic glove with integrated sensing for intuitive grasping assistance post spinal cord injury," Proc. - IEEE Int. Conf. Robot. Autom., vol. 2019-May, pp. 9059–9065, 2019, doi: 10.1109/ICRA.2019.8794367.

[28] K. H. L. Heung, R. K. Y. Tong, A. T. H. Lau, and Z. Li, "Robotic Glove with Soft-Elastic Composite Actuators for Assisting Activities of Daily Living," Soft Robot., vol. 6, no. 2, pp. 289–304, 2019, doi: 10.1089/soro.2017.0125.
[29] M. Gerle, D. Jakobsson, M. Makris, and E. Nordqvist, "A Chalmers University of Technology Bachelor ' s thesis The human in the loop robot," 2018.
[30] O. Sandoval-Gonzalez et al., "Design and development of a hand exoskeleton robot for active and passive rehabilitation," Int. J. Adv. Robot. Syst., vol. 13, no. 2, 2016, doi: 10.5772/62404.
[31] M. Ariyanto, R. Ismail, A. Nurmiranto, W. Caesarendra, Paryanto, and J. Franke, "Development of a low cost anthropomorphic robotic hand driven by modified glove sensor and integrated with 3D animation," IECBES 2016 - IEEE-EMBS Conf. Biomed. Eng. Sci., pp. 341–346, 2016, doi: 10.1109/IECBES.2016.7843470.
[32] D. Popescu, M. Ivanescu, S. Manoiu-Olaru, M. I. Burtea, and N. Popescu, "Robotic glove development with application in robotics rehabilitation," EPE 2014 - Proc. 2014 Int. Conf. Expo. Electr. Power Eng., no. Epe, pp. 168–173, 2014, doi: 10.1109/ICEPE.2014.6969890.
[33] S. W. Pu and J. Y. Chang, "Robotic hand system design for mirror therapy rehabilitation after stroke," Microsyst. Technol., vol. 3, 2019, doi: 10.1007/s00542-019-04483-3.
[34] T. Vanteddu, P. Ben-Tzvi, S. C. Southward, and A. Leonessa, "Grasp Stability with a Robotic Exoskeleton Glove," 2019.
[35] S. U. N. Zhong-sheng, G. U. O. Zhong-hua, and T. Wei, "Design of wearable hand rehabilitation glove with soft hoop-reinforced pneumatic actuator," pp. 0–2, 2019.
[36] P. Bernocchi, C. Mulè, F. Vanoglio, G. Taveggia, A. Luisa, and S. Scalvini, "Home-based hand rehabilitation with a robotic glove in hemiplegic patients after stroke: a pilot feasibility study," Top. Stroke Rehabil., vol. 25, no. 2, pp. 114–119, 2018, doi: 10.1080/10749357.2017.1389021.
[37] B. Radder et al., "A wearable soft-robotic glove enables hand support in ADL and rehabilitation: A feasibility study on the assistive functionality," J. Rehabil. Assist. Technol. Eng., vol. 3, p. 205566831667055, 2016, doi: 10.1177/2055668316670553.
[38] D. Popescu, M. Ivanescu, S. Manoiu-Olaru, L. C. Popescu, and N. Popescu, "Development of robotic gloves for hand rehabilitation post-stroke," Proc. - 2015 20th Int. Conf. Control Syst. Comput. Sci. CSCS 2015, pp. 838–844, 2015, doi: 10.1109/CSCS.2015.95.
[39] N. Norouzi-Gheidari, A. Hernandez, P. S. Archambault, J. Higgins, L. Poissant, and D. Kairy, "Feasibility, safety and efficacy of a virtual reality exergame system to supplement upper extremity rehabilitation post-stroke: A pilot randomized clinical trial and proof of principle," Int. J. Environ. Res. Public Health, vol. 17, no. 1, pp. 1–11, 2020, doi: 10.3390/ijerph17010113.
[40] A. Yurkewich, I. J. Kozak, D. Hebert, R. H. Wang, and A. Mihailidis, "Hand Extension Robot Orthosis (HERO) Grip Glove: Enabling independence amongst persons with severe hand impairments after stroke," J. Neuroeng. Rehabil., vol. 17, no. 1, pp. 1–17, 2020, doi: 10.1186/s12984-020-00659-5.
[41] M. C. Barba et al., Augmented Reality VS Virtual Reality, vol. 1. Springer International Publishing, 2019.
[42] Martinez Luna, Carlos Humberto, Michael Alfred Delph, Philip Walter Gauthier, and Sarah Anne Fischer. "Rehabilitative Robotic Glove." (2012).
[43] M. Seçkin and N. Yaman Turan, "Rehabilitation Glove Device Design," J. Eng. Technol. Appl. Sci., vol. 3, no. 1, pp. 75–81, 2018, doi: 10.30931/jetas.391297.
[44] B. Aparna, B. Anithakrithi, P. Naveena, M. Yaswanth Kumar, M. Avinash, and S. Sivanandam, "Design and simulation of bionic glove for rehabilitation of the paralytics," Int. J. Eng. Technol., vol. 7, no. 2, pp. 1–6, 2018, doi: 10.14419/ijet.v7i2.8.10314.

DOI: 10.37917/ijeee.sceeer.3rd.13 *(15-16) June 2020*

Open Access

Iraqi Journal for Electrical and Electronic Engineering
Conference Article

Enhancement the Sensitivity of waveguide Coated ZnO thin films: Role of Plasma irradiation

Marwan Hafeedh Younus *, Muayad Abdullah Ahmed, Ghazwan Ghazi Ali
Physics Department, College of Education for Pure Science, University of Mosul, Iraq

Correspondence
*Marwan Hafeedh Younus
Physics Department, College of Education for Pure Science,
University of Mosul, Iraq
Email: marwan82hafed@gmail.com

Abstract
In this study, Dielectric Barrier Discharge plasma irradiation (DBD) is applied to treatment and improve the properties of the ZnO thin film deposited on the glass substrate as a sensor for glucose detection. The ZnO is prepared via a sol-gel method in this work. ZnO is irradiated by the DBD high voltage plasma to improve of its sensitivity. The optical properties, roughness and surface morphology of the waveguide coated ZnO thin films before and after DBD plasma irradiation are studied in this work. The results showed a significant improvement in the performance of the sensor in the detection of concentrations of glucose solution after plasma irradiation. Where the largest value in sensitivity was equal to 62.7 when the distance between electrodes was 5 cm compared to the sensitivity before irradiation, which was equal to 92. The high response showed in results demonstrating that the fabricated waveguide coated ZnO after plasma irradiation has the excellent potential application as a sensor to detect small concentration of glucose solution.

KEYWORDS: waveguide sensor, Sensitivity, ZnO thin film, plasma irradiation .

I. INTRODUCTION

The sensors have broad applications for gas and chemical liquids sensing in a variation of fields such as food, environmental sensing, and security [1] .Solid state has been achieved as by researchers a sensors to monitor different chemical and gases [2].

Due to their unique advantages of developed sensors based on metal oxide semiconductors such as inexpensive, uncomplicated fabrication and good compatibility with microsystem processes make it to use widely to measure a diverse array of chemicals and gases.
Nowadays, due to the environmental pollution concerns and the requirements of life safety, sensors development become essential to detect volatile and toxic materials. Thin films and nanoparticles have acquired a lot of attractive due to their potential applications in different fields of technology. ZnO has been considered as a promising material as a sensors because of its high electrochemical stability, non-toxicity, suitability to doping , and low cost [3-6]. In addition, ZnO has many unique properties, such as a large exciting bonding energy of 60 meV, non-toxicity, good electrical, optical and piezoelectric behavior, and low cost [7-11].
Many methods have been developed to produce ZnO [12-20]. Generally, the porous thin films can be fabricated through different ways such as screen printing [21], brush coating [22] Vapor–liquid–solid (VLS), [23] chemical vapor deposition (CVD) [24]. Overall, the facile fabrication of sensing thin films with uniform porosity and cracks is still a challenge. A low-temperature and mild approach is highly desired for the creation of crack-free homogenous films.
In recent years, non-thermal plasma dielectric barrier discharge (NTPDBD) techniques including radio frequency (RF) discharge, glow discharge and silent discharge have been used for treatment, modified and changes in the morphology of thin films surface [25–27]. Plasma treatment has various industrial applications because of their low-cost high speed and the ability to operate without vacuum. Plasma surface modification involves the interaction of the plasma generated excited species with a solid interface.
Moreover, the high energy electrons of NTPDBD low temperature lead to generate of physical on the thin film surface. Thus, plasma treatment is suitable to irradiate the thermal sensitive materials such as ZnO thin films [28]. The surface activation typically takes places with oxygen containing gas mixtures such as ambient air which is change the surface properties of the external layers of the material [29-30].
In this work, We have carried out and established our own high voltage pulse generator for atmospheric pressure plasma system by using dielectric barrier discharge. we improvement the sensitivity of waveguide coated with ZnO sensors via plasma irradiation at low temperature. The as-

prepared ordered porous thin films are stable and homogenous which leads to significant enhancement in the sensing performance. This technique also appropriate for the fabrication of other metal oxide homogenous thin films sensors with suitable quality at a low temperature.

II. DBD Dielectric Barrier Discharge Plasma Setup

The schematic diagram of experimental setup for pulse high voltage power supply (PHVPS) is shown in Figure 1a. The circuit of low voltage pulse uses the TL494 integrated circuit which represents a pulse width modulation control circuit that generates variation pulse width.

The pulse width varying is performed by changing the applied voltage on the pin 4 as shown in Figure 1b. The frequency can be adjusted by the value of resistance which is connected with pin 6 and the capacitance in pin 5. In order to obtain high current to ignite the high voltage stage, MOSFET transistors are used to ensure obtaining appropriate output high voltage stage.

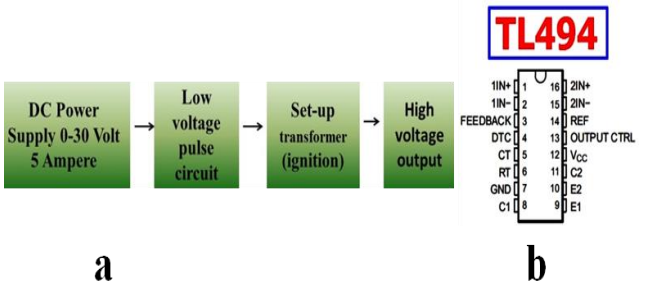

Fig. 1: (a) Schematic presentation of dielectric barrier discharge used for surface, (b) Diagram of TL494 integrated circuit.

PHVPS was launched as shown in Figure 2. The low voltage pulse was generated, which represents a pulse width modulation control circuit. This circuit can be operated safely from power supply as high as (+12 volt). It generates a successive sequence pulses with a peak varying from 0 to 2 volt when the input DC power supply ranging between 0 to 30 volts, and 5Ampere. The UNT-I 60 MHz digital storage oscilloscope (Model UT2062CE, China) and the GOULD-15 MHz oscilloscope (Model OS255, England) were used to measure the voltage value of pulse and the current passed through a resistance of 1.2 Ω respectively.

On the other hand, the high voltage pulse was measured using a probe pulse high tension type Tesla (Model BS375A, England). Figure 3 shows the atmospheric pressure plasma (APP) using the dielectric barrier discharge (DBD) method floating discharge [1, 2]. The high voltage obtained from PHVPS was used in the dielectric barrier discharge system for surface treatment. After that, the samples of ZnO coated glasses substrate were placed between the two electrodes of the DBD plasma discharge to irradiate the ZnO film. The exposure time of 20 second was fixed for the samples during the plasma irradiation process, while the distance between the two electrodes of plasma was chosen to be 0.5 cm, 1 cm, 1.5 cm.

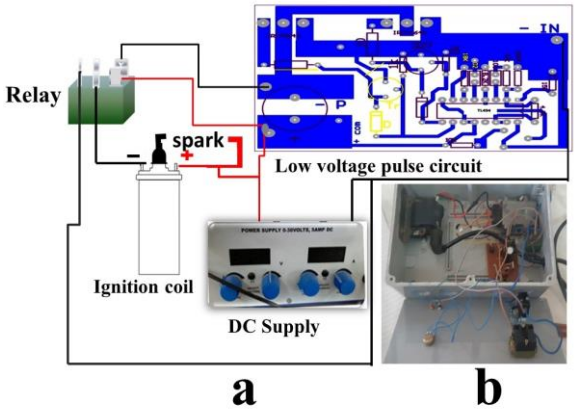

Fig. 2: (a) The circuit of high voltage pulse power supply, (b)the high voltage power supply components.

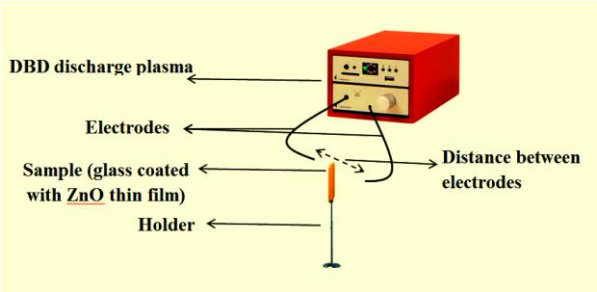

Fig. 3: Schematic presentation of dielectric barrier discharge used for treatment surface.

III. Waveguide Sensor Coated ZnO Setup

The fabrication of the waveguide sensor coated with ZnO thin film is carried out according to our previous work [14]. Figure 4 illustrates the setup of waveguide sensor coated with ZnO thin film for glucose detection. Its tested in the transmission system where optical source (Broad Band Source supplied by JDS Uniphase) placed near the one end of the waveguide sensor, and the Optical Spectrum Analyzer (ANDO AD6317B) was placed near the other end. The ZnO was cleaned by distilled water and ethanol respectively before the detection process. The experiment was conducted with the sensor being immersed in a container to be in contact with the glucose solution. The container was covered with a glass slide to prevent the impurity during the experiment. All the experiments were achieved at room temperature and were carried out for different concentrations of glucose ranging from 1% to 5%. In addition, the light from the source was effectively passed into the surface of the waveguide coated ZnO and the light exiting from the other end was detected directly by Optical Spectrum Analyzer to record the spectrum.

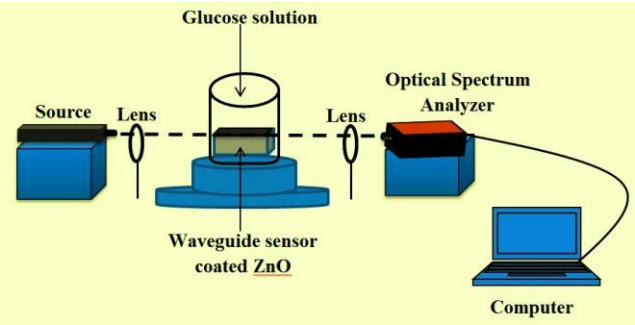

Fig. 4: waveguide Sensor Coated ZnO Setup for glucose detection.

IV. Results and Discussion

A. Absorption Analysis

ZnO thin film was exposed to plasma irradiation in order to improve its sensitivity to detect the glucose solution. The distance between the electrodes of the plasma was chosen to be 0.5 cm, 0.8 cm and 1 cm respectively. Figure 5 shows the absorption spectra of ZnO thin film before and after plasma irradiation in UV-visible range from 300 to 800 nm. It can be seen that the ZnO thin film has strong absorption in the visible range with the absorption edge from 380 to 450 nm, which can be attributed to the fundamental absorption of ZnO. In addition, the absorption of ZnO has been increased after plasma irradiation as the distance between the electrodes is decreased, which can be ascribed to increase the roughness of the ZnO surface after irradiation.

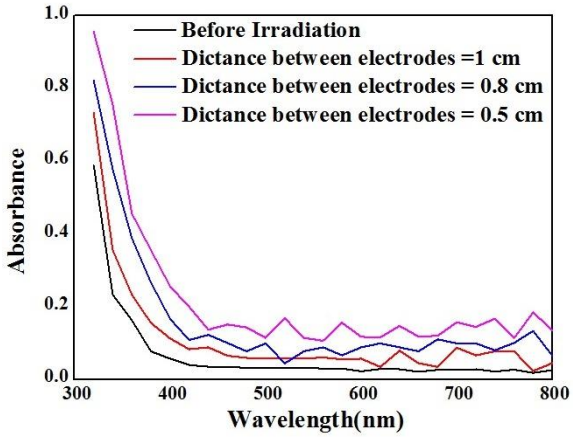

Fig. 5: Optical absorbance spectrum of ZnO thin films at different plasma irradiation.

B. Roughness Surface Morphology

Atomic force microscope (AFM) was used to study the surface topography of ZnO thin films before and after plasma irradiation as shown in Figure 6. The ZnO thin film before irradiation is packed and continuous without the presence of porosity or voids due to the homogeneous distribution of ZnO grains on the surface as shown in Figure 6a. However, the porosity and voids started to appear on the ZnO surface after plasma irradiation. Moreover, the porosity and the voids were increased as the distance between the electrodes of plasma is decreased as shown in Figure 6 b,c and d. The increase in porosity and voids on the surface of irradiated ZnO thin films were due to the occurrence of cracks on the surface of irradiated ZnO thin films. The appearance of the cracks is also significant to improve in the sensitivity of the waveguide sensors to detect the glucose solution.

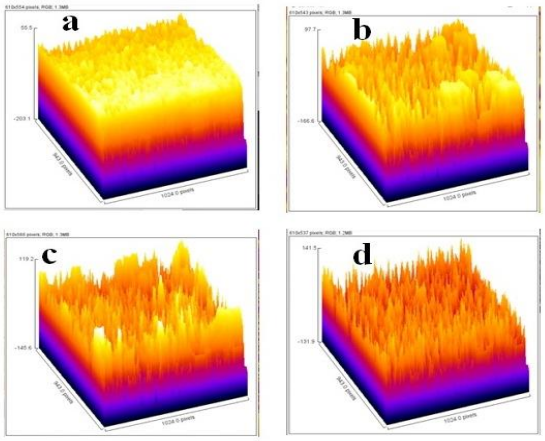

Fig. 6: AFM morphology of waveguide coated ZnO thin films (a) before exposed to DBD irradiation (b) after DBD irradiation (distance at 1 cm) (c) after DBD irradiation (distance at 0.8 cm) (d) after DBD irradiation (distance at 0.5 cm).

C. SEM Morphology

The SEM morphology of the deposited ZnO thin films before and after plasma irradiation is depicted in Figure 7. Figure 7a illustrates that the surface of the ZnO thin film before irradiation is smooth, packed and continues as well no cracking is observed. However, the ZnO thin film after plasma irradiation ()shows considerable morphological differences as shown in Figure 7 b, c, d for the electrodes distance of 1 cm, 0.8 cm and 0.5 cm respectively. As can be seen, the surface of the resulting ZnO films were directly influenced by the irradiation which leads to display the porosity, voids and cracks, suggesting that the irradiation plasma improve the sensitivity of the waveguide sensor coated with ZnO for glucose solution detection.

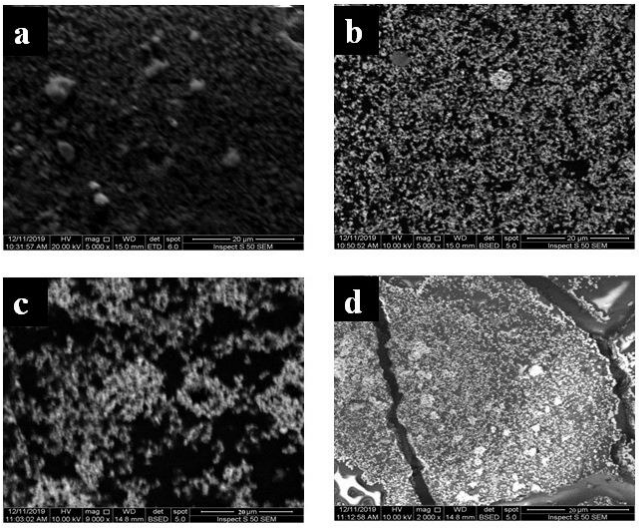

Fig. 7: SEM micrographs of waveguide coated ZnO thin films (a) before plasma irradiation (b) after plasma

irradiation (distance at 1 cm) (c) plasma irradiation (distance at 0.8 cm) (d) after plasma irradiation. (distance at 0.5 cm) irradiation (distance at 0.5 cm) .

D. Response of Waveguide Coated with ZnO Thin Films for Glucose Detection

As a proof of the waveguide coated with ZnO sensor principle, our sensor before and after plasma irradiation was immersed in different concentrations (1% to 5%) of glucose solution. Figure 8 shows the spectrum of output intensity of the ZnO coated waveguide sensor before and after plasma irradiation for different glucose concentrations. From Figure 6, it can be observed that the transmittance intensity of waveguide sensor after plasma irradiation decreases at all the glucose concentrations, indicating that the sensor presents a good response to glucose. Further, the response of the waveguide sensor after plasma irradiation is more when the distance between the electrodes of 0.5 cm, this due to the increasing in the porosity and cracks via plasma irradiation which leads to increase the absorbance of the ZnO surface during the glucose detection. While the response of the sensor was less when the distance between the electrodes of 0.8 cm and 1 cm.

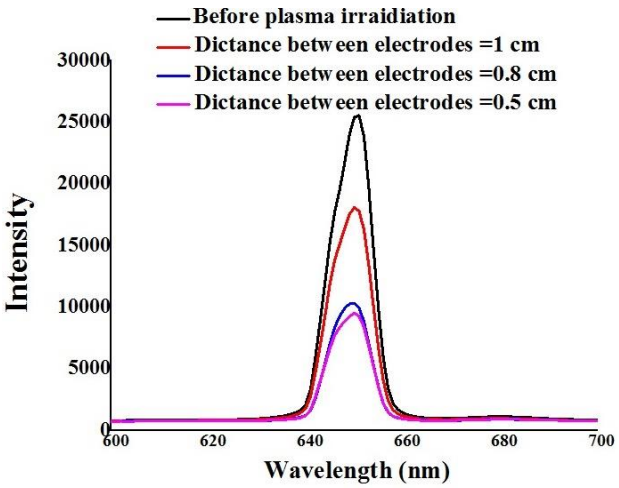

Fig. 8: spectrum of output intensity of the sensor coated ZnO before and after plasma irradiation at different glucose concentrations.

To understand the spectral response of the sensors more clearly, we have plotted the variation of normalized intensity (it is the ratio between the initial intensity to the intensity falling on the detector) with glucose concentration before and after plasma irradiation as shown Figure 9. It can be seen that the normalize intensity of sensor increases with increase in the value of glucose concentrations after plasma irradiation. The normalized intensity is found to be the maximum for sensor when the distance between the electrodes of 0.5 cm than the other sensors.

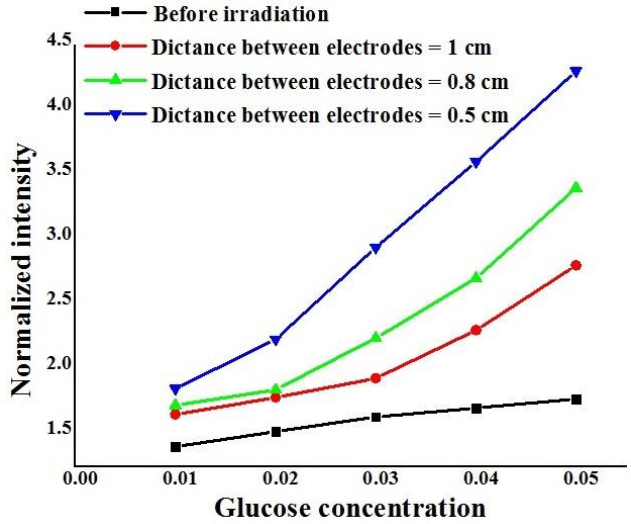

Fig. 9: Normalized intensity of the waveguide sensor versus different glucose concentrations.

To compare the performance of waveguide sensor before and after plasma irradiation, we have plotted the variation of sensitivity (the ratio between the normalized intensity and the glucose concentration) with the distance between the electrodes in Figure 10. It is found that the sensitivity increases with decreasing in the distance between the electrodes, because the possibility of produced the porosity and cracks increases when the distance between the electrodes is decreased, which leads to increase the impact of plasma irradiation on the surface of ZnO thin film. A maximum sensitivity of 62.7 is achieved when the distance between the electrodes was 0.5 cm which is at least six times larger than the sensitivity of the waveguide sensor before irradiation (9.2). Additionally, the sensitivity of sensors at distance between the electrodes of 1 cm and 0.8 cm found to be 28 and 42.2 respectively. The large value of the sensitivity obtained in the sensor can be used to detect a small changes in the surrounding medium which may be used to detect the presence of chemical or biological agents.

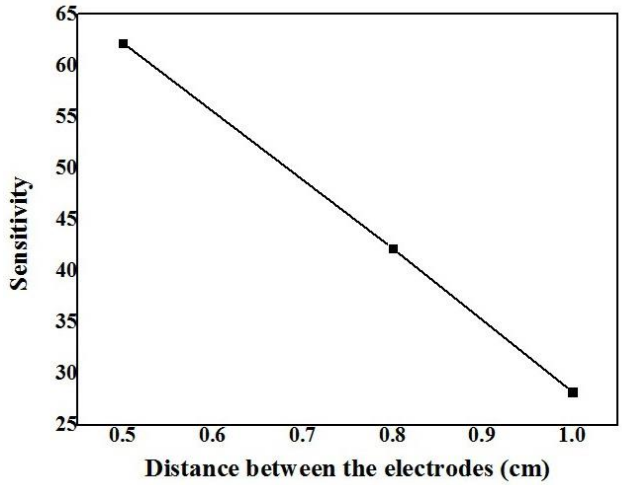

Fig. 10: Sensitivity of the waveguide sensor versus distance between the electrodes of DBD plasma.

IV. Conclusion

The waveguide coated ZnO thin films as sensor for glucose detection is fabricated and characterized in this study. The Physical properties of the sensor before and after (DBD) plasma irradiation are analyzed by uv-visible-IR, AFM and SEM analysis. The observation from AFM and SEM revealed that the morphology of the ZnO thin films are completely changed and the porosity and cracks produced on the ZnO surface after irradiation which enhancement the sensitivity of the sensor during the detection process. The results show that the waveguide sensor has a high sensitivity of 62.7 when the distance between the electrodes is 0.5 cm which is higher at least six time than the sensitivity of the sensor before irradiation (9.2). The high sensitivity obtained exhibits that the fabricated waveguide coated with ZnO thin film can be used as sensor to detect small concentration of glucose after plasma irradiation.

Acknowledgment

The authors want to thank and appreciate the staff at Department of physics, College of Education for Pure Science , University of Mosul for providing research facilities required to complete this study.

References

[1] Dai, Zhengfei, et al. "Crack-Free Periodic Porous Thin Films Assisted by Plasma Irradiation at Low Temperature and Their Enhanced Gas Sensing Performance." Chemistry–A European Journal 19.40 (2013): 13387-13395.

[2] Choi, Kwon-Il, et al. "Rh-catalyzed WO 3 with anomalous humidity dependence of gas sensing characteristics." RSC Advances 4.95 (2014): 53130-53136.

[3] Kumar, Ravi, et al. "Single phase formation of Co-implanted ZnO thin films by swift heavy ion irradiation: Optical studies." Journal of applied physics 100.11 (2006): 113708.

[4] Franco Jr, A., and H. V. S. Pessoni. "Enhanced dielectric constant of Co-doped ZnO nanoparticulate powders." Physica B: Condensed Matter 476 (2015): 12-18.

[5] Shash, Nabil M., and Ibrahim S. Ahmed. "Structure and electrical properties of ZnO doped barium-metaphosphate glasses." Materials Chemistry and Physics 137.3 (2013): 734-741.

[6] Moafi, Hadi Fallah, Mohammad Ali Zanjanchi, and Abdollah Fallah Shojaie. "Tungsten-doped ZnO nanocomposite: Synthesis, characterization, and highly active photocatalyst toward dye photodegradation." Materials Chemistry and Physics 139.2-3 (2013): 856-864.

[7] Wang, Liwei, et al. "ZnO nanorod gas sensor for ethanol detection." Sensors and Actuators B: Chemical 162.1 (2012): 237-243.

[8] Jayakumar, O. D., et al. "A rare defect free 3D ZnO rod structure with strong UV emission." CrystEngComm 13.7 (2011): 2187-2190.

[9] Peleckis, Germanas, et al. "Co valence and possible spin transformation in diluted magnetic semiconductors Zn/sub 1-z/Mg/sub z/Co/sub 0.15/O and Zn/sub 1-x/Co/sub x/O." 2005 IEEE International Magnetics Conference (INTERMAG). IEEE, 2005.

[10] Han, S. J., et al. "A key to room-temperature ferromagnetism in Fe-doped ZnO: Cu." Applied Physics Letters 81.22 (2002): 4212-4214.

[11] Sharma, Parmanand, et al. "Ferromagnetism above room temperature in bulk and transparent thin films of Mn-doped ZnO." Nature materials 2.10 (2003): 673-677.

[12] Kang, Si Woo, et al. "Realization of vertically well-aligned ZnO: Ga nanorods by magnetron sputtering and their field emission behavior." Crystal Growth and Design 8.5 (2008): 1458-1460.

[13] Kim, Dahye, and Young-Duk Huh. "Morphology-dependent photocatalytic activities of hierarchical microstructures of ZnO." Materials Letters 65.14 (2011): 2100-2103.

[14] YOUNUS, MH, ALI GG, and Aswad Tahseen A.. "Effect of Annealing Temperature on Response of ZnO Sensor Deposited on Glass Substrate." The African Review of Physics 14 (2019).

[15] Miculescu, Florin, et al. "Hierarchical nanostructures of ZnO obtained in the presence of water soluble polymers." Powder technology 239 (2013): 56-58.

[16] Fan, Donghua, Rong Zhang, and Xianghu Wang. "Synthesis and optical property of ZnO nanonail arrays with controllable morphology." Physica E: Low-dimensional Systems and Nanostructures 42.8 (2010): 2081-2085.

[17] Pawar, B. N., S. R. Jadkar, and M. G. Takwale. "Deposition and characterization of transparent and conductive sprayed ZnO: B thin films." Journal of Physics and Chemistry of Solids 66.10 (2005): 1779-1782.

[18] Chen, M., et al. "Structural, electrical, and optical properties of transparent conductive oxide ZnO: Al films prepared by dc magnetron reactive sputtering." Journal of Vacuum Science & Technology A: Vacuum, Surfaces, and Films 19.3 (2001): 963-970.

[19] Cao, Bingqiang, et al. "Ultraviolet-light-emitting ZnO nanosheets prepared by a chemical bath deposition method." Nanotechnology 16.9 (2005): 1734.

[20] Khataee, Alireza, et al. "Conversion of natural clinoptilolite microparticles to nanorods by glow

discharge plasma: a novel Fe-impregnated nanocatalyst for the heterogeneous Fenton process." Industrial & Engineering Chemistry Research 52.51 (2013): 18225-18233.

[21] Fan, Zhiyong, et al. "Toward the development of printable nanowire electronics and sensors." Advanced Materials 21.37 (2009): 3730-3743.

[22] Li, Xiaopeng, et al. "Novel sensor array based on doped tin oxide nanowires for organic vapor detection." Sensors and Actuators B: Chemical 162.1 (2012): 251-258.

[23] Park, Jae Young, Sun-Woo Choi, and Sang Sub Kim. "Junction-tuned SnO2 nanowires and their sensing properties." The Journal of Physical Chemistry C 115.26 (2011): 12774-12781.

[24] Zhang, Zhenyu, et al. "Highly aligned SnO 2 nanorods on graphene sheets for gas sensors." Journal of Materials Chemistry 21.43 (2011): 17360-17365.

[25] Khataee, Alireza, et al. "Conversion of natural clinoptilolite microparticles to nanorods by glow discharge plasma: a novel Fe-impregnated nanocatalyst for the heterogeneous Fenton process." Industrial & Engineering Chemistry Research 52.51 (2013): 18225-18233.

[26] Yang, Zen-Hung, Chun-Hsien Ho, and Szetsen Lee. "Plasma-induced formation of flower-like Ag2O nanostructures." Applied Surface Science 349 (2015): 609-614.

[27] Moafi, Hadi Fallah, et al. "The effects of non-thermal plasma on the morphology of Ce-doped ZnO: synthesis, characterization and photocatalytic activity of hierarchical nanostructures." Plasma Chemistry and Plasma Processing 37.1 (2017): 159-176.

[28] Raoufi, Davood, and Taha Raoufi. "The effect of heat treatment on the physical properties of sol–gel derived ZnO thin films." Applied surface science 255.11 (2009): 5812-5817.

[29] Wang Y, Yang J, Li Y, Jiang T, Chen J, Wang J (2015) Controllable preparation of ZnO nanostructure using hydrothermal-electrodeposited method and its properties. Mater Chem Phys 153:266–273

[30] Meena, Jagan Singh, et al. "Effect of oxygen plasma on the surface states of ZnO films used to produce thin-film transistors on soft plastic sheets." Journal of Materials Chemistry C 1.40 (2013): 6613-6622.

DOI: 10.37917/ijeee.sceeer.3rd.14 (15-16) June 2020

Open Access

Iraqi Journal for Electrical and Electronic Engineering
Conference Article

Synchronization and tracking control of a novel 3 dimensional chaotic system

Basil H. Jasim*, Mofeed Turky Rashid, Khulood Moosa Omran
Electrical Engineering Department, University of Basrah, Basrah, Iraq

Correspondence
* Basil H. Jasim
Electrical Engineering Department,
University of Basrah, Basrah, Iraq
Email: hanbas632@gmail.com

Abstract
In this article, a novel three dimensional chaotic systems is presented. An extensive analysis including Lyapunov exponents, dissipation, symmetry, rest points with their properties is introduced. An adaptive tracking control system for the proposed chaos system has been designed. Also, synchronization system for two identical systems has been designed. The simulation results showed the effectiveness of the designed tracking and synchronization control systems.
KEYWORDS: Chaotic, dissipation, Lyapunov exponents, Synchronization.

I. INTRODUCTION

chaotic motion of dynamical systems is a special behavior arises in nonlinear systems, furthermore these systems are very sensitive to the initial conditions [1]. Chaotic systems received considerable attention in last three decades due to possible applications in varies science and engineering fields [2-5]. At other hand, chaos phenomena was investigated in many real systems [6], such as in double and triple pendulums [7,8] and brushless DC motor [9]. This leads to the fact that studying chaos systems and investigating their dynamical properties beside designing control systems for them are very advantageous and may be critical in some cases.

Lyapunov exponents represent sufficient indication on existence of chaotic behavior [10], where the system is chaotic when it has positive Lyapunov exponent. Systems with more than one positive exponent is said to be hyperchaotic [11].

Despite of that there was many chaotic and hyperchaotic systems proposed [12-15] since the first appear of chaotic systems by Lorenz [16], but it still benefits to find and analyze new chaotic systems for both theoretical and practical aspects [17].

Chaotic synchronization means using two identical chaotic systems, the first one called the master and the second is the slave. The two systems are synchronized where the controlled (slave) system should track the uncontrolled (master) system outputs. Due to complex dynamics of chaotic system, chaotic synchronization still a challenging problem [18]. Different control techniques have been used for chaotic synchronization system design [18-20].

In this work, a novel three dimensional chaos system is introduced. The proposed system has 5 terms with 2 quadratic nonlinearities. The system has been analyzed where its properties have been investigated. Lyapunov exponents have been found and from which and phase portrait, the system has been proved to be chaotic. Symmetry, dissipation, rest points and Kaplan York fractal dimension of the system have been found and discussed.

A tracking control system for all states of system assuming uncertain parameter values is designed. The design process uses simple algorithm with Lyapunov theory to find adaptive laws to estimate the uncertain parameters of the system. Also, and by using similar algorithm, a synchronization system has been designed to synchronize two identical systems.

The proposed system and the designed controllers have been simulated using Matlab. The simulation showed the effectiveness of the designed control systems.

The rest of this article is organized as follows: in section 2, the new chaotic system is introduced. In section 3, the system dynamical properties are investigated. In section 4, a tracking control system for the system is designed. In section 5, a synchronization controller for two identical systems is designed. Section 6 is a simulation study where Matlab18a has been used to write simulation programs for the control and synchronization systems. Finally, in section 7 the paper has been concluded.

II. THE PROPOSED SYSTEM

The proposed three dimensional chaos system is described by the following sate equations: -

$$\left.\begin{aligned}\dot{x}_1 &= ax_1x_2\\ \dot{x}_2 &= 70 - x_1x_3\\ \dot{x}_3 &= bx - cx_{3_1}\end{aligned}\right\} \quad (1)$$

This system exhibits chaotic behavior for wide range of values of the parameters a,b and c. we selected a,b,c equal to 10, 0.2 and 0.6 respectively. The system has been simulated for initial conditions x_1, x_2 and x_3 = {0.2,0.2,0.2}. Figures below show phase portrait of the system. Figs.1 and 2 show the 2 dimensional phase portrait of x_1, x_2 and x_1, x_3 planes and fig.3 shows the 3 dimensional portrait of x_1, x_2, x_3.

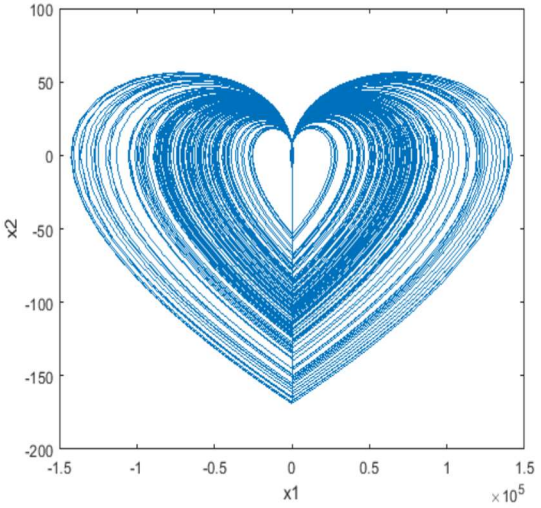

Fig. 1: 2 D phase portrait of x_1, x_2.

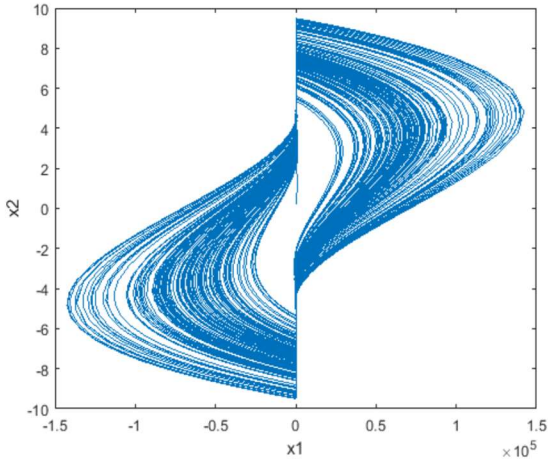

Fig. 2: phase portrait of x_1, x_2.

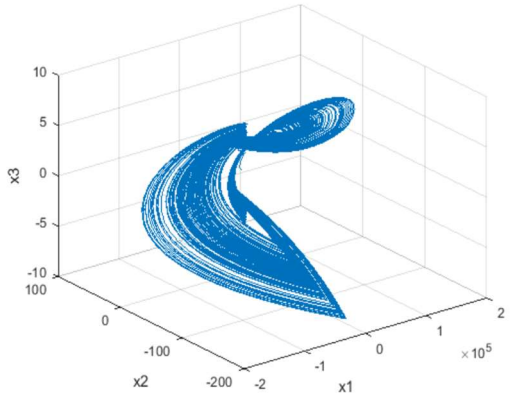

Fig. 3: phase portrait of x_1, x_2, x_3.

III. Dynamical Analysis

A. The Lyapunov exponents

The Lyapunov exponents for the proposed system with the selected parameter values have been found using Wolf algorithm [21] and $X(0) = 0.5, 0.5, 0.5$. The Lyapanove exponents dynamics for 1000 seconds are shown in fig. 4, and their steady state values are L1= 1.1, L2= -0.37 and L3=-1.3324. the maximum exponent is positive which indicate clearly that the system is chaotic.

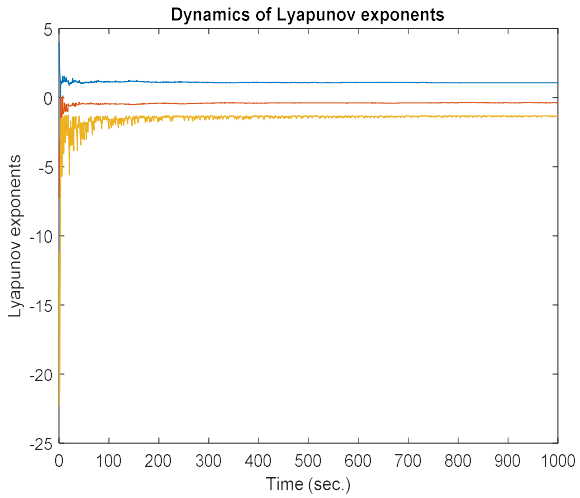

Fig. 4: Lyapunov exponents dynamics.

The Kaplan-York fractal dimension which can be used as a measure of system complexity is determined as follow :
The Lyapunov dimension which used as an indication about the degree of chaotic behavior of the system, can be found by Kaplan-York conjecture [23]. Using this formula, the following can be obtained:

$$D_{KY} = 2 + \frac{L1+L2}{|L3|} = 2.5479 \quad (2)$$

D_{KY} is The Lyapunov dimension.

B. Dissipation

Let us express the proposed system as a vector function f(x):

$$f(x) = \begin{bmatrix} ax_1x_2 \\ 70 - x_1x_3 \\ bx_1 - cx_3 \end{bmatrix} \quad (3)$$

The divergence of the system described by f(x) can be found as in the following:

$$\nabla . f = \sum_{i=1}^{3} \frac{\partial f_i}{\partial x_i} = -c = -0.6 \quad (4)$$

Since $\nabla . f = -0.6 < 0$, then the system is dispative because

$$\dot{V}(t) = (\nabla . f)V(t) = -0.6V(t) \quad (5)$$

Then, any volume element V(t) will shrink to 0 as t goes to zero.

C. The Equilibrium points

The equilibrium or rest points can be found by setting the system questions equal to zero, i.e.

$$\left.\begin{array}{ll} ax_1x_2 = 0 & 1 \\ 70 - x_1x_3 = 0 & 2 \\ bx_1 - cx_3 = 0 & 3 \end{array}\right\} \quad (6)$$

In solving these questions, first we notice from 6-1 that either x_1=0 or x_2=0, but from 6-2, $x_1$can not equal to zero, then x_2=0. Solving 6-2 and 6-3, we find $x_1 = \pm 14.4914 \ and \ x_3 = \pm 4.8305$. Then, the system has two equilibrium points ($E_1$and E_2) :-

$$E_1 = \begin{bmatrix} 14.4914 \\ 0 \\ 4.8305 \end{bmatrix}, \quad E_1 = \begin{bmatrix} -14.4914 \\ 0 \\ -4.8305 \end{bmatrix}$$

The general Jacobian matrix of the system with the specified parameters is given by the following: -

$$J(x) = \begin{bmatrix} 20x_2 & 20x_1 & 0 \\ -x_3 & 0 & -x_1 \\ 0.2 & 0 & 0.6 \end{bmatrix} \quad (7)$$

Using this matrix, we can find the spectral values of E_1 and E_2 ($J(E_1)$ and $J(E_2)$). The spectral values for both E_1 and E_2 are the same: -

$$\lambda_{1,2} = 3 \pm j37.4156 \ , \ \lambda_3 = 0$$

It is clear that E_1 and E_2 are non-hyperbolic points. Then, the stability of these points cannot be ensured by linearization and the system can be self-excitation or hidden attractor.

IV. Controller Design

In this section, a tracking controller is designed using simple procedure. Rewriting the system model as: -

$$\left.\begin{array}{c} \dot{x}_1 = ax_1x_2 + u1 \\ \dot{x}_2 = 70 - x_1x_3 + u2 \\ \dot{x}_3 = bx_1 - cx_3 + u3 \end{array}\right\} \quad (8)$$

Where U={u1,u2,u3} is the control inputs. The design procedure based on satisfying the following error question: -

$$\dot{e}_\iota + k_i e_i = 0 \ , \quad i=1,2,3 \quad (9)$$

Where, e_i=r_i-x_i, r_i is the desired state outputs. k_i is the design parameters.

Combining (8) and (9) and solving for U, the following results can be obtained;

$$\left.\begin{array}{c} u1 = \dot{r}_1 + k_1e_1 - a(t)x_1x_2 \\ u2 = \dot{r}_2 + k_2e_2 - 70 + x_1x_3 \\ u3 = \dot{r}_3 + k_3e_3 - b(t)x_1 + c(t)x_3 \end{array}\right\} \quad (10)$$

Substituting (10) into (8), the following equations are obtained: -

$$\left.\begin{array}{c} \dot{x}_1 = \dot{r}_1 + k_1e_1 + (a - a(t))x_1x_2 \\ \dot{x}_2 = \dot{r}_2 + k_2e_2 \\ \dot{x}_3 = \dot{r}_3 + k_3e_3 + (b - b(t))x_1 - (c - c(t))x_3 \end{array}\right\} \quad (11)$$

Substituting x_i = r_i - e_i and $\dot{x}_i = \dot{r}_i - \dot{e}_\iota$ into (11), the error dynamics of the system can be written as in the following questions :-

$$\left.\begin{array}{c} \dot{e}_1 = e_ae_1e_2 - e_ae_1r_2 - e_ae_2r_1 + e_ar_1r_2 - k_1e_1 \\ \dot{e}_2 = -k_2e_2 \\ \dot{e}_3 = e_br_1 - e_be_1 + e_cr_3 + e_ce_3 - k_3e_3 \end{array}\right\} \quad (12)$$

Where, e_a=a-a(t), e_b=b-b(t) and e_c=c-c(t).

To stabilize the error dynamics of the system, we must obtain suitable update laws for a(t), b(t) and c(t) which ensures convergence to real values. For this purpose, Lyapunov theory has been used.

The following positive definite function is selected as a Lyapunov function candidate:

$$V(t) = 1/2(e_1^2 + e_2^2 + e_3^2 + e_a^2 + e_b^2 + e_c^2) \quad (13)$$

Differentiating V(t), we obtain: -

$$\dot{V}(t) = e_1\dot{e}_1 + e_2\dot{e}_2 + e_3\dot{e}_3 + \dot{a}e_a + \dot{b}e_b + \dot{c}e_c \quad (14)$$

Substituting (12) into (14) and rearranging, the following result is obtained :-

$$\dot{V}(t) = -k_1e_1^2 - k_1e_2^2 - k_1e_3^2 + e_a(\dot{a} + e_1^2e_2 - e_1^2r_2 - e_1e_2r_1 + e_1r_1r_2) + e_b(\dot{b} + r_1e_3 + e_1e_3) + e_c(\dot{c} + e_3^2 - r_3e_3) \quad (15)$$

Selecting

$$\left.\begin{array}{c} \dot{a} = e_1^2e_2 - e_1^2r_2 - e_1e_2r_1 + e_1r_1r_2 \\ \dot{b} = r_1e_3 + e_1e_3 \\ \dot{c} = e_3^2 - r_3e_3 \end{array}\right\} \quad (16)$$

$\dot{V}(t)$ becomes: -

$$\dot{V}(t) = -k_1e_1^2 - k_1e_2^2 - k_1e_3^2 \quad (17)$$

(17) is negative definite and controller stability is ensured.

V. Synchronization System Design

In this section, a synchronization system for two identical of the proposed chaotic system is designed. The master is the uncontrolled system described by (1). The slave system takes the following form: -

$$\left.\begin{array}{c} \dot{y}_1 = ay_1y_2 + u1 \\ \dot{y}_2 = 70 - y_1y_3 + u2 \\ \dot{y}_3 = by_1 - cy_3 + u3 \end{array}\right\} \quad (18)$$

Where U={u1,u2,u3} is the control inputs to be designed to synchronize the two systems.
The error between the two systems (synchronization error) is defined as: -

$$e_i = y_i - x_i, \quad i = 1,2,3 \tag{19}$$

Using $\dot{e}_i = \dot{y}_i - \dot{x}_i$ and substuting (1) and (18), the following error dynamics can be easily obtained :-

$$\left.\begin{array}{c} \dot{e}_1 = a(y_1y_2 - x_1x_2) + u1 \\ \dot{e}_2 = x_1x_3 - y_1y_3 + u2 \\ \dot{e}_3 = be_1 - ce_3 + u3 \end{array}\right\} \tag{20}$$

To stabilize the dynamics described by (20), we designed the control inputs to satisfy the following stable dynamics: -

$$\dot{e}_i + k_i e_i = 0 \ , \qquad i=1,2,3 \tag{21}$$

Where k_i is the design parameters.
Substituting (21) into (20) and solving for U, the following result is obtained: -

$$\left.\begin{array}{c} u1 = -k_1e_1 - a(t)(y_1y_2 - x_1x_2) \\ u2 = -k_2e_2 - x_1x_3 + y_1y_3 \\ u3 = -k_3e_3 - b(t)e_1 + c(t)e_3 \end{array}\right\} \tag{22}$$

Substituting (22) into (20), we get:-

$$\left.\begin{array}{c} \dot{e}_1 = -k_1e_1 + e_a(y_1y_2 - x_1x_2) \\ \dot{e}_2 = -k_2e_2 \\ \dot{e}_3 = -k_3e_3 + e_be_1 - e_ce_c \end{array}\right\} \tag{23}$$

Where, $e_a = a - a(t), e_b = b - b(t), e_c = c - c(t)$.
To obtain stable update laws for time varying design parameters, we use Lyapunov theory. Selecting the Lyapunov function candidate as: -

$$V(t) = 1/2(e_1^2 + e_2^2 + e_3^2 + e_a^2 + e_b^2 + e_c^2) \tag{24}$$

Differentiating V, the following is obtained:-

$$\dot{V}(t) = e_1\dot{e}_1 + e_2\dot{e}_2 + e_3\dot{e}_3 + \dot{a}e_a + \dot{b}e_b + \dot{c}e_c \tag{25}$$

Substituting from (23), the following result is obtained: -

$$\dot{V}(t) = -k_1e_1^2 - k_1e_2^2 - k_1e_3^2 + e_a(\dot{a} + e_1(y_1y_2 - x_1x_2)) + e_b(\dot{b} + e_1e_3) + e_c(\dot{c} - e_2e_3) \tag{26}$$

Selecting:

$$\left.\begin{array}{c} \dot{a} = -e_1(y_1y_2 - x_1x_2) \\ \dot{b} = -e_1e_3 \\ \dot{c} = e_2e_3 \end{array}\right\} \tag{27}$$

Result in,

$$\dot{V}(t) = -k_1e_1^2 - k_1e_2^2 - k_1e_3^2 \tag{28}$$

Which is a negative semi definite function.

VI. Simulation Study

In this section, the designed control and synchronization systems are tested by simulation. Matlab18a is used to write the simulation programs.

A. Control system

The designed controller is simulated for two cases. First, a stabilization ability is tested by assuming starting from an initial condition and the reference target is:
$R = \{0,0,0\}$.
The initial condition is assumed to be:
$X(0) = \{1, -2, 3\}$
Fig.5 shows system states responses and it is clearly shows the high performance of the control system.

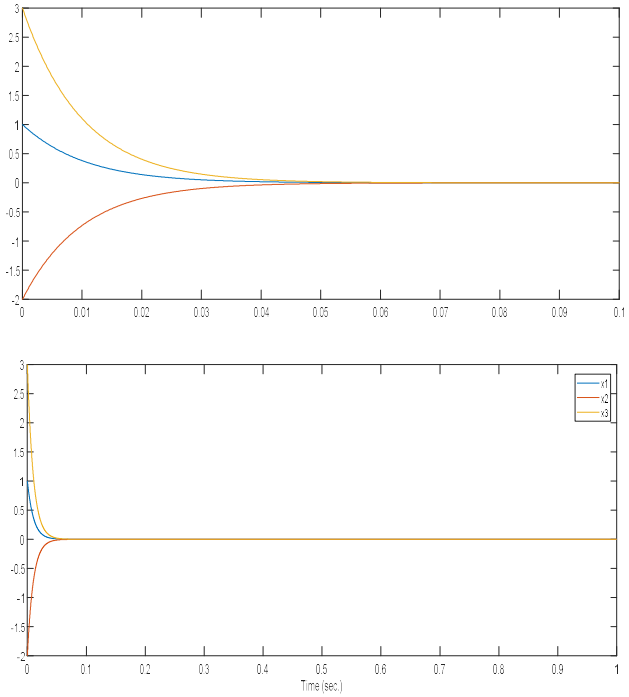

Fig. 5: States response of the stabilized system

Secondly, a tracking ability for the designed control system is tested by assuming sinusoidal reference signals and as follows:
$R = \{\sin(20t), 2\sin(20t), 3\sin(20t)\}$
The initial condition is taken as:
$X(0) = \{1, -2, 3\}$.
Fig. shows the states responses of the system and it shows high performance tracking ability.

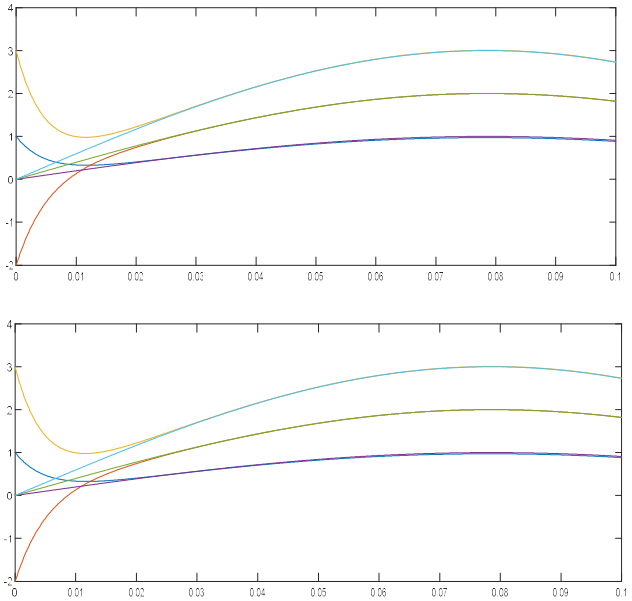

Fig. 6: States response of sinusoidal tracking system

B. synchronization system

The designed synchronization system is simulated assuming the following initial conditions for the master and slave states:

$X(0) = \{3, -1, 2\}$

$Y(0) = \{1, 2, 3\}$

Fig.7 shows the synchronization errors and it clearly shows the high performance synchronization of the system with very small and acceptable transient time.

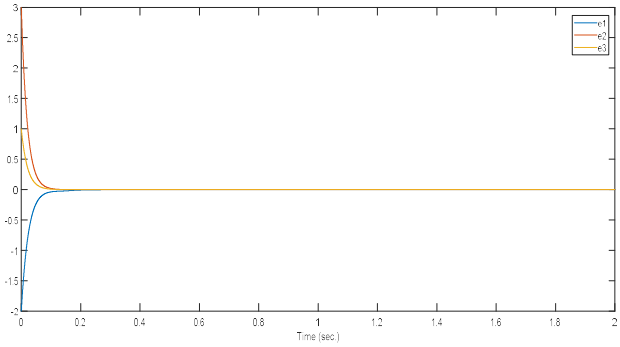

Fig. 7: Synchronization error.

The synchronization system is also simulated as a secure communication system where a sinusoidal signal $s = 3\sin(20t)$ is assumed as the signal to be transmitted. This signal is added to $x_1$and the resultant signal t_r is transmited to the receiver side where the slave system. The received signal should be extracted by subtracting it from y_1. The initial conditions for the master and slave are:

$X(0) = \{3, -1, 2\}$

$Y(0) = \{1, 2, 3\}$

Fig.8 shows the transmitted and received signals.

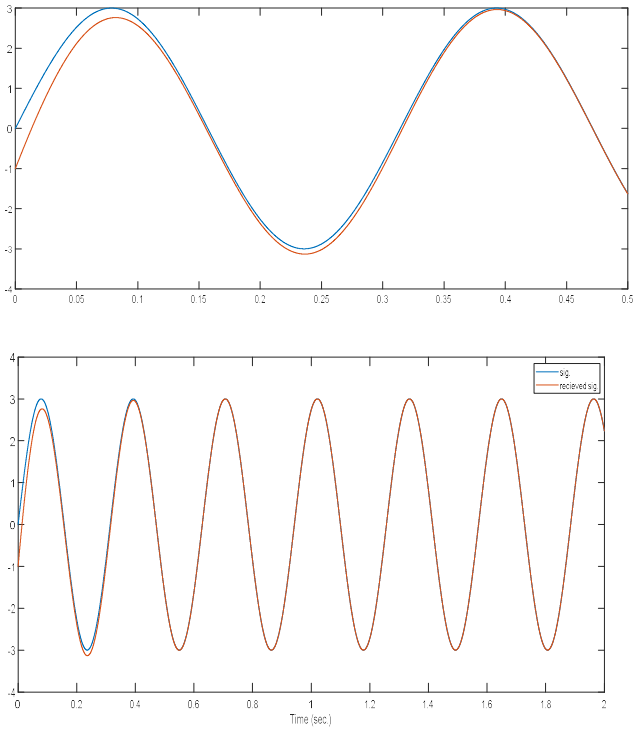

Fig. 8: Transmitted and received signal.

VII. Conclusion

A novel 3 dimensional chaotic systems are presented in this paper. The dynamical properties of the proposed system are studied. Control and synchronization systems using simple control design procedure are designed. Simulation study is used to validate the designed control and synchronization systems and to investigate their performances. The simulation study shows that the controllers designed to control and synchronize the system have very high performances and that the synchronization system is suitable and easy to use in secure communication application.

References

[1] Ahmad Azar, Sundarapandian Vaidyanathan, (2015), "Chaos Modeling and Control Systems Design", 2015. DOI: 10.1007/978-3-319-13132-0.

[2] Saeed Khorashadizadeh, Mohammad-Hassan Majidi, "Chaos synchronization using the Fourier series expansion with application to secure communications", AEU - International Journal of Electronics and Communications, Vol. 82, 2017.

[3] Ghaida Al-Suhail, Fadhil Tahir, Mariam Abd, Viet-Thanh Pham, Luigi Fortuna, "Modelling of Long-Wave Chaotic Radar System for Anti-Stealth Applications", Communications in Nonlinear Science and Numerical Simulation, Vol. 57, 2017.

[4] Amin Yousefpour, Hadi Jahanshahi, J.M. Munoz-Pacheco, Stelios Bekiros, Zhouchao Wei, (2019), "A fractional-order hyper-chaotic economic system with

transient chaos", Chaos Solitons & Fractals, Vol. 130, 2019. DOI: 10.1016/j.chaos.2019.109400.

[5] Philippe Faradja, Guoyuan Qi, "Analysis of multistability, hidden chaos and transient chaos in brushless DC motor", Chaos Solitons & Fractals, 2020. DOI: 132. 10.1016/j.chaos.2020.109606.

[6] Miillin T, "Chaos in physical systems. In: Crilly AJ, Earnshow RA, Jones H, edi- tors", Fractals and chaos. New York: Springer, 1991, pp. 237–245.

[7] Shinbrot T, Grebogi C, Wisdom J, Yorke JA. "Chaos in a double pendulum", Am J Phys, Vol. 60, Issue 6, 1992.

[8] Zhu Q, Ishitobi M, "Experimental study of chaos in a driven triple pendulum", J Sound Vib, Vol. 227, Issue 1, 1999.

[9] Hemati N, "Strange attractors in brushless DC motors", IEEE Trans Circuits Syst, Vol. 41, Issue 1, 1994.

[10] Emad Mahmoud, Fatimah Abood, "A novel sort of adaptive complex synchronizations of two indistinguishable chaotic complex nonlinear models with uncertain parameters and its applications in secure communications", Results in Physics, Vol. 7, 2017. DOI: 10.1016/j.rinp.2017.07.050.

[11] Amin Yousefpour, Hadi Jahanshahi, J.M. Munoz-Pacheco, Stelios Bekiros, Zhouchao Wei, "A fractional-order hyper-chaotic economic system with transient chaos. Chaos Solitons & Fractals, Vol. 130, 2019. DOI: 10.1016/j.chaos.2019.109400.

[12] Emad Mahmoud, "Dynamics and synchronization of new hyperchaotic complex Lorenz system", Mathematical and Computer Modelling, Vol. 55, 2012. DOI: 10.1016/j.mcm.2011.11.053.

[13] Maitreyee Dutta, Krishna Binoy, Roy, "A new fractional-order system displaying coexisting multiwing attractors; its synchronisation and circuit simulation", Chaos Solitons & Fractals, Vol. 130, 2020. DOI: 109414. 10.1016/j.chaos.2019.109414.

[14] Mohammad Ababneh, "A new four-dimensional chaotic attractor", Ain Shams Engineering Journal, Vol. 9, 2016. DOI: 10.1016/j.asej.2016.08.020.

[15] Sundarapandian Vaidyanathan, Aceng Sambas, Mustafa Mamat, W. S. Mada Sanjaya, "A new three-dimensional chaotic system with a hidden attractor, circuit design and application in wireless mobile robot", Archives of Control Sciences, Vol. 27, 2017. DOI: 10.1515/acsc-2017-0032.

[16] E.N. Lorenz, "Deterministic nonperiodic flow," J. Atmos. Phys., Vol. 20, pp 131-141, 1963.

[17] Mohammad Ababneh, "A new four-dimensional chaotic attractor. Ain Shams Engineering Journal, Vol. 9, 2017. DOI: 10.1016/j.asej.2016.08.020.

[18] Homayoon Arabyani, Hassan Saberi-Nik, "Synchronisation of the hyperchaotic complex Lorenz system in a finite time", International Journal of Modelling, Identification and Control, Vol. 25, 2016. DOI: 138. 10.1504/IJMIC.2016.075273.

[19] L.M. Pecora, T.L. Carroll, "Synchronization in chaotic systems", Phys. Rev. Lett., Vol. 64, pp 821-824, 1990.

[20] Mengjiao Wang, Xiaohan Liao, Yong Deng, Li Zhijun, Yongxin Su, Yicheng Zeng, "Dynamics, synchronization and circuit implementation of a simple fractional-order chaotic system with hidden attractors", Chaos, Solitons & Fractals, Vol. 130, 2020. DOI: 109406. 10.1016/j.chaos.2019.109406.

[21] Wolf A, Swift J, Swinney H, Vastano J., "Determing Lyapunov exponents from a time series", Phys Lett B, Vol. 737, 1985.

[22] P. Frederickson, J.L. Kaplan, E.D. Yorke, J.A. Yorke, "The Liapunov dimension of strange attractors", J. Differ. Equ., Vol. 44, pp. 185–207, 1983.

Open Access
Iraqi Journal for Electrical and Electronic Engineering
Conference Article

Design and implementation of monitoring and warning (IOT) system for electricity poles

Jumana Amer AL-Hammoudi*, Basil H. Jasim
Electrical Engineering Department, University of Basrah, Basrah, Iraq

Correspondence
* Jumana Amer AL-Hammoudi
Electrical Engineering Department,
University of Basrah, Basrah, Iraq
Email: jumana.fnmr@yahoo.com

Abstract
There are many serious accidents on human life caused by electric current columns, and it is possible for the Internet of Things to find solutions to prevent the risks that occur, as in many fields such as medicine, agriculture, industry and others. In this paper, we will show monitoring and tracking of the current that passes through the electrical poles and the possible leakage, in addition to monitoring the temperature and humidity in the area, and knowing the condition of the light in the column according to morning and evening, this proposed system that will perform a general purpose added to the region. using Open source NODE MCU board, GPS positioning, current sensor, temperature and humidity sensor that provide desired data via open source platforms that we have chosen to be ThingSpeak that easily to handle.

KEYWORDS: IOT, Node MCU board, ACS712sensor, ThingSpeak, DHT11, GPS, LDR.

I. INTRODUCTION

A long time ago, the Internet of things (or the Internet of everything) appeared in the military fields, but with the development of technology and the increase in the use of the Internet and wireless technologies and the widespread use of mobile phones. The existence IOT became necessary to provide human services with high technology and quality. Cloud computing and IPV6 foster an integrated development between the Internet and IOT, as the Internet of Things acts as a huge network of objects that connect with each other and with the individual across the Internet by making each device associated with a single definition capable of collecting and processing information in real time individually. The entry of IPV6 with IOT has made it possible to mix an unknown number of things on the Internet [1][2]. In 1999 IOT was launched by Kevin Ashton, who dreams of a system in which anything physical can be connected to the Internet via sensors everywhere. In 2013, the Global Standards Initiative (GSI) determined that the Internet of Things was the infrastructure for the information society [3].

The Internet of Things has become a supporter of many areas in the process of connecting devices with sensors surrounding the Internet and facilitating the access to information, exchange and processing of required information anywhere in the world and at any time through ready-made software platforms from anywhere in the world via the Internet. The Internet of Things has made life and business faster and easier than it has been, as well as flexibility in dealing with devices and making people more free in their lives.

Fig. 1: Internet of thing (iot)

The rest of this paper is organized as follows. Section II introduces IOT applications, Section III presents the proposed system for monitoring. and warning IoT system for the electrical poles, while Section IV presents the hardware components used in system, Section V displays the software part and results, and finally, Section VI presents the concludes of the paper.

II. IOT APPLICATIONS

The applications in the Internet of things appeared clearly over its ability to communicate with humans and devices, as we will present some of them:
In the literature [4] the researcher describes home appliances more intelligent with(IoT) through sensors and microcontrollers that collect and continuously transmit data via the Internet via phones / personal computers and process them remotely without the need to stick to the place and restrict human freedoms.
In the literature [5], the entry of the Internet has revealed things in the medical field when discussing cases of heart patients, as it monitors and follows patients through sensors and sends their data to the Internet to follow up on the matter by the specialist doctor and also gives treatment via the Internet, these techniques avoided many risks for the elderly and cases Fast, which can lead to the loss of the patient and thus be safer in his health.

The author in [6] describes the possibility of monitoring water quality and turbidity and controlling this in real time through sensors that send their data through the micro-controllers to the official in handling the matter through the Internet. What led to the Internet of things to have a role in finding a valid and self-sustaining environment High quality water and serve humans and living organisms in drinking water.

In this [7] research, the monitoring system used to distribute and transfer electrical energy is mentioned, at the present time, interest in introducing smart systems and devices to achieve comfortable purposes for life has become. The electric power sector has created what is known as a smart grid that works to offset the demand for electricity supplies and benefit from electrical resources. Effectively. The network monitors the distribution and transmission of energy and establishes several smart communications in the system to enhance energy services to make them more responsive, powerful and communicative.
Many developing countries, such as Indonesia, are working with a combination of wireless transmission with the ZigBee and GPRS to meet the basic requirements in terms of real-time communication and long distances for a monitoring system through the Internet of things that are displayed on the computer and even the mobile phone, and the development is still ongoing to design the power distribution system devices more effectively.

On this page [8] he talked about using the library system that enables it to continuously update data and information for employees and students without the need for the human factor. It was designed with GMS technology with a built-in server to send SMS to the user what he needs and requests. For the customer. He also made it possible to store previous notes and notifications that were sent.
In this proposed work, we will explain the process of monitoring and tracking electrical and leakage cases using the ACS712 sensor, as well as changes in the area in terms of humidity and heat using the DHT11 sensor and tracking the light used in the column next to the light sensor, using the NODE MCU controller board, in addition to GPS, and send all data to ThingSpeak online platform.

III. PROPOSED SYSTEM

In this paper, we proposed monitoring the current passing through the electrical poles and discovering the current leakage and tracking that in platform ThingSpeak site, so that get a warning from electrical leakage. the ACs712 sensor, that be sensing the current passed in poles and transmit data in real time to ThingSpeak. this propose will lead to find a solutions speed up to prevent danger from controller room.
In addition to the presence of the DHT11 temperature and humidity sensor, which shows the temperature and humidity of the area, as we know its influence on the columns and wires, as the humidity increases, the probability of leakage will increase in the electrical column and that the high temperature affecting the state of the wires and their expansion, which will lead to merging and leakage cases. It will send the DHT11 sensor information to the platform.

With the addition of a light sensor that monitors the work of light at day and night during the day, as the data sent to the site indicates the state of light at the column, it becomes clear to us the safety of the light attached to the column. In this work, we have linked the GPS locator, which helps to facilitate the process of determining the leakage current, thus reducing much time and speeding up the processing task.

Where depended in this paper to find the problem only, using one of the microcontrollers that are characterized by their small size and low cost is NodeMCU and we will explain in the following paragraphs, where it is installed within the Arduino IDE environment working on it in the same well-known Arduino programming language. The following Fig. (2) shows the hardware connection proposed system.

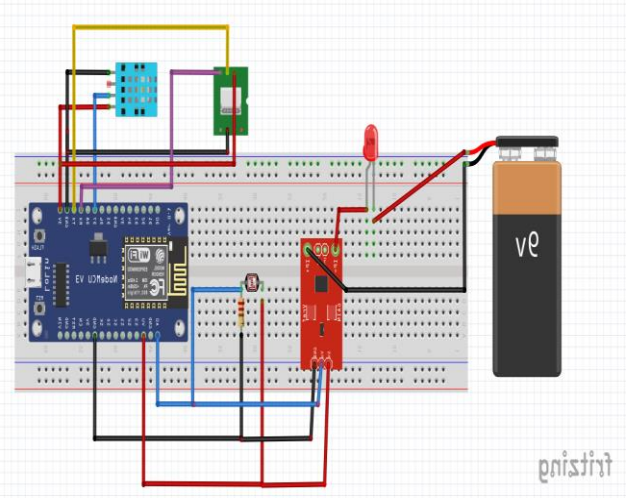

Fig. 2: Hardware connection system

We notice in Fig. (2) that the NODE MCU board microcontroller will be the main board at work, and is considered to be the gateway between the sensors and the cloud computing that stores information sent via the Internet from the sensors. Fig. (3) show block diagram system

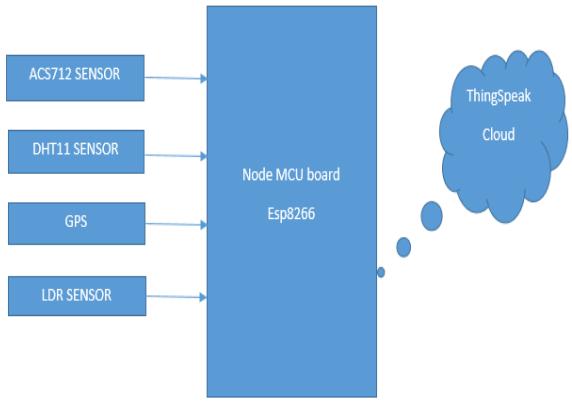

Fig. 3: block diagram for the system

IV. COMPONENTS REQUIRED

A. ACS712 Current Sensor

The ACS712 provides economical and precise solutions for AC or DC current sensing in industrial, commercial, and communications systems. The device package allows for easy implementation by the customer. Typical applications include motor control, load detection and management, switched-mode power supplies, and overcurrent fault protection The ACS712 Current Sensors offered on the internet are designed to be easily used with micro controllers like the Arduino and other that. These sensors are based on the Allegro ACS712ELC chip. These current sensors are offered with full scale values of 5A, 20A and 30A [9].

the Fig. (4) below present the circuit connected with current sensor in the two poles and the other side connected with microcontroller NodeMCU have three pin, pin Vcc connect with PIN power, GND PIN, and PIN analog signal.

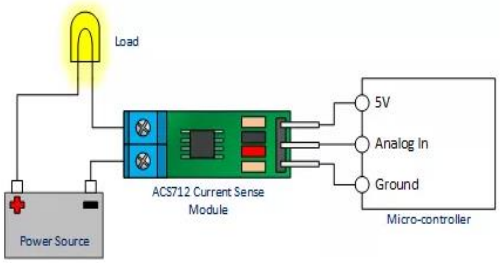

Fig. 4: circuit diagram current sensor

B. GPS

The NEO-6 module collection is a family of stand-alone GPS receivers providing excessive-overall performance u-blox 6 positioning engine. These bendy and fee-effective receivers offer a couple of connectivity alternatives in a miniature 16 x 12.2 x 2.4 mm bundle. The compact architecture, energy and reminiscence alternatives make the NEO-6 modules best for battery operated cell devices with limited price and area constraints. Innovative layout and era suppresses jamming sources and mitigates multipath consequences which provide NEO-6 GPS receivers first rate navigation overall performance even within the most difficult environments [10].

C. LDR Sensor

It is a component made up of highly resistant semiconductor materials or called photo conductors or photo cells only or optical cells. These resistors are
distinguished by their dependence on the light intensity they are exposed to, as the resistance decreases with increasing light intensity. This resistance entered in many areas because of its low cost and ease of use .as it was in automatic street lights systems and in smart home systems and other light sensing circuits [11] [12]. In the proposed system for this page, as resistance sensitive to the dark and when it is darkness will be Turn on the lights and when there is light it will work opposite that.

*D. **Te**mperature and Humidity Sensor DHT11:*

It is a low-cost, easy-to-use digital sensor, it utilizes a capacitive humidity sensor and a thermistor to gauge the surrounding air, what is wrong with this sensor is its ability

to give new information when every two seconds pass when using our library.it works on 3-5V power supply, Humidity ranges between 20-80% and heat ranges from 0-50 ° C [13] [14].

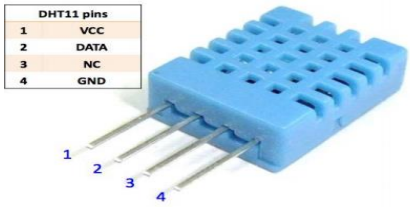

E. NODE MCU Board

NodeMCU board is an open source and can operate with in IDE Arduino. It consists of firmware which runs on ESP8266. It is programmable, low cost, and smart Wi-Fi enabled. NodeMCU has ESP-12 based serial Wi-Fi integrated on-board to provide GPIO, PWM, ADC, I2C and built-in USB-TTL serial as shown in Fig. below. NodeMCU has powerful processing and storage capabilities that, allows the sensors to be integrated with it.it is Operating voltages (3.3-3.6V), Uses IPV4, HTTP, FTP, UDP & TCP network protocols, operating frequency range (2.4-2.6 GHz), Configured in both Android and iOS devices [15].

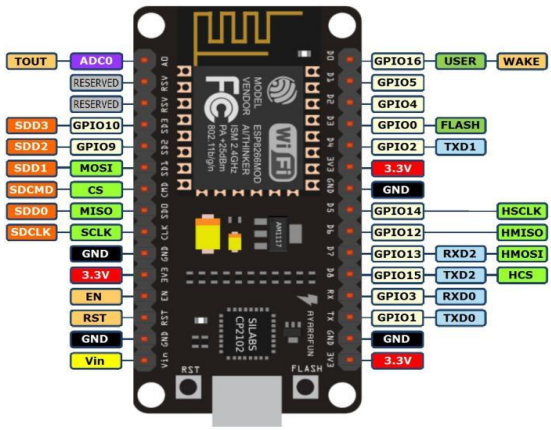

V. SOFTWARE WORK AND RESULT

A. ThingSpeak Platform

ThingSpeak is an open source platform that appeared in 2010. It is used in many internet of things applications. It stores the data collected in real time from the sensors and stored inside the channels. It includes 4 channels and each channel allows to store up to 8 data fields, using up to 255 characters each. There are also 4 fields dedicated to the data on the site, and it consists of: description, length, length, height. Also, each channel can be public for all users and display its information without requiring a key, but when you make it private, the channel will give you a writing key and read key to make it private, it features a very easy visualization of the data collected from the sensors using simple and easy graphics.
ThingSpeak has the ability to integrate with small controls like Arduino, Raspberry Pi and others. ThingSpeak source includes HTTP request processing, data storage (alphanumeric), digital data processing, site tracking, and status updates [16] [17].

B. Getting Start

At the beginning of the worked, we will define the microcontroller that we are dealing with it, as our worked will be linked to the Internet. We choose a microcontroller with Wi-Fi inside it to make work easier, it's Nodemcu. Initially, we will define NodeMCU within the Arduino environment to allow us to work within the environment and download the code on it, and the steps to defined it inside the Arduino environment itself with any other microcontroller. Now in IDE environment file > Preferences> Additional URL Fields for board Manager: (https://arduino.esp8266.com/stable/package_esp8266com_index.json).Then Tools> board> board manager, search about esp8266 and install it. After finishing, we find in the boards all esp8266 boards - includes it NodeMCU and its various versions.

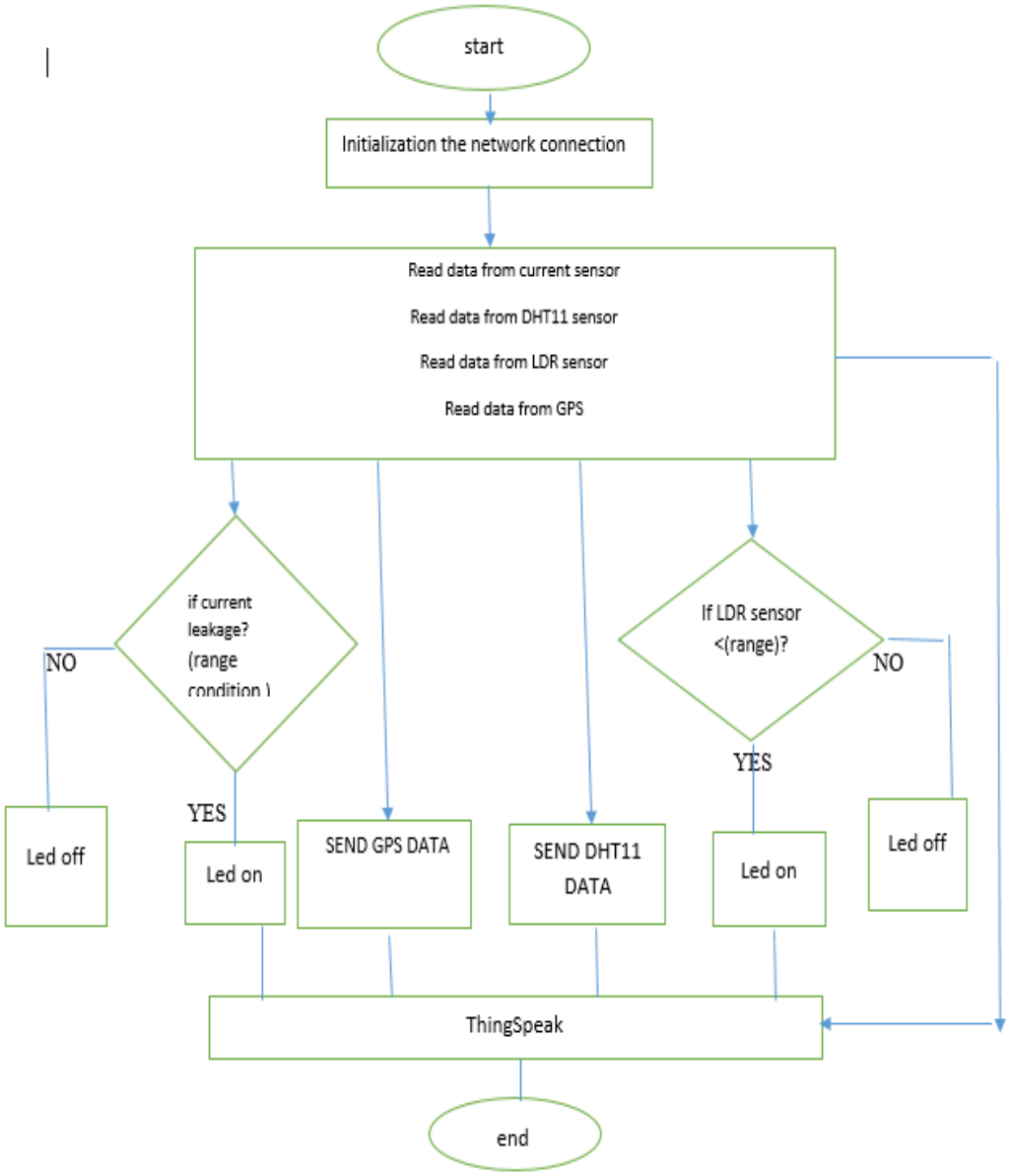

Fig. 5: System flowchart.

And the previous flowchart shows the work followed in the proposed system.

Then we need to create an account inside the API ThingSpeak, which contains the channels that are the storage location for the data loaded from the devices and sensors, this is done by creating an account and after logging in we will choose Channels> My Channels and then create a new channel. The channel has a unique identifier key that is used to identify the channel when reading or downloading data. After that, we defined the required libraries for the devices used in the system and we also linked the proposed system as we showed it through the block diagram in advance and we started recording the results and examined the system and its work after downloading the program to the NODE MCU We saw the results for more than once and they were giving similar results. as the DHT11 sensor that records the workplace temperature and humidity properly, as well as the light sensor, we noticed that when the brightness of the light increases the optical resistance increases, and by darkness it will follow the condition in the program and give a signal there are darkness by ON LED. the ACS712 sensor the current passing in the circuit used in the system, the GPS determines the work site properly .and this results data uploaded to the site ThingSpeak, show Fig. 6.

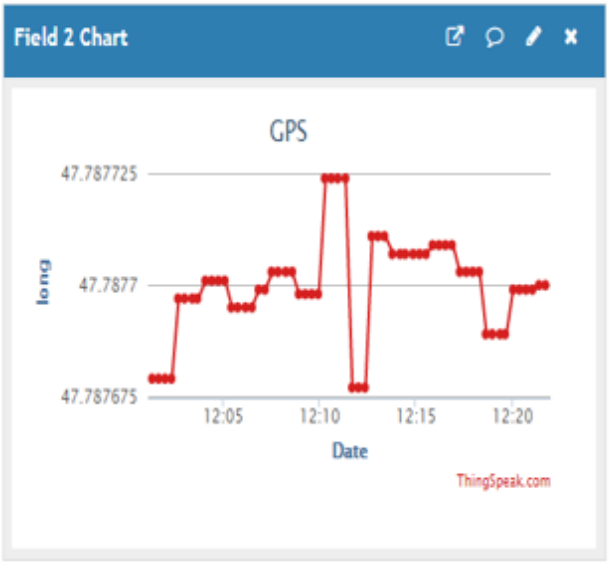

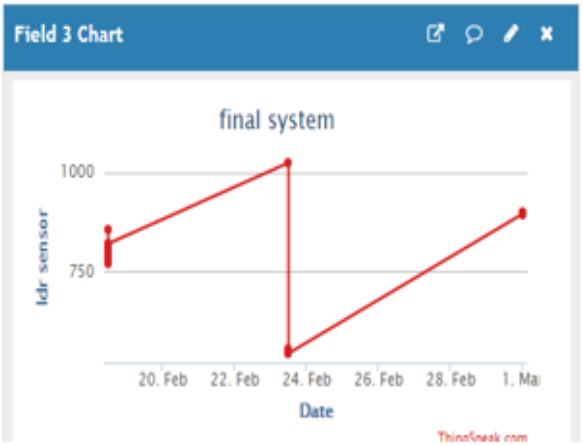

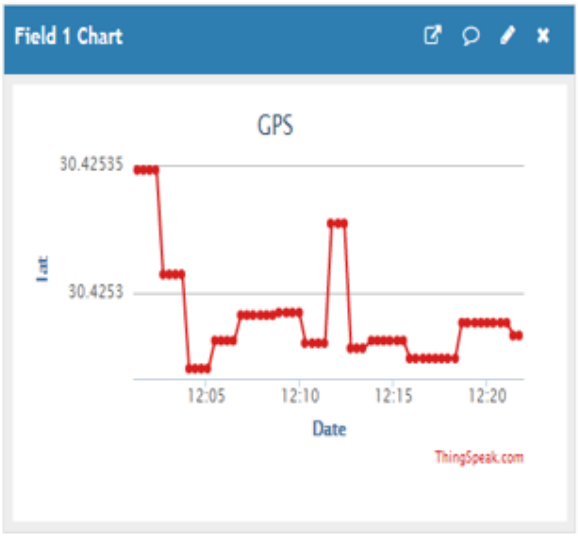

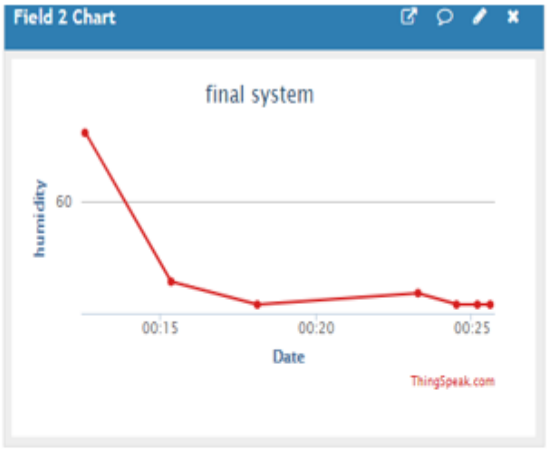

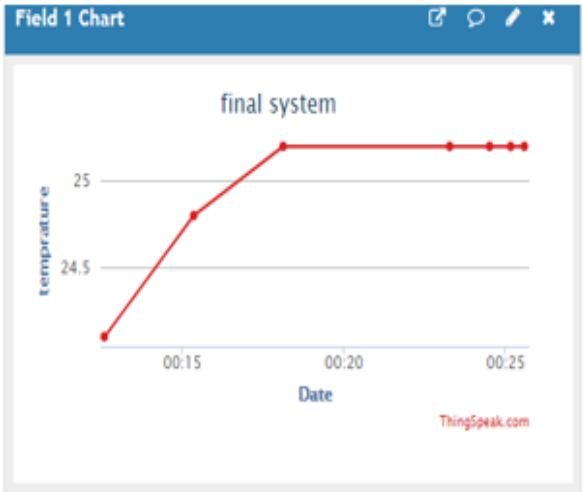

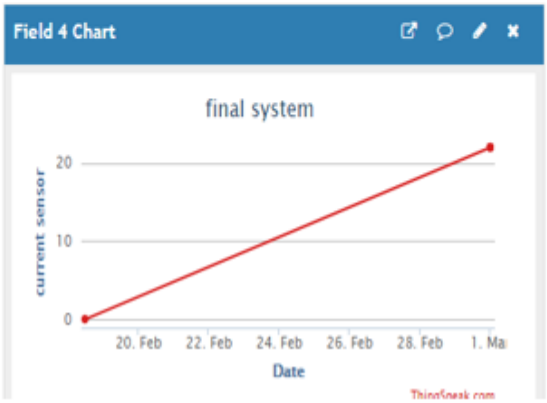

Fig. 6: Display the data received from sensors in ThingSpeak site.

VI. CONCLUTION

We have shown on this page what is the Internet of Things and its many uses in various fields, and here we have worked to show the status of tracking the current and the possible leakage in the electrical poles and get the location of the column by through the GPS, adding the ability to know the lighting in the column and measure the temperature and humidity of the column area and raise all these data to ThingSpeak online. This technology can be a topic to protect from the danger of the current leading to death in many places, as well as the possibilities of development at work according to the required need, which works to serve man and facilitate many of the complexities of life and the possible risk with modern technologies.

REFERENCES

[1] Rose, Karen, Scott Eldridge, and Lyman Chapin. "The internet of things: An overview." *The Internet Society (ISOC)* 80 (2015).

[2] Davies, Ron. "The Internet of Things opportunities and challenges." *European Parliamentary Research Service* (2015).

[3] Patel, Keyur K., and Sunil M. Patel. "Internet of things-IOT: definition, characteristics, architecture, enabling technologies, application & future challenges." *International journal of engineering science and computing* 6, no. 5 (2016).

[4] Suresh, Dalli Sai, and Sivah Akash. "Implementation of Home Automation with Thingspeak Cloud."

[5] Gurjar, A. A., and Neha A. Sarnaik. "Heart attack detection by heartbeat sensing using Internet of Things: IoT." *Heart* 5, no. 03 (2018).

[6] Shirode, Mourvika, Monika Adaling, Jyoti Biradar, and Trupti Mate. "IOT based water quality monitoring system." *Int. J. Sci. Res. Comput. Sci. Eng. Inf. Technol* 3, no. 1 (2018): 5447-5454.

[7] Hidayatullah, N. A., A. C. Kurniawan, and Akhtar Kalam. "Power Transmission and Distribution Monitoring using Internet of Things (IoT) for Smart Grid." In *IOP Conference Series: Materials Science and Engineering*, vol. 384, no. 1, p. 012039. IOP Publishing, 2018.

[8] Memon, Azam Rafique, Bhawani Shankar Chowdhry, Syed M. Shehram Shah, Tarique Rafique Memon, and Syed MZ Abbas Shah. "An electronic information desk system for information dissemination in educational institutions." In *2015 2nd International Conference on Computing for Sustainable Global Development (INDIACom)*, pp. 1275-1280. IEEE, 2015.

[9] ACS712, Datasheet. "Fully Integrated, Hall Effect-Based Linear Current Sensor IC with 2.1 kVRMS Isolation and a Low-Resistance Current Conductor." (2006). www.allegromicro.com

[10] www.u-blox.com. NEO-6 u-blox 6 GPS Modules Data Sheet.

[11] Ome, Nerella, and G. S. Rao. "Internet of Things (IoT) based Sensors to Cloud system using ESP8266 and Arduino Due." *International Journal of Advanced Research in Computer and Communication Engineering* 5, no. 10 (2016): 337-343.

[12] Zailan, Fatin Syamimi. "IMPLEMENTATION OF HOME AUTOMATION USING WIRELESS COMMUNICATION." IRC, 2016.

[13] https://www.adafruit.com/product/386

[14] Dangi, Nagendra. "Monitoring environmental parameters: humidity and temperature using Arduino based microcontroller and sensors: Microcontroller based building monitoring system." (2018).

[15] GHOSH, KUNDAN. "Globally controlled multiple relays using NODE MCU." PhD diss., University of Technology, 2018.

[16] Maureira, Marcello A. Gómez, Daan Olden of, and Livia Teernstra. "ThingSpeak–an API and Web Service for the Internet of Things." *World Wide Web* (2011).

[17] Mohamad, Auday AH, Noor Kareem Jumaa, and Sameer Hameed Majeed. "ThingSpeak Cloud Computing Platform Based ECG Diagnose System." *International Journal of Computing and Digital Systems* 8, no. 01 (2019): 11-18.

DOI: 10.37917/ijeee.sceeer.3rd.16 *(15-16) June 2020*

Open Access

Iraqi Journal for Electrical and Electronic Engineering
Conference Article

Control Strategy of Reactive Power Sharing in an Islanded Microgrids

Ali Q. Almousawi*[1], Ammar A. Aldair[2]
[1]Electrical Engineering Department, Faculty of Engineering, University of Kufa, Iraq
[2]Electrical Engineering Department, College of Engineering, University of Basrah, Iraq

Correspondence
* Ali Q. Almousawi
1Electrical Engineering Department,
Faculty of Engineering, University of Kufa, Iraq
Email: ali.almousawi@uokufa.edu.iq

Abstract
Precise power sharing considered is necessary for the effective operation of an Autonomous microgrid with droop controller especially when the total loads change periodically. In this paper, reactive power sharing control strategy that employs central controller is proposed to enhance the accuracy of fundamental reactive power sharing in an islanded microgrid. Microgrid central controller is used as external loop requiring communications to facilitate the tuning of the output voltage of the inverter to achieve equal reactive power sharing dependent on reactive power load to control when the mismatch in voltage drops through the feeders. Even if central controller is disrupted the control strategy will still operate with conventional droop control method. additionally, based on the proposed strategy the reactive power sharing accuracy is immune to the time delay in the central controller. The developed of the proposed strategy are validated using simulation with detailed switching models in PSCAD/EMTDC.

KEYWORDS: **Microgrid, reactive power control, Droop control, voltage control, central controller.**

I. INTRODUCTION

With the expanded penetration of distributed generation (DG) units on the electrical grid systems, the renewable energy sources (RESs) including photovoltaic (PV) systems, fuel cells, microturbines, and wind energy systems have been widely used in the distributed power systems in the past decades [1]. The DG units play an important role in decreasing power transmission losses, reducing pollution, and improving local operation of RESs.

A Microgrid (MG) consists of a collection of the distributed interconnection energy resource (DER) and many loads controlled intelligently by using a central controller. Most the DG, such as energy storage systems and RES, require interfaced by a power electronics such as inverter, rectifier to be linked to the MG, which permits them to be further adaptable in their control and operation [2].

DG also get difficulties to the distribution network system for example: voltage fluctuations, voltage profile, and inverse power flow. if an among of DG units are tied close proximity, this connection can make a MG have ability to solve the difficulties occurs by high penetration of DG effectively and makes the application of large-scale for DG systems possible [3]. Actually, the DG placed in various geographic sites therefore this methodology considered ineffective.

MG can operate in two basic modes: islanded mode (autonomous) and grid connected mode. When the MG working in autonomous mode, the MG must share loads and each DG unit must be it has the ability to deliver the power proportion to its rating in order to share the total load [4]. Also, DG unit must adjust its own voltage and frequency separately dependent on the local information comes from the same DG and any DG activity mode exchanging must not influence the MG steady state operation. Many papers, focus on the load sharing specially with reactive power, what's more, how to control the voltage and frequency of an autonomous droop-controlled MG.

In operation of MG, to guarantee stability should be the active and reactive power of DG units shared instantaneously. The droop control method provides a decentralized control and the preferred favored strategy to control an enormous number of DG since does not required any type from communication lines between inverters and this enhances the reliability of the system, enables "plug-and-play" interfacing [5], and also can be utilized to accomplish each of the real and reactive power sharing by mimic the steady state features of the synchronous generator in autonomous MG.

Several configurations and control schemes of droop control exist so as to permit great quality load sharing for nonlinear and fixed loads. The traditional droop control utilizes the reactive power-voltage (Q-V) control and the real

power-frequency (P-w) control to understand decoupling control for each real and reactive power [6].

Under extreme situation, the frequency droop control can achieve accurate real power sharing because the frequency of the microgrid is not affected and remains constant during the whole microgrid. therefore, the active power provided by the DG units is shared accurately between the DG unit in any even when mismatches are existing. also, the local load demand should be not exceeding the maximum power rating of the inverters connected to the whole MG.

The voltage droop control commonly results in poor reactive which cause circulating current between the inverter units and make microgrid network instability because the various ratings of the DG units and the various values in the impedances of the DG unit feeders. Communication lines can be used, however, in addition to the droop control method to improve the system performance without reducing reliability and achieve accurate reactive power sharing [7].

various control techniques have been proposed in the literature recently to address the reactive power sharing issue.

in [8] islanded microgrid could operate with two operation modes, the first mode with single master operation which has one master inverter entrusted with voltage/frequency control and real-time load balancing thereby offering a more straightforward control. The multi-master operation used as the second mode, this mode have more than one master inverter entrusted with supporting coordinated voltage/frequency control and real-time load sharing.

The virtual impedance idea presented in [9] to reduce errors focus on reactive power sharing with the different values in the output impedances for closed-loop controlled inverters that are utilized to connect between PCC and the DG units. using suitable strategy of the voltage controller, for the closed-loop the output impedances should be negligible especially at steady state about the reference operating frequency. So, the virtual impedance is prevailing under this condition, which yields precise reactive power sharing. the study, However, the mismatch in the feeder's impedance did not consider, including links, transformers, and the interface inductors related with every DG unit.

in [10] is proposed a unique approach to realize precise reactive power sharing. The technique dependents injection in the system a small AC voltage signal, but the quality of line current and the result voltage may be reduced when injection small voltage signal. Also, processing and generating this signal may result in a difficult achievement.

A control technique utilizing only inductive virtual impedance is used in [11] to guarantee precise reactive power sharing. Design method and analysis in [11] are depend on the virtual impedance which is a known parameter is dominate when assumption that the impedance of feeder is small. furthermore, to enhance the precision should be the feeder physical impedance is estimated, and to contain the impact of the impedance resistive part. The problem in this method, the estimation method needs the MG it works first in grid connected before islanded mode and simulated the system with identical feeder physical impedances.

in [12] the analysis and control strategy require that the impedances of feeder are resistive. Therefore, the control method and the analysis yields in perfect power sharing if used only the resistive. Actually, the feeders may have resistive and inductive components and both cannot negligible.

Communication is used in [13] to set the virtual impedances to guarantee precise reactive power sharing after estimation the impedances of feeders. using the point of common coupling (PCC) voltage information transferred through a communication link in order to estimate the feeder impedance at each the local DG controller. This study established on the hypothesis that the power angle variance between the inverter output and the voltages at the PCC is negligible. This assumption considered not appropriate for higher power levels or for long feeders.

The distributed strategy presented in [14] coordinates the voltage control mode (VCM) and power control mode (PCM) units to share the real and reactive power. The droop control and opposite droop control are added to the VCM and PCM compensators to adjust the reactive power adaptively.

graph theory is presented in [15] utilizing optimized algorithm to realize the sharing in reactive power when the different values feeder impedance situation.

A secondary control technique is developed in [16] to ensure precise reactive power sharing. Also, to restore the voltage and the frequency. the controller is applied in every DG unit for this technique instead of executing it in the MG central controller unit. the state of a whole communication when failure, however, is not studied.

in [17] a control strategy which combines droop control and the MG central controller (MGCC) in order to share the reactive power. In this paper, The MGCC is utilized to regulate reactive power references to the corresponding inverter units and compute the averaged reactive power. basically, the physical modes of the MG are complex and the reactive power can be seriously influenced by the communication delay.

in [18] used only MGCC as a control method to share both the active and reactive power. Also, The MGCC is used to regulate active and reactive power references to the corresponding DG units dependent on two paradigms derived, quantity of real power bound and the quantity of optimized reference active power. basically, the analysis and control strategy in this proposed assuming that the feeder impedances are inductance only. Also, if the MGCC is disrupted the control strategy will not operate the droop control.

In this paper, a central controller strategy is developed to improve reactive power sharing precision. central controller is used to tuning of the output voltage of the inverter to achieve equal reactive power sharing dependent on reactive power load to avoid time delay unlike [19] which be used reactive power from all DG to compensate for the different values in voltage drops across each feeder.

The layout of the remainder of the paper is as per the following. In section II, explain the proposed structure and control of an islanded microgrid, control of inverter unit with explain the outer and inner control loop. Section III, power sharing strategy discussed for the reactive power sharing and explain the function of MGCC and how to operating in system. Sections IV and V consist of simulation results and conclusion respectively.

II. ISLANDED MICROGRID STRUCTURE AND CONTROL

A. *Structure of the proposed Microgrid*

The structure of the IEEE 4-bus test feeder [20] with one-line diagram as appeared in Fig. 1 used to confirm the reactive power sharing capability. The system is modified by adding two cumulative loads, it is indicated L1 and L2, additionally, switch will be used with each load. the loads in this paper, are modeled as linear loads. Also, in the system used, three DGs the MG contain: DG1, DG2, and DG3. Every unit is demonstrated as a droop-controlled inverter linked DG. PSCAD/EMTDC is used to develop the droop control inverter model.

In this paper, the microgrid considered runs with low voltage distribution level (480 V_{ll}). LC output filters (not appear in Fig.1) connected to output three phase inverters, the feeder and then the isolation transformer connected each inverter unit to the point of common connection (PCC). the voltage converted by the transformer to the distribution network close of (4.16 kV_{ll}). The focus in this work is on the basic active and reactive power sharing. All quantities are in per unit with base voltage used in the inverter side is 0.48 kV_{ll} and base power is 1 MVA.

The switch (s) is open when operating in islanding mode, and each inverter work alone to regulate the frequency. local grid voltage regulated by MGCC for accurate load sharing.

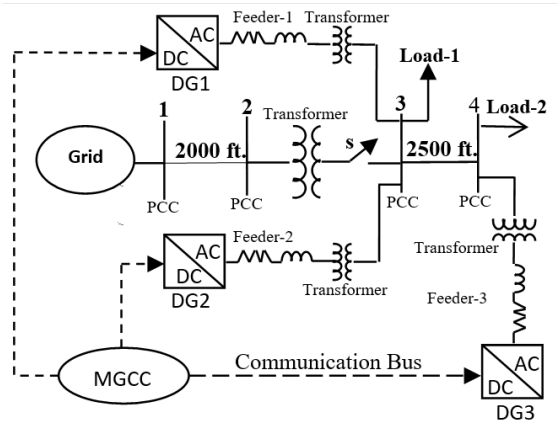

Fig. 1 Structure of proposed Microgrid

B. *inverter unit control*

The basic control structure in islanded microgrid, outer droop control loop which is also called primary loop used to control on the real power and reactive power for the microgrid, and Inner control loop to regulate the voltage and current in three phase inverter voltage.

The (P-w) and (Q-V) droop control considered a straight technique utilized to solve active and reactive load sharing problem in MG. to developed the droop control method, using Fig.2 to explain the power flow between two nodes can expressions as (1) and (2) [11].

$$p = \frac{V^*}{R^2 + X^2}(V^*R - V_{PCC}R\cos\delta + V_{PCC}X\sin\delta) \quad (1)$$

$$Q = \frac{V^*}{R^2 + X^2}(V^*X - V_{PCC}X\cos\delta - V_{PCC}R\sin\delta) \quad (2)$$

Where V_{PCC} and V^* are the terminal node voltage and magnitudes of the power output node, R represent the resistance of the feeder impedance while X represent the reactance, the phase angle variance between the two nodes represented as δ. For high power flow the value of inductive larger than resistance, may be neglect the resistance. additional, when the δ is typically small, the (1) and (2) can be simplified as:

$$p = \frac{V^*\, V_{PCC}\sin\delta}{X} \quad (3)$$

$$Q = \frac{V^*}{X}(V^* - V_{PCC}) = \frac{V^*}{X}\Delta V \quad (4)$$

Therefore, the output active power is relative to δ and the active power from every inverter can be controlled by adjusting the inverter output frequency. Also, the reactive power is proportional to ΔV and the inverter reactive power can be adjusted by varying the inverter output voltage value.

The straightforward idea of droop control, if the power output of a inverter exceeds the set point value, the power output will be reduced by the droop control characteristics (P-w) and (Q-V), which can be statement as:

$$w = w^* - m\,(p_m - p^*) \quad (5)$$

$$V = V^* - n\,(Q_m - Q^*) \quad (6)$$

Where p^* and Q^* are the set point real and reactive power outputs that the DG can supply; w^* and V^* represented frequency and the root mean square value of the nominal voltage, respectively; p_m and Q_m represented the output measurement for real and reactive power of the DG, respectively; w and V represented the output reference frequency and voltage value, respectively; m and n represented the relative angular frequency and the voltage drooping coefficients, respectively. These coefficients are selected as a deviation in frequency and voltage divided by set point active and reactive power, respectively.

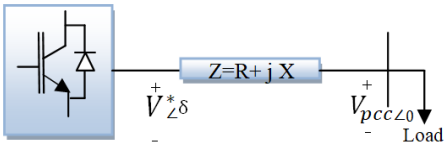

Fig. 2 Equivalent Circuit MG in Islanded Mode

In this paper, the structure of each DG shown in Fig.3, V_{DC} represented the DC prime mover operating as input for three

phase voltage source inverter, where L_f and C_f represented the filter inductor and filter capacitor, respectively. v represented the capacitor voltage while i is the inductor current.

Inner control loop identified as low-level current and voltage compensators. This loop consists of a filter inductor current control loop, a filter capacitor voltage control loop also used, and maintains feed-forward compensators and the feedback together with the linear control loop. The Clark and park transformation (ABC-dq0) which be used in this loop.

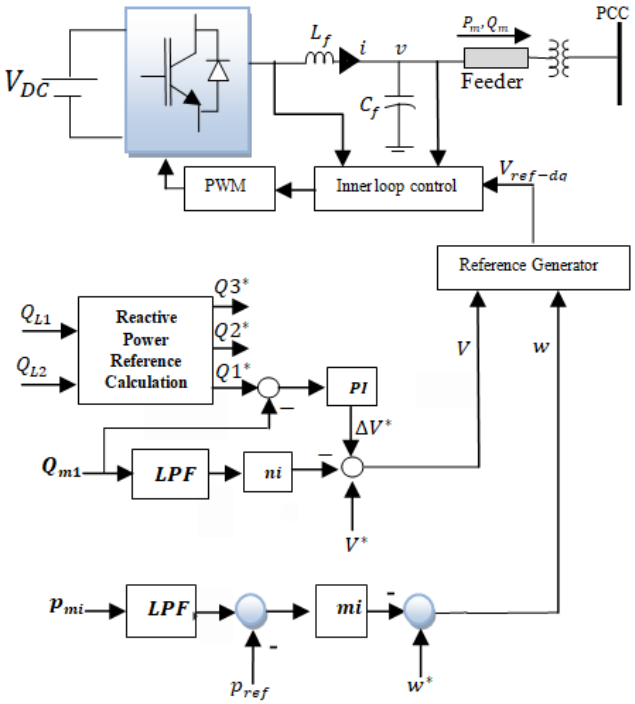

Fig. 3 local controls and structure of a DG unit

III. POWER SHARING STRATEGY

Completing equivalent reactive power sharing for islanded system among the DG that are linked to the MG is a difficult job. When dependent on only local voltage and current information the inverters cannot compensate for mismatches in their reactive power productions, since the working parameters of the other DG are unidentified. To improve the work of the DG and complete equivalent sharing of the reactive power request, must be made the MGCC to adjust the reactive power provided by every DG connected to the MG.

Every of the loads delivers information to the MGCC related of the reactive power distributed to the microgrid (Q_{L1} and Q_{L2}). The MGCC than determines the quantity of reactive power that every DG must be provide and adjusts the reactive power of every DG through an external loop as illustrate in Fig.3.

To allow good sharing of the reactive power, each inverter should send the droop gain (n) to the MGCC. This operation achieved through the setup time only i.e. when the DG is linked to the MG for the first time. The reactive power request for each DG can be determined by:

$$Q_x^* = \frac{Q_{load}}{n_x \sum_{i=1}^{3} \frac{1}{n_i}} \qquad (7)$$

where Q_{load} is the reactive power consumed by all the loads, the droop gain of inverter x represented by n_x, $\sum_{i=1}^{3} \frac{1}{n_i}$ is the summation for all droop gains of the DG connected with MG, and Q_x^* is the reactive power request namely required to be provided by inverter X.

The MGCC adjusts the reactive power of each inverter by using PI controllers. PI controllers in this paper, deliver an extra modification in voltage production which additional to the droop control output (ΔV^*).

IV. SIMULATION RESULTS

In this paper, the case study simulated with program PSCAD/EMTDC, there are three sequence of actions with each lasting 4 seconds. Also, The MGCC was assumed to adjust the voltage reference starting from the beginning of the simulation. In this paper, two case study discussed: the first case, the rating of the three DG units have same rating with different feeder impedance, while another case discussed the rating of the three DG units with different ratings.

A. *First Case*

At beginning, the three DGs were operated together with load 1, while the load 2 were off. Loads were shared between the inverter's unit for both real and reactive power load sharing according to the droop control and the equation (7). Reactive power when the DG in the same rating was shared in the same ratio. Additionally, reference points for voltage inverter output for the droop controllers were determined as previous discussed and transmitted to the every DGs by the MGCC.

The rating of each DG in this case (0.2 MVA) while the load 1 represented the fixed load with (0.27 MW, 0.135 MVAR). At 4 seconds simulation time, the load 2 was turned on with (0.135 MW, 0.045 MVAR). Also, the real and reactive power was shared according to droop control and the equation (7). At 8 seconds, load 2 increased to (0.27 MW, 0.09 MVAR). Table 1 explained the parameters used for both MG and DG while the results for real and reactive powers, frequency, and voltage inverter output are shown in Fig. 4 and Fig. 5. Examining the plots in Figs. 4 (a) and (b), notice that the active and the reactive power was shared accurately.

TABLE. 1
MG and DG parameters

Description	parameter	value
Rating of each DG system	MVA	0.2
Nominal voltage	V_o	480 V (L-L)
Nominal Frequency	w_o	377 rad/s
Input DC voltage	V_{DC}	850 V
Feeder 1 impedance	R + J X (Ω)	1.1 + j 0.434
Feeder 2 impedance	R + J X (Ω)	1.0 + j 0.563
Feeder 3 impedance	R + J X (Ω)	1.2 + j 0.372

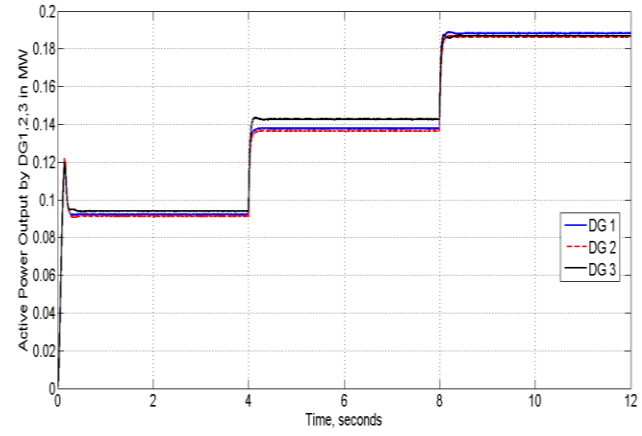

(a)

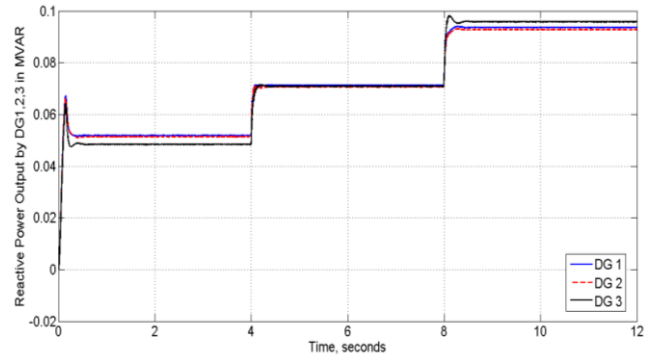

(b)

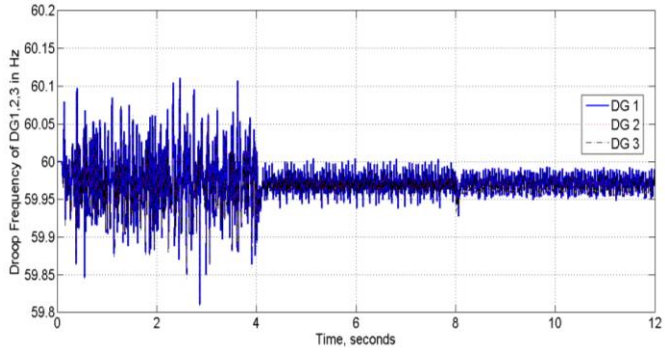

(c)

Fig. 4 Output of (a) Real power (b) The reactive power (c) drop frequency for three DG

We note that at the beginning of the simulation, the transient will be occurring but quickly removed with less than (0.03 sec.) by controlling ability for each of the real and reactive power. In this paper, the droop frequency selected as 0.25 Hz and the result as shown in Fig. 4 (c). Also, it can be seen that the DG3 differs slightly from the DG1 and DG2 because the distance between them.

Fig. (5) shown that the minimum drop voltage occurs when any new load appears in the MG and then this drop quickly removed.

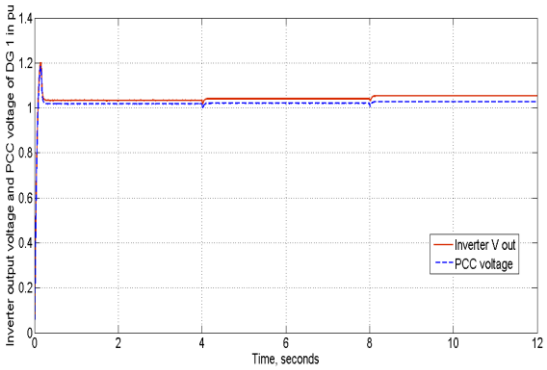

(a)

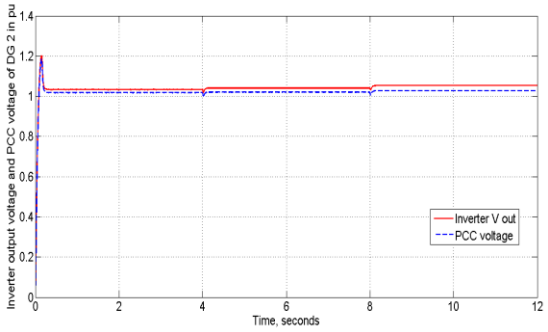

(b)

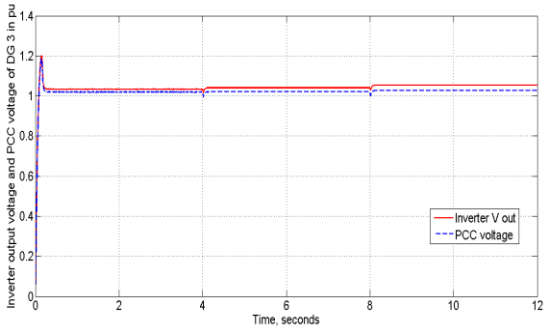

(c)

Fig. 5 Inverter output voltage for (a) DG1 (b) DG2 (c) DG3

B. Second Case

In this case, the DG operating with different rating (0.3 MVA for DG1, 0.2 MVA for DG2, and 0.1 MVA for DG3). The active and reactive power sharing the load according to rating of each DG with ratio (3:2:1).

At beginning, the three DGs were operated together with load 1, while the load 2 were off. Loads were shared between the inverter's unit for both real and reactive power load sharing according to the droop control and the equation (7).

Reactive power was shared according to ratio. The reference points for voltage inverter output for the droop controllers were determined as previous discussed and transmitted to the DGs by the MGCC. Remaining parameters used the same parameters in Table 1. The results for real and reactive powers, frequency, voltage inverter output, and current inverter output are shown in Fig. 6, Fig. 7, Fig. 8, and Fig. 9.

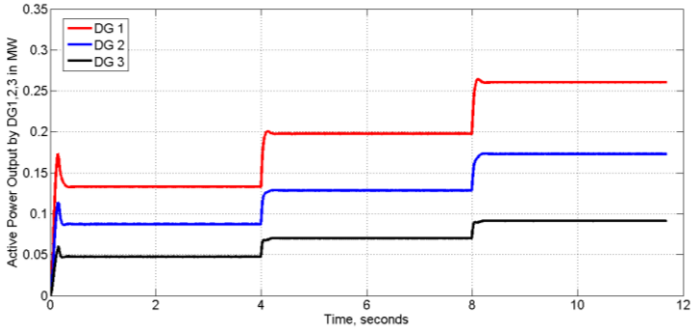

(a)

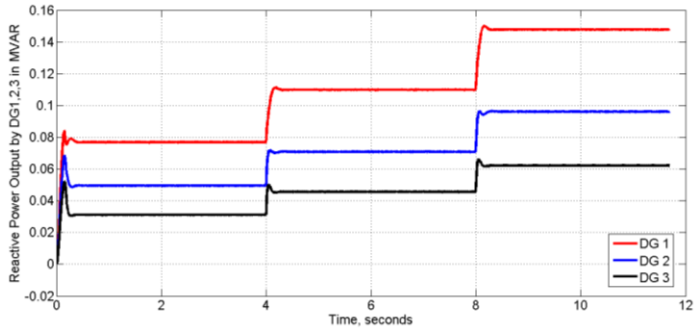

(b)

Fig. 6 Output of (a) Real power (b) The reactive power

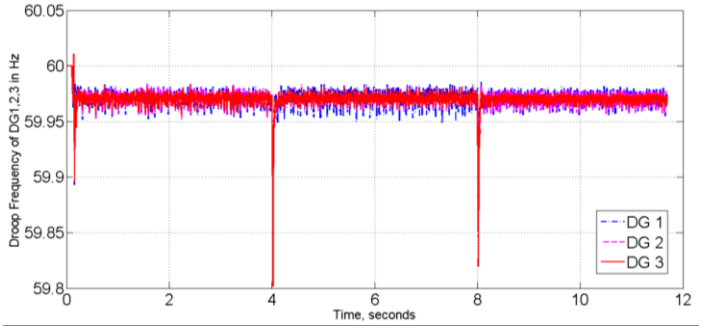

(a)

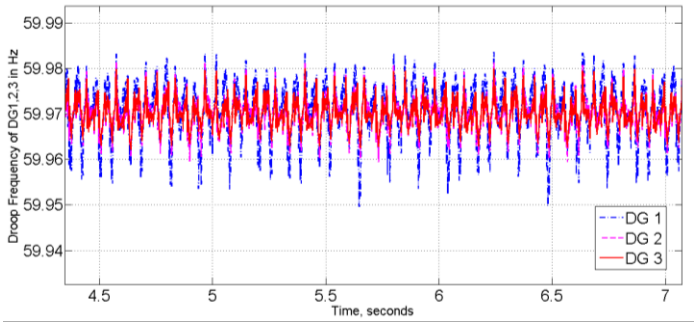

(b)

Fig. 7 Output of (a) drop frequency for three DG (b) Zoom the droop frequency

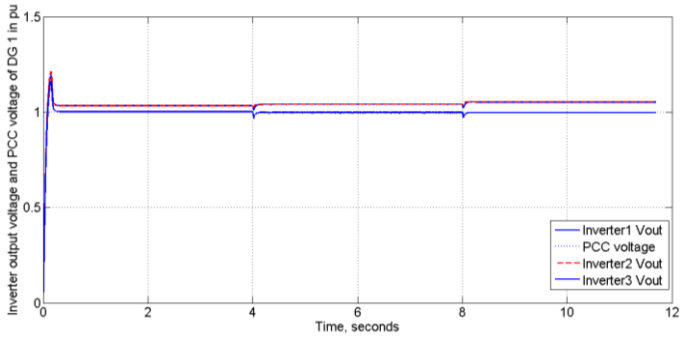

Fig. 8 Inverter output voltage for DG1, DG2, and DG3

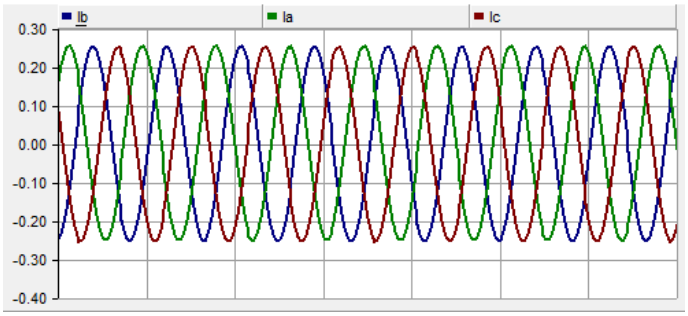

Fig. 9 Inverter output current for DG1

V. CONCLUSION

In this work, an enhanced MG reactive power load sharing strategy was proposed for parallel DGs in an islanded microgrid. This strategy uses reactive power load information to help calculated power sharing according to power rating for each DG then compared with reactive measurement, the error of reactive power load sharing is compensated by utlizing PI controller. The output of PI controller used to adjust the voltage reference output from each inverter.

Modelling of MG has been established by using PSCAD/EMTDC. The simulated MG consist of three DG units with two linear loads. DG operating with the equal power rating and in this case DG units segment the load equally. Also, DG operating with the different power rating and in this case DG units share the load according to rating for each DG. In two case, the feeder impedance different from each DG to PCC.

REFERENCES

[1] Wang, Keyou et al. "Decentralized Power Sharing Control for Parallel-Connected Inverters in Islanded Single-Phase Micro-Grids." *IEEE Transactions on Smart Grid* 9 (2018): 6721-6730.

[2] Rezaee, Saeed et al. "Accurate and fast power sharing among inverters in AC microgrids with constant power loads." *2017 IEEE 18th Workshop on Control and Modeling for Power Electronics (COMPEL)* (2017): 1-8.

[3] Yang, Jian et al. "A Distributed Cooperative Control Algorithm for Optimal Power Flow and Voltage Regulation in DC Power System." *IEEE Transactions on Power Delivery* 35 (2020): 892-903.

[4] Guerrero, Josep M. et al. "Advanced Control Architectures for Intelligent Microgrids—Part I: Decentralized and Hierarchical Control." *IEEE Transactions on Industrial Electronics* 60 (2013): 1254-1262.
[5] Afshar, Zakaria et al. "A Novel Accurate Power Sharing Method Versus Droop Control Include Autonomous Microgrids With Critical Loads." *IEEE Access* 7 (2019): 89466-89474.
[6] Milczarek, Adam et al. "Reactive Power Management in Islanded Microgrid—Proportional Power Sharing in Hierarchical Droop Control." *IEEE Transactions on Smart Grid* 6 (2015): 1631-1638.
[7] Guo, Qian et al. "Secondary Voltage Control for Reactive Power Sharing in an Islanded Microgrid." (2016).
[8] Chandorkar, M. C. et al. "Control of parallel connected inverters in stand-alone AC supply systems." *Conference Record of the 1991 IEEE Industry Applications Society Annual Meeting* (1991): 1003-1009 vol.1.
[9] Yao, Wei et al. "Design and Analysis of the Droop Control Method for Parallel Inverters Considering the Impact of the Complex Impedance on the Power Sharing." *IEEE Transactions on Industrial Electronics* 58 (2011): 576-588.
[10] Tuladhar, Anil et al. "Control of parallel inverters in distributed AC power systems with consideration of line impedance effect." (2000).
[11] Li, Yun Wei and Ching-Nan Kao. "An Accurate Power Control Strategy for Power-Electronics-Interfaced Distributed Generation Units Operating in a Low-Voltage Multibus Microgrid." *IEEE Transactions on Power Electronics* 24 (2009): 2977-2988.
[12] Zhong, Qing-Chang. "Robust Droop Controller for Accurate Proportional Load Sharing Among Inverters Operated in Parallel." *IEEE Transactions on Industrial Electronics* 60 (2013): 1281-1290.
[13] He, Jinwei et al. "An islanding microgrid reactive power sharing scheme enhanced by programmed virtual impedances." *2012 3rd IEEE International Symposium on Power Electronics for Distributed Generation Systems (PEDG)* (2012): 229-235.
[14] Wu, Dan et al. "Autonomous active and reactive power distribution strategy in islanded microgrids." *2014 IEEE Applied Power Electronics Conference and Exposition - APEC 2014* (2014): 2126-2131.
[15] Simpson-Porco, John W. et al. "Secondary Frequency and Voltage Control of Islanded Microgrids via Distributed Averaging." *IEEE Transactions on Industrial Electronics* 62 (2015): 7025-7038.
[16] Shafiee, Qobad et al. "Distributed Secondary Control for Islanded Microgrids—A Novel Approach." *IEEE Transactions on Power Electronics* 29 (2014): 1018-1031.
[17] Zhu, Yixin et al. "Accurate power sharing strategy for complex microgrid based on droop control method." *2013 IEEE ECCE Asia Downunder* (2013): 344-350.
[18] Bassey, Ogbonnaya et al. "Active and Reactive Power Sharing in Inverter Based Droop-Controlled Microgrids." *2019 IEEE Power & Energy Society General Meeting (PESGM)* (2019): 1-5.
[19] Micallef, Alexander et al. "Secondary control for reactive power sharing in droop-controlled islanded microgrids." *2012 IEEE International Symposium on Industrial Electronics* (2012): 1627-1633.
[20] PES Test Feeder [Online]. Available: http://sites.ieee.org/pes-testfeeders/resources/

Open Access
Iraqi Journal for Electrical and Electronic Engineering
Conference Article

Novel Memory Structures in QCA Nano Technology

Ali H. Majeed*[1,2], Esam Alkaldy[2], Mohd S. Zainal[1] and Danial MD. Nor[1]
[1]FKEE, UTHM, Johor, Malaysia
[2]Electrical Department, Faculty of Engineering, University of Kufa, Kufa, Iraq

Correspondence
*Ali H. Majeed
Electrical Department, Faculty of Engineering,
University of Kufa, Kufa, Iraq
Email: alih.alasady@uokufa.edu.iq

Abstract
Quantum-dot Cellular Automata (QCA) is a new emerging technology for designing electronic circuits in nanoscale. QCA technology comes to overcome the CMOS limitation and to be a good alternative as it can work in ultra-high-speed. QCA brought researchers attention due to many features such as low power consumption, small feature size in addition to high frequency. Designing circuits in QCA technology with minimum costs such as cells count and the area is very important. This paper presents novel structures of D-latch and D-Flip Flop with the lower area and cell count. The proposed Flip-Flop has SET and RESET ability. The proposed latch and Flip-Flop have lower complexity compared with counterparts in terms of cell counts by 32% and 26% respectively. The proposed circuits are designed and simulated in QCADesigner software.

KEYWORDS: QCA technology, D Flip-Flop, Memory unit, Nanotechnology.

I. INTRODUCTION

The limitations in CMOS technology such as high lithography, short channel effects, and power consumption encouraged scientists to think about alternatives. Many nanotechnologies were emerged to overcomes these limitations such as Single Electron Transistor [1, 2], Carbon Nanotube Field-Effect Transistor [3-7], FinFET [8-10] and Quantum-dot Cellular Automata (QCA). QCA technology was introduced for the first time by Lent et al in 1993 [11] and it is reliability was studied in [12]. QCA building block is a square shape that has four dots and two electrons. This technology is reviewed in details by [13, 14] QCA depends on the principle of electron's repulsion [15]. The memory unit is very important in all electronic circuits. Designing efficient memory units in QCA technology still in the competition. The researchers in QCA technology looking for finding a good circuit with minimum complexity (cells and area). This paper introduces a novel latch with minimum complexity then uses this latch for designing an optimum form of D Flip-Flop with set/reset ability.

II. BACKGROUND

The basic QCA technology block is a quantum cell. This cell consists of four holes (dots) in addition to a couple of electrons. The electrons configuration inside the cell gives it a certain polarization. Only two configurations can be formed by a QCA cell so, it can represent the binary numbers. Cell with polarized -1 represents binary 0 and the binary 1 can be represented by a cell with polarized +1 as shown in Figure 1.

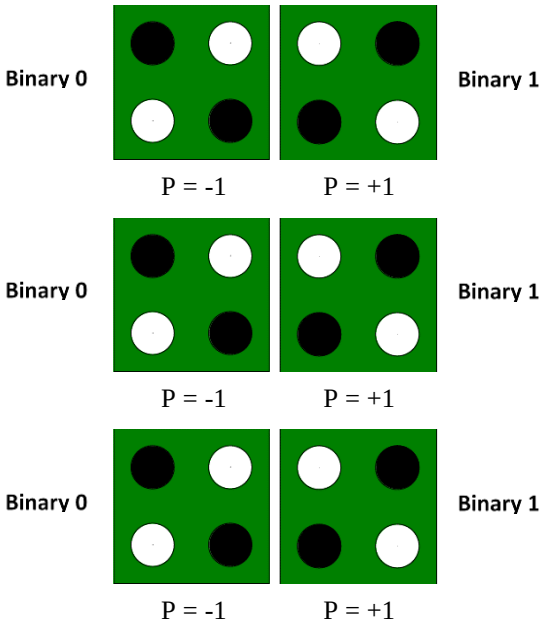

Fig.1: QCA cell configuration

The dominant gate in QCA technology is the majority gate where AND/OR gates can be built using this gate. Majority gate constructed with 5 cells as illustrated in Figure 2. The

basic gates (AND/OR) designs shown in Figure 3. Multi-input majority gate are also available as in [16].
In QCA, there is also another important block beside the majority gate called an inverter. The two main structures of the inverter depicted in Figure 4.

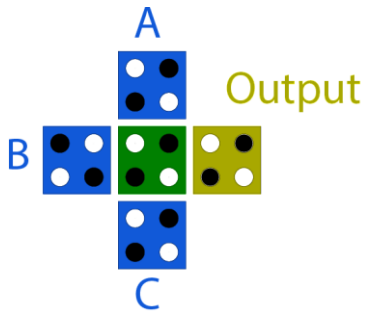

Fig. 2: QCA majority gate

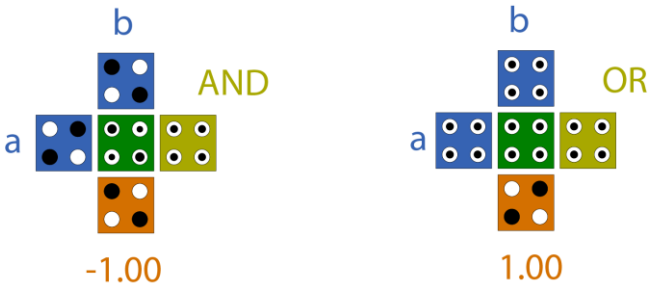

Fig. 3: The general form of AND and OR gates

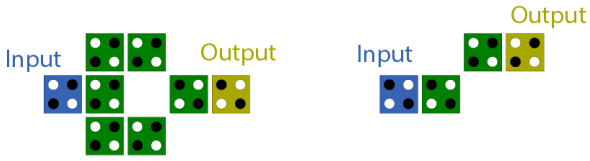

Fig. 4: Two main structures of QCA-inverter

Binary wire in QCA technology can be constructed by a set of cells put beside each other as shown in Figure 5.

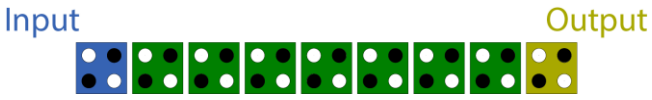

Fig. 5: QCA wire

Generally, QCA circuits need a clock signal for many reasons such as synchronization and control of the direction of flowing signals [17, 18]. The large circuits in QCA can be divided into four zones each zone has four clock phases (switch, hold, release and relax) as shown in Figure 6 to ensure adiabatic switching and keep the circuit close to the ground state. The clock signal controls the barriers between dots to allow or prevent the flowing of electrons. QCA cells give true value during hold state only. Therefore, in this phase, the cells will act as the drive to the adjacent cells.

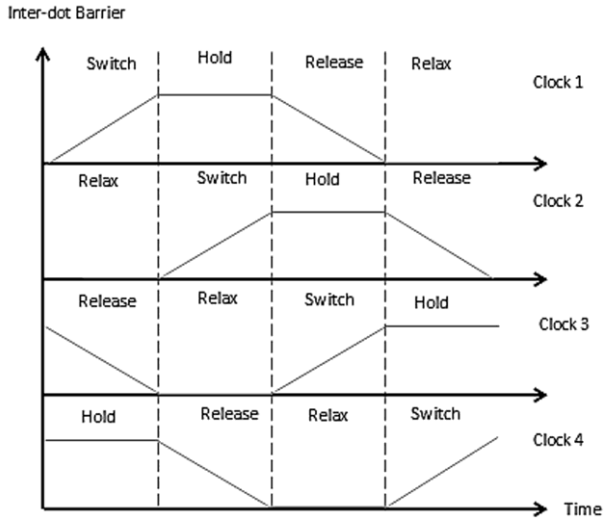

Fig. 6: QCA-clock signal

III. Related Work

In QCA literature, the counters and flip-flops are discussed a lot [19]. Many structures of D-lathes and flip-flops were introduced in QCA technology. All of them aiming to find an optimum structure in terms of area and cell counts. Some best relevant of such circuits are shown in Figure 7. In Figure 7(a) proposed by [20], the authors proposed D flip-flop without set/reset ability where D flip-flop having the ability to set and reset the output is proposed in [21] as shown in Figure 7(b). In Figure 7(c), the design reported in [22] is shown with better performance.

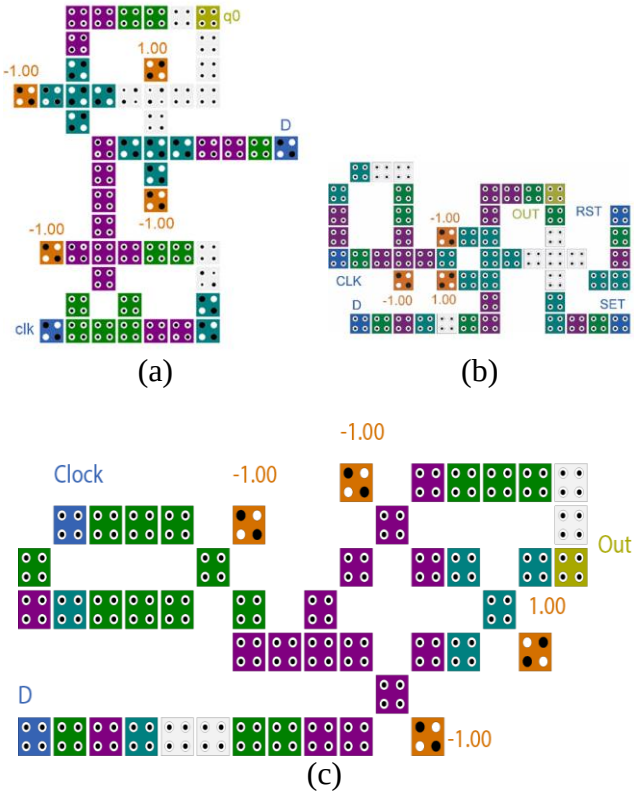

Fig. 9: D flip-flop proposed (a) in [20] (b) in [21] (c) in [22]

IV. Proposed Design

In this section, a novel QCA-design of D latch will be proposed. The block diagram that will be followed to design the latch is depicted in Figure 8. Although many multiplexers are presented in QCA literature discussed in [23], the multiplexer structure that will be utilized in this work is proposed in [24]. So, the proposed D latch is illustrated in Figure 9. From the proposed D latch, D Flip-flop in both positive and negative edge triggers are constructed by adding small circuit called level to edge converter as shown in Figure 10.

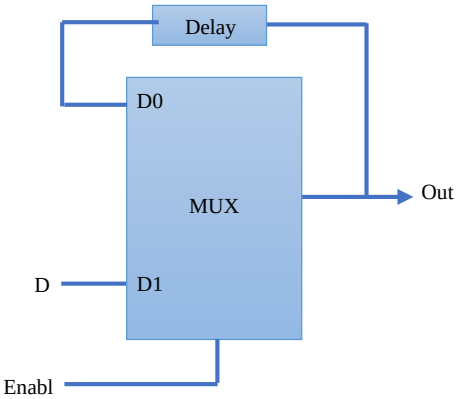

Fig. 8: D flip-flop Block diagram

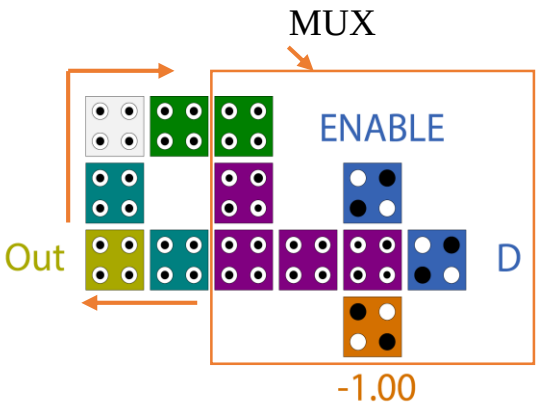

Fig. 9: Proposed D latch

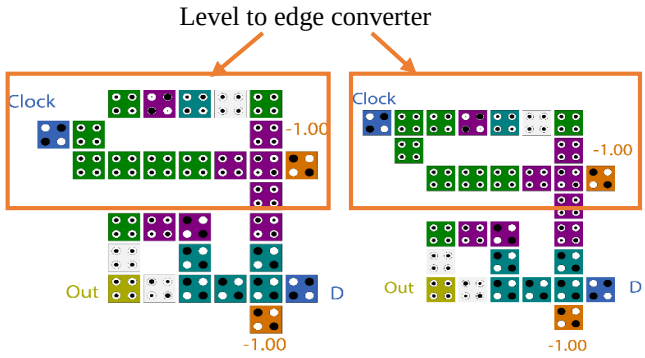

(a) (b)

Fig. 10: Proposed D Flip-Flop (a) +Ve edge trigger (b) -Ve edger trigger

From designs shown in Figure 10, it can add set and reset feature by adding majority gate at the output. The proposed Flip-Flop with set/reset ability will be as depicted in Figure 11. The functionality table of the proposed flip-flop is detailed in Table 1. The proposed structures in this work are very efficient compared to the early reported ones in terms of number of cells and layout area, and adopting them to larger circuits will cause significant improvements.

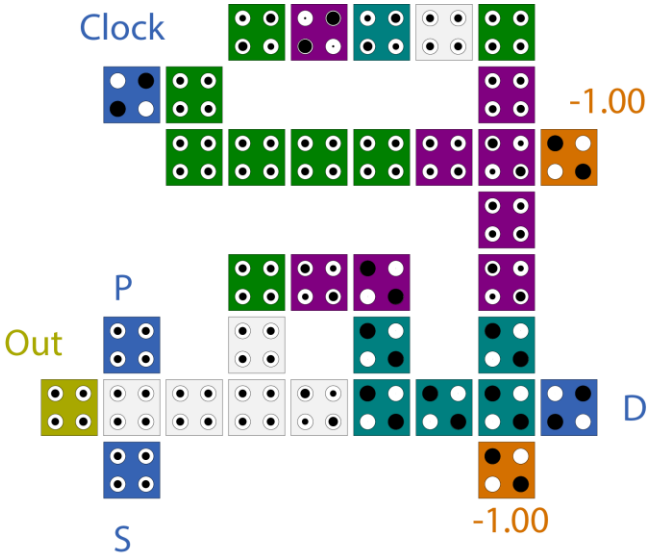

Fig. 11: Proposed D Flip-Flop (+Ve) with Set/reset ability

TABLE 1:
Proposed D Flip-Flop (+Ve) functionality table

P	S	Clock transition	D	Out(t+1)
0	0	x	x	0 (reset)
1	1	x	x	1 (set)
0	1	0 to 1	0	0
1	0			
0	1	0 to 1	1	1
1	0			
0	1	1 to 0	X	Out
1	0			

V. Simulation Result and Comparison

This section will explain the simulation result of the proposed circuits using QCADesigner software [25]. The output waveforms prove that the proposed circuits are free of error as illustrated in Figure 12. The proposed D latch and D Flip-Flop are compared with counterparts as detailed in Tables 2 and 3. It's clear from Table 2 that the proposed D Latch has a better structure than the best reported in terms of cell count of about 32 %, and in terms of geometry and layout the proposed design is optimized and this improves the circuit area by 50 %. The comparison results in Table 3 for the D-FF are also encouraging. Although the improvement in cell count is around 26 %, the geometry optimization of the proposed structure is very effective and caused circuit area improvement of 57 %. The major cause of the improvements in the proposed structures is the used Multiplexer structure.

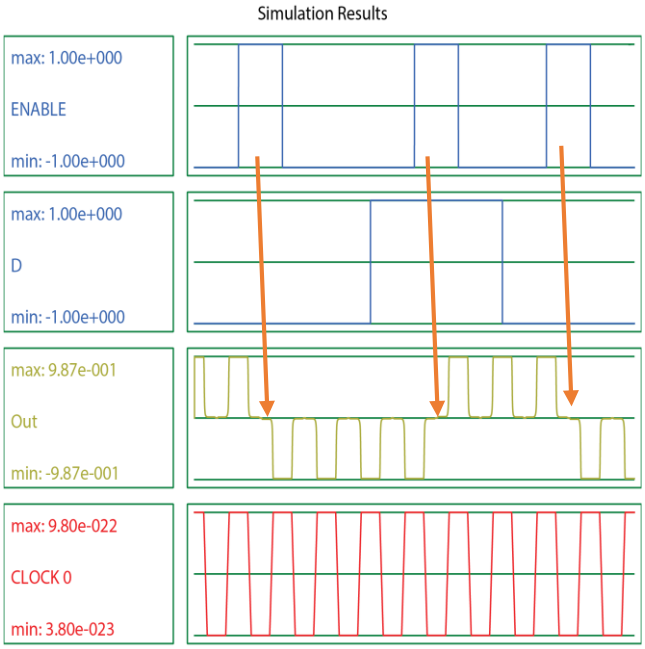

Fig. 12: Output waveforms of the proposed D-latch

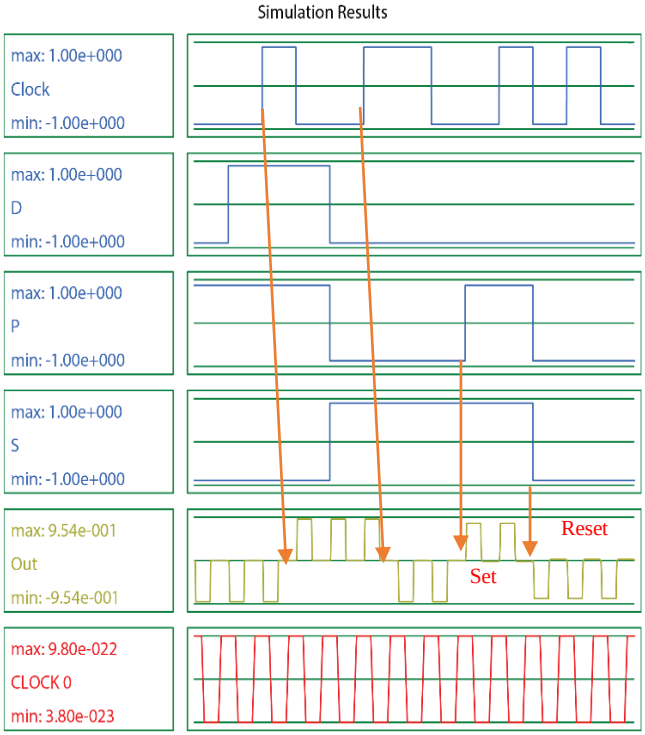

(a)

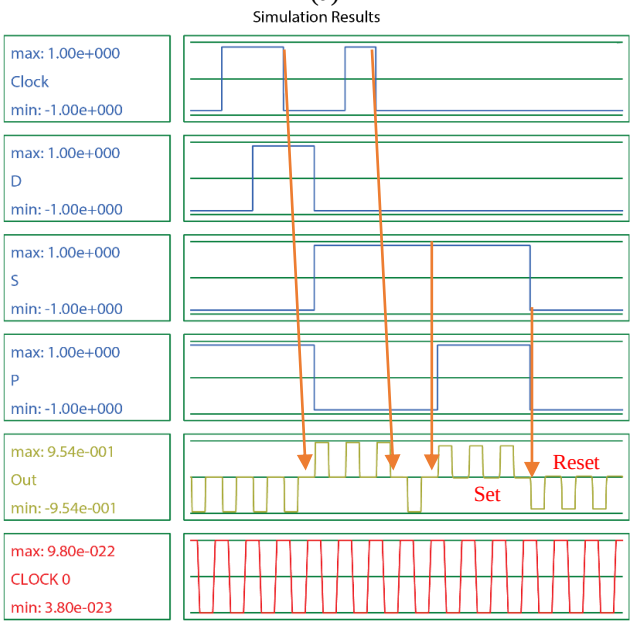

(b)

Fig. 13: Output waveforms of the proposed D-FF with set/reset (a) positive edge (b) negative edge

TABLE 2:
Proposed D latch comparison table

Design	Area (μm2)	Cell count	Clock phases
D Latch in [26]	0.05	48	4
D Latch in [27]	0.06	43	4
D Latch in [28]	0.02	28	2
D Latch in [21]	0.02	19	3
Proposed D latch	0.01	13	3

TABLE 3:
Proposed D Flip-Flop comparison table

Design	Area (µm2)	Cell count	Clock phases	S/R ability
D-FF in [29]	0.11	84	11	No
D-FF in [30]	0.06	56	10	No
D-FF in [21]	0.04	53	9	Yes
D-FF in [22]	0.07	47	7	No
Proposed D-FF	0.03	35	8	Yes

VI. Conclusion

This paper presents novel structures of memory units (D latch and D Flip-Flop) in QCA technology. The proposed circuits are in optimal form in terms of area and cell counts. The proposed flip flop has the ability to set the output and reset it. The proposed circuits have more efficient than previously published in almost all metrics as explained in comparison tables. The output waveforms indicate that the proposed structures are free of error.

References

[1] M. H. A. Khan, "Single-Electron Transistor Based Implementation of NOT, Feynman, and Toffoli Gates," in *2015 IEEE International Symposium on Multiple-Valued Logic*, 2015, pp. 66-71.

[2] S. Tannu and A. Sharma, *Low power random number generator using single electron transistor*, 2012.

[3] M. Reshadinezhad, M. Moaiyeri, and K. Navi, "An energy-efficient full adder cell using CNFET technology," *IEICE Transactions on Electronics*, vol. E95.C, pp. 744-751, 04/01 2012.

[4] S. A. Ebrahimi and P. Keshavarzian, "Fast low-power full-adders based on bridge style minority function and multiplexer for nanoscale," *International Journal of Electronics*, vol. 100, pp. 727-745, 2013/06/01 2013.

[5] Y. Safaei Mehrabani and M. Eshghi, "Noise and Process Variation Tolerant, Low-Power, High-Speed, and Low-Energy Full Adders in CNFET Technology," *IEEE Transactions on Very Large Scale Integration Systems (TVLSI), Accepted*, vol. 24, 02/01 2016.

[6] E. Alkaldy, K. Navi, F. Sharifi, and M. H. Moaiyeri, "An Ultra High-Speed (4; 2) Compressor with a New Design Approach for Nanotechnology Based on the Multi-Input Majority Function," *Journal of Computational and Theoretical Nanoscience*, vol. 11, pp. 1691-1696, // 2014.

[7] E. Alkaldy, K. Navi, and F. Sharifi, "A Novel Design Approach for Multi-input XOR Gate Using Multi-input Majority Function," *Arabian Journal for Science and Engineering*, vol. 39, pp. 7923-7932, 2014/11/01 2014.

[8] D. Hisamoto, L. Wen-Chin, J. Kedzierski, H. Takeuchi, K. Asano, C. Kuo, *et al.*, "FinFET-a self-aligned double-gate MOSFET scalable to 20 nm," *IEEE Transactions on Electron Devices*, vol. 47, pp. 2320-2325, 2000.

[9] H. Xuejue, L. Wen-Chin, C. Kuo, D. Hisamoto, C. Leland, J. Kedzierski, *et al.*, "Sub-50 nm P-channel FinFET," *IEEE Transactions on Electron Devices*, vol. 48, pp. 880-886, 2001.

[10] F. Sabetzadeh, M. H. Moaiyeri, and M. Ahmadinejad, "A Majority-Based Imprecise Multiplier for Ultra-Efficient Approximate Image Multiplication," *IEEE Transactions on Circuits and Systems I: Regular Papers*, pp. 1-9, 2019.

[11] C. S. Lent et al, "Quantum cellular automata," *Nanotechnology*, vol. 4, pp. 49-57, 1993.

[12] E. Alkaldy and K. Navi, "Reliability Study of Single Stage Multi-Input Majority Function for QCA," *International Journal of Computer Applications*, vol. 83, 2, 2013.

[13] A. H. Majeed, M. S. B. Zainal, and E. Alkaldy, "Quantum-dot Cellular Automata: Review Paper," *INTERNATIONAL JOURNAL OF INTEGRATED ENGINEERING*, vol. 11, 2019.

[14] U. Mehta and V. Dhare, *Quantum-dot Cellular Automata (QCA): A Survey*, 2017.

[15] A. Sadoghifar and S. R. Heikalabad, "A Content-Addressable Memory structure using quantum cells in nanotechnology with energy dissipation analysis," *Physica B: Condensed Matter*, vol. 537, pp. 202-206, 2018.

[16] Ali H. Majeed, E. AlKaldy, MSB Zainal, and Danial BMD Nor, "A new 5-input Majority Gate Without Adjacent Inputs Crosstalk Effect in QCA Technology," *Indonesian Journal of Electrical Engineering and Computer Science*, vol. 14, pp. 1159-1164, 2019.

[17] Y. Zhang, G. Xie, and J. Han, "A robust wire crossing design for thermostability and fault tolerance in quantum–dot cellular automata," *Microprocessors and Microsystems*, vol. 74, p. 103033, 2020/04/01/ 2020.

[18] A. H. Majeed, M. S. B. Zainal, E. Alkaldy, and D. M. Nor, "Full Adder Circuit Design with Novel Lower Complexity XOR Gate in QCA Technology," *Transactions on Electrical and Electronic Materials*, 2020/01/07 2020.

[19] A. H. Majeed, E. Alkaldy, M. S. bin Zainal, and D. Bin Md Nor, "Synchronous Counter Design Using Novel Level Sensitive T-FF in QCA Technology," *Journal of Low Power Electronics and Applications*, vol. 9, 2019.

[20] Z. Amirzadeh and M. Gholami, "Counters Designs with Minimum Number of Cells and Area in the Quantum-Dot Cellular Automata Technology," *International Journal of Theoretical Physics*, vol. 58, pp. 1758-1775, 2019/06/01 2019.

[21] M. Gholamnia Roshan and M. Gholami, "Novel D Latches and D Flip-Flops with Set and Reset Ability in QCA Nanotechnology Using Minimum Cells and Area," *International Journal of Theoretical Physics*, vol. 57, pp. 3223-3241, 2018/10/01 2018.

[22] T. N. Sasamal, A. K. Singh, and U. Ghanekar, "Design of QCA-Based D Flip Flop and Memory Cell Using Rotated Majority Gate," in *Smart Innovations in Communication and Computational Sciences*, Singapore, 2019, pp. 233-247.

[23] E. Alkaldy, A. H. Majeed, M. S. bin Zainal, and D. Bin Md Nor, "Optimum multiplexer design in quantum-dot cellular automata," *Indonesian Journal of Electrical Engineering and Computer Science*, vol. 17, pp. 148-155, 2020.

[24] H. Majeed Ali, E. Alkaldy, S. Zainal Mohd, K. Navi, and D. Nor, "Optimal design of RAM cell using novel 2:1 multiplexer in QCA technology," *Circuit World*, vol. 46, pp. 147-158, 2019.
[25] K. Walus, T. J. Dysart, G. A. Jullien, and R. A. Budiman, "QCADesigner: a rapid design and Simulation tool for quantum-dot cellular automata," *IEEE Transactions on Nanotechnology*, vol. 3, pp. 26-31, 2004.
[26] S. Hashemi and K. Navi, "New robust QCA D flip flop and memory structures," *Microelectronics Journal*, vol. 43, pp. 929-940, 2012.
[27] M. A. Dehkordi and M. Sadeghi, "A new approach to design D-ff in QCA technology," in *Proceedings of 2012 2nd International Conference on Computer Science and Network Technology*, 2012, pp. 2245-2248.
[28] M. M. Abutaleb, "Robust and efficient quantum-dot cellular automata synchronous counters," *Microelectronics Journal*, vol. 61, pp. 6-14, 2017/03/01/ 2017.
[29] P. Dutta and D. Mukhopadhyay, "New Architecture for Flip Flops Using Quantum-Dot Cellular Automata," in *ICT and Critical Infrastructure: Proceedings of the 48th Annual Convention of Computer Society of India- Vol II*, Cham, 2014, pp. 707-714.
[30] R. Binaei and M. Gholami, "Design of novel D flip-flops with set and reset abilities in quantum-dot cellular automata nanotechnology," *Computers & Electrical Engineering*, vol. 74, pp. 259-272, 03/01 2019.

DOI: 10.37917/ijeee.sceeer.3rd.18 *(15-16) June 2020*

Open Access

Iraqi Journal for Electrical and Electronic Engineering
Conference Article

Automatic Storage and Retrieval System using the Optimal Path Algorithm

Hanan M. Hameed*, Abdulmuttalib Turky Rashid, Kharia A. Al Amry
Electrical Engineering Department, University of Basrah, Basrah, Iraq.

Correspondence
* Hanan M. Hameed
Electrical Engineering Department,
University of Basrah, Basrah, Iraq.
Email: ranamajeed90@gmail.com

Abstract
The demand for application of mobile robots in performing boring and extensive tasks are increasing rapidly due to unavailability of human workforce. Navigation by humans within the warehouse is one among such repetitive and exhaustive task. Autonomous navigation of mobile robots for picking and dropping the shelves within the warehouse will save time and money for the warehousing business. Proposing an optimization model for automated storage and retrieval systems by the goals of its planning is investigated to minimize travel time in multi-robot systems. This paper deals with designing a system for storing and retrieving a group of materials within an environment arranged in rows and columns. Its intersections represent storage locations. The title of any subject is indicated by the row number and the column in it. A method was proposed to store and retrieve a set of requests (materials) using a number of robots as well as one receiving and delivery port. Several simulation results are tested to show this improvement in length of path and time of arrival.
KEYWORDS: Multi-mobile robot, AS/RS system, static environment.

I. INTRODUCTION

Warehousing is the function involving storage and retrieval of raw materials, components, and finished goods as well as shipments of goods. However, auto-store is a new way of thinking when it comes to warehousing where main purpose for the product is to improve the quality of the internal logistics. In auto-store, the heart of the systems is an automatic storage system operated by robots. This is the key product under the Logistics branch. It can reduce the need of labor, maximize the use of storage and run 24 hours per day, as well as being a green energy product when it comes to distribution[1]. Consumers demand faster delivery, access to labor increasingly difficult, and increased competition. So, Goods to Person (G2P) robotics is one solution where (G2P) robotics can be classified into three types such as Pick Assistant with Autonomous Mobile Robot (PA-AMR's), Autonomous Mobile Robot (AMR) and Automated Storage and Retrieval System (ASRS). A comparison between them showing in the following table 1 [2, 3]. Robotics & automation is rapidly becoming a key success factor in ecommerce and is about to make a very large impact on the world of logistics. From AMRs and AS/RS to track & trace technologies and advanced supply chain software, it is a game changer enabling increasingly speedy, safe and error-free distribution, shorter time to market and ultimately lower costs to businesses and consumers. Robots can work in "harsher" conditions than humans, requiring less light and heating, and they also require less energy than traditional trucks [4, 5]. Multi Robot System MRS can be characterized as a field of research that investigates the use of multiple robots operating in the same environment.

TABLE 1
COMPARISON BETWEEN PA-AMR'S, AMR AND ASRS SYSTEMS.

PA-AMR	AMR	ASRS
• Pick Assistant with AMR base, often including Lidar. ▪Human collaborative robots	• Autonomous Mobile Robot, (incl. AGV's using fiducials) • 'Dark warehouse.	• Automated Storage and Retrieval System. • Dark warehouse.
• Deployed in existing warehouse infrastructure • Augmented picking. • Highest H&S specifications, such as lifting heavy goods, working among humans. • Low pick speed.	•Mainly deployed in existing warehouse infrastructure. • Move pods (shelves) to a pick & pack station. •Flexible & fast changing warehouse/sorting space. • Space efficiencies. • Low-medium pick speed.	• Mainly deployed in new warehouses. • Includes high speed shuttle systems. • Medium to high goods density • Auto Store type warehouse pick speed is low-medium.
Fetch, MIR, VECNA	Swiss log, VECNA, GREY, …	EXOTIC, DEMATIC, OPEX,….

Robotic systems are mobile platforms, equipped with sensors and actuators, able to interact with other similar devices and with the environment in order to perform (simple or complex) tasks [6]. A multi-robot exploration task consists of the locations of n robots and m targets as well as a cost function that specifies the cost of moving between locations. The objective of the multi-robot exploration task is to find an allocation of targets to robots and a path for each robot that visits all targets allocated to it so that the team objective is achieved. In this paper, In this paper, one team objectives is investigated which minimize the sum of the path costs over all robots that leads to minimum time required for each cycle There are a lot of path planning algorithms which give minimization for path and time where going from one point to another is one of the challenges that mobile robots have to face today. The problem of robot navigation deals with finding a path with the shortest distance and hence the shortest time of travel, through a terrain that may be partially or totally defined by a lane, track or just specified by one or more way points between a starting point and ending point even in the presence of stationary or moving obstacles [9, 10]. The multi-robot exploration task is to find an allocation of targets to robots and a path for each robot that visits all targets allocated to it so that the team objective is achieved. In this paper, one team objectives is investigated which minimize the sum of the path costs over all robots that leads to minimum time required for each cycle [7, 8].

Line follower robots can be used in path planning to design the object storage system [11-15]. The performance of the robot can be increased by assuming that the line follower robot moves on a predetermined path [16]. The line follower system has the property to drive the robot properly [17]. Many fields nowadays use follower robot, such as transport building materials and transport luggage which increase the use of this type of system [18].

Efficient navigation of mobile robots defined as a generation of collision-free path and design of control law, which gives the desired path following. A great effort has been made to solve Robot Motion Planning (RMP) problems. Path planning for a mobile robot, which is an important content in the field of intelligent robot research, is typically stated as finding a sequence of state transitions for the robot from its initial state to some desired goal state. The path is optimal if the sum of the transition costs is minimal across all possible sequences through the map [19-22]. There are a lot of path planning algorithms that give minimization for path and time where the going from one point to another is one of challenges that mobile robots have to face today. The problem of robot navigation deals with finding a path with the shortest distance and hence the shortest time of travel, through a terrain that may be partially or totally defined by a lane or track or just specified by one or more way points between a starting point and ending point even in the presence of stationary or moving obstacles [9, 10]. In engineering, there are two different approaches to problem solving: mathematical or heuristic approach. In the mathematical approach, it is more concerned with the solution than with the calculations are feasible for algorithms. In the heuristic approach, the algorithm has to use special knowledge of the problem area. The heuristic approach can use multiple different ways of solving problem from looking from start to finish [23, 24]. Planning the layout of our AS/RS is based on a table of inquiry and the frequencies when manufacturing individual products. Distribution of products during an AS/RS operation depends on factor of inquiry (FOI), product height (PH), storage space usage (SSU) and path to dispatch (PD). Another boundary condition included within any optimization algorithm is that the factor of inquiry may change dynamically during AS/RS operation regarding actual market

requirements. Considering all the parameters resulted in a multi-objective optimization problem.
In this paper, the study investigate one team objectives which minimize the sum of the path costs over all robots that leads to minimum time required for each cycle [25].

The goal of this paper is to provide a simple of low-cost high accuracy AS/RS system, suitable for store and retrieval more than one order using multi-mobile robot. The proposed algorithm is described in section II. Simulations results are explained in Section III. The conclusions discussed finally.

II. Automatic Storage and Retrieval System

This section deals with designing an optimization model for automated storage and retrieval systems by the goals of its planning to minimize travel time in multi-robot systems. This research deals with designing a system for storing and retrieving a group of materials within an environment arranged in rows and columns. Its intersections represent storage locations. The title of any subject is indicated by the row number and the column in it, as shown in Fig. 2. A method was proposed to store and retrieve a set of requests (materials) using a number of robots as well as one receiving and delivery port.

Optimal Path Algorithm

The idea of this algorithm is based on determining the delivery point after each order, firstly, and how far it is from all robots. Second, calculate all possibilities for delivery from each robot and all orders back and forth to the delivery point. All probabilities are calculated using the compatibility algorithm where the total paths to deliver all orders are calculated to deliver all orders and at every possibility for the distribution of orders on robots, the longest path is taken as the worst case for this possibility, then look for the possibility that the worst case is the least possible to represent the best possibility Optimal paths to complete the task in the shortest time. The steps for implementing this algorithm are as follows:

Step1: Estimation the distance between the orders and the received point: The coordinate axis of the order and the received point are shown in Fig. 2. The distance between the order i and the received point (Fig. 3 is computed by using the following equation:

$$Disrcv(i) = Abs(Xor(i) - Xrec) + Abs(Yor(i) - Yrec) \quad (1)$$

Step2: Estimation the distance between the orders and all the robots: The distance between the order i and the robot j (Fig. 4 is computed by using the following equation:

$$Disrbt(I,j) = Abs(Xor(i) - Xrob(j) + Abs(Yor(i) - Yrob(j)) \quad (2)$$

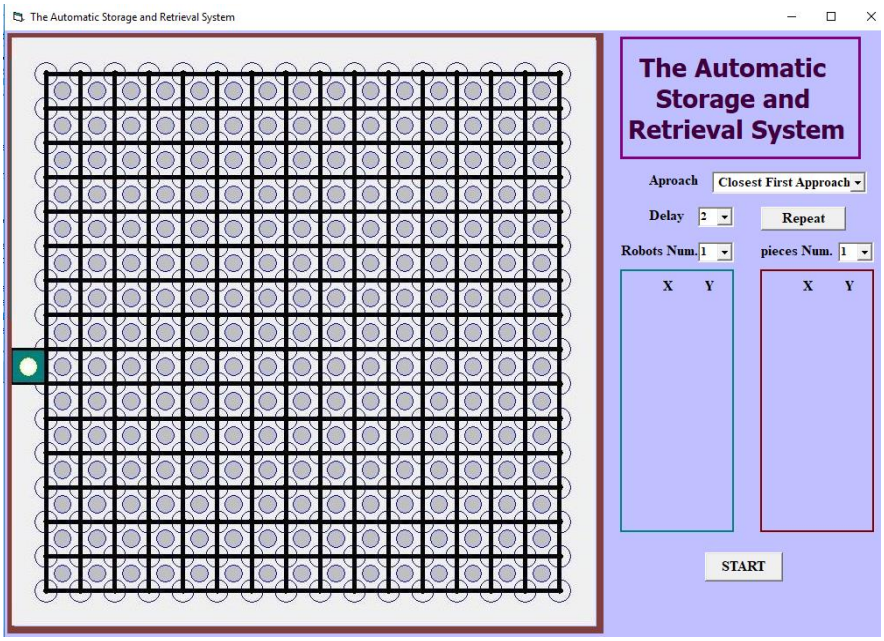

Fig.1 The automatic storage and retrieval environment.

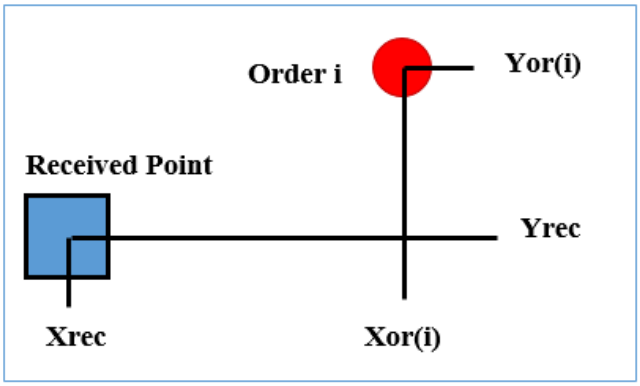

Fig.2 The coordinate axis of the order and the receiver point.

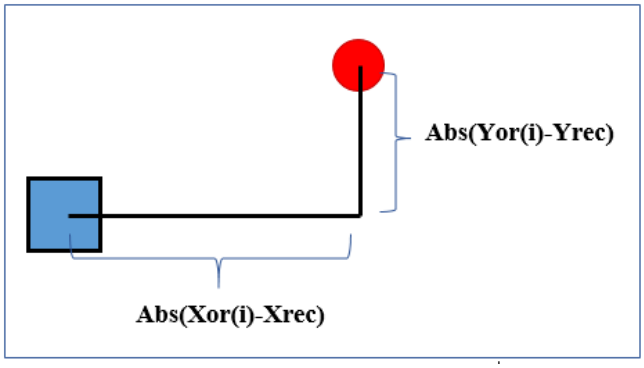

Fig.3 The distance between any order i and the receiver point.

Step3: Use one of the permutation algorithms to compute the length of total paths. The summing of the lengths of the paths for back and forth between the orders and receipt with the addition of the distance between each robot.

$$Total(I,j) = 2 * disrcv(i) + disrb(j) \quad (3)$$

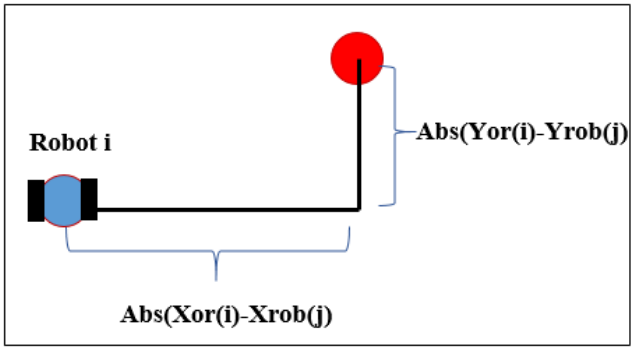

Fig.4 The distance between the order I and the robot j.

Step 4: choose the maximum distance: For each probability choose the maximum distance: Max of total (j,j)

Step 5: search for the minimum distance among all the maximum ones. This path represents the probability of the optimal path.

Step 6: move the robot according to the arranged sequence

Step 7: Collision avoidance among the robots when they move.

1. Arranged the robot in decreasing manner according to their distances from the received place.
2. Through the moving of the robots, each robot check the distances with the other robots.
3. If the distance is less than the length of one cell in the environment then the robot with the higher order must stop his movement.
4. The last step is repeated until the distance with the other robot is greater than the size of one cell.
5. The last two steps are repeated until all robots complete their tasks.

III. Simulation Results

The proposed algorithm (optimal path algorithm) is simulated to investigate the store and retrieval operation using Visual basic programming language and tested in the Windows environment using an Intel core i5. Two methods were implemented to simulate the performance of the algorithm and its estimator. The first is to implement the algorithm with the assumption of avoiding collision between robots while performing tasks. The second represents the application of the same algorithm with cause's collision between robots.

Two simulation experiments are implemented in this section: The first is to calculate the optimum time to complete the task while the second simulation is done by calculating the average path length during the execution of the tasks. For a measurable analysis of these approaches, the following performance metrics are used:

1. The storage and retrieval completing path (L): this metric is used to measure the total path for the storage and retrieval process to the number of the orders.
2. The storage and retrieval completing time (t): this metric is used to measure the percentage of the completing time to the number of the orders.

Fig. 5 (a)–(f) represent the Screenshots of the simulation at different time steps using the optimal path algorithm (No collision among the robots).

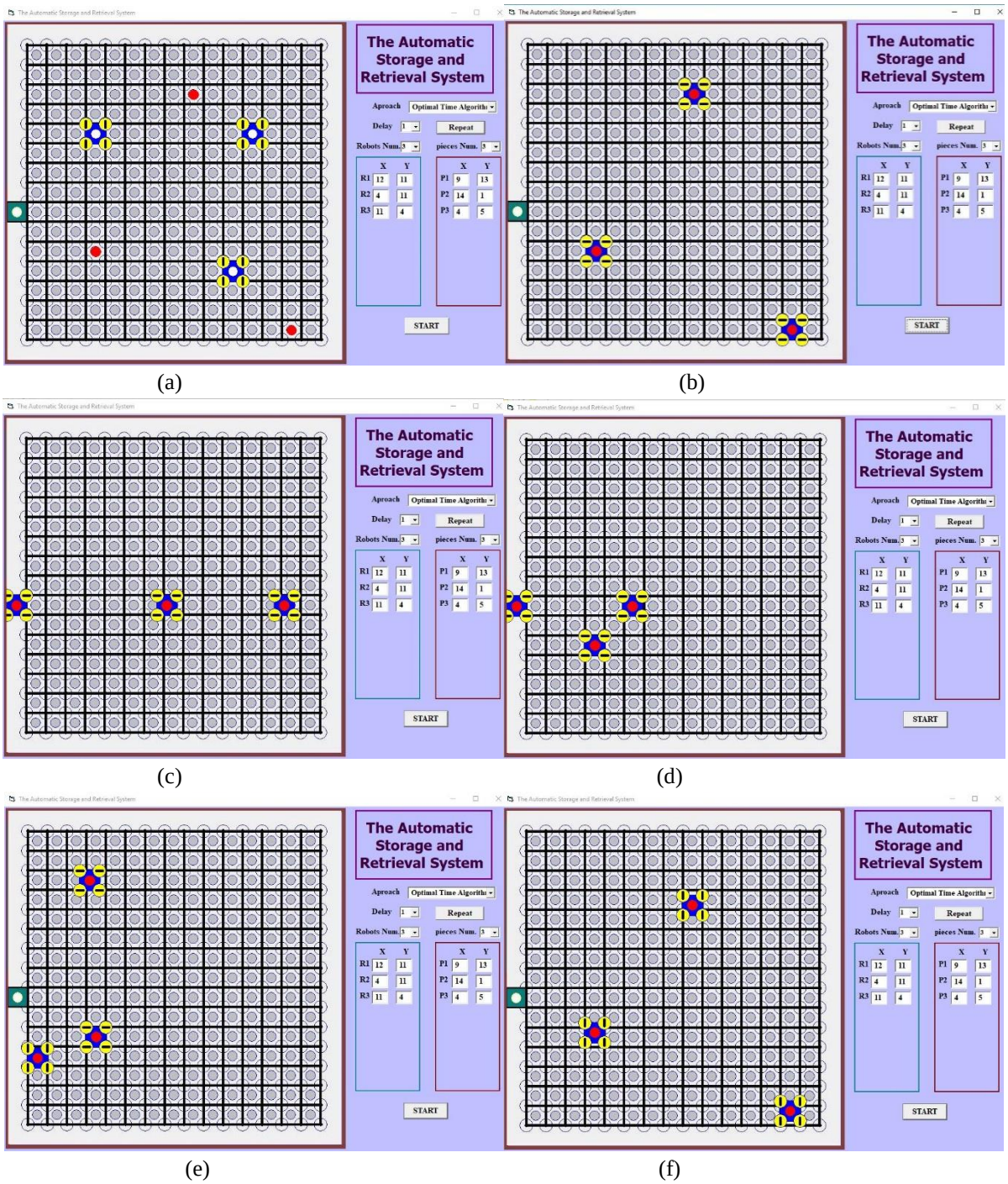

Fig. 5 The average of the arrival time using the optimal time algorithm (No collision among the robots).

Fig. 6 (a)–(f) represent the Screenshots of the simulation at different time steps using the optimal path algorithm (With collision among the robots). The main goal of this simulation is to show the relation between the number of orders and the store and retrieval accomplishment time for both cases.

Fig. 7 (a)–(6) represents the simulation of the minimum path for a different number of orders and robots (1, 2, 4 and 6) using the optimal path algorithm

Fig. 8 shows a comparison between the number of orders and the accomplishment percentage. As the number of the orders increases in the collision and non-collision environment, the accomplishment percentage increases, too.

Fig. 9 shows a comparison between the number of orders and the minimum accomplishment path for both the collision and non-collision environment. As the number of orders increases in the environment, the accomplishment increases, too.

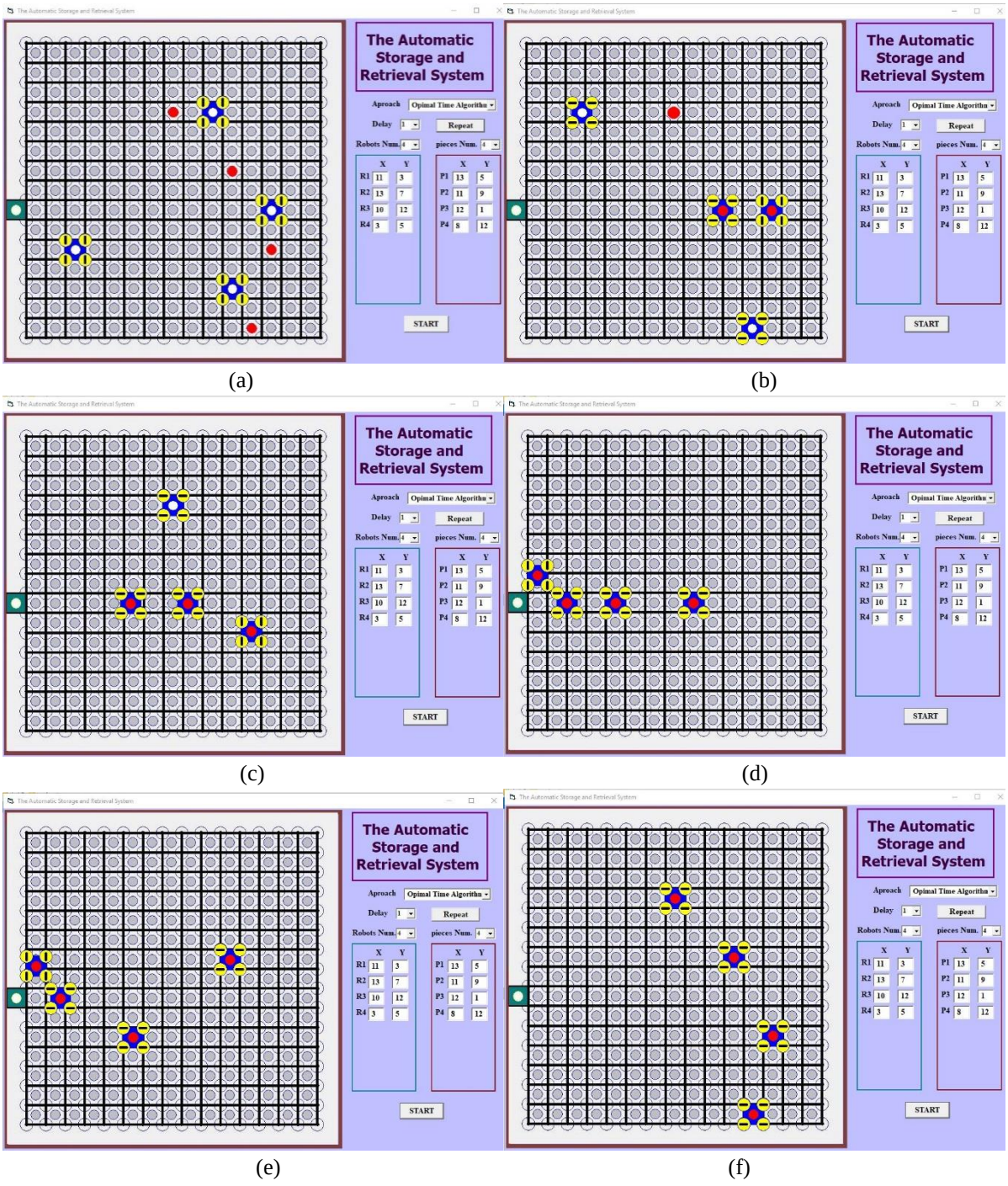

Fig. 6 The average of the arrival time for the optimal time algorithm (Collision avoidance algorithm).

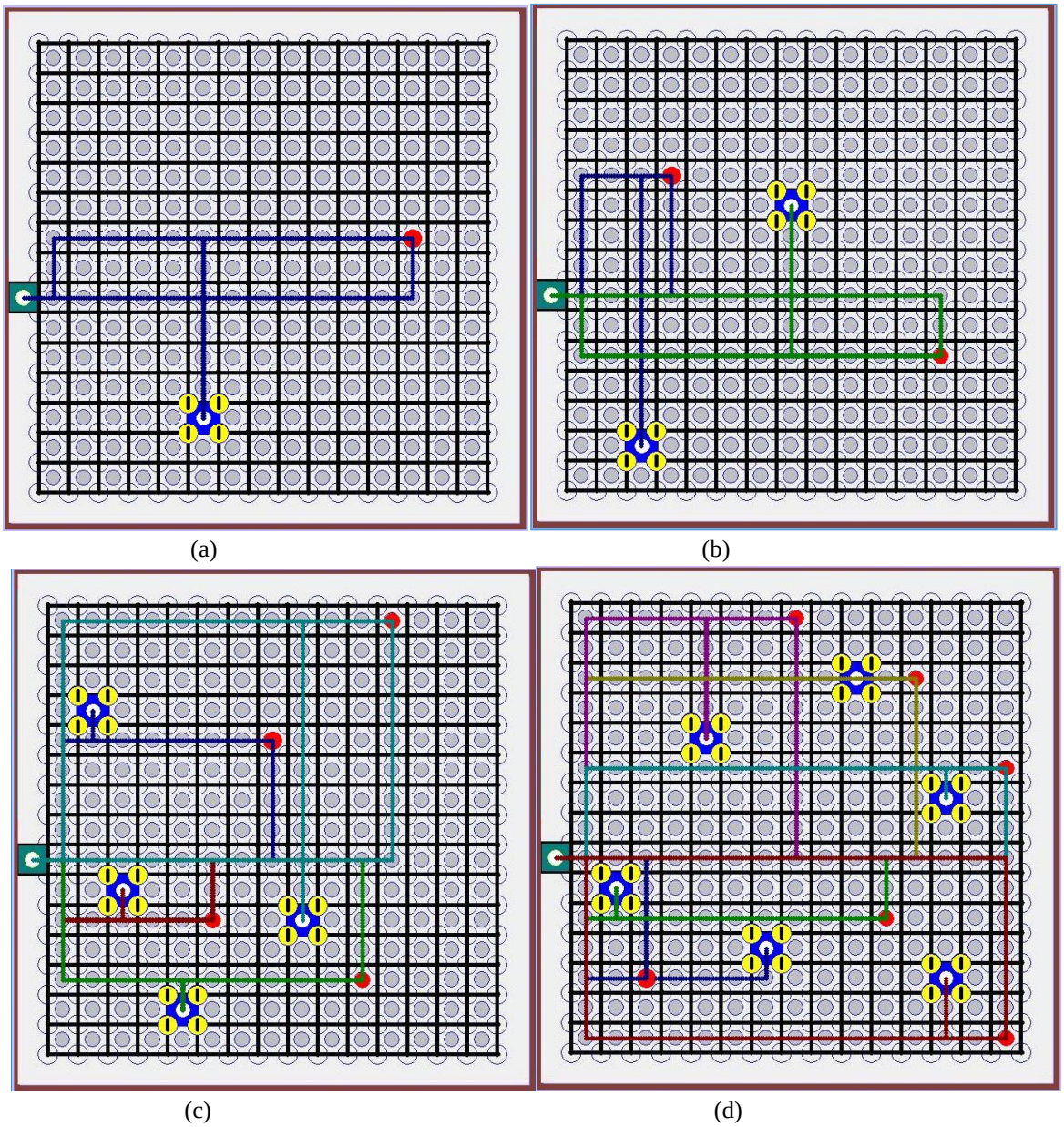

(a) (b)

(c) (d)

Fig. 7 The average of the total path for the optimal paths algorithm. a) one robot b) Two robots c) Four robots d)Six robots.

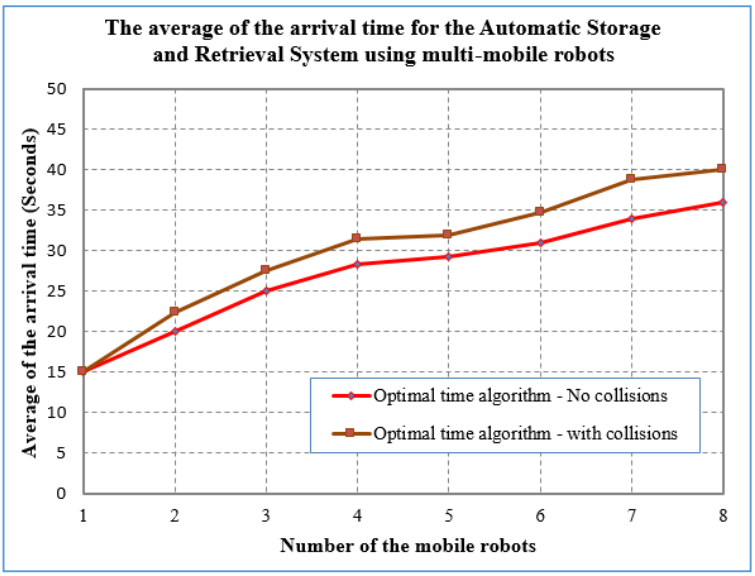

Fig. 8 Comparison the average of the arrival time for both the collision and not collision avoidance mobile robots.

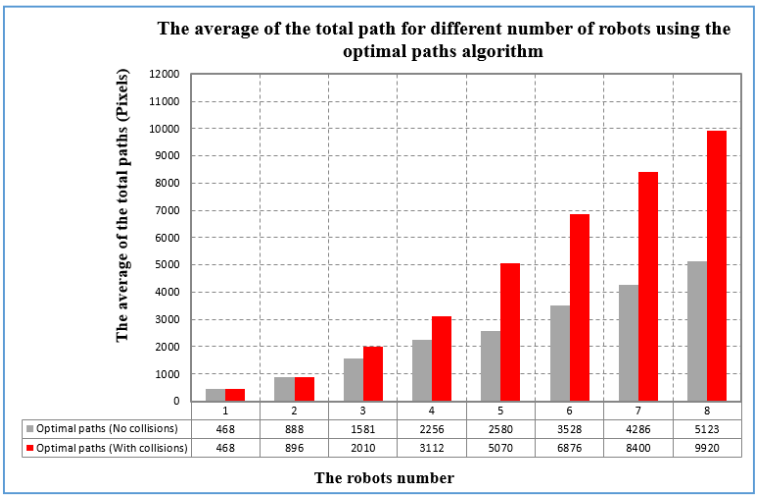

Fig. 9 Comparison the average of the total path for the optimal paths algorithm (collide and not collide robots).

IV. Conclusions

In this paper, a storage and retrieval approach (optimal path algorithm) in the static environment is proposed by using several numbers of orders with several number of mobile robots. Simulation results are implemented in an environment with a different number (1 to 8) of orders and robots. The results show that as the number of orders increases, the accomplishment time also increases for both collision and non-collision among robots The Non-collision environment has the best performance than the other one in an accomplishment time. From results, it is found that The accomplishment path increases when the number of orders increases for both environment. Also, the non-collision environment has the shortest accomplishment path comparing to the other approach.

References

[1] H. Hameed, Kh. Al-amry and A. Rashid, " The Automatic storage and retrieval system: an overview", *International Journal of Computer Applications* (0975 – 8887), Vol. 177, No.16, pp. 36-43, 2019.

[2] K. Azadeh, D. Roy, and R. de Koster, "Vertical or horizontal transport -comparison of robotic storage and retrieval systems", *SSRN Electronic journal*,dio:102139/ssrn.2888615.1,2016.

[3] F. Mauro, *Towards the design of an effective and robust parcel-sorting system* , master degree, Monday August 28, 2017.

[4] L. Parker, F. Fgan, and A. Schultz, "Multi-robot systems. From Swarms to intelligent automata", Volume III, Proceedings from the 2005 International Workshop on Multi-Robot Systems, Published by

Springer, P.O. Box 17, 3300 AA Dordrecht, The Netherlands.2005.

[5] S. Sarkar, *Industrial Engineering, Path planning and obstacle avoidance in mobile robots*, MsC . thesis, 16th November 2007.

[6] M. Reeves, *An analysis of path planning algorithms focusing on a * and d**, thesis Master degree, Dayton university, Ohio, May, 2019.

[7] D. Singh, *Path planning and evolutionary optimization of wheeled robots* . MsC thesis, Cleveland State University, May 2013.

[8] J. Debnath, *Path planning and resource management algorithms for robotic fully-automated and multi-story parking structure*, MsC thesis, The University of Toledo August 2016.

[9] M. Cunkas, and O. Ozer, "Optimization of location assignment for unit-load as/rs with a dual- shuttle", *International Journal of Intelligent Systems and Applications in Engineering IJISAE*, 7(2), 66–71 | 66, 2019.

[10] Y. Zhang, Zh.Lin, P. Tsai, J. Zhou1, and J. Dai, "Stacking storage scheduling optimization for profile automated warehouse robot based on mixing-degree", International Conference on Electrical Engineering and Automation (ICEEA 2016) ISBN: 978-1-60595-407-3, 2016

[11] A. T. Rashid, F. R. Ali, and O. T. Rashid, "Design and Construction a Dynamic Store System using the Bezier Curve Algorithms", *International Journal of Computer Applications*, vol. 179, No. 42, pp. 22-29, 2018.

[12] A. T. Rashid, F. R. Ali, and O. T. Rashid, "Software implementation of a static store system using the digital differential analyzer algorithm", International Iraqi Conference on Engineering Technology and their Applications, The Islamic University - Najaf – Iraq, 2018.

[13] F. R. Ali, and A. T. Rashid, "Design and implementation of static and dynamic objects store systems using line follower robots", International Conference on Advances in Sustainable Engineering and Applications, Wasit university - Iraq, 2018.

[14] F. R. Ali, and A. T. Rashid, "Software implementation of objects store system using line follower robots", Second Al-Sadiq International Conference on Multidisciplinary in IT and Communication Science and Applications, 2017.

[15] F. R. Ali, A. T. Rashid and O. T. Rashid, "Design and Construction Objects Store System using Line Follower Robot", *International Journal of Computer Applications*, vol. 181, No. 15, pp. 27-35, 2018.

[16] P. Goel, G. Arora, and V.K. Panchal, "Incorporating Perception Radius to the Line Follower Robot ", IEEE, 2014.

[17] O. Gumus, M. Topaloglu, and D. Ozcelik, "The use of computer controlled line follower robots in public transport", 12th International Conference on Application of Fuzzy Systems and Soft Computing, ICAFS, 2016.

[18] R. H. Rafi , S. Das, N. Ahmed, I. Hossain, and S. T. Rezae, " Design & implementation of a line following robot for irrigation based application", 19th International Conference on Computer and Information Technology, pp. 480-483 , 2016.

[19] N. Sariff 1 and N. Buniyamin 2 , "An overview of autonomous mobile robot path planning algorithms", 4th Student Conference on Research and Development (Scored 2006), June 2006.

[20] S.MahmoudZadeh, D. Powers, K. Sammut, A. Lammas, and A.M. Yazdani , "Optimal route planning with prioritized task scheduling for auv missions", Centre for Maritime Engineering, Control and Imaging Flinders University, Adelaide, SA 5042, Australia,2016

[21] Z. Y. Ibrahim , A. T. Rashid, and A. F. Marhoon, " An algorithm for path planning with polygon obstacles avoidance based on the virtual circle tangents", Iraq J. *Electrical and Electronic Engineering*, Vol. 12, No. 2, pp. 221-234 , 2016.

[22] Z. Y. Ibrahim , A. T. Rashid, and A. F. Marhoon, " Prediction-based path planning with obstacle avoidance in dynamic target environment ", Basrah Journal for Engineering Sciences, Vol. 16, No. 2, pp. 48 – 60, 2017.

[23] H. Zheng, "Trust-based multi-robot symbolic motion planning with a human-in-the-loop", *ACM Transactions on Interactive Intelligent Systems*, Vol. 9, No. 4, Article 39. Publication date: March 2017.

[24] H.Zhang, W. Lin and A. Chen , "Path Planning for the Mobile Robot: A Review", *Symmetry* 2018, 10, 450; doi:10.3390/sym10100450, www.mdpi.com/journal/symmetry

[25] K. Solovey, *Multi-robot motion planning: theory and practice*, doctor in philosophy, Tel-Aviv University, March 2018

DOI: 10.37917/ijeee.sceeer.3rd.19 *(15-16) June 2020*

Open Access

Iraqi Journal for Electrical and Electronic Engineering
Conference Article

Design a Compact Coplanar Wideband Antenna Used in Radio Frequency Identification Systems

Sufyan Hazaa Ali[1], Ahmed Hameed Reja[2], Yousif Azzawi Hachim*[3]
[1,3]Departement of Electrical Engineering, Tikrit University, Tikrit, Iraq
[2]Department of Electromechanical Engineering, University of Technology, Baghdad, Iraq

Correspondence
*Yousif Azzawi Hachim
Tikrit University, Tikrit, Iraq
Email: yousifazzawi@st.tu.edu.iq

Abstract
In this paper, a new compact coplanar antenna used for Radio frequency identification (FID) applications is presented. This antenna is operated at the resonant frequency of 2.45 GHz. The proposed antenna is designed on an epoxy substrate material type (FR-4) with small size of (40 × 28) mm² in which the dielectric thickness (h) of 1.6 mm, relative permittivity (ε_r) of 4.3 and tangent loss of 0.025. In this design the return loss is less than −10 dB in the frequency interval (2.12 − 2.84) GHz and the minimum value of return loss is -32 dB at resonant frequency. The maximum gain of the proposed antenna is 1.22 dB and the maximum directivity obtained is 2.27 dB. The patch and the ground plane of the proposed antenna are in the same surface. The proposed antenna has a wide bandwidth and omnidirectional radiation pattern with small size. The overall size of the compact antenna is (40 × 28 × 1.635) mm³. The Computer Simulation Technology (CST) microwave studio software is used for simulation and gets layout design.

KEYWORDS: Antenna, Gain, Return loss, RFID, Wideband.

I. INTRODUCTION

A Radio Frequency Identification (RFID) is rapidly growing technology for automatic identification and it is being exploited in many areas such as healthcare, airport, libraries, military, passport, supply chain etc. [1]. The prodigious development in the field of RFID corresponding uses and applications has increased the requirement of smaller size and low profile elements that appropriate for application in RFID systems. RFID technologies have risen interest to realize several commercial implementations, like security, manufacturing, management of automatic retail, industrial work, access control and transportation, electronic toll collection and distribution systems [2]. A standard RFID system contains a tag and reader devices. The antenna of reader sends an electromagnetic wave (EMW) signal to the tag then RFID reader receives a signal as an information from tag's antenna [3].

The bands of frequency of an RFID are the high frequency (HF) band operates at 13.56 MHz, ultra-high frequency (UHF) band from 860 to 960 MHz, and Industrial, Scientific, and Medical (ISM) band at 2.4GHz [4],[5]. The applications of an RFID in the ultra-high frequency (UHF) divided to intervals of band of frequencies in many countries. These bands of frequencies are subdivided with respect to countries to: 840.5–844.5 MHz and 920.5–924.5 MHz in China, 902–928 MHz in North America, 950–956 MHz in Japan, 866–869 MHz in Europe, 865–867 MHz band in India, 920–926 MHz in Australia, and 908.5–914 MHz in South Korea [6], [7], [8]. The comprehensive coverage of ultra-high frequency (UHF) band used in RFID in each country is about 840–960 MHz. In practical using, the reader antennas usually are circularly polarized (CP) to ensure best communication between tags and reader [9]. A linearly polarized (LP) antenna is necessary for tag antenna, and the RFID tags are mostly oriented arbitrarily [9]. Several limitations are occurs of using distributed patch antennas such as; low gain, narrow bandwidth (NBW) and low efficiency, which leads to reduce the antenna performance [10], [11].

Generally, the basic configuration of conventional microstrip antenna are a conducting patch which is made of metal such gold or copper. The patch is printed on the upper side of the substrate material that has dielectric or relative permittivity value in the range of $2.2 \leqslant \varepsilon\_r \leqslant 12$, which set on the ground layer on the other side as shown in Fig. 1 [12], [13]. The substrate material type FR-4 is used in most designs where the FR-4 dielectric combines good electrical features, price, and availability [14].

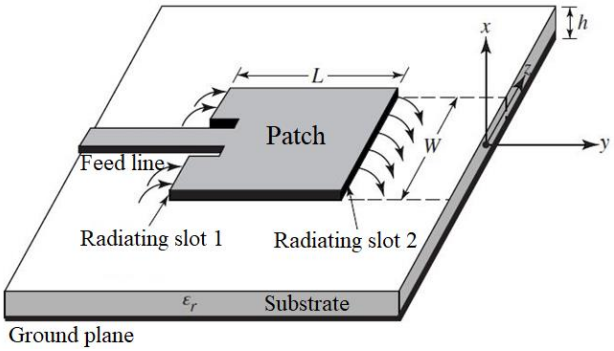

Fig. 1: Microstrip antenna configuration

The main disadvantages of microstrip patch antennas are narrow bandwidth, lesser gain and poor efficiency, which disturbed the efficiency of this antenna. Various researchers currently studied different shapes of antenna design for RFID readers by applying a varied approach of patch and ground geometry [14] . Generally, the miniaturization in size, broad bandwidth and good directivity of RFID antenna systems are important requirements of microstrip antenna and most researches try to develop and modified the antenna specifications.

A. K. Gautam et al. [15] presented a compact antenna made with size of (30 × 30 × 1.6) mm^3 and narrow bandwidth with acceptable gain value, so the proposed coplanar antenna improved bandwidth. N. O. Parchin et al. [16] presented an antenna to cover dual band of 2.4/5.8 GHz RFID operation bands with good realized gain with overall size of (38 × 45 × 1.6) mm^3, so the proposed coplanar antenna improved the size where it has smaller size . M. Z. Aziz et al. [17] presented a dual band omnidirectional antenna to operate at 2.45 GHz in which the dimensions of substrate material are (l5 × 85.75) mm^2 and dielectric thickness of 1.6 mm. The return loss at the resonance frequency of -10.61dB with bandwidth is 122 MHz and the gain that has been achieved is 3.798 dB, so the proposed coplanar antenna improved to achieved best return loss. M. R. Reader [18] presented a microstrip stacked patch antenna operates at 2.45 GHz passive RFID reader. The antenna has dimensions of (58 × 58) mm^2 with large thickness of 11 mm with narrow bandwidth and the peak gain achieves 6.32 dB in the resonance frequency.

In this work, a microstrip antenna resonated at 2.45 GHz to use in RFID band is designed. This presented antenna is not similar to the traditional microstip antenna, where the patch and the ground are together in same plane (upper surface) as a coplanar technique with omnidirectional radiation. The size of this design is (40 × 28 × 1.635) mm^3 achieves best impedance matching, acceptable gain, suitable bandwidth and best Voltage Standing Wave Ratio (VSWR). When the value of the VSWR is less than 2 at the frequency band interval, the antenna can be able to work correctly in this band [19].. In detailed structure configuration, design, and simulation results of this design are discussed and explained in the following paragraphs.

II. ANTENNA DESIGN

The presented coplanar antenna geometry has partial ground in two separate sections as illustrated in Fig. 2. The presented antenna is printed on substrate material type FR-4 that has thickness (h) of 1.6 mm and relative permittivity (ε_r) of 4.3 and loss tangent ($\tan\delta$) of 0.025. The proposed antenna works at the band of frequency in interval (2.12 – 2.84) GHz. The dimensions of the general microstrip patch antenna have been obtained [20]. The effective dielectric constant (ε_{eff}) depends on width of the patch antenna (W), dielectric constant (ε_r) and the height substrate (h).

The effective dielectric constant (ε_{eff}) is calculated as

$$\varepsilon_{eff} = \frac{\varepsilon_r+1}{2} + \frac{\varepsilon_r-1}{2}\left[1+\frac{12h}{W}\right]^{-1/2} \quad (1)$$

The physical dimensions of the microstrip antenna looks smaller than its electrically the patch due to fringing effects. The length of antenna increases due to fringing effect as

$$\frac{\Delta L}{h} = 0.412h\frac{(\varepsilon_{eff}+0.3)\left(\frac{W}{h}+0.264\right)}{(\varepsilon_{eff}-0.258)\left(\frac{W}{h}+0.8\right)} \quad (2)$$

ΔL is the extension patch length due to fringing

The effective length is calculated by

$$L_{eff} = \frac{1}{2f_o\sqrt{\varepsilon_{reff}}\sqrt{\mu_o\varepsilon_o}} = \frac{v_o}{2f_o\sqrt{\varepsilon_{reff}}} \quad (3)$$

The width of patch antenna is calculated by

$$W = \frac{1}{2f_o\sqrt{\mu_o\varepsilon_o}}\sqrt{\frac{2}{\varepsilon_r+1}} = \frac{v_o}{2f_o}\sqrt{\frac{2}{\varepsilon_r+1}} \quad (4)$$

v_o is speed of light in free space

f_o is resonance frequency

Where $v_o = 3\times10^8\ m/s$, $\mu_o = 4\pi\times10^{-7}\ H/m$ and $\varepsilon_o = 8.85\times10^{-12}\ F/m$

The actual length ($L_{act.}$) of the patch is calculated by

$$L_{act.} = L_{eff} - 2\Delta L \quad (5)$$

The dimensions of the substrate as Length ($L_{substrate}$) and Width ($W_{substrate}$) are specified as

$$W_{substrate} = W + 6h \quad (6)$$

$$L_{substrate} = L + 6h \quad (7)$$

By using the above equations, the dimensions of antenna are achieved as shown in Fig. 2.

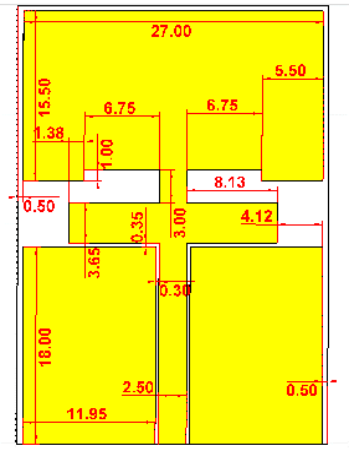

Fig. 2: Geometry of the proposed antenna

From this design we conclude that to achieved the resonant frequency demanded with suitable size we must add the slots, also to achieve good impedance matching, best return loss, wide bandwidth and minimum VSWR. To achieved omnidirectional radiation pattern, the ground must be partial ground.
The materials of this antenna and its dimensions and thicknesses are registered in Table I.

TABLE I DIMENTIONS OF THE PROPOSED ANTENNA

Elements	Material type	Dimensions in mm^2	Thickness in mm
Substrate	FR-4	40 × 28	1.6
ground element	Copper	18 × 11.95	Too low
Patch	Copper	21.65 × 27	Too low
Feed line	Copper	18.35 × 2.5	Too low

III. SIMULATION RESULTS AND DISSCUISIONS

At first, the return loss (RL) or reflection coefficient |S11| is calculated as a function of frequency and illustrated in Fig. 3. The simulated bandwidth evaluated at −10 dB is 720 MHz that is measured in the frequency range (2.12 – 2.84) GHz.
Thereafter, the other important parameter with return loss, that effects on antenna performance and related to the bandwidth, is Voltage Standing Wave Ratio (VSWR), and it is less than or equal to 2. (VSWR ≤ 2).
The VSWR response of the proposed antenna is illustrated in Fig. 4. As can be showed in Fig. 4, the deepest or less value of VSWR is 1.05 occurs at the resonance frequency of 2.45 GHz that means the maximum power will be transferred at the operated frequency (2.45 GHz).

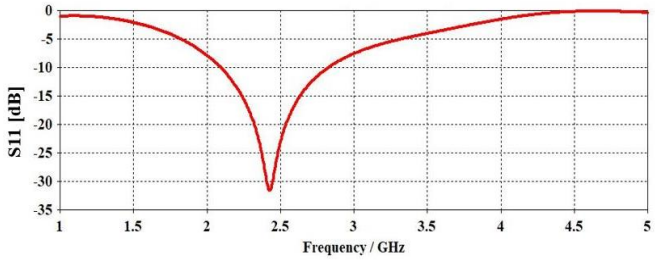

Fig. 3: Return loss verses frequency

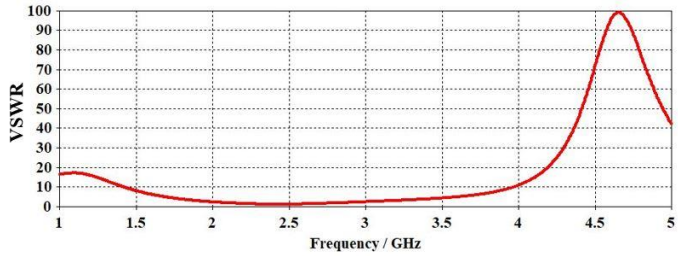

Fig. 4: The VSWR of the proposed antenna

As observed from the appreciated gain curve of the presented antenna design in Fig. 5, a suitable amount gain of 1.22 dB is obtained.

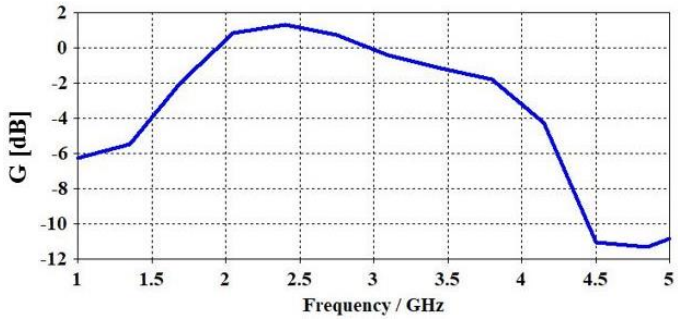

Fig. 5: The response gain of the proposed antenna

The other considerable parameter related to the gain (G) that interested in antenna performance is the directivity (D). Fig. 6 shows the directivity of radiation pattern of the presented antenna. Theoretically, the relation between the gain (G) and directivity (D) is related to antenna efficiency factor (η) as in (8).

$$G = \eta D \quad (8)$$

The antenna efficiency factor value is enclosed by ($0 \leq \eta \leq 1$). If η =1, that means the antenna is lossless. In practice, gain (G) is always less than the directivity (D). As showed in the Fig. 6, the omnidirectional radiation pattern is obtained. Thus the maximum value of directivity resulted is 2.27 dB.

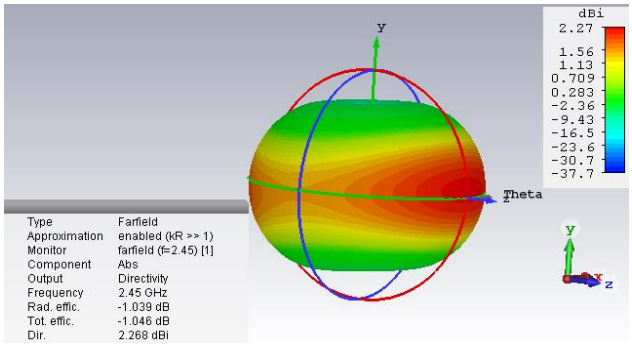

Fig. 6: Radiation pattern with all defined parameters

The brief of simulated results for the offered antenna is listed in Table Ⅱ.

TABLE II
SUMMARY RESULTS OF SIMULATED PARAMETERS

Antenna parameters	Value
Frequency range	2.12 – 2.84 GHz
Resonance frequency (f_o)	2.45 GHz
Bandwidth	720 MHz
Return Loss at f_o	-32 dB
VSWR at f_o	1.05dB
Directivity	2.27 dB
Gain	1.22 dB

IV. CONCLUSION

This work presented a wideband microstrip slots loaded patch antenna as a coplanar with microstrip feed line. By using partial ground method (i.e. this theory used to obtain omnidirectional radiation pattern) the antenna performance has been improved where the parameter results of the suggested antenna present less return loss, broad bandwidth, minimum VSWR and proper directivity with reasonable value of gain furthermore miniaturization in antenna size. The suggested antenna has small size and operates in the frequency band of (2.12 – 2.84) GHz which represent the suitable band to cover RFID applications at resonant frequency of 2.45 GHz, the gain and directivity values are 1.22 dB and 2.27 dB respectively.

REFERENCES

[1] F. Xavier, O. K. Hikage, M. S. de Paula Pessôa, and A. L. Fleury, "A View about RFID Technology in Brazil," in *PICMET 2010 Technology Management for Global Economic Growth*, 2010, pp. 1–9.

[2] K. Finkenzeller, *RFID handbook: fundamentals and applications in contactless smart cards, radio frequency identification and near-field communication*, 3rd ed., John wiley & sons, Munich, Germany, 2010.

[3] W.-S. Chen and Y.-C. Huang, "A Novel CP Antenna for UHF RFID Handheld Reader," *IEEE Antennas Propag. Mag.*, vol. 55, no. 4, pp. 128–137, 2013.

[4] J.-H. Lim, B.-S. Kang, J.-W. Jwa, H.-S. Kim, and D.-Y. Yang, "RFID Reader Antenna with Hilbert Curve Fractal Structure over Partially Grounded Plane," *J. Korea Contents Assoc.*, vol. 7, no. 4, pp. 30–38, 2007.

[5] Y. Jin, J. Tak, and J. Choi, "Quadruple Band-notched Trapezoid UWB Antenna with Reduced Gains in Notch Bands," *J. Electromagn. Eng. Sci.*, vol. 16, no. 1, pp. 35–43, 2016.

[6] Z. N. Chen and X. Qing, "Asymmetric-circular Shaped Slotted Microstrip Antennas for Circular Polarization and RFID Applications," *IEEE Trans. Antennas Propag.*, vol. 58, no. 12, pp. 3821–3828, 2010.

[7] R. Cao and S.-C. Yu, "Wideband Compact CPW-fed Circularly Polarized Antenna for Universal UHF RFID Reader," *IEEE Trans. Antennas Propag.*, vol. 63, no. 9, pp. 4148–4151, 2015.

[8] J. H. Yoon, S. J. Ha, and Y. C. Rhee, "A Novel Monopole Antenna with Two Arc-shaped Strips for WLAN/WiMAX Application," *J. Electromagn. Eng. Sci.*, vol. 15, no. 1, pp. 6–13, 2015.

[9] X.-Z. Lai, Z.-M. Xie, Q.-Q. Xie, and X.-L. Cen, "A Dual Circularly Polarized RFID Reader Antenna with Wideband Isolation," *IEEE Antennas Wirel. Propag. Lett.*, vol. 12, pp. 1630–1633, 2013.

[10] G. Kaur, G. Singla, and S. Kaur, "Design of Wideband Micro strip Patch Antenna Using Defected Ground Structure for Wireless Applications," *Int. J. Adv. Res. Comput. Sci. Softw. Eng.*, vol. 3, no. 10, 2013.

[11] J. M. Patel, S. K. Patel, and F. N. Thakkar, "Comparative Analysis of S-shaped Multiband Microstrip Patch Antenna," *Int. J. Adv. Res. Electr. Electron. Instrum. Eng.*, vol. 2, no. 7, pp. 3273–3280, 2013.

[12] B. S. Sandeep and S. S. Kashyap, "Design and Simulation of Microstrip Patch Array Antenna for Wireless Communications at 2.4 GHz," *Int. J. Sci. Eng. Res.*, vol. 3, no. 11, pp. 1–5, 2012.

[13] S. A. Ali, U. Rafique, U. Ahmad, and M. A. Khan, "Multiband Microstrip Patch Antenna for Microwave Applications," *IOSR J. Electron. Commun. Eng.*, vol. 3, no. 5, pp. 43–48, 2012.

[14] D. G. Fang, *Antenna Theory and Microstrip Antenna*, United States of America: Taylor and Francis Group, LLC, 2010.

[15] A. K. Gautam, N. Agrawal, and K. Rambabu, "Design and Packaging of a Compact Circularly Polarised Planar Antenna for 2 . 45-GHz RFID Mobile Readers," vol. 13, pp. 2310–2314, 2019.

[16] N. O. Parchin, H. J. Basherlou, R. A. Abd-Alhameed, and J. M. Noras, "Dual-band Monopole Antenna for RFID Applications," *Futur. Internet*, vol. 11, no. 2, 2019.

[17] M.Z.A. A. Aziz, M. Md. Shukor, M.K. Suaidi, B.H. Ahmead, M.F. Johar, H. Nornikman, F.A. Azmin, S.N. Salleh and M.F. Abd. Malek, "Printed Omnidirectional Antenna for RFID Applications," *2013 IEEE Int. Conf. RFID-Technologies Appl. RFID-TA 2013*, pp. 4–5, 2013.

[18] M. R. Reader, "A Compact and Broadband Microstrip Stacked Patch Antenna With Circular Polarization for 2.45-GHz Mobile RFID Reader," *IEEE Antennas and Wireless Propagation Letters*, vol. 12, pp. 623–626, 2013.

[19] B. Niboriya, C. Choudhary, and G. Prabhakar, "S-shape Wideband Microstrip Patch Antenna with Enhanced Gain and Bandwidth for Wireless Communication," *Int. J. Comput. Appl.*, vol. 73, no. 7, pp. 975–8887, 2013.
[20] C. A. Balanis, *Antenna Theory Analysis and Design*, 4th ed. United States of America: John Wiley Sons, 2016.

DOI: 10.37917/ijeee.sceeer.3rd.20 *(15-16) June 2020*

Open Access

Iraqi Journal for Electrical and Electronic Engineering
Conference Article

Fair and Balance Demand Response application in Distribution Networks

Ibrahim H. Al-Kharsan *[1,2], Ali.F. Marhoon[1], Jawad Radhi Mahmood[1]
[1]Electrical Engineering department, University of Basrah, Basrah, Iraq
[2]Computer Technical Engineering Department, College of Technical Engineering, The Islamic University, Najaf, Iraq

Correspondence
* Ibrahim H. Al-Kharsan
Electrical Engineering department,
University of Basrah, Basrah, Iraq
Email: smrtg809@gmail.com

Abstract
The unprogrammed penetration for the loads in the distribution networks make it work in an unbalancing situation that leads to unstable operation for those networks. the instability coming from the imbalance can cause many serious problems like the inefficient use of the feeders and the heat increased in the distribution transformers. The demands response can be regarded as a modern solution for the problem by offering a program to decreasing the consumption behavior for the program's participators in exchange for financial incentives in specific studied duration according to a direct order from the utility. The paper uses a new suggested algorithm to satisfy the direct load control demand response strategy that can be used in solving the unbalancing problem in distribution networks. The algorithm procedure has been simulated in MATLAB 2018 to real data collected from the smart meters that have been installed recently in Baghdad. The simulation results of applying the proposed algorithm on different cases of unbalancing showed that it is efficient in curing the unbalancing issue based on using the demand response strategy.
KEYWORDS: Algorithm, Demand Response, Direct load control, Distribution Networks, Unbalance Loads.

I. INTRODUCTION

The modern technologies entered the electrical power system make it more flexible and provide a method to achieve better control. In the same time, it created a series problem like that related to the reliability, the efficiency, the high losses in the energy, the pollution results from the gases emission to the atmosphere, the high cost of power generation and the high ratio of peak to average in the consumption. The high energy consumption was seen as an urgent matter because the solution calls for more money to be spent and professional experts available. The high demand issue results from the fixed tariff of electricity that makes the consumers not take the amount of consumption in their consideration, and that leads to a high peak to average ratio (PAR) [1]–[3]. In spite of the high demand not continuous for extended periods (may few hours in one day) but there is a high investment to overcome the problem if the problem solves by increasing the generation. The adding of new generation plants requests an overall reconsideration for the transmission and distribution infrastructures. The smart grid in this century has an essential role in changing the philosophy of electrical power engineering. In the past, the power generation should be equivalent to the consumed power, but with the advent of the non-conventional grids, everything has been changed, and users can consume energy in the same quantity as already generated from the units by using of the DR strategy. DR can alter the consumption pattern of the consumers based on some motivations beside it represent an effective solution for all the issues mentioned above[4]. The DR can lead to a low consumption curve instead of the sharp one that leads to additional
costs coming increasing the generation plants to cover the peak periods in the load curve, and that represents a non-economic solution. DR idiom means “changes in electric usage by end-use customers from their normal consumption patterns in response to changes in the price of electricity over time, or to incentive payments designed to induce lower electricity use at times of high wholesale market prices or when system reliability is jeopardized” [3], [5], [6]. The DLC regarded one of the popular programs that applied to convert the consumption behaviors when the load on the generation stations becomes more and more, and that threatens the stability of the system if the problem stays without a solution [7]–[9]. In the DLC program, specific consumers or appliances have been recorded, and the utility can operate with full freedom to shut down or scheduling the operation of them in the events to need for that like in the hours of peak

demand. The participating in this program received an incentive for allowance to the utility to control their loads [10].

II. The Proposed Algorithm

The implementation of the Direct Load Control Program (DLC) in the Secondary Distribution Networks (SDN) is has a paramount importance as there are many loads consumed large amount of energy and it has a vital role to play in generating the circumstances that could place the network in a position that could threaten its stability. Fair Demand Response with Direct Load Control Mechanism (FDR-DLCM) is the proposed algorithm to achieve the DLC program in the SDN that spread in the residential areas. The paper discussed in this section applying for the DLC program on the AL-Qahera sector in Baghdad, and we suppose it has 48 homes. The utility success in contracting with all the owners of the homes to participate in this program. The utility is responsible for paying a financial incentive in exchange for the full control of the registered phases ($R_{Phs-DLC}$). It has the right to switch off or to schedule the $R_{Phs-DLC}$ as necessary for reducing the power consumption in the peak demand hours. The participators can dedicate some deferrable loads (the not essential loads that can work at any time in the day or night like the washing machine) to the program and let the critical loads out the authority of the utility. The novelty for the suggested mechanism is the fairness, which means justice in switching the $R_{Phs-DLC}$. The loads participated in the program ready to shut down at any time without any alert to the consumers, but it is a good matter if the algorithm satisfied the equality in switching off that loads.

The general framework for the DLC DR procedure that done starting from the utility to the last stage in the system (the consumers) clarified in twelve steps below:

1. The utility checks the generated and consumed energy, and if there is dispatching, nothing, in this case, should do, but if the consumed energy started to be more than the produced here, some loads should be shedding.
2. MCC (Main Control Computer) is sending a signal to the control units (CUs) that installed in the secondary transformers of the SDN to measure the consumption of the RPhs-DLC (see Fig. 1).
3. The CUs sending signals to the SMs to measure the consumption of the targeted nodes.
4. The aggregated amount of consumption that measured by all the CUs in the region sending back to the MCC in the utility.
5. Depending on the received data, the MCC divided the reduction requested to achieve the optimal power dispatching on the regions.
6. MCC Determine the reduction in consumption for each region and sending that to the CUs.
7. The CU receives the data and memorize it and readiness to achieve the DLC on the registered loads.
8. The algorithm avoids any load that used in the previous event and trying to use all those loads not participated in any event, or its participation is low.
9. The proposed algorithm performing an accumulative summing for all the choices loads and check if it equal to the amount that the MCC asked to shed.
10. If it is enough, stop the algorithm and leave.
11. If the algorithm needs switching OFF additional loads, it looking again for the fewer loads that participated in the previous event reach the demanded current consumption.

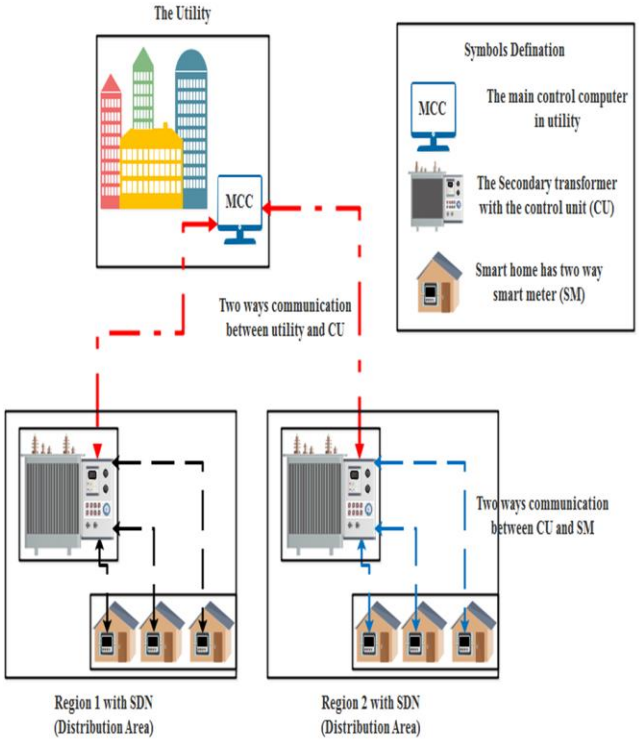

Fig. 1: The communicate mechanism between MCC, CUs and SMs to achieve the DLC program.

The previous steps that explain the procedure followed by the utility to satisfying the DLC program in the critical events illustrated in Fig.2. The proposed algorithm has been designed to give the participators in the DLC program the right to give the loads registered in the DLC program a particular priority, and this regarded the second novelty. In other words, we suppose the algorithm care about the following load indications:

- High priority (HP): the consumer announced not shut down this load if there any alternative solution.
- Moderate priority (MP): it means the consumer can abandon the load in spite he needs it.
- Low priority (LP): the consumer declares the load is permissible for shutting down in any event.

The proposed algorithm measured all the load consumption and the priority of each load and, depending on the data collected, and it was able to decide what the loads that should remain in operation and the loads should be stopped to

overcome the event under consideration. The proposed algorithm operation illustrated in the flowchart in Fig.2.

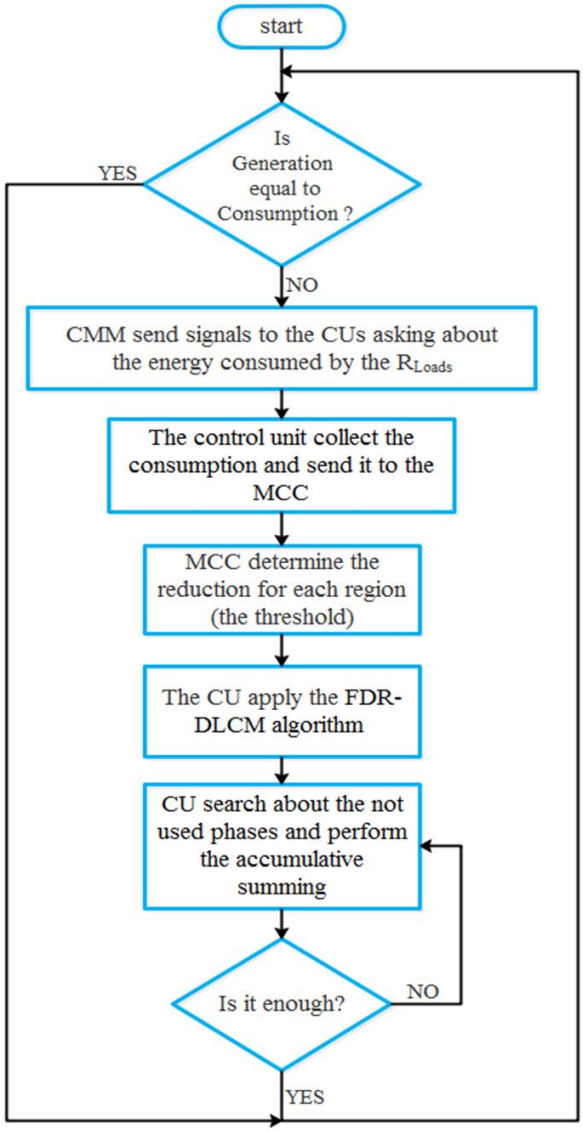

Fig. 2: The flowchart of the main steps for achieving the online DLC program.

According to the instruction signal from the MCC, the FDR-DLCM algorithm installed in the CUs pursue the following steps to achieve the DLC program on the $R_{Phs\text{-}DLC}$ to reduce the power consumption:

1. CU is sending a signal to the SMs in the region under its responsibility, ordering it to measure the consumption of all the Rphs-DLC and return measured data to it. The CU saves the coming information in the (PhaseCurrent) matrix.
2. The CU sending another signal to the SMs requesting the desired priorities by the participators. The priorities saved in the memory of the CU in the (Priority) matrix.
3. The CU Recall the saved (TimeStep) matrix in the CU memory. It showed the times every phase shut down according to the events that happened in the past.
4. The CU Recall the saved (TimeStep) matrix in the CU memory. It showed the times every phase shut down according to the events that happened in the past.
5. The CU Recall the saved (TimeStep) matrix in the CU memory. It showed the times every phase shut down according to the events that happened in the past.
6. The CU has four cases to handle the DR program: **CASE1:** If the (**total consumption < TransCurrent**) does not do anything and let all the phases on its previous state.
   a. CASE1: If the (total consumption < TransCurrent) does not do anything and let all the phases on its previous state.
   b. CASE2: if ((ColCurrent2 +ColCurrent3) < TransCurrent) the limited consumption in this situation enough to operate all the phases with MP and HP. The algorithm computes first the remaining amount of consumption (RestCurrent) and determine how many phases with LP enough to energize and switch OFF the others.
   c. CASE3: if (RestCurrent=TransCurrent-(ColCurrent3)) The algorithm, in this case, switching OFF all the low priority loads and chooses some of the Rphs-DLC with a moderate priority. The high priority phases stay in ON state because of the limitation of the utility enough for that.
   d. CASE4: if (RestCurrent=TransCurrent) The limitation, in this case not enough to cover all the Rphs-DLC with HP. The important event is hard, and the algorithm forced to switch OFF the request phases until if it has the most significant priority. Axiomatically, all the phases with low and moderate priority are switched OFF.
7. In all the four cases, when there is a new event that happened, the algorithm chooses a new phase to switch off and avoided the phases switched off in the previous event except in the cases that the algorithm compiles to that action in the massive emergency to achieve the fairness principle.

The flow chart that shown in Fig. 3 illustrate the trajectory that the proposed algorithm sticks to reach the desired reduction in the consumption by using the direct load control program. The following steps achieved in the CU that installed in the secondary transformer in each region.

CU represents the aggregator of data for all the consumers in a specific region because the utility does not directly deal with the final consumers because the CU collects all the demanded data requested by the MCC from the consumers. The CU represent an advance microcontroller that can programing to achieve the targeted tasks that it designs for.

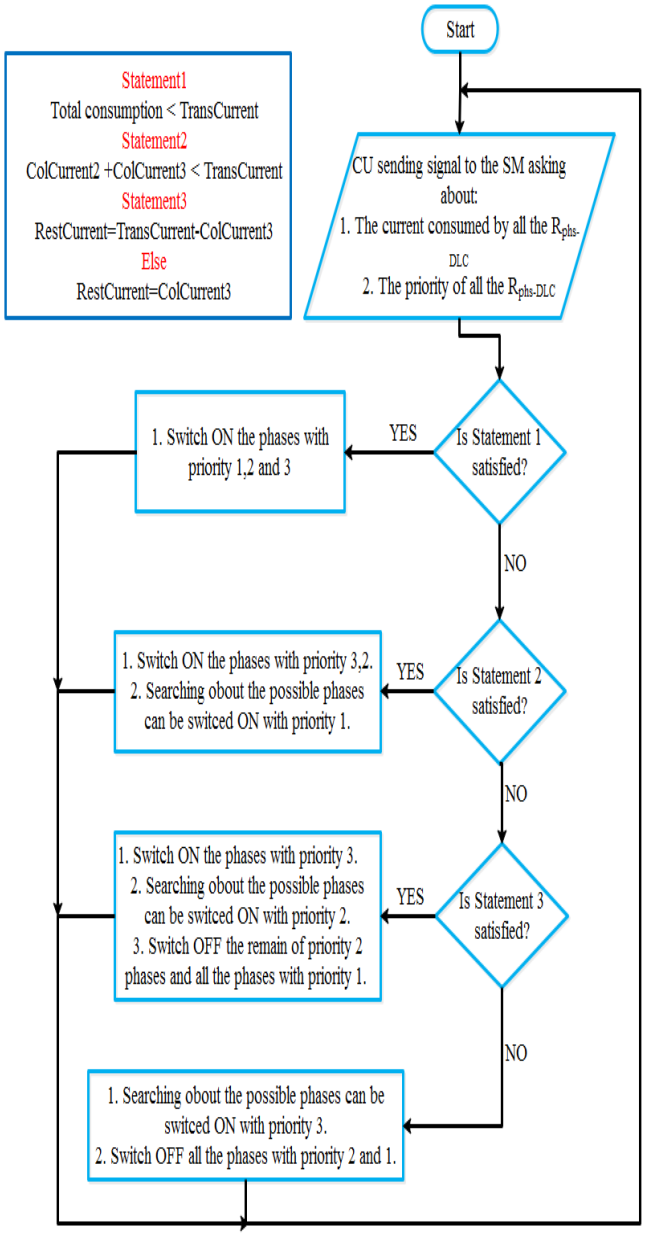

Fig. 3: The flowchart of the online algorithm that installed in the CU.

III. The Results

The simulation results obtained in this paper have been satisfied by using MATLAB2018b on a real and row data obtained from the 50 SMs that installed in the AL-Qahera sector in Baghdad by Al-Rasikh company. We regarded it has 48 residential homes, and the utility reach a contract with all of them. The utility registered the phases of the contracted homes as a supported load used in case there is an important event. The utility agreed to pay a specific amount of money as an incentive, in any event, to take place in the power system. The utility has full control over all the loads in the contract and can apply for the DLC program at any time without prior permission from the homeowners. The results divided into two parts; the first part discussed all the possible four cases that may cause the algorithm encounter in the real environment. The second part is for affirmation of the fairness principle that the proposed algorithm should achieve in case many events happened in the system.

1. Demonstration the Algorithm Performance

In order to testing the algorithm performance, all the home phases in Al-Qahera regarded as a $R_{phs\text{-}DLC}$. The real measured current in the mentioned area showed in Fig. 4. The total current consumption is equal to 459.06A according for that

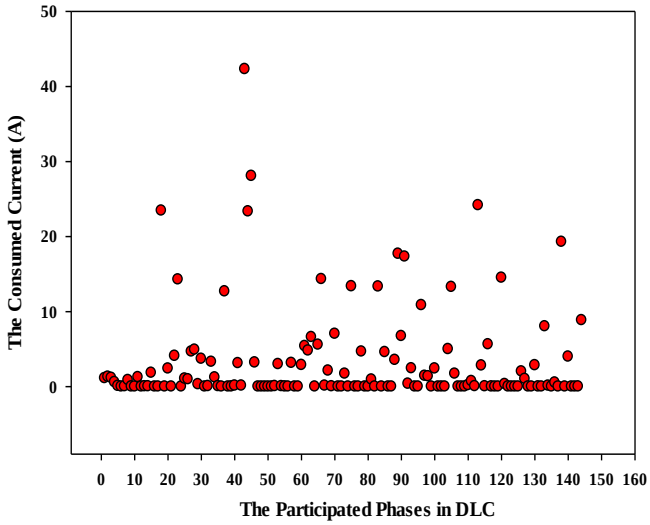

Fig. 4: The Al-Qahera current consumption that used in testing the performance of the proposed algorithm.

The priority of the consumers generated virtually in a MATLAB environment randomly because the DR is not applied yet in Iraq, as shown in Fig. 5.

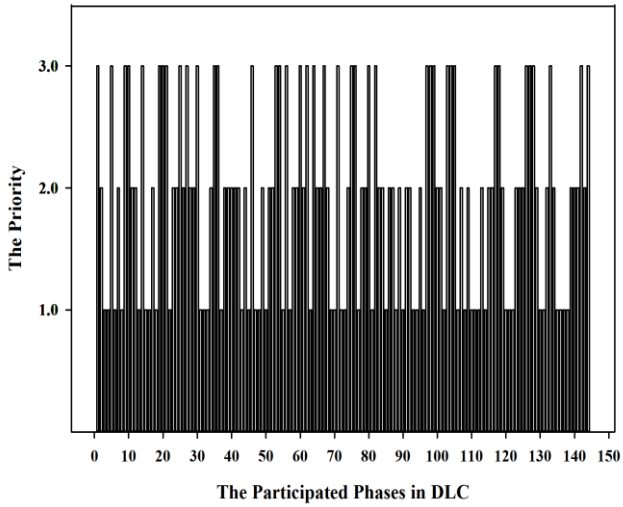

Fig. 5: The proposed priority for the Al-Qahera registered consumers in DLC program.

The consumers give a low priority for most of the phases. Some of the consumers prefer the moderate priority due to the moderate importance of these phases by their opinion. The fewer chooses the high priority for a specific reason like the connection of necessary tools or machines that achieve particular tasks during the period take the measurements taking into consideration they may lose the incentive paid by the utility if during this time there is an event that has been occurred as that depicted in Fig. 5 above.

The consumed data and the priority not have constant configuration and not take fix style, but it changed continuously between day and night or between different seasons in the year. The four cases of the instructions that may reach to the CU from the MCC has been studied depending on the data and priority has been shown in Fig. 4 and Fig. 5.

- **The Overall Consumption < The MCC Limitation**

The first case that may encounter the CU in a specific region is that when the MCC ordered it not to take any action because the reduction of the consumption in the other sectors was enough to pass the event safely. Table I shown detailed information about the consumption due to each priority and what the overall consumption of AL-Qahera under the recoded data and the new consumption limit that the area must consume less than it.

TABLE I
THE CASE1 PARAMETERS

ColCurrent1	ColCurrent2	ColCurrent3	Overall Consumed current	The permissible consumed current (The MCC limitation)
209.2 A	168.34 A	81.52 A	459.06A	500A

From the table, we notice that the MCC limitation (500A) can cover all the region consumption (459.06A), so the algorithm not switching OFF any phase with any priority and the consumption before and after applying the algorithm is same as shown in Fig. 6. The first bar explains the total consumption of all the houses that registered in the program, and the second one showed the consumption after applying the algorithm. Usage still the same due to the working in case1 that performs nothing and all the phases in ON state.

Initially, suppose the following:

- ✓ The CUs have two ways of communication with all the SMs of the registered homes in the DLC program in the region.
- ✓ The SMs have the ability to perform the phase swapping technique depending on 9 CRs installed in the SMs.
- ✓ The phases are connected to the same SFs. For example, phase1 in all the homes has been connected to the first SF and phases 2 and 3 connected to the second and third SF, respectively.
- ✓ When the CU send (1) that activated the CR to be in ON state and connected the registered phase to the SF and vice versa.

In Case1, the CU switched ON all the phases by sending an operating signal - High signal or (1) - to trigger ON CRs in the SMs.

The balancing of the SFs is a critical issue and the question arising here about the effecting of the DLC program on the state of the SFs after applying for the DLC DR program.

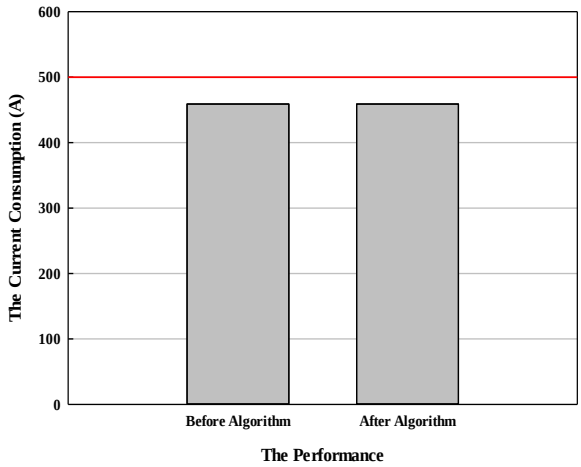

Fig. 6: The result of CASE1.

Fig. 7 shown the current consumed after the operation of the proposed algorithm.

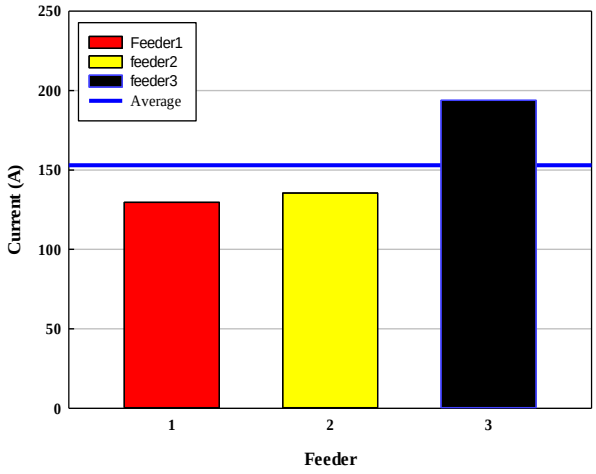

Fig. 7: The SFs after applying the DLC program**.**

There is clear unbalance that may lead to not desired results in the view of the secondary transformers if the temperature of the coil increased, and that leads to inefficient operation for the transformers.

- **CASE2: (ColCurrent2 +ColCurrent3) < TransCurrent**

In this case, there is an amount of reduction that must be happening to the phases with LP. The other two priorities not be impressed by the reduction, and the CU lowering the consumption based on the SMs of targeted phases. From Table I the phases with priory 2 and 3 consume 249.86A and if we suppose the message that reaches to the CU from the MCC was " Decrease the consumption to 270A", that mean the algorithm switching ON a specific number of the LP phases that consume around 20.14A (**RestCurrent** that is over the current consumed by the MP and HP Rphs-DLC) as shown in Fig. 8.

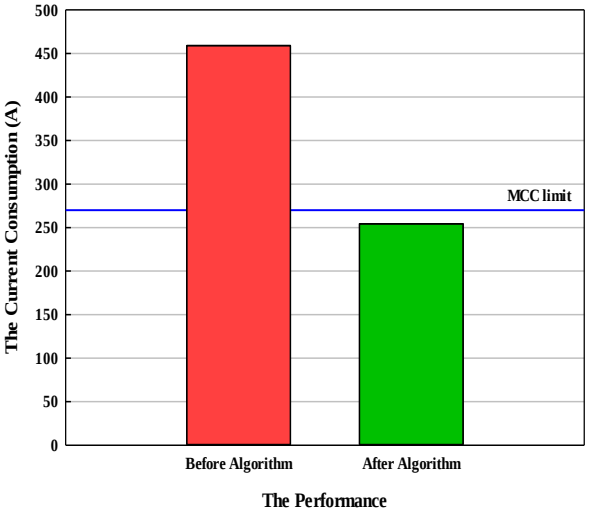

Fig. 8: The old and new consumption in CASE2.

MCC ordered the algorithm for decreasing the consumption to 270A, but when the algorithm checks the accumulative sum for $R_{phs\text{-}DLC,}$ it found the last load can be switched ON make the consumption equal to 254.38A and in case adding any new load the consumption exceeded the limit of the utility. The CU sending signal to the SMs that reduced the consumption due energizing 70.9% of the overall phases in Al-Qahera, as shown in Fig. 9.

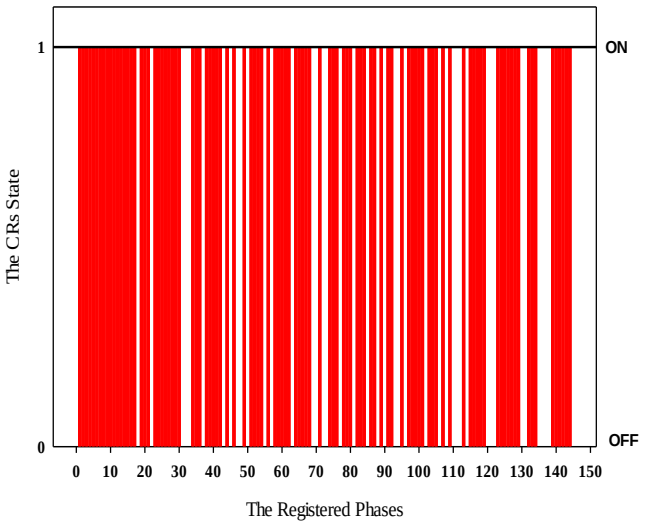

Fig. 9: The CRs state in CASE2.

The last portion wondering about the effect of the proposed algorithm on the balancing situation and to what extent it is good or bad. Fig. 10 illustrated the current after applying the DLC and comparing with the average value, and it showed the following:

- ✓ The current consumption after applying the algorithm is less in all the feeders comparing with the consumption before applied the DLC program (refer Fig. 8).
- ✓ The CUI reach to (59.4819%) and that indicate to serious unbalance.

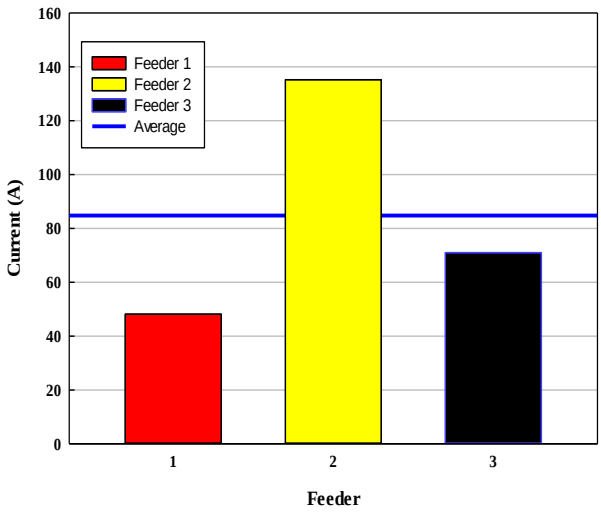

Fig. 10: The SFs when CASE2 applied by algorithm.

- **CASE3:RestCurrent=TransCurrent-ColCurrent3**

The third case happened when there is urgent hard event, and the MCC ordered the CU to reduce the region consumption to an amount enough just to the loads with HP and some loads with MP as an example if TransCurrent =150A. The algorithm searching smartly about the suitable phases with MP that can be operated in the remaining current that allowed to be consumed above the consumption of the phases with HP. The remaining current for the MP phases equal to 68.48A. The total phases energized in this case, to achieve the threshold of consumption are 64 phases that represent 44% of the total phases of the Al-Qahera sector as that clear in Fig. 11.

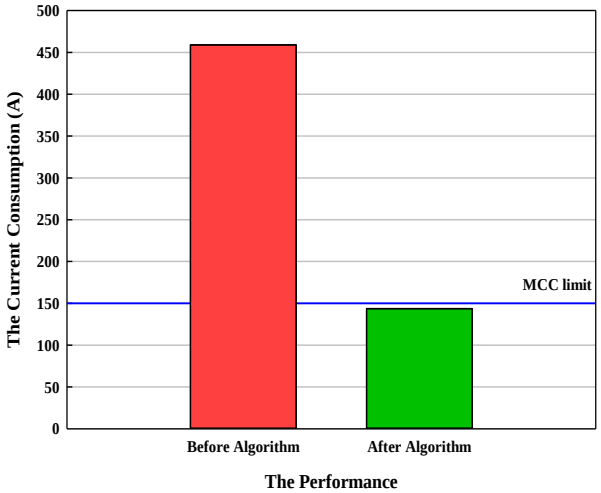

Fig. 11: The reduction in consumption due CASE3.

The operation signal generated by the CU and sent to the SMs illustrated in Fig. 12, where the HIGH signal energized the load and vice versa. The consumption after applying the algorithm reach 143.61A, as illustrated in Fig. 11, with the current consumed before the urgent cases in the power system. The SFs situation is illustrated in Fig. 13 that highlighted the amount of current consumed by each one among the SFs and appear the following facts:

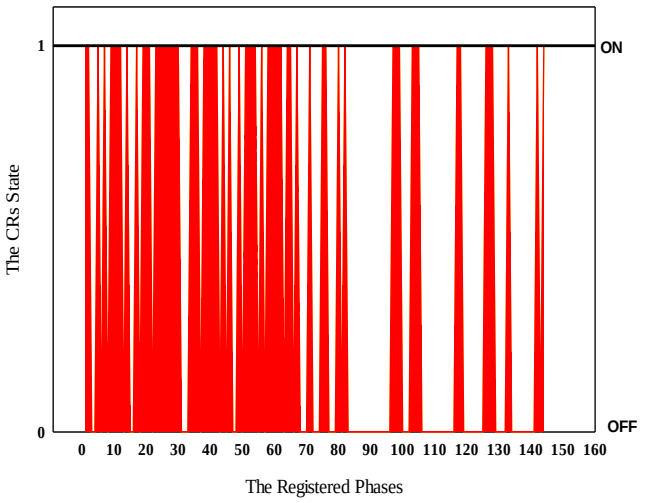

Fig. 12: The CRs situation due to the CASE3.

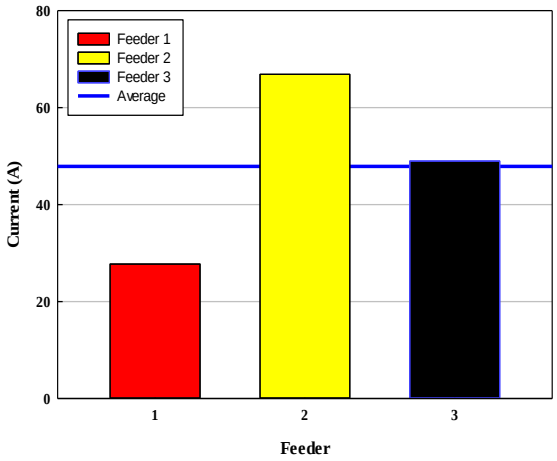

Fig. 13: The SFs after applying the CASE3.

- ✓ The consumption under the determined threshold has been satisfied.
- ✓ The reduction creates a bad unbalance in the SDN where in this case, the CUI reaches 42.0305% compare with 26 before applying the algorithm and this problem should be solved.

- **CASE4: RestCurrent=TransCurrent**

This case regarded the hardest case because there is a significant event that makes the MCC shut down all the LP and MP phases and allows for specific HP loads to still energized. To test the algorithm, the MCC supposed to send a message with the following content to the CU "Reducing the consumption to 50A ". The algorithm should search for the HP phases that can consume 50A only. The algorithm reaches to operate the suitable phase that consumed 48.33A and shut down all the others. Fig. 14 illuminated the SFs situation before and after applying the proposed algorithm. There are 31 HP phases still energized that represent 21.5% form the total phases in Al-Qahera, as showing in Fig. 15. The CUI% recorded after applying the algorithm was 56.9212%, and that means the SFs in an unbalancing situation. The imbalance happens in this case worse than the unbalance before applying the proposed algorithm 26%, and this case also needs to solve the unbalancing to avoid the harmful effects in the future. The SFs after applying the algorithm has been illustrated in Fig. 16.

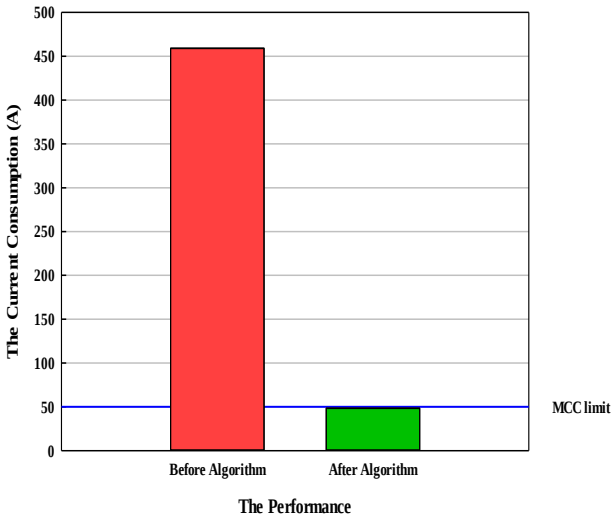

Fig. 14: The Consumption before and after specific event.

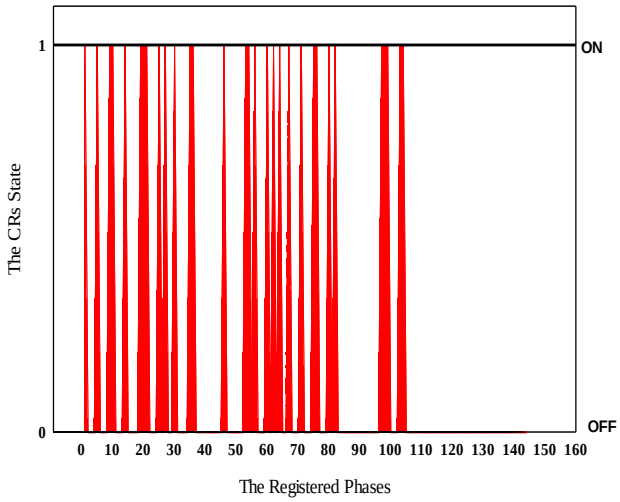

Fig. 15: The signals that reach the CRs in CASE4.

2. Proving the Fairness Principle

The fairness used by the suggested FDR-DLCM algorithm that can contribute effectively in changing the behavior of the last consumer means the justice and balancing in choosing the phases that shut down when there is an event required that. To full clearance, the MATLAB simulation environment used to prove the fairness principle by supposing the utility contract with 3ph 6 homes in the Al-Qahere sector in Baghdad and the DLC DR program has been applied on during 100 events. The total consumption of specific homes is 65.92A. The algorithm should choose different phases in each event and not stick to specific ones because that represents a comfort factor to the consumers who participated in the program. The fairness for the CASE2, CASE3, and CASE4 proved and neglected the CASE1 because the algorithm does not act any action in CASE1.

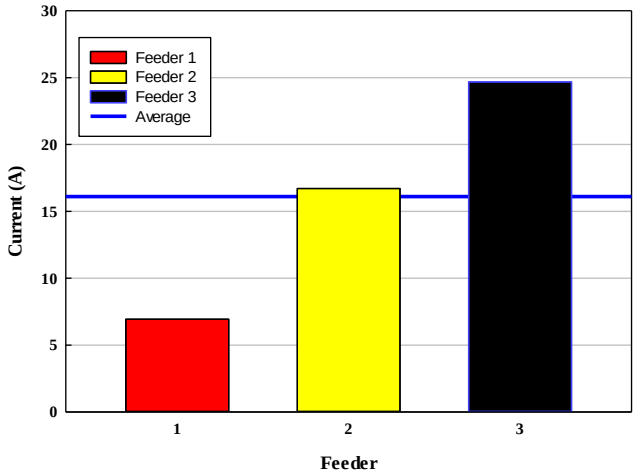

Fig. 16: the SFs after applying the CASE4.

- **CASE2: The threshold =40A**

The Fig. 17 illustrates the situation of the Rphs-DLC if there are 100 tests performed during four hours to maintain the consumption under 40A. In each test, the algorithm supposes the consumers changed the load priorities due to some reasons, and that called the variable priority test (VPT).

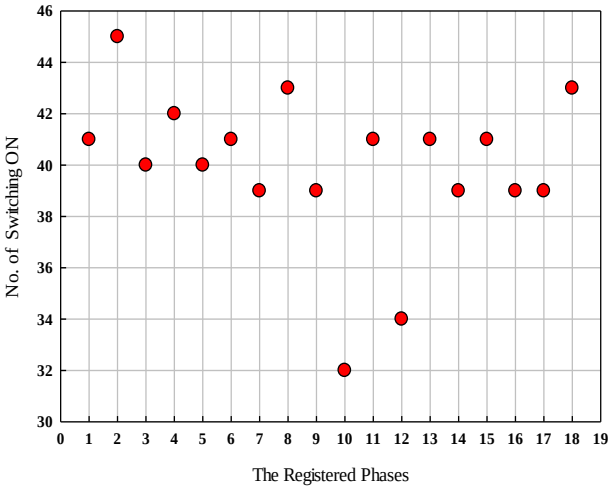

Fig. 17: The Shutdown times for the $R_{phs\text{-}DLC}$ if there are repeated events

The registered loads in the DLC program used in an unbiased manner, and there is no load, not shut down, and some loads still ON during all the events. Within all the 100 events, the algorithm satisfied the threshold demanded by the MCC. The threshold was not let the six homes consuming more than 40A by measuring the consumption of the phases and choosing the suitable candidates among it to energized and switching off all the others. The Fig. 18 showed the consumed current amount during the four hours with 100-times testing. The algorithm efficiently gives a satisfying result along the experimental time. In the previous part, we supposed the consumers are changing the priority of the phases with all tests. In this part, the algorithm has been tested under the assumption "the phases priority is fixed in all events in the test period" and that called by the fixed priority test (FPT).

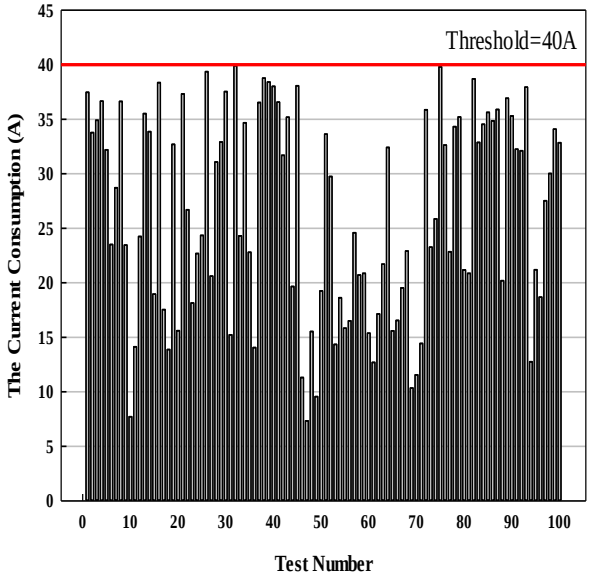

Fig. 18: The current consumption during the experiment period.

The Fig. 19 illustrated the FPT result if the algorithm encountered the CASE2, and it means the threshold cover the HP and MP phases and some of the LP phases. The outcome showed that the LP phases switched off throughout the test and the remain phases used fairly manner during the test. Depending on the data in Table II the algorithm performance under the FPT scenario has been tested. It used to prove the algorithm validity for the two next cases (CASE3 and CASE4).

During the FPT, the algorithm reaches to the demanded consumption in addition to the fair using of the phases, as depicted in Fig. 20.

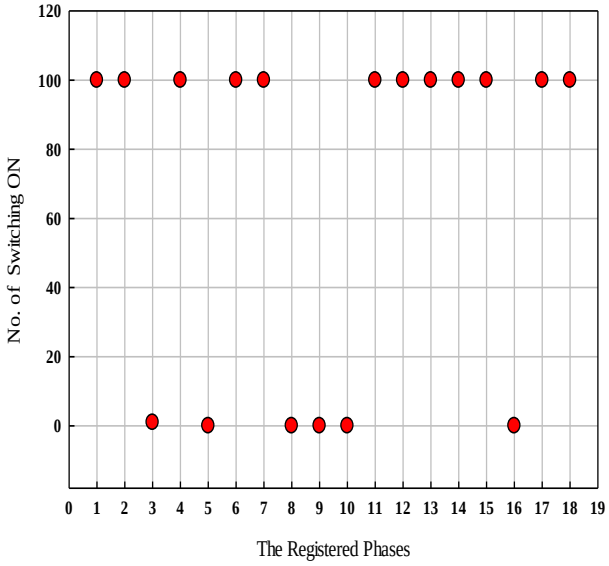

Fig. 19: The Registered loads under the similar priority test.

TABLE II
THE FPT PARAMETERS

Parameter	Value
Phases current (A)	[1.12,1.32,1.17,3.55,17.71,6.73,0 .04,0.04,1.84,1.06,0.96,4.66,4.91, 0.31,3.7,5.4,4.8,6.6]
Priority	[2,3,1,3,1,3,3,1,1,1,3,3,2,3,3,1,2, 2]
The total Consumption	65.92A
The consumption by LP phases	27.22A
The consumption by MP phases	17.43A
The consumption by HP phases	21.27A
The Threshold of CASE2	40A
The Threshold of CASE3	25A
The Threshold of CASE4	17A

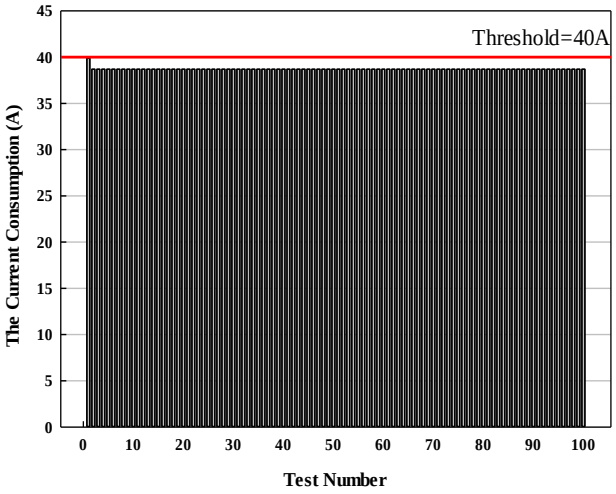

Fig. 20: The consumption not exceed the threshold in CASE2 FPT.

- **CASE3: The Threshold= 25A**
  - **VPT**

Fig. 21 and Fig. 22 illustrate the success in applying the fairness principle and the reduction in current consumption. In Fig. 22, we notice there is a high reduction in some of tests like the test number 13,47 and 65 and that coming because one the fairness principle forced the algorithm to energize the HP or MP phases that not used before (to satisfy the fairness principle), and in chance, all the candidate phases were consuming low current, so the final consumption will be low but under the utility threshold.

  - **FTP**

Fig. 23 and Fig. 24 illustrate the success in applying the fairness principle and the reduction in current consumption in the FPT. Eight phases that have HP as recorded in Table 4.2, and it consume an amount of current reach to the threshold, and for that, there is no enough current to operate any other loads with MP or LP as it is shown in Fig. 23

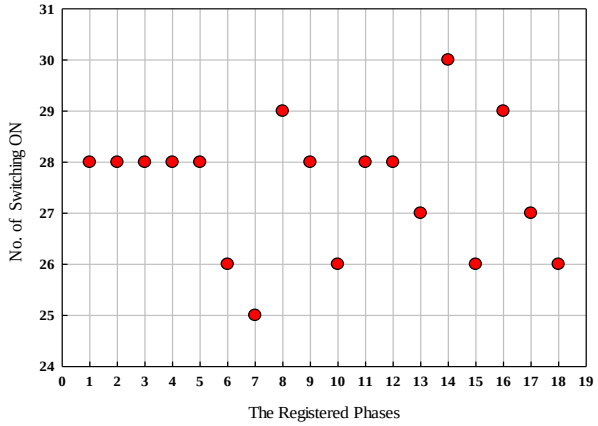

Fig. 21: The fairness principle in CASE3 VPT.

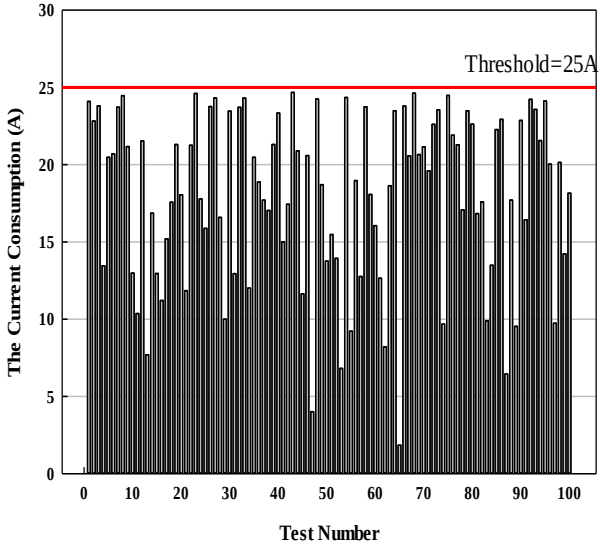

Fig. 22: The current consumption reduction below the threshold level.

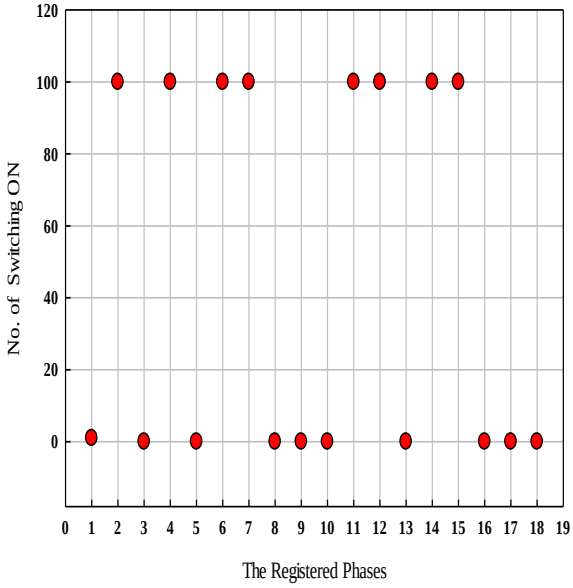

Fig. 23: The fairness principle in CASE3 FPT.

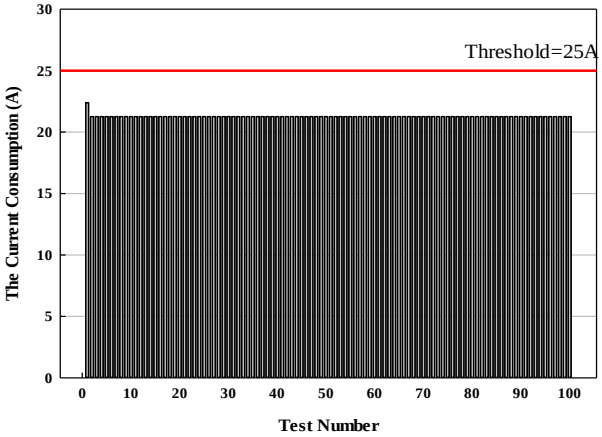

Fig. 24: The consumption reduction below the threshold level in FPT.

- **CASE4: The Threshold= 15A**

The current, in this case not enough to energize all the phases with HP, so the algorithm chooses wisely the candidate loads that satisfied the threshold demanded by the utility and caring to the fairness in the phase electing.

- VPT

The fairness principle and amount of consumption are satisfied in Fig. 25 and Fig. 26.

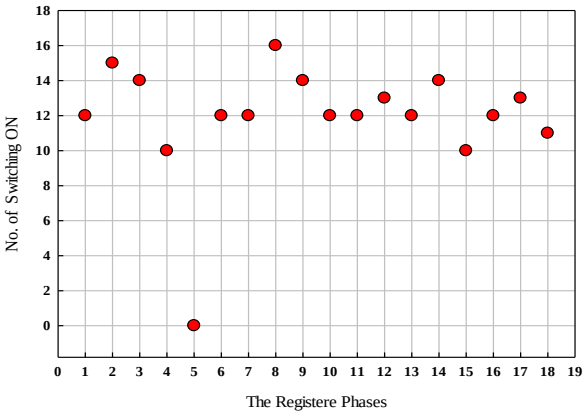

Fig. 25: The fairness principle in CASE4 VPT.

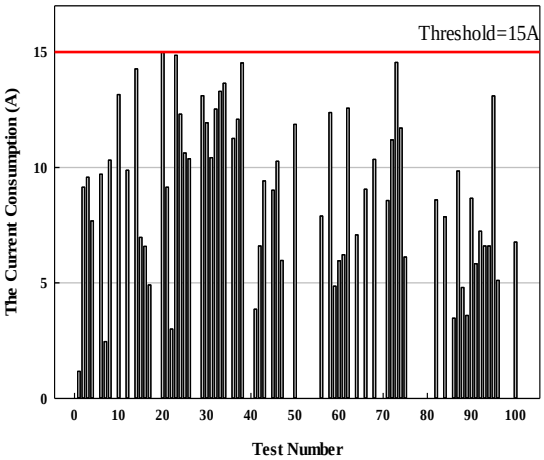

Fig. 26: The consumption reduction below the threshold level in VPT.

- FPT

The fairness validation and the consumption that is under the MCC threshold level are depicted in Fig. 27 and Fig. 28.

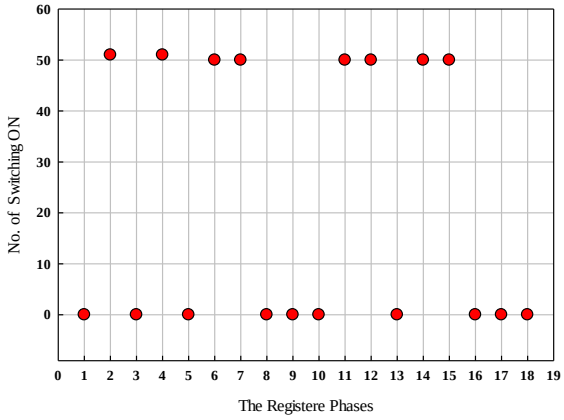

Fig. 27: The fairness principle in CASE4 FPT.

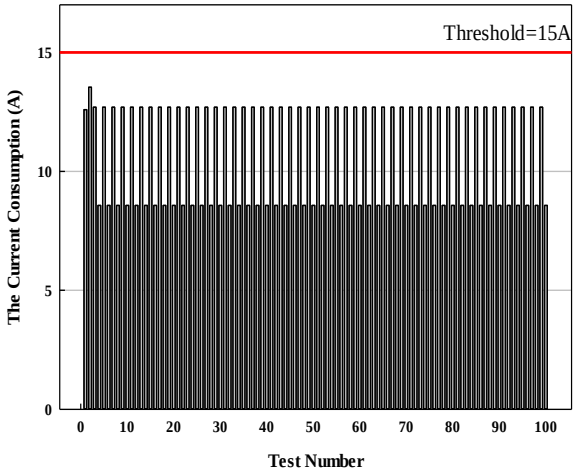

Fig. 28: The consumption reduction of CASE4 FPT.

3. The Treatment of the Load Balancing Problem

The proposed algorithm achieves the main target that it designs for with additional important feature that called the fairness. The reduction in consumption and altering the final behavior of the consumers in the distribution area is demanded to achieve the optimal power dispatching with reasonable costs. The algorithm treats the essential events that result from there is a sudden peak demand that may be a critical factor from the stability point of view. The shedding loads treatment created from another viewpoint a severe problem in the SDN. The current reduced in all the SFs but not in a regular rate that leads to sharp unbalancing cases, as it showed so far. The proposed algorithm adapted to balance the SFs by using the phase swapping technique to change the position of the choose phases by the DR algorithm. The MOGWO algorithm is merged with the FDR-DLCM to create a new hybrid algorithm that can perform the balanced DLC DR program. The SMs installed in all the 48 homes in the Al-Qahera sector supposed to have a swapping mechanism that represents attached 9CRs with the SMs. The flowchart that explains the hybrid algorithm is illustrated in

Fig. 29. The four cases have been studied in section 4.4.1, severing from sharp unbalancing that results from a reduction of the consumption or switching OFF some phases on specific feeders and let the others ON. The balancing of the SDN leads to an efficient investment of the available equipment and lowering the probability of discomforting the consumer's relief by sudden events like damaging the secondary transformers.

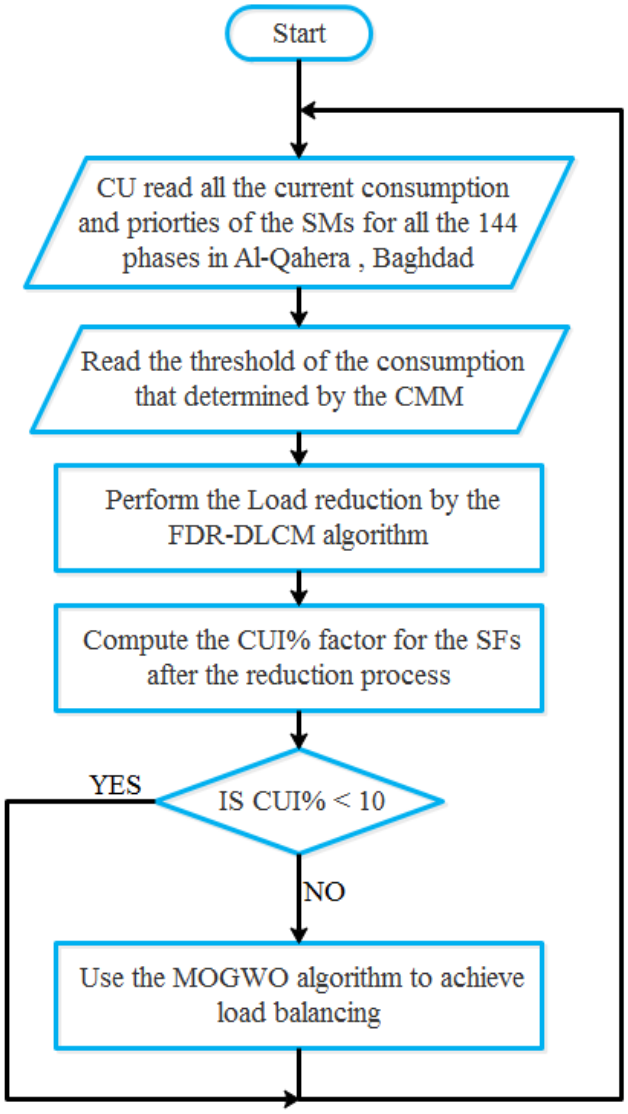

Fig. 29: The online hybrid algorithm to perform balanced reduction in current consumption during the peak demand events.

- **Case1:**

In case 1, the result of applying the FDR-DLCM on the RPhs-DLC in Al-Qahera showed it not alter anything, and the consumption stays itself (refer to Fig. 6) because of the threshold, in this case, can cover all consumption of the LP, MP and HP phases. The CUI% for the SFs reach 26%, and that means there are unbalancing that need for a solution (refer to Fig. 7). Outcomes of applying the hybrid algorithm showed in Table III that illustrated the consumption before and after DR and the CUI% that indicate to the unbalancing ratio in the SFs.

TABLE III
THE HYBRID ALGORITHM CASE1 RESULS

The consumption before DR	The consumption after DR	CUI% for the SFs
459.06A	459.06A	0.5163

The CUI% achieved by the hybrid algorithm is less than one percent, and it is in the accepted level of unbalancing. The consumption of SFs is illustrated in Fig. 30.

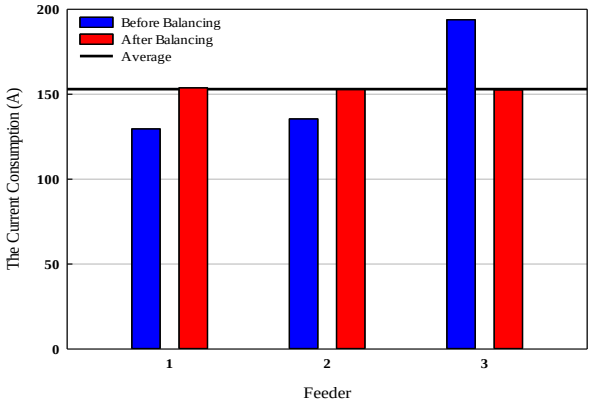

Fig. 30: The SFs after and before using the hybrid algorithm (CASE1).

- **Case2:**

In this case, the proposed FDR-DLCM algorithm has succeeded in altering the consumption pattern and make it under the threshold of the utility, as illustrated in Fig. 8. The problem that appears after reducing the phases consumed energy form the SFs is the hard unbalancing where the CUI% equal to 59.481 (refer to Fig. 10). The balancing situation is worse compared to the CUI% before applying for the DR program. The hybrid algorithm solved the problem and satisfied the threshold in consumption, as illustrated in Table IV and in additional for that in Fig. 31.

TABLE IV
HYBRID ALGORITHM OUTCOMES OF CASE2

The consumption before DR	The consumption after DR	CUI% for the SFs
459.06A	254.38A	0.3459

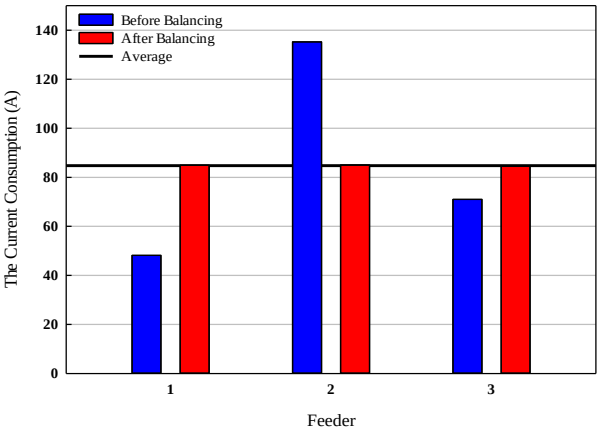

Fig. 31: The SFs after and before using the hybrid algorithm (CASE2).

- **Case3:**

As in the CASE2, the FDR-DLCM algorithm achieved the demanded reduction (refer to Fig. 11) but with a not proper balancing where the CUI% equal to 42.0305 and that still out the range of the accepted ratio (less than 10%) and the state of the SFs was better before applying the reduction (refer to Fig. 13). The applying of the hybrid algorithm gives a satisfactory result depicted and tabulated in Fig. 32 and Table V respectively.

TABLE V
THE HYBRID ALGORITHM CASE3 RESULTS

The consumption before DR	The consumption after DR	CUI% for the SFs
459.06A	143.61A	0.1253

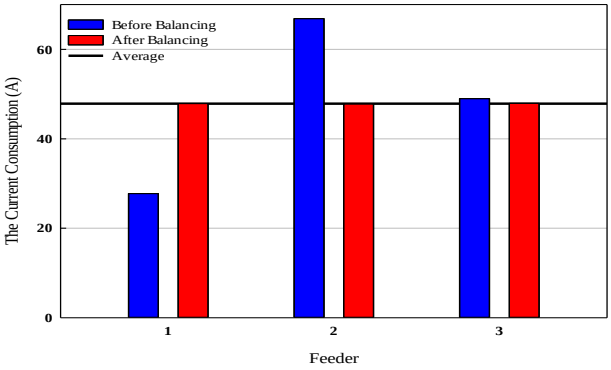

Fig. 32: The SFs after and before using the hybrid algorithm (CASE3).

- **Case4:**

As in the two cases before, the consumption is reduced according to the threshold determined by the MCC of the utility, as that appears in Fig. 14. The CUI% for this case was 56.92%, and it is rejected because of it much higher than the accepted ration for balancing in the SDN that results in severe unbalancing in the SFs, as that clear in Fig. 16. The hybrid algorithm exceeded the balancing problem and reduced the consumption to the desired level of the utility, as it clear in Fig. 33 and tabulated in Table VI.

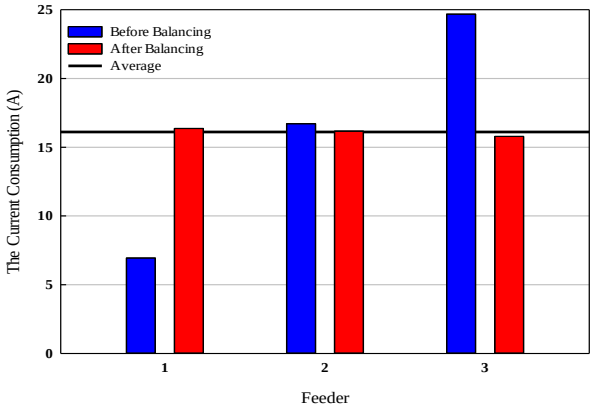

Fig. 33: The SFs after and before using the hybrid algorithm (CASE4).

TABLE VI
HYBRID ALGORITHM RESULT OF CASE4

The consumption before DR	**The consumption after DR**	**CUI% for the SFs**
459.06A	48.33A	1.9863

IV. CONCLUSIONS

This chapter discusses the mechanism for achieving the demand response in the Al-Qahera sector in Baghdad. There are many programs under the DR, but the choice program in this thesis was the direct load control program that gives the utility the full authority on the phases that registered under the program as an exchange to the monetary incentives that paid to the participators in the program. The result achieved can be summarized in the following points:

1. In the beginning, the proposed algorithm (FDR-DLCM) has been succeed in altering the consumption behavior for the consumers in the peak load periods and reduced the consumption to the determined level by the utility. The algorithm applied on four different scenarios allowed to test the performance under all the expected events from the viewpo int of the hardness of the event that it may encounter when it applied.
2. The FDR-DLCM has been succeed in all the different four cases, but it causes serious balancing problems that caused as an effect of the unsymmetrical choosing of the phases that must be switching OFF. The random phases electing make some SFs heavily loaded and the others with low load. The CUI% indicated in all the four cases to the possibility of damaging the secondary transformers by increasing the temperature in its coils or it leads to the inefficient investment of the equipment of the SDN like the feeders.
3. The balancing problem leads to changing the FDR-DLCM algorithm to a new algorithm that is a hybrid algorithm that it represents a smart mixture between the FDR-DLCM and the MOGWO algorithm.

4. The hybrid algorithm attains an efficient outcome due to its ability to reach the requested level of reduction as the FDR-DLCM algorithm and, at the same time, have the ability to balance like the MOGWO algorithm [11], [12]. The hybrid algorithm tested again on the four operation cases, and it proves itself in the consumption reduction and the load balancing.

REFERENCES

[1] S. S. Reka and V. Ramesh, "Demand response scheme with electricity market prices for residential sector using stochastic dynamic optimization," in *2016 Biennial International Conference on Power and Energy Systems: Towards Sustainable Energy (PESTSE)*, 2016, pp. 1–6.

[2] F. Kamyab, M. Amini, S. Sheykhha, M. Hasanpour, and M. M. Jalali, "Demand response program in smart grid using supply function bidding mechanism," *IEEE Trans. Smart Grid*, vol. 7, no. 3, pp. 1277–1284, 2015.

[3] M. H. Yaghmaee, A. Leon-Garcia, and M. Moghaddassian, "On the performance of distributed and cloud-based demand response in smart grid," *IEEE Trans. Smart Grid*, vol. 9, no. 5, pp. 5403–5417, 2017.

[4] P. Du, N. Lu, and H. Zhong, *Demand Response in Smart Grids*. 2019.

[5] M. Parvania, M. Fotuhi-Firuzabad, and M. Shahidehpour, "ISO's optimal strategies for scheduling the hourly demand response in day-ahead markets," *IEEE Trans. Power Syst.*, vol. 29, no. 6, pp. 2636–2645, 2014.

[6] D. T. Nguyen, M. Negnevitsky, and M. de Groot, "Market-based demand response scheduling in a deregulated environment," *IEEE Trans. Smart Grid*, vol. 4, no. 4, pp. 1948–1956, 2013.

[7] S. Paul, "Day Ahead Bi-Level Direct Load Control in Smart Residential Apartment Building : A Stackelberg Game Approach," no. September, 2019.

[8] F. Ruelens, B. J. Claessens, P. Vrancx, F. Spiessens, and G. Deconinck, "Direct Load Control of Thermostatically Controlled Loads Based on Sparse Observations Using Deep Reinforcement Learning," vol. 5, no. 4, pp. 423–432, 2017.

[9] J. M. Lujano-Rojas, G. Zubi, R. Dufo-López, J. L. Bernal-Agustín, E. García-Paricio, and J. P. S. Catalão, "Contract design of direct-load control programs and their optimal management by genetic algorithm," *Energy*, vol. 186, 2019.

[10] A. R. Jordehi, "Optimisation of demand response in electric power systems, a review," *Renew. Sustain. Energy Rev.*, vol. 103, no. September 2017, pp. 308–319, 2019.

[11] I. H. Al-Kharsan, "a New Strategy for Phase Swapping Load Balancing Relying on a Meta-Heuristic Mogwo Algorithm," *J. Mech. Contin. Math. Sci.*, vol. 15, no. 2, pp. 84–102, 2020.

[12] I. H. Al-Kharsan, A. F. Marhoon, and J. R. Mahmood, "The Balancing of Secondary Distribution Feeders by Two Techniques GWO and PSO Applied in Baghdad, Comparative Study," *IOP Conf. Ser. Mater. Sci. Eng.*, vol. 745, no. 1, 2020.

DOI: 10.37917/ijeee.sceeer.3rd.21 *(15-16) June 2020*

Open Access

Iraqi Journal for Electrical and Electronic Engineering
Conference Article

Performance of Non-Orthogonal Multiple Access (NOMA) with Successive Interference Cancellation (SIC)

Ali K. Marzook*[1], Hayder J. Mohammed[2], Hisham L. Swadi Roomi[3]
[1] Petroleum Engineering Department, University of Basrah, Basrah, Iraq
[2]Alfurat Alawsat Technical University, Najaf, Iraq
[3] Electrical engineering Department, University of Basrah, Basrah, Iraq

Correspondence
* Ali K. Marzook
Petroleum Engineering Department,
University of Basrah, Basrah, Iraq
Email: ali.marzook@uobasrah.edu.iq

Abstract
Non-Orthogonal Multiple Access (NOMA) has been promised for fifth generation (5G) cellular wireless network that can serve multiple users at same radio resources time, frequency, and code domains with different power levels. In this paper, we present a new simulation compression between a random location of multiple users for Non-Orthogonal Multiple Access (NOMA) and Orthogonal Multiple Access (OMA) that depend on Successive Interference Cancellation (SIC) and generalized the suggested joint user pairing for NOMA and beyond cellular networks. Cell throughput and Energy Efficiency (EE) are gained are developed for all active NOMA user in suggested model. Simulation results clarify the cell throughput for NOMA gained 7 Mpbs over OMA system in two different scenarios deployed users (3 and 4). We gain an attains Energy Efficiency (EE) among the weak power users and the stronger power users.

KEYWORDS: **Non-orthogonal multiple access; successive interference cancellation, energy efficiency, and throughput maximization.**

I. INTRODUCTION

Non-Orthogonal Multiple Access (NOMA) system has been recently proposed as candidate multiple access technique for 5G and beyond 5G systems by 3GPP in different applications [1]. NOMA system gained a wide interest as a technique of increasing the number of users that can be served simultaneously by scheduling multiple users over same spectrum resources but at different power levels [2].

Pairing of users schemes have been proposed for NOMA cellular downlink scenario with randomly deployed users [3-5]; where, the comprehensive performance of NOMA system is very affected with targeted data rates and allocated power of the deployed users. Another group of researches focused on the advantage of NOMA over Orthogonal Multiple Access (OMA) in a power allocation and fairness index in system to motivate the NOMA system as prospective system; a dynamic power allocation scheme is proposed in [6], which ensures that the individual rates for both strong and weak users in NOMA are higher than the corresponding ones in Orthogonal Multiple Access (OMA). The power allocation strategies are discussed in [7]; where they measure per-user outage probability to prove the superiority of NOMA system on OMA.

Successive Interference Cancellation (SIC) is very important toll in NOMA system which is applied at the receiver(s) for multiuser detection and decoding. To obtain of each user desired signal, the SIC processor in transmitter/receiver (uplink/downlink detection) deciphers an eminent interferences firstly and then deducts them from the superimposed signal. Since in downlink each User Equipment (UE) receives the other user's signal (the desired and interfering signals) over it channel, the superimposing of different signals with different power levels is decisive to diversifying each user signal and to perform SIC at a given UE end [8-9]. Some of authors try to improve the NOMA capacity by allocate the users into three categories (singletons, weak users, and strong users) and to derive the data rate and Signal to Interference Noise Ratio (SINR) for these categories, emphasizing the Quality of Service (QoS) of weak users [10].

The aforementioned studies motivated us to formulate the users allocation scenario to unification the fairness index around unity value for all users and maximization of the throughput cell of NOMA systems as a pairing optimization problem. In this paper, the performance of NOMA system is investigated in a downlink network with specific calculated positions for mobile users and Show the usefulness of this model compare with random location of users. This step is a prelude to generalizing these calculations to suggest a new uniform a cluster regions for the mobile users based on a successive values for SIC and throughput cell for all users.

The rest of the paper is organized as follows. Section II presents NOMA downlink system. Section III presents performance comparison. Sections IV and V presents the simulation results and the conclusion, respectively.

II. NOMA DOWNLINK SYSTEM

In NOMA downlink, we consider a standard single-cell cellular system that consists of a BS equipped with single antenna and serving m users, as shown in Fig. 1

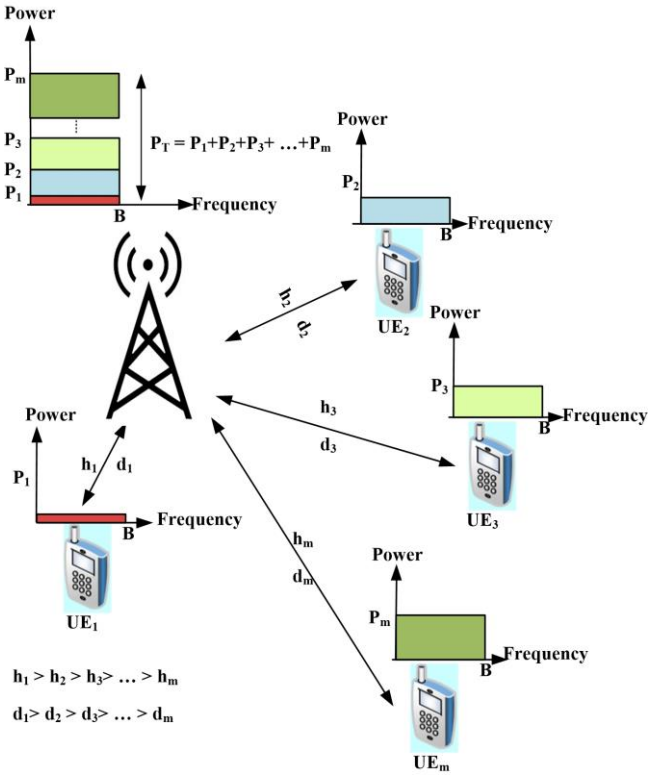

Fig. 1 NOMA downlink system

The gathering of User Equipment (UE) of all active users and SIC are employed to detect their assigned signals. Fig. 2 shows NOMA downlink system of m number of UEs end followed by SIC receivers. In the cellular network, it is supposed that the nearest user to the base station (BS) is UE_1 , while UE_m is the farthest one.

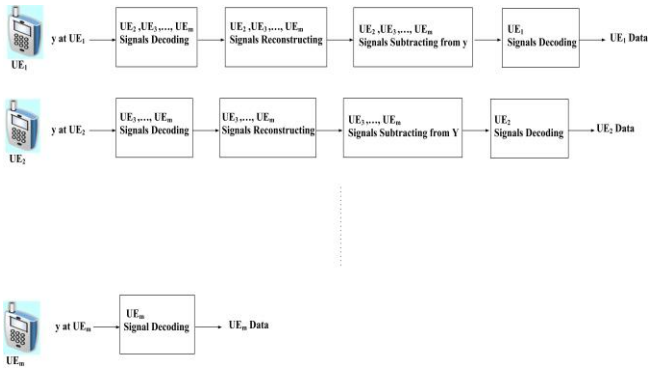

Fig.2 SCI stages for the active users

The allocated power for each user, whereas the least power assigned to the closest user and highest power assigned to the farthest and the power difference increase distributed by the most distant and the farthest among the other users, is consider the main challenge for BS. In the cellular network, each UE received the same transmitted signal that holds the data signal for the active users. Started by the farthest user which receives the high power signal, and then deducts the decoded signal from the received signal (y) to has won signal; that means the strongest user forward the signal intended for the weakest user. SIC will be carried out at the users.

Let us consider a NOMA cellular network in downlink scenarios, in which single base station has a single antenna and m users, each user has a single antenna too. The propagation channel between the UE_i and the BS is presented by [3]:

$$h_i = \frac{g_i}{\sqrt{1+d_i^{\gamma}}} \qquad for\ i = 1,2,\dots m \tag{1}$$

Where g_i denotes the channel gain with Rayleigh fading, d_i represents the distance from the user to the BS, and γ is the path loss coefficient. The channel of the users are sorted as $|h_1|^2 \le |h_2|^2 \le \cdots \le |h_m|^2$.

According to NOMA system, the superimposed transmitted signal which sent by the BS for all users can be expressed as:

$$x(t) = \sum_{i=1}^{m} \sqrt{\propto_i P_T} x_i\,(t) \tag{2}$$

where $x_i(t)$ represents the intended data signal of OMA system, $\propto_i$ is the factor of power allocation for the UE_i , and P_i is the total average power available at the BS end.

The power allocated to for the weak and strong user UE_i is $P_i = \propto_i P_T$. The power allocated of each UE_i is follows the distance of the userUE_i from the BS; where, it distributed inversely depended on near or far the user UE_i from the BS. The closest user UE_1 the least power, while farthest user UE_m has the strongest power.

The individual received signal at the user end UE_i represents as:

$$y_i(t) = x(t)h_i + w_i(t) \quad (3)$$

where h_i is the factor of channel attenuation between the UE_i user and BS, and $w_i(t)$ denotes the received mean zero AWGN at the UE_i with spectral density N_o (W/Hz).

The signal of the farthest user will decoded at the first that has the most allocated power compare with the other users. While the signals for residual users will look like interference.

The signal to noise ratio (SNR) for farthest UE_m will be indicated by [4],

$$SNR_m = \frac{P_m h_m^2}{N_o W + \sum_{i=1}^{m-1} P_i h_m^2} \quad (4)$$

where the transmission bandwidth of the system is denoted by W.

Finally, the signal nearest user UE_1 signal will be decodes and it denoted as

$$SNR_1 = \frac{P_1 h_1^2}{N_o W} \quad (5)$$

The SNR for residual users UE_i can written as,

$$SNR_i = \frac{P_i h_i^2}{N_o W + \sum_{k=1}^{i-1} P_k h_i^2} \quad (6)$$

The data rate achievable (the throughput) for each UE_i that measured by (bps) is given by

$$R_i = W log_2 \left\{1 + \frac{P_i h_i^2}{N + \sum_{k=1}^{i-1} P_k h_i^2}\right\} \quad (7)$$

In OMA, the total bandwidth system and power transmitted by BS are divided equally among the UEs, the data ratet for each UE in OMA is given by

$$R_i = W_i log_2 \left\{1 + \frac{P_i h_i^2}{N_i}\right\} \quad (8)$$

Where W_i individual bandwidth for each user and equal to $W_i = \frac{W}{m}$ and N_i noise for each user and equal to $N_i = N_o W_i$.

The sum capacity of the systems (NOMA and OMA) can be expressed as

$$R_T = \sum_{i=1}^{m} R_i \quad (9)$$

III. Data Rate and Power Performances

In this section, we demonstrate the performance of the NOMA system with OMA system.
First, we follow the cell throughput

$$\text{Targeted R is } \max_{\propto_i, Pt} W log_2 \left\{1 + \frac{P_i h_i^2}{N + \sum_{k=1}^{i-1} P_k h_i^2}\right\} \quad (11)$$

Subject to

C1: $\sum_{i=1}^{m} P_i \leq P_T$;
C2: $P_i \geq 0, \forall i$
C3: $P_1 < P_2 < P_3 < \cdots < P_m$

The relation between power the individual power of each user P_i and its channel attenuation factor $|h_i|^2$ supposed to be inversely proportional, it will present by:

$$P_i \alpha \frac{1}{|h_i|^2} \quad (12)$$

The Constraint C1 denotes the total power constraint of the BS and the sum of UEs power don't exceed P_T , Constraint C2 ensures the has a bit of power that depend on it position from BS, and Constraint C3 ensures the power that assign by BS for nearest user is lower than the farthest one.
Second, the power consuming at the UEs will be exemplified as the sum of the data signal power adding to power consumed by the power amplifiers in transmitter circuits. In downlink transmitting, the consumption power in the BS can be represented as

$$P_{BST} = P_T + P_{cct} \quad (13)$$

where P_{BST} is the consumption power by BS and P_{cct} is the consumption power by amplifiers circuit at the transmitter end. Energy efficiency (EE) is defined as the sum rate over the total consumed power of the BS [6]

$$EE = \frac{R_T}{P_{total}} = \frac{\sum_{i=1}^{m} R_i}{P_{total}} = \frac{mR}{P_{total}} \quad \left[\frac{bits}{J.Hz}\right] \quad (14)$$

where R_T is the sum of rates transmitted by UEs in terms of (bits/Hz) as mentioned earlier.

IV. Simulation Results

The first group of simulation results are investigated the throughput performances of the downlink NOMA system in two scenarios of users deployed (first one has a 3 users for model 1 and the second is 4 users in model 2) as cleared in Fig.3 and Fig.5 while the second group of simulation results are investigated the energy efficiency performances for the two models that mentioned before.
The main simulation parameters are presented in Table. 1

TABLE 1
The main simulation parameters.

Parameters	value	Model
Rang of transmit power	10-80 dbm	1 and 2
The Bandwidth	5 MHz	1 and 2
Initial channel gain of UE_1	20 dB	1 (m=3 users)
Initial channel gain of UE_2	14 dB	
Initial channel gain of UE_3	1 dB	
Initial channel gain of UE_1	20 dB	2 (m=4 users)
Initial channel gain of UE_2	14 dB	
Initial channel gain of UE_3	6 dB	
Initial channel gain of UE_4	1 dB	
N_o	1 µ watt	1 and 2
P_{cct}	100 m watt	1 and 2
Antennas of BS	1	1 and 2
Antennas of UEs	1	1 and 2

In Fig.3; the advantage of NOMA system over OMA system is very clear in cell throughput for the whole system and each user individually in model 1 (m=3); for example; at $P_T = 50$ watt the NOMA system gained 6.92 Mbps and each users gained 4.55 Mbps, 1.32 Mbps, and 0.74 Mbps for UE_1 , UE_2, and UE_3respectively.

In Fig.4; the peak of the EE-SE curve that corresponding the derivative of the curve is where the system has the maximum energy efficiency that occur when $P_T = 34$ watt for NOMA and OMA systems. At this power, both the systems are achieved the maximum EE, where the NOMA performance is clear has outperforms OMA system at maximum point and beyond for both EE and SE.

In Fig.5; the advantage of NOMA system over OMA system is clear too in cell throughput for the whole system and each user individually in model 2 (m=4); for example; at $P_T = 70$ watt the NOMA system gained 7 Mbps and each users gained 4.83 Mbps, 1.03 Mbps, 0.36 Mbps , and 0.67 Mbps for UE_1 , UE_2, UE_3,and UE_4respectively.

For model 2, the system has the maximum energy efficiency that occur when $P_T = 36$ $P_T = 34$ watt for NOMA and OMA systems respectively. The NOMA performance is clear has outperforms OMA system at maximum point and beyond for both EE and SE that was clear in Fig. 6.

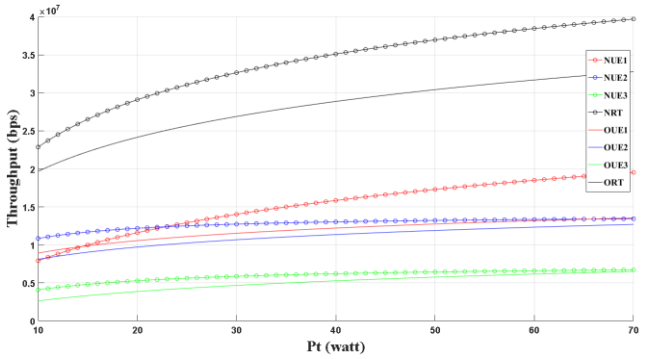

Fig. 3 Cell throughput rates for downlink NOMA and OMA systems at m=3.

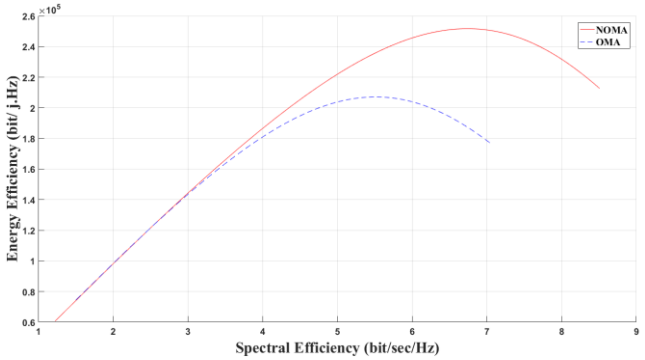

Fig.4 EE-SE curves for NOMA and OMA systems at m=3.

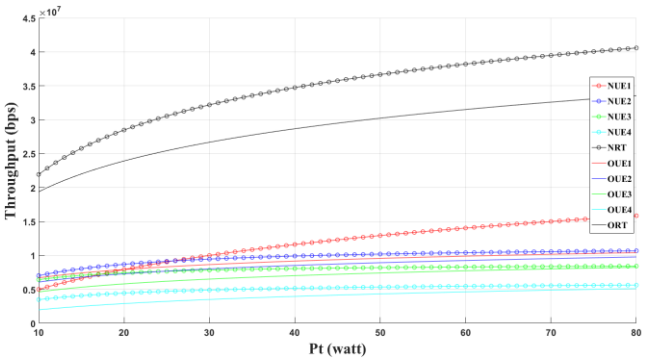

Fig. 5 Cell throughput rates for downlink NOMA and OMA systems at m=4.

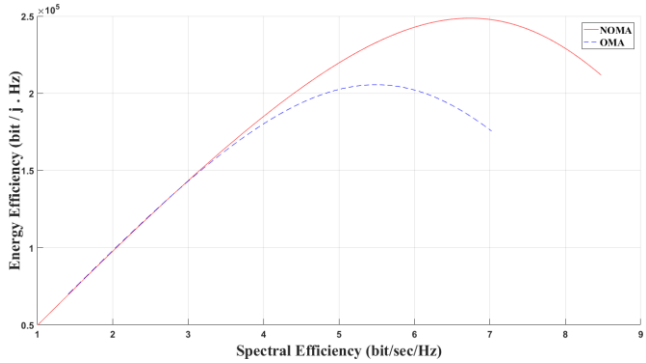

Fig.6 EE-SE curves for NOMA and OMA systems at m=4.

V. CONCLUSIONS

In this paper, the throughout performance in NOMA and OMA systems have been examined. We compare its performance for two different scenarios of deployed users (3 users for model 1 and 4 users for model 2). Through the simulation the highest throughput cell can be achieved at specific range of total base station power. Based on the utility of NOMA system can be suggested as a potential technique for 5G mobile communication system. There are many direction for future work like a power allocation of each user and gathering them in clusters. SIC techniques will enhance the performance due to can consider it as a hot area research.

REFERENCES

[1] J. Choi, "Minimum power multicast beamforming with superposition coding for multiresolution broadcast and application to NOMA systems," IEEE Trans. Commun., vol. 63, no. 3, pp. 791–800,2015.
[2] Z. Ding, X. Lei, G. K. Karagiannidis, R. Schober, J. Yuan, and V. K. Bhargava, "A survey on non-orthogonal multiple access for 5g networks: Research challenges and future trends," IEEE Journal on Selected Areas in Communications, vol. 35, no. 10, pp. 2181–2195, 2017.
[3] Zhiguo Ding, Zheng Yang, Pingzhi Fan, and H. Vincent Poor, "On the Performance of Non-Orthogonal Multiple Access in 5G Systems with Randomly Deployed Users". IEEE Signal Processing Letters, vol. 21, no. 12, pp. 1501 - 1505, 2014.
[4] Peng Xu, Zhiguo Ding, Xuchu Dai and H. Vincent Poor "NOMA: An Information Theoretic Perspective. Multiple Access Techniques for 5G Wireless Networks and Beyond, Springer, pp 167-193". 2015
[5] Z. Ding, P. Fan, and V. Poor, "Impact of User Pairing on 5G NonOrthogonal Multiple Access Downlink Transmissions," IEEE Trans. Veh. Technol., vol.65, no. 8, pp. 6010 - 6023, 2016.
[6] E. Hossain, M. Rasti, H. Tabassum, and A. Abdelnasser, "Evolution toward 5G multi-tier cellular wireless networks: An interference management perspective," IEEE Wireless Communications, vol. 21, no. 3, pp. 118–127, 2014.
[7] M. F. Sohail, C. Y. Leow, and S. Won, "Non-orthogonal multiple access for unmanned aerial vehicle assisted communication," IEEE Access, vol. 6, no. 1, pp. 22716 - 22727, 2018.
[8] M. Saideh, Y. Alsaba, I. Dayoub, and M. Berbineau, "Joint interference cancellation for multi-carrier modulation-based non-orthogonal multiple access," IEEE Commun. Lett., vol. 23, no. 11, pp. 2114–2117, 2019.
[9] K. Higuchi and A. Benjebbour, "Non-orthogonal multiple access (NOMA) with successive interference cancellation for future radio access," IEICE Transactions on Communications, vol. 98, no. 3, pp.403-414, 2015.
[10] S. Dhakal, P. A. Martin, and P. J. Smith, "Noma with guaranteed weak user qos: Design and analysis," IEEE Access, vol. 7, no. 2, pp. 32884–32896, 2019.